Photochemical characterisation of some novel luminescent materials.

Rofe, Karen

Photochemical Characterisation of some Novel Luminescent Materials

Karen Rofe

2009

A Thesis Submitted to the University of Wales, in Fulfilment of the Requirements for the Degree of Doctor of Philosophy

ProQuest LLC.
789 East Eisenhower Parkway
P.O. Box 1346
Ann Arbor, MI 48106 – 1346

Declaration

This work has not previously been accepted in substance for any degree and is not being concurrently submitted in candidature for any degree.

.....

(Signature of candidate)

16/1/10

(Date)

Statement 1

This thesis is the result of my own investigations, except where otherwise stated.

Other sources are acknowledged by footnotes giving explicit references. A bibliography is appended.

.....

(Signature of candidate)

16/1/10

(Date)

Statement 2

I hereby give consent for my thesis, if accepted, to be available for photocopying and for inter-library loan, and for the title and summary to be made available to outside organisations.

.....

(Signature of candidate)

16/1/10

(Date)

Acknowledgements

The last four years I have spent in Swansea have been extremely enjoyable and this has been in a large part due to the people I have met and had the privilege to work with. Firstly, I would like to thank my supervisor Dr. Peter Douglas for all his help, encouragement, support and enthusiasm towards my PhD work and also for being a good friend. I would also like to thank Dr. Chris Morley who has given me invaluable supervision, help and support in all aspects of my work. Many thanks go to Professor Hugh Burrows for allowing me the opportunity to go and complete research in the Chemistry Department at the University Of Coimbra, Portugal, and also for the help and assistance he gave me whilst I was there. I would like to thank Professor Andy Monkman at the University of Durham for giving me the opportunity to use the TCSPC equipment. I am also very grateful to Dr. Chris Webster for introducing me to new techniques and equipment which resulted in me being able to develop my synthetic skills.

Much of the work I completed would not have been possible without the help of Stan. He has been not only an invaluable help in the lab but also a great friend during my time at Swansea. I would also like to thank Dr. Mike Garley and Dr. Rod Mason, who have also helped make my time at Swansea very memorable.

Thanks go to my friends from the photochemistry research group in Swansea, Rachel and Matt who have not only been great friends and people to work with but also share my passion for red wine. I would like to thank Jeremie for all his help with the DFT calculations, and his constant positive attitude and also Steve and Suaud. Special thanks goes to Su Jing who has been a good friend and helped scientifically especially

when I first started in Swansea also, Nat, Lee, Mabsy, Martyn, Dave and Des. Many thanks go to Sofia, Pina, Carmen, Joana and Ana Teresa who made my time in Portugal very enjoyable. I would also like to thank Helen Vaughan and the Photonics Research group at the University of Durham for the help they have given me.

My friends outside chemistry have also provided me with much support especially Bev, Lily, Sian, Kate. D, Claire, Darren, Katy, Charlotte, Louise, Laura and James.

This work would have not been possible without the sponsorship I received. For this, thanks go to Swansea University Chemistry Department, EPRSC, ERASMUS and Johnson Matthey for loan of platinum and palladium salts.

Last but most importantly, I would like to thank my parents, my brother Graham and my Nan and Grandma and Jazz for all their invaluable help, encouragement and support which are very much appreciated.

Symbols and Abbreviations

α4	4 thiophene units
CP	Conjugated Polymer
DCM	Dichloromethane
DFT	Density Functional Theory
dppe	1,2- Bis(diphenylphophinoethane)
dppm	Bis (diphenylphosphinomethane)
dppp	1,3-Bis(diphenylphosphinopropane)
EDT	1:2:1 Ethanol: Diethylether: toluene glass
ET	Energy Transfer
f	Ratio of End Groups to Repeat Units
FC	Franck Condon
FRET	Förster Resonance Energy Transfer
HOMO	Highest Occupied Molecular Orbital
IL	Intra-Ligand Transition
IR	Infra-Red
J	Joules
J	Spectral Overlap
K	Kelvin
k	Rate constant
LED	Light Emitting Diode
LFT	Ligand Field Transition
LMCT	Ligand to Metal Charge Transfer
LUMO	Lowest Unoccupied Molecular Orbital
MLCT	Metal to Ligand Charge Transfer
n	Repeat Units between End Groups
nm	Nanometre

OLED	Organic Light Emitting Diode
PF	Polyfluorene
PF2/6	Poly [9,9'-(di 2-ethyl hexyl) fluorene)
PF 8	Poly [9,9'-(di,n,octyl) fluorene)
PFPT	poly (9,9, dialkylfluorene) poly(3-diethylphosphonato-hexyl thiophene
P_n	Probability of a Chain with n Repeat Units
P_{nd}	Polymer Containing x % Defects
PT	Polythiophene
R_n	Number of Repeat Units in Chains of Length,n.
RT	Room Temperature
s	Second
T	Tau, lifetime
TCSPC	Time Correlated Single Photon Counting
UV	Ultra Violet
Vis	Visible
λ	Lambda, wavelength

Thesis Summary

The photochemical characteristics of two phosphorescent palladium diselenolenes $[Pd_2(Se_2C_8H_{12})_2(PBu_3)_2]$ (**1**) and $[Pd_2(Se_2C_8H_{12})_2(PPh_3)_2]$ (**2**) are described. These are believed to be the first reported examples of luminescent Pd-Se compounds. Both compounds exhibit broadband near-infrared phosphorescence in the solid state and at 77 K in organic glasses with emission yields of 0.12 (±0.01) for **1** and 0.13 (±0.01) for **2** in an ethanol:diethylether:toluene (1:2:1) (EDT) glass. Emission lifetimes at 77 K are the same whether in the solid state or an organic glass with first order fit lifetimes of τ = 18.8 (±0.7) μs and 11.5 (±0.3) μs for **1** and **2** respectively. In the solid state at 298 K emission lifetimes are 1.83 (±0.02) μs and 7.0 (±0.3) μs for **1** and **2** respectively. No transients were detected by ns flash photolysis that could be assigned to the triplet state in room temperature solution, and no emission assignable to singlet oxygen across the wavelength range 1200-1350 nm upon 550 nm excitation of either **1** or **2** in acetonitrile solution was observed. DFT calculations of the S_0 to S_1 and T_1 transitions show a shift in molecular orbital character from one with significant -ene π involvement but very little P involvement in the ground-state to one with less –ene π but greater P involvement in the excited-states; there is also a significant shift in the distribution of involvement of atomic orbitals on the four Se atoms.

The synthesis, structure and photochemistry of a group of novel platinum diselenolenes of the general formula $[Pt(Se_2C_8H_{12})(PR_3)_2]$ where R is Et, Bu, or Ph and $[Pt(Se_2C_8H_{12})(L)]$ where L = dppm, dppe, or dppp are described. The photochemistry of these compounds is complex. In solution, molecular phosphorescence with a quantum yield of 0.05% can be observed upon excitation at 355 nm. It is also possible to excite this phosphorescence using 532 nm irradiation, where there is very little absorption, which suggests a quantum yield of ca. 1 for excitation at this wavelength. Triplet formation was confirmed by the generation of singlet oxygen. A long lived transient absorbance with a lifetime comparable to that of molecular phosphorescence was observed in ns- flash photolysis. The compounds also emit blue fluorescence with a quantum yield of ca. 7%. It has not been possible to identify the origin of the orange/red broad band solid state emission, which is very different to that seen in solution, however it is tentatively attributed to an intermolecular charge transfer transition.

Polyfluorenes (PFs) are blue emitters with potential application in OLEDs. Steady-state and time resolved methods have to used to examine energy transfer processes in PFs which have been: a) doped with defects, and b) incorporated into polyfluorene-polythiophene (PT) block co-polymers. Increasing the defect concentration in the polymer chain reduces the emission from PF but increases that from the defect, and excitation spectra show conclusive evidence for energy transfer from PF to PT in the block co-polymer. Förster energy transfer rate constants of 1.47 $x10^{12}$ s^{-1} at the PF-PF distance of 8.5Å; and 8.3 x 10^{-13} s^{-1} at the PF-PT distance of 6.9 Å have been calculated. PF-PF energy transfer along PF polymer chains has been modelled using a new kinetic curve fitting method which gives energy transfer rate constants of ca. 1 $x10^{12}$ s^{-1} in good agreement with that obtained by FRET theory, which provides very strong support for the validity of the interpretation of the energy transfer kinetics and the modelling approach taken. The photophysical properties of the polythiophenepolyfluorene co-block polymer are strongly solvent dependent, behaviour which is thought to arise from complex aggregation properties.

Contents

Chapter 1:

Introduction

1.1 The importance of photochemistry

Photochemistry has been defined in many different ways, including 'the study of light-induced chemical reactions'.[1] Another definition is 'the study of the interactions between atoms, small molecules and light or electromagnetic radiation'.[2] The word 'light' with regards to photochemistry has a somewhat broad meaning. In principle, it refers to any part of the spectrum, which can promote a chemical change.[3] The best description of photochemistry that suits the work presented in this thesis is a definition used by Turro: 'the study of chemical and physical reactions induced by the absorption of photons',[4] so for the purpose of this thesis the term 'photochemistry' includes what others might define as 'photophysics'. Photochemistry is considered a very broad discipline which describes a range of energetic, structural and dynamic processes.[3] A key part of photochemistry is understanding the way in which the particular excited states of atoms or molecules play a part in the physical and chemical processes which occur after the absorption of a photon.[2,5]

Photochemistry occurs naturally on a grand scale. Photochemical reactions are of great importance to everyday life, playing a predominant role in, for example, the processes of vision and photosynthesis.[2,6] Photochemistry has, over the past few decades, and especially since the introduction of the laser, advanced tremendously.[2] There is a huge demand for further understanding of photochemical processes for use in varied applications in science and technology, such as photography,[2,7] fluorescent lighting, [8]electroluminescent displays,[9] and physical and biological sensors.[10,11]

To take just one example, the study of organic light emitting diodes (OLEDs) [12] has been the subject of a lot of interest from both academia and industry in recent years.

The aim of the work presented in this thesis was to investigate the photochemistry of some novel and known emissive materials, namely: (i) palladium diselenolenes, (ii) platinum diselenolenes and (iii) a range of polyfluorene co-polymers. Although these compounds were studied with no specific technological application in mind, many of the applications described above require emissive materials, and it is hoped that the studies presented here will be generally useful to those interested in the practical applications of photochemistry.

In this chapter a general overview of photochemistry will be given, in which both the physical and chemical principles which are important to this work will be described.

1.2 First and second laws of photochemistry

In the early 1800s Grotthus and Draper formulated the *first law of photochemistry,* which states that only light which is absorbed by the molecule can produce a photochemical change in that molecule. This law relates photochemical activity to the fact that each chemical substance absorbs only certain wavelengths of light: the presence of light alone is not enough to induce a photochemical reaction; the light must also be of the correct wavelength to be absorbed by the reactant species.[14]

The quantum theory of light was developed in the early 1900s. The idea that light is absorbed in discrete packets of energy called photons was introduced. This led to the *second law of photochemistry* described by Stark and Einstein which states that any molecule absorbs only one photon of light at a time, although now, with the advent of

very high intensity laser sources the study of multiphoton processes in which an individual molecule absorbs two or more photons is possible.[14]

1.3 Spectral transitions and selection rules

1.3.1 Definition of state

Electrons make transitions between atomic/molecular orbitals. When a lumophore absorbs light, electrons may be promoted from their normal ground state configuration to a higher, shorter-lived excited state. The excited state then will decay back down to the ground sate, losing energy via numerous non-radiative processes and in the case of lumophores, the emission of light. The emitted light is of lower energy than the absorbed light due to some of the energy being also converted into vibrational, rotational and translational energy.[4]

1.3.2 Definition of electron spin

The existence of electron spin was reported by Otto Stern and Walther Gerlach in 1921. The spin of an electron is an intrinsic angular momentum that every electron possesses and cannot be changed or eliminated. Electron spin is described by a spin quantum number (s) which is fixed at the single (positive) value of ½ at all times. The spin can be clockwise or anticlockwise. These two states are distinguished by the spin magnetic quantum number, m_s, which can take only values of +½ or –½. An electron with m_s = +½ is denoted as ↑or α and an electron with m_s= –½ is denoted as ↓ or β. [4,13]

1.3.3 Definition of electronic state

Electronic states can be classified as singlet, doublet, triplet, quartet, *etc.* The term defines the multiplicity of the state. It is common to specify a state by its spin

multiplicity 2S+1 whereby S is equal to the total spin of the state. In some states the electron spins are paired in an antiparallel manner (↑↓). Such states have no resultant spin magnetic moment and are referred to as singlet states since 2S+1 = 1. Singlet states are denoted as S_0 for the singlet ground state, S_1 for the lowest energy excited singlet state, and S_n for higher singlet states. In the other common state two electron spins are unpaired and parallel (↑↑). Such a state possesses a net spin magnetic moment of S = 1 and is termed a triplet state as 2S +1 = 3. The lowest energy triplet is denoted by T_1 with higher states shown as T_n.[4]

1.3.4 Optical selection rules

1.3.4.1 Spin selection rule

Selection rules govern the feasibility of a transition from one state to another. Transitions between states of different multiplicities are forbidden i.e. singlet-singlet and triplet-triplet transitions are allowed whereas triplet-singlet transitions are forbidden.[2-5] This is usually written as:

$$\Delta S = 0 \qquad \textbf{(eq. 1.1)}$$

However, even though "forbidden" transitions between states of different spin multiplicity do occur, these transitions generally have a low probability and occur much more slowly than allowed transitions. As a result this allows processes such as quenching to occur.[3] For lighter atoms the spin selection rule tends to be obeyed. Spin-forbidden transitions occur more commonly for heavier atoms. This is known as the heavy atom effect. This occurs due to the interaction between the spin and orbital magnetic moments, which are both generated by an electron as it orbits the nucleus. This phenomenon is known as spin-orbit coupling. Spin-orbit coupling mixes the singlet and triplet states so that transitions between them become allowed. The

strength of the coupling depends on the size of the spin-orbit coupling constant. In addition to spin-orbit coupling the spin selection rule has also been shown to break down in the presence of collisions and electric or magnetic fields. This is due to the fact that the spin selection rule is derived on the basis that the system is unperturbed. [3-5, 14-16]

1.3.4.2 Laporte Selection Rule

The second selection rule is the Laporte selection rule. This is particularly relevant to the electronic spectroscopy of transition metals and lanthanides. The rule states that electronic transitions conserving either symmetry or asymmetry with respect to an inversion centre, *e.g.* gerade (g→g) and ungerade (u→u), are forbidden. Hence, d-d and f-f transitions are Laporte-forbidden. [3-5, 14-16]

$$\Delta L = +/- 1 \qquad \textbf{(eq.1.2)}$$

As in the case of the spin selection rule, transitions which are Laporte forbidden have been seen to occur experimentally. This is a consequence of the interaction between the vibrational and electronic motions which gives rise to vibronic coupling. The vibronic coupling results in the mixing of asymmetric vibrations, which allows the absorption of light due to the deviation from perfect symmetry.

The Jahn-Teller effect means that some complexes are not perfectly symmetric, which will again allow theoretically forbidden processes to occur. The molar absorption coefficients of these transitions are very small and the corresponding absorption bands exhibit well-defined vibronic bands. This is the case in, for example, most n→π* transitions in solvents which cannot hydrogen bond (ε is *ca.* 100-1000 M^{-1} cm^{-1}). [3-5, 14-16]

1.3.4.3 The Born-Oppenheimer approximation

The Born-Oppenheimer approximation states that since the motion of electrons in orbitals is far more rapid than nuclear motion, electronic and nuclear motions may be treated separately.

1.3.4.4 The Franck-Condon principle

The promotion of an electron to an antibonding molecular orbital is very rapid (*ca.* 10^{-15} s) in comparison to the time take for a molecular vibration (*ca.* 10^{-10}-10^{-12} s). It is this observation that is the basis of the Franck-Condon principle, which states that an electronic transition is most likely to occur without changes in the positions of the nuclei.

At room temperature most of the molecules are in the lowest vibrational level of the ground state. An electronic transition requires a net positive overlap of the vibrational wavefunctions of the initial and final states in the transition. The Franck-Condon factors are a measure of the degree of this overlap and correspondingly are an indication of the transition intensity. The most probable and intense transition occurs between states with the maximum overlap of vibrational wavefunctions. This is shown in Figure 1.1. The larger the difference in vibrational quantum number (v) in the initial and final states, the more likely the shape and the momentum are to be different which means a transition is less likely to occur.

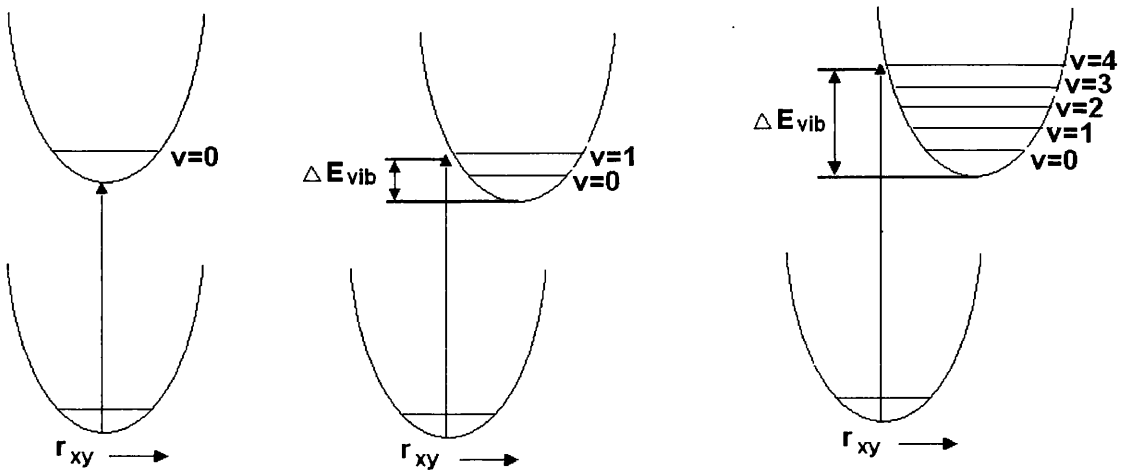

Figure 1.1: A mechanical analogue to the Franck-Condon principle for radiative transitions. [4]

1.4 Photoexcitation and classification of the excited state

When a species absorbs a quantum of UV or visible radiation, an electron is promoted from a low-energy ground-state orbital to a higher energy excited-state orbital. [4,12] Excited state species can exhibit a dramatically altered behaviour from the ground state. This is due to both the increased energy and the new electronic arrangement. This allows the excited state to participate in reactions which are not possible in the ground state.[4]

This excited state then relaxes back down to the ground state. This involves the loss of energy by either non-radiative or radiative processes. Radiative decay mechanisms include (i) fluorescence and (ii) phosphorescence. The principal non-radiative decay mechanisms are (i) internal conversion (IC) and (ii) intersystem crossing (ISC). A Jablonski diagram which represents these processes is shown in Figure 1.2.

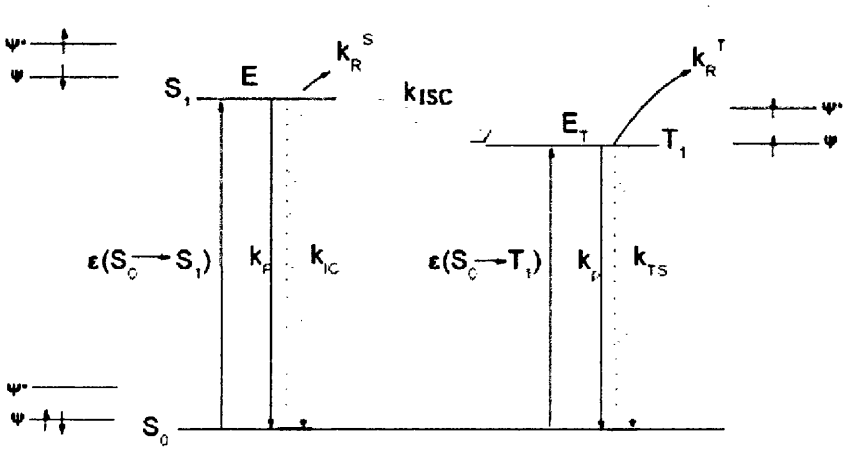

Figure 1.2: Jablonski Diagram[4]. S_0 = Singlet ground state, S_1 = First singlet excited state, k_f = fluorescence rate constant. k_{IC} = intersystem conversion rate constant from the singlet state. k_p = phosphorescence rate constant. k_{isc} = intersystem crossing rate constant. k_{TS} = intersystem crossing from the triplet state. k_{RT} = rate constant for a triplet reaction.

1.4.1 Fluorescence

The term 'fluorescence' was first introduced by Stokes in his famous paper 'On the refrangibility of light' in 1852.[17] Fluorescence is a spin allowed emission.

Fluorescence is characterised by the rate constant k_f. It is relatively short lived with k_f being equal to *ca.* $10^9 \rightarrow 10^6$ s^{-1}. The observed rate constant for the deactivation of the excited singlet state (k_{obs}) is generally a lot higher, typically in the range $10^{11} \rightarrow 10^8$ s^{-1}; this is due to other deactivation processes such as IC (internal conversion) and ISC (intersystem crossing) which occur in competition with fluorescence.

1.4.2 Phosphorescence

Phosphorescence is a forbidden transition between states of differing multiplicity *e.g.* $T_1 \rightarrow S_0$ emission. τ_p typically lies in the range of *ca.* $10^{-1} \rightarrow 10^{-5}$ s^{-1}. As a result phosphorescent materials generally emit light with a low efficiency in comparison to fluorescent materials. In order to generate an emissive triplet state it is necessary that the rate of ISC is significant. In solution at room temperature, non-radiative de-excitation from the triplet state T_1 is predominant over phosphorescence. Due to the spin-forbidden nature of phosphorescence the radiative rate constant is very low. During such a slow process, numerous collisions with solvent molecules favour intersystem crossing and vibrational relaxation in S_0. Phosphorescence is more often observed at low temperatures and in rigid systems where these collisions are inhibited. The lifetime of the triplet state under these circumstances may be very high. The phosphorescence emission spectrum is at longer wavelengths than fluorescence because the lowest vibrational level of the triplet state T_1 is lower than that of S_1. [3-5, 14-15]

1.4.3 Internal conversion (IC)

Internal conversion is a non-radiative transition between vibronic levels in states of the same multiplicity. In solution this process is followed by a vibrational relaxation

towards the lowest vibrational level of the final electronic state. Internal conversion occurs on a time scale of 10^{-13}-10^{-11} s.

1.4.4 Intersystem crossing (ISC)

Intersystem crossing is a non-radiative transition between two isoenergetic vibrational levels belonging to electronic states of different multiplicities. Crossings between states of different multiplicity are a spin-forbidden process, but can occur if the spin-orbit coupling is large enough to let it happen. The probability of ISC depends on the singlet and triplet states involved. If the transition $S_0 \rightarrow S_1$ is for example, $n \rightarrow \pi^*$, intersystem crossing is very efficient. The presence of heavy atoms also increases the spin-orbit coupling which will favour intersystem crossing.

1.4.5 Competition between radiative and non-radiative transitions

The rates of non-radiative and radiative transitions depend on the size of the energy gap between the initial and final state and the overlap between the vibrational wavefunctions within those states. The excited singlet state can deactivate via IC to the S_0 ground state or via intersystem crossing to a T_n state. For the quantum yield of fluorescence to be high both internal conversion and intersystem crossing must be suppressed. Internal conversion can be controlled with the correct choice of ligand which will suppress the vibrations which promote it. The rate of intersystem crossing depends on the energy gap between the triplet and singlet states involved as well as the electronic configuration of these states. The two mechanisms by which ISC can occur are (i) direct spin-orbit coupling of the S_1 to the upper vibrational levels of T_1 or (ii) via spin-orbit coupling of S_1 to a higher triplet state, this would then be followed by internal conversion through the triplet manifold. In order to prevent ISC a large

singlet-triplet energy gap is required which will then prevent deactivation of the excited singlet state by ISC.

1.5 Further pathways of deactivation of the excited state

As described, once formed the excited state molecule then loses the excess energy via a combination of radiative and non-radiative pathways and either returns to the ground state or reacts. There are several ways in which this can occur which include luminescence, such as phosphorescence and fluorescence which have been previously described, intermolecular and intramolecular energy transfer, and quenching. The possible routes for deactivation are summarised in Figure 1.3. [4]

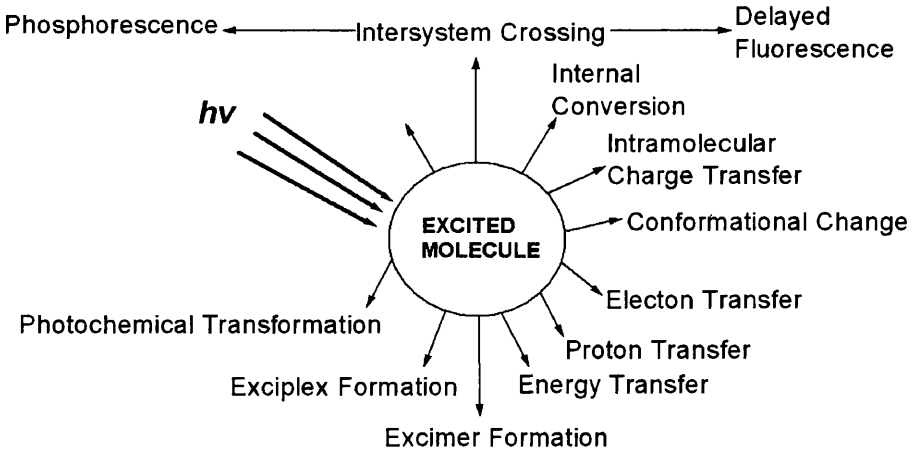

Figure 1.3: Possible deactivation pathways of an excited molecule.[3]

1.5.1 Energy transfer

A substance which accelerates the decay of an electronically excited state to the ground state is known as a quencher. Quenching can be observed as a reduction in the

quantum yield of emission. There are many different quenching processes, some of which are shown in Figure 1.4 below. [3]

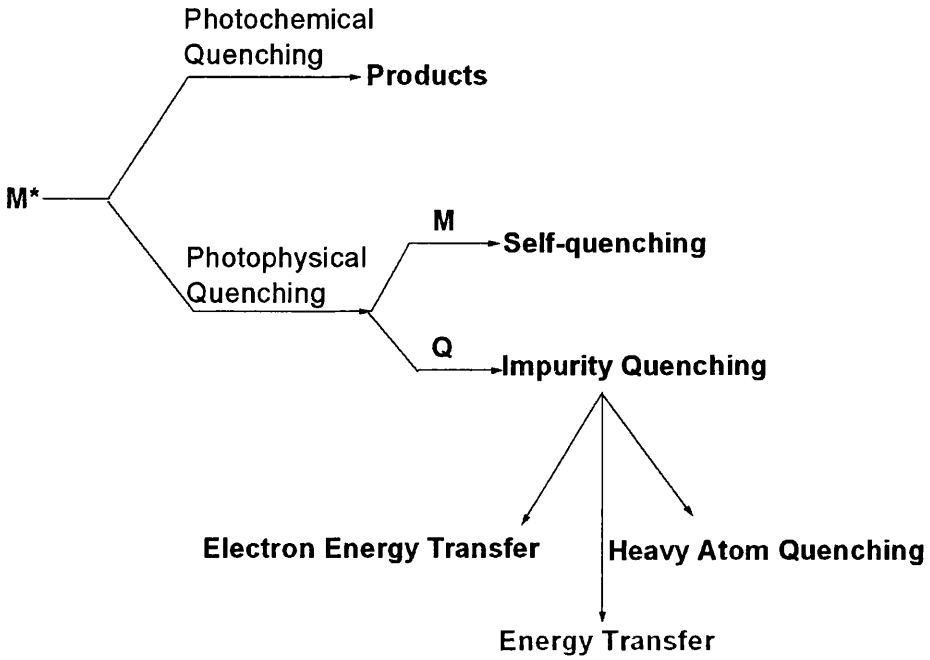

Figure 1.4: Quenching processes.[3]

In Chapters 5 and 6 the energy transfer between a polyfluorene and defect unit and polyfluorene and polythiophene unit in a block co-polymer will be presented. Therefore in this section of the introduction, the concept of energy transfer will be addressed.

Hetero-energy transfer from an excited molecule (donor) to another that is chemically different (acceptor) can be described according to:

$$D^* + A \rightarrow D + A^* \qquad \textbf{(eq. 1.3)}$$

Whereas homo-transfer occurs when the donor and acceptor are the same species:

$$D^* + D \rightarrow D + D^* \qquad \textbf{(eq.1.4)}$$

When the process of energy transfer can repeat itself so that the excitation migrates over several molecules, as in the polymers described in Chapter 5 and 6, this is referred to as energy migration or excitation transport. [2-3]

1.5.2 Radiative and non-radiative energy transfer

Radiative transfer depends on the 'capture' of photons emitted by a donor. This is observed when the average distance between D and A (or D) is larger than the wavelength.

$$D^* \rightarrow D + h\nu \qquad \textbf{(eq. 1.5)}$$

$$h\nu + A \rightarrow A^* \text{ or } h\nu + D \rightarrow D^* \qquad \textbf{(eq.1.6)}$$

Radiative transfer does not require an interaction between the acceptor and the donor but does require spectral overlap. It is also dependent on the acceptor concentration and the sample configuration with respect to excitation and observation. Radiative energy transfer occurs over a scale from large molecular to fully macroscopic. This process can also be referred to as trivial energy transfer. In the region of spectral overlap there is a decrease in donor fluorescence intensity. This results in a distortion of the fluorescence spectrum, which is also sometimes referred to as the inner filter effect. [2-5, 12-15]

Non-radiative energy transfer has a large significance in many applications ranging from photosynthesis to OLED technology. In order for the excitation energy to be transferred some interaction between the donor and acceptor molecule is required. This allows some of the vibro-electronic transitions in the donor to have practically

the same energy as transitions in the acceptor. Such transitions are then considered to be coupled (or are in resonance with one another). [2]

1.5.3 Förster energy transfer

Förster's interest in the energy transfer process was initially inspired by the efficiency of the photosynthetic process.[18-21] He published his first work on energy transfer in Naturwissenschaften in 1946,[19] which was a extension of the work firstly completed by Perrin who in his work outlined the transfer of energy between two molecules non-radiatively. In the 1946 paper Förster described the quantum mechanical behaviour of electronic excitation energy between two molecules in the solution phase.[18-21] From this paper the term FRET was introduced, which is now a thoroughly used acronym for Förster Resonance Energy Transfer. In some papers it is said to denote fluorescence resonance energy transfer, but according to Valeur this expression is incorrect because it is not the fluorescence which is transferred but rather the electronic energy of the donor.[3] Förster successfully developed a set of equations, which can, via the use of experimental results, predict whether energy transfer occurs in a system.[18-21]

FRET involves the interaction between the electric fields of the transition dipole of the donor and the acceptor. The first step of FRET is the absorption of a quantum of energy by the donor molecules. Once the excited molecule exists in thermal equilibrium with the surrounding medium it will then return to the ground state via spontaneous radiative and non-radiative pathways. There is an interaction between the electric fields of the transition dipole moments of the donor emission and acceptor absorption. This means that most of the emitted fluorescence comes from the acceptor molecule and not from the donor molecule which was originally excited. In order for the transfer to be efficient, it is essential for the acceptor to have a strong absorption, and hence a high extinction coefficient. The emission spectrum of the donor must

overlap with the absorption spectrum of the acceptor. The extent of energy transfer can also be influenced by the effect of molecular collisions on the motion of the donor and acceptor during the period when it is in the excited state. [2-5, 18-21]

According to Förster's theory the rate of energy transfer $\mathbf{k_{et}}$ in units of s^{-1} and the efficiency of transfer **e** are given by Equations 1.7 and 1.8 respectively. [3,21]

$$\mathbf{k_{et}} = 0.8 \times 10^{17}\, r^{-6}\kappa^2 J n^{-4} k_f \qquad \textbf{(eq.1.7)}$$

$$\mathbf{e} = r^{-6}/(r^{-6} + R_0^{-6}) \qquad \textbf{(eq.1.8)}$$

$$\text{where } R_0 = 0.97 \times 10^3\, (J\kappa^2\Phi_0 n^{-4})^{1/6} \qquad \textbf{(eq.1.9)}$$

in which:

r is the distance between the centres of the donor and acceptor

κ^2 is the orientation factor for dipole-dipole interactions

n is the refractive index of the medium between the donor and the acceptor

k_f is the rate constant for fluorescence emission by the donor

Φ_0 is the quantum yield of fluorescence of the donor in the absence of the acceptor

J = spectral overlap between the donor and the acceptor.

FRET can be used as a 'spectroscopic ruler' in the ranger of 10-100 Å from the variations in transfer efficiency. R_0 is the distance at which a half of the energy is transferred to the acceptor. A typical donor-acceptor pair will have values of R_0 ranging from 10-70 Å. As seen from Equation 1.3 above, R_0 is affected by the donor quantum yield since the energy cannot be transferred if it is lost too quickly via non-radiative decay routes, the refractive index, the orientation factor and the spectral overlap between the donor and the acceptor. Figure 1.5 shows an energy level scheme

which illustrates the coupling of isoenergetic donor and acceptor transitions which is necessary for FRET to occur. [2-5, 18-21]

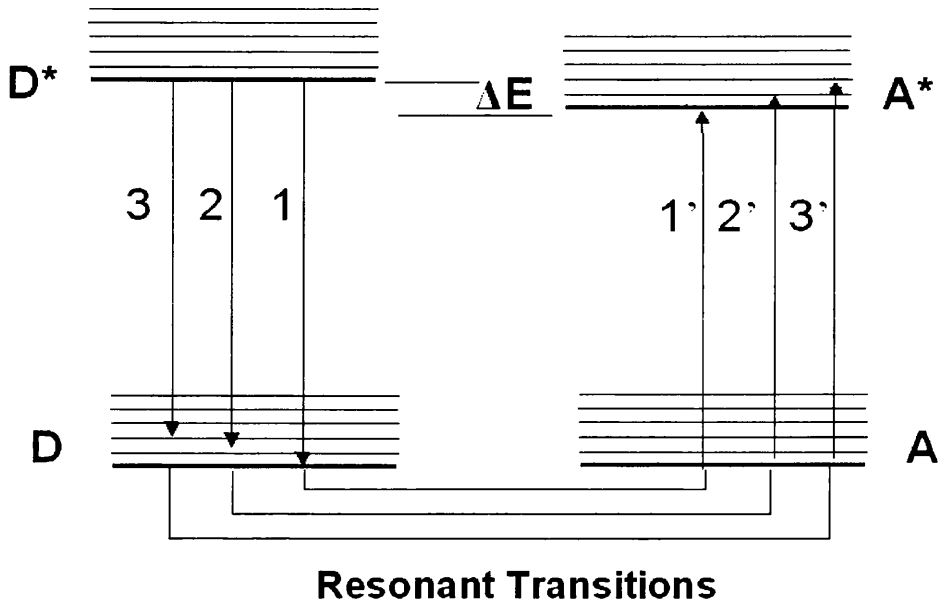

Figure 1.5: Energy level scheme of donor and acceptor molecules showing the coupled transitions in the case where vibrational relaxation is faster than the energy transfer, *i.e.* very weak coupling.[2]

1.5.4 Dexter energy transfer

The Dexter theory of energy transfer, sometimes referred to as the exchange mechanism, involves some sort of intermolecular orbital overlap which can include electron exchange. [12-13, 22]

Dexter energy transfer occurs over much shorter ranges than FRET (~10 Å). Important features of Dexter transfer are that the spin selection rules are always obeyed and because the energy rate does not depend on the transition moments, triplet- triplet energy transfer as well as singlet-singlet transfer is possible. [12-13, 22]

$$^1D^* + {}^1A \rightarrow {}^1D + {}^1A^*$$

$$^3D^* + {}^1A \rightarrow {}^1D + {}^3A^*$$

The rate constant for Dexter energy transfer can be given by Equation 1.4. [12]

$$k_{DA} = K' J \exp(-2R_{DA}/L) \qquad (1.4)$$

Where:

L = the average Bohr radius

K' = the rate constant which is related to the specific orbital interactions. However, it is not derived from any spectroscopic data, which makes it difficult to characterise Dexter energy transfer experimentally.

J = the spectral overlap integral

R_{DA} = the donor and acceptor separation relative to their van der Waals radii.

1.6 Electroluminescent polymers

1.6.1 Polymer-based organic light-emitting diodes

Organic molecules, especially conjugated polymers, have been known to be electroluminescent since the 1960s.[23-27] Polyacetylene was focused on initially; it is however, not easily processable. Burroughs and co-workers in 1990 reported the first example in the literature of a polymer-based light-emitting diode. From this point more complex polymers were soon developed, with focus towards the development of π-conjugated polymers with non-degenerate ground states. These included

polythiophene (PT), polyaniline (PANI) , polypyrrole (PPy) and poly(*p*-phenylene) (PPP). The significance of these classes of polymer was recognised in 2002 by the Nobel Prize in chemistry being awarded to H. Shirakawa, A. G. MacDiarmid, and A. J. Heeger who are considered to be the pioneers in this type of materials research. These materials which have been most specifically studied for application in OLED technology can also be used effectively as polymer lasers, photodiodes, sensors, and solar cells.

This has led to the discovery of a large series of conjugated polymers which include polyfluorenes, which are excellent for blue LED applications and are now becoming a core building block in a range of new device technologies. This will be discussed further in the introduction to Chapter 5.

1.7 Transition metal photochemistry

Over the past 50 years transition metal compounds have attracted much interest from numerous researchers due to their unique photochemical properties which can be finely tuned for utilisation in several fields such as; solar energy conversion, [28] electroluminescence,[29-30] chemical sensors [31-32] and OLED technology.[13,33-35]

In organic photochemistry the general features of electronic excitation, as well as resulting photochemical reactions, can be described effectively by three electronic states: the singlet ground state, first singlet excited state, and the corresponding longer-lived first triplet excited state.[13] The photochemistry of transition metal complexes is more varied than organic molecules due to the possibility of different orbital types and spin multiplicities. It is important to understand the electronic

structure of the transition metal complexes and to assign correctly the electronic transitions involved. Normally emission from a transition metal complex will occur from the lowest excited state. The identity of the excited state can be controlled via the judicious selection of ligands. This is particularly important when designing a complex for a specific application.[12-13] Transition metal complexes demonstrate four main types of transitions. These are shown in Figure 1.6, which is a simplified MO scheme of an octahedral complex, with the various types of electronic transitions defined.[36]

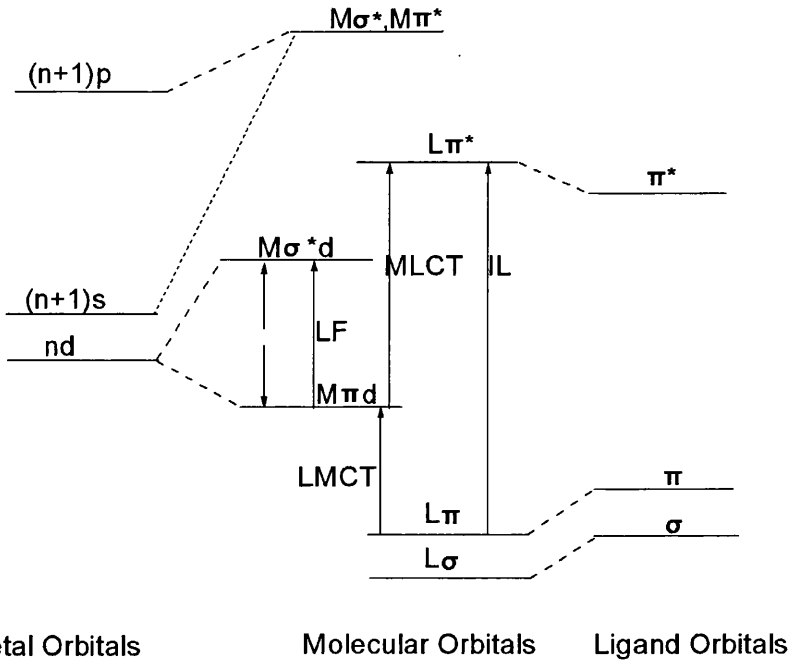

Figure 1.6: MO scheme of an octahedral complex, with the various types of electronic excitation defined. Correlation lines lead to the atomic orbitals which dominate in the respective molecular orbitals.[13,36]

LF = Ligand field transition. This occurs between orbitals with dominant metal (nd) character.

MLCT = Metal to ligand charge transfer. This involves excitation of a metal-centred electron to a π^* antibonding orbital located on the ligand system.

LMCT = Ligand to metal charge transfer. This arises from the transfer of electronic charge from the ligand π-system onto a metal-centred orbital.

IL= Intra-ligand transition. This involves the promotion of an electron from a π-bonding or non-bonding orbital to a higher energy antibonding orbital.

1.7.1 1st row transition metal compounds

Phosphorescence from 1st row transition metal compounds is limited by weak spin-orbit coupling. Emission from glasses at 77 K has been noted for Ni(0),[37-38] Mn(II)[39] and Mn(I)[40] complexes. However, phosphorescence at room temperature is not commonly observed. Complexes of Cr(III) have been reported to show phosphorescence with a quantum yields of 10^{-2}. [41] which can be enhanced by the incorporation of rigid ligands which suppress non-radiative decay. Some copper (I) cluster complexes have been shown to be phosphorescent.

1.7.2 2nd and 3rd row transition metal compounds

Interest in the photochemistry of 2nd and 3rd row complexes grew rapidly in the 1970s due to the discovery of compounds such as $[Ru(bpy)_3]^{2+}$,[43] which is luminescent and undergoes both intermolecular excited state energy and electron transfer reactions, with applications ranging from electrochemical luminescence to DNA binding.[43] The interest in 2nd and 3rd row transition metal complexes has been maintained with much attention also being shown towards d^6, d^8 and d^{10} coordination complexes including those of Re(I), [13,44-47] Os(II),[13,48,49] Ir(III),[13, 50-53] and Pt(II).[13, 54-57] All these metals have high spin-orbit coupling constants which effectively promote the triplet radiative

decay making them particularly appropriate for application as phosphorescent dopants to enhance the electroluminescent quantum yield in OLEDs. [13,54] The chemistry of Pd^{2+} and Pt^{2+} will be discussed further in Chapters 3 and 4.[13,54]

1.8 Theoretical and computational chemistry

The term theoretical chemistry can be defined as a mathematical description of chemistry.[58,59] The term computational chemistry however, is often used to describe a mathematical method which applies computer-based models to simulate chemical processes and properties. Computational chemistry is not a new technique, but improved desktop computers have allowed computational methods to become more available to scientists who are not necessarily specialists in computational chemistry.[58-62] While the results from computational chemistry have generally been used to complement the information obtained by chemical experiments, they have also, in some cases, provided a route towards results which would have not been possible practically such as in the design of drugs and materials.[61]According to Jenson "Today, the situation has been reached where, in many cases the computational chemist can substitute the computing machine for the test tube".[60-61] Properties frequently calculated using computational techniques include: structural data (*i.e.* expected positions of constituent atoms), molecular energies, dipoles, vibrational frequencies, and reactivity and spectroscopic properties. Methods employed can cover both static and dynamic situations .[61]

1.8.1 Ab initio

Computational methods can range from being highly accurate to very approximate. Ab initio processes are 'based on theory from first principles' and considered to be one of the most accurate techniques. The term 'ab initio' was first used in a letter

between Parr and Craig, who later introduced it into a research paper regarding the excited states of benzene, published in 1950.[58-61] The methods used in ab initio calculations are based on quantum mechanical calculations (solving the Schrödinger equation). Most ab initio calculations make use of the Born-Oppenheimer approximation, which serves to simplify the Schrödinger equation by freezing the nuclei in place during the calculation. The calculations should converge to the exact solution of the underlying equations, but realistically it's impossible to eliminate all the approximations resulting in some residual error remaining. [58-59]

The major disadvantage of ab initio calculations is the heavy demand made on computer power, as the computer time required for a calculation scales with the 4^{th} power of the size of the basis set. Significant errors can exist in ab initio models comprising many electrons. This for example, complicates the study of molecules interacting with high atom mass units, such as transition metals. A variety of ab initio methods now exist whereby large calculations are possible and the treatment of larger molecules can be modelled computationally by methods such as Density Functional Theory (DFT), Hartree Fock and Quantum Monte Carlo (QMC). In terms of CPU time, memory and disc space DFT is the least expensive method, due to it being based on electron density rather than wave functions. It is commonly thought that DFT calculations show the most promising approach to accurate quantum chemical calculations for large systems. [58-62]

In the early 1970s efficient ab initio computer programmes such as ATMOL, GAUSSIAN, IBOL, and POLYATOM began to be used to speed up ab initio calculations. Of these programmes, only GAUSSIAN has expanded and is now the

most frequently used. The GAUSSIAN programme is based on Gaussian orbitals (sometimes referred to as Gaussian type orbitals, GTOs or Gaussians). These are functions which are used as atomic orbitals in the LCAO (Linear Combination of Atomic Orbitals) model for the computation of electron orbitals in molecules. [58] A further discussion of the particular DFT calculations used for the work presented in this thesis is given in the introduction to Chapters 3 and 4 where DFT calculations are used to model ground and excited states of Pd and Pt diselenolenes.

1.9 Thesis Overview

The work which will be detailed in this thesis describes the photochemical characterisation of novel complexes. Chapter 2 will describe the experimental techniques used in this study. Chapters 3 and 4 describe the synthesis and photochemical characterisation of some novel palladium and platinum diselenolenes which have been identified as a new group of lumophores. Chapter 5 describes the photochemistry of a range of polyfluorene compounds, commonly used as blue emitters in OLED technology. This chapter looks at the possible causes for defect formation in this type of compound. Chapter 5 presents time-correlated single photon counting data on these compounds and looks at possible energy transfer between the polyfluorene sections and the defect. Chapter 6 describes the photochemical characterisation of a polyfluorene-polythiophene block co-polymer in different solvent systems. The possibility of energy transfer from the polyfluorene unit into the polythiophene unit is discussed.

1.10 References

1. International Union of Pure and Applied Chemistry *Photochemistry Compendium of Chemical Technology*. Internet edition, Pac, **1996**, 68, 2223.
2. Coyle, J.D, Hill, R.R, Roberts, D.R, *Light, Chemical Change and Life: a source book in photochemistry*, The Open University Press, Milton Keynes, 1988.
3. Valeur, B, *Molecular Fluorescence: Principles and Applications.*, Wiley-VCH Verlag Weinheim, Germany, 2002.
4. Turro, N. J. *Modern Molecular Photochemistry*, University Science Books, Sausalito, California, 1999.
5. Wayne, C.E, Wayne, R.D, *Photochemistry*, Oxford Science Publications, Oxford, 1996.
6. http://www.chemlin.net/chemistry/photochemistry.htm
7. Drake, N. A.; Haines, W. J.;Knauff, R.E.; Nelson, E. D. *Anal. Chem.* **1956**, *28*, 2036
8. Eckelman, M. J.; Anasta, P. T.; Zimmerman, J. B. *Environ. Sci. Technol.* **2008**, *42*, 8564.
9. Mullen, K.; Scherf, U. *Org. Process. Res. Dev.* **2006**, *10*, 1081.
10. Parkesh, R.; Mohsin, S.; Lee, T. C.; Gunnlaugsoon T, *J. Chem. Mater.* **2007**, *19*,1656.
11. Huang, C.-C.; Chang, H.-T. *Anal. Chem.*, **2006**, *78*, 8332
12. Evans R. C. *Efficient Emitters for Technological Applications*, PhD Thesis, University of Wales Swansea, 2007.
13. Evans, R.C.; Douglas, P.; Winscom, C. *Coord. Chem. Rev.* **2006**, *250,* 2093.
14. Wayne, R. P. *Principles and Applications of Photochemistry*, Oxford University Press, Oxford, 1988.

15. Gilbert, Baggot *Essentials of Molecular Photochemistry.* Blackwell Scientific, Oxford, 1991.

16. Blasse, G.; Grabmeier, B. C., *Luminescent Materials*, 1st Ed, Springer, Berlin, 1999.

17. Stokes, G. C. *Philosophical Transactions of the Royal Society of London,* **1852**, *142*, 463.

18. Förster, T. *Disc. Faraday Soc.* **1959**, *27*, 7.

19. Förster, T. *Naturwissenschaften* **1946**, 6, 166.

20. Braismiche, D.; Frecht, S. J.; Lin, H. G.; Chung, S.; Prasad, P. *J. Am. Chem. Soc.* **2003**, *125*, 1448.

21. Lakowicz. J. R. *Principles of Fluorescence Spectroscopy,* 2nd Ed, Kluwer Academic, New York, 1999.

22. Dexter, D.L. *J. Chem. Phys.* **1953**, *21*, 836.

23. Shirakawa, H.; Louis, E. J.; MacDiarmid, A. G.; Chiang, C. K.; Heeger, A. J. *Chem. Commun.* **1977**, 578.

24. Tang, C.W.; Vanslyke, S. A. *Appl. Phys. Lett.* **1987**, *51*, 913.

25. Burroughs, J. H.; Bradley, D. D. C.; Brown, A. K.; Burn, P. L.; Marks, R. N.; Mackay, K.; Friend, R. H.; Holmes, A. B. *Nature* **1990**, *347*, 539.

26. Arif, M. A. I. *Raman Scattering Studies and Charge Transport in Polyfluorenes,* PhD Thesis, University of Missouri-Columbia, 2007.

27. Nazeruddin, K.; Humphry-Baker, R.; Berner, D.; Rivier, S.; Zuppiroli, L.; Grätzel, M. *J. Am. Chem. Soc.* **2003**, *125*, 8790.

28. Grätzel, M. *Nature* **2001**, *414*, 338.

29. Zu, Y.; Bard, A. J. *Anal. Chem.* **2001**, *73*, 3960.

30. Lee, J. K.; Yoo, D.; Rubner, M. F. *Chem. Mater.* **1997**, *9*, 1710.

31. Amoa, Y.; Ishikawa, Y.; Ikura, I. *Anal. Chim. Acta* **2001**, *445*, 177

32. Zakeeruddin, S. M.; Fraser, D. M.; Nazeruddin, M. K.; Grätzel, M. *J. Electroanal. Chem.* **1993**, *337*, 2536.

33. Adachi, C.; Baldo, M.; Forrest, S. R.; Thompson, M. E. *Appl. Phys. Lett.* **2000**, *77*, 6904.

34. Gao, F. G.: Bard, A. *J. Chem. Mater.* **2002**, *14*, 3465.

35. Handy, E. S.; Pal, A. J.; Rubner, M. F. *J. Am. Chem. Soc.* **1999**, *121*, 3525.

36. Elschenbroich, C.; Salzer, A. *Organometallics*, VCH, Weinheim, 1992.

37. Frem, R. C. G.; Massabrini, A. C.; Massabrini, A. M. G.; Mauro, A. E. *Inorg. Chim. Acta* **1997**, *255*, 53.

38. Kunkely, H.; Vogler, A. *J. Organomet. Chem.* **2003**, *684*,113.

39. Rossenaar, B. D.; Lindsay, E.; Stufkens, D. J.; Vleek, J. A. *Inorg. Chim. Acta* **1996**, *250*, 5.

40. Carlos, R. M.; Neumann, M. G. *J. Photochem. Photobiol. A* **2000**, *131*,17

41. Forster, L. S. *Chem. Rev.* **1990**, *41*, 331.

42. Yam, V. W.-W.; Lo, K. K.-W. *Chem. Soc. Rev.* **1999**, *28*, 323.

43. Juris, A. ; Balzani, V. ; Barigelletti, F.; Campagna, S.; Belser, P.; von Zelewsky, A. *Coord. Chem. Rev.* **1988**, *84*, 85.

44. Kunkley, H.; Vogler, A. *Inorg. Chem. Commun.* **1999**, *2*, 533.

45. Kunkley, H.; Vogler, A. *Inorg. Chem. Commun.* **1998**, *1*, 398.

46. Wrighton, M. S.; Morse, D. L. *J. Am. Chem. Soc.* **1974**, *96*, 998.

47. Striplin, D. R.; Crosby, G. A. *Coord. Chem. Rev.* **2001**,*163*,163.

48. Carlson, B.; Phelan, G. D.; Karninsky, W.; Dalton, X. Z.; Jiang, S.; Jen, A. X. Y. *J. Am. Chem. Soc.* **2002**, *124*, 14162.

49. Wu, P. C. ; Yu, J. K. ; Song, Y.-H. ; Chi, Y. ; Chou, P. T. ; Lu, T. H. *Chem. Commun.* 2003, 3046.

50. Adachi, C. ; Kwong, R. C. ; Djurivuch, P.; Adamovich, V.; Baldo, M. A.; Thompson, M. E.; Forrest, S. R. *Appl. Phys. Lett.* **2001**, *79*, 2082.

51. Finkenzeller, W. J, Yersin, H. *Chem. Phys. Lett.* **2004**, *397*, 289.

52. Schaffner-Hamann, C.; von Zelewsky, A.; Barbieri, A.; Barigelletti, F.; Muller, G.; Riehl, J. P.; Neels, A. *J. Am. Chem. Soc.* **2004**, *126*, 9339.

53. Neve, F.; Crispini, A.; Campagna, S.; Serroni, S. *Inorg. Chem.* **1999**, *38*, 2250.

54. Williams, J. A. G. *Coord. Chem. Rev.* **2008**, 252, 2596.

55. Yam, V. W. W. W. *Acc. Chem. Res.* **2002**, *35*, 555.

56. Zipp, A. P. *Coord. Chem. Rev.* **1998**, *84*, 47.

57. Bevillacqua, J. M.; Eisenberg, R. *Inorg. Chem.* **1994**, *33*, 2913.

58. http://en.wikipedia.org/wiki/Computational_chemistry

59. Smith, S. J.; Sutcliffe, B. T. *Rev. Comp. Chem.* **1997**, *70*, 271.

60. Jenson, F. *Introduction to Computational Chemistry*, John Wiley and Sons, Chichester, 1998.

61. Lewars, E. *Computational Chemistry. Introduction to the Theory and Applications of Molecular and Quantum Mechanics*, Kluwer Academic Publishers, USA, 1998.

Chapter 2:

Experimental

2.1 Introduction

General experimental/instrumental techniques are reported in this section. Where necessary a more detailed description of the materials and specific experimental conditions used are given at the beginning of each chapter.

2.2 Chemicals

Details of all general solvents and standards used and their origin are provided in Table 2.1.

Chemical	Supplier	Relevant chapter
Acetonitrile	Fisher/ Reidel-de Haen	3
Diethylether	Fisher or BDH	3,4
Ethanol	Fischer or Jose Manuel Gomes Dos Santos LDA	3,4
Methylcyclohexane (MCH)	Fisher	3,4
Tetrahydrofuran (THF)	Fisher	5,6
Toluene	Fisher	3,4
Tetraphenylporphyrin (TPP)	Sigma-Aldrich	3,4
Acetone	Fisher	6
Chloroform	Fisher	6
9-H-Fluoren-9-one	Gift from J. Pina University of Coimbra	3,4
Alpha-4	Standard used for quantum yield calculations. Gift from Hugh Burrows University of Coimbra	6
Rhodamine-6G	Sigma Aldrich	6

Table 2.1: Details of general solvents and standards used in this thesis and their origin.

2.3 Chemical synthesis

2.3.1 Schlenk techniques

Reactions requiring an inert atmosphere, *i.e.* the synthesis of both the palladium and platinum diselenolenes as described in the literature,[1-2] and the drying of toluene following standard procedures, involved using a Schlenk line. This is a glass manifold containing two-way taps which allow manipulation of vacuum and inert gases within reaction vessels, as shown below in Figure 2.1.[3]

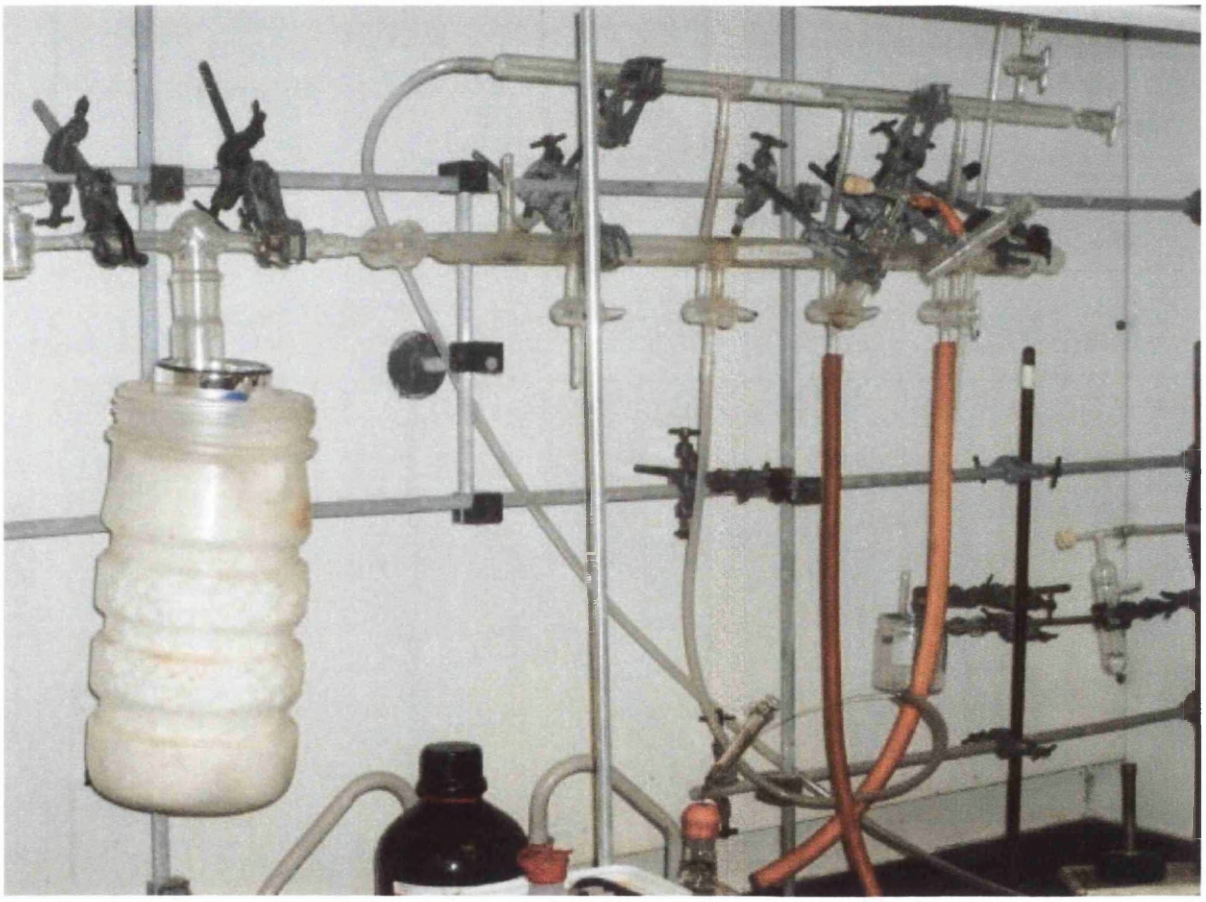

Figure 2.1: Photograph of the Schlenk line used for inert atmosphere experiments.[3]

2.4 Physical characterisation techniques

2.4.1 Mass spectrometry

Mass spectrometry was used to confirm that the structures of products obtained from the synthesis of the palladium diselenolenes described in this work were consistent with the data available in the literature. Spectra were recorded at the EPSRC Mass Spectrometry Centre at Swansea University using electrospray ionisation (ES).

2.4.2 Infrared spectroscopy

Infrared spectra were recorded on a PC-controlled Perkin Elmer "Spectrum-one" FT-IR spectrophotometer fitted with a universal ATR (attenuated total reflection) sampling attachment.

2.4.3 UV-vis absorption spectroscopy

UV-visible spectra recorded at Swansea University were obtained using either a Unicam UV300 spectrometer or a Hewlett Packard HP 8452A single beam diode array spectrophotometer. UV-visible spectra recorded at the Chemistry Department, University of Coimbra, Portugal were obtained using a Shimadzu 2100 spectrometer. All absorption spectra were measured against the appropriate background reference and were recorded in 1 cm path length quartz cells unless stated otherwise.

The molar extinction coefficients were obtained from absorption measurements in quartz absorption cells with path lengths ranging from 1 mm to 10 cm. Experimental oscillator strengths, f_{exp}, were calculated from: $f_{exp} \equiv 4.3 \times 10^{-9} \int \varepsilon d\upsilon$, where $\int \varepsilon d\upsilon$ is the area under the curve of molecular extinction coefficient plotted against wavenumber. [4]

2.5 Luminescence studies

2.5.1 Steady state emission and excitation measurements

Room temperature and 77 K emission measurements were carried out using either a Perkin Elmer MPF-44E fluorescence spectrometer or a Horiba-Jobin-Yvon SPEX Fluorolog 3-22 spectrometer. In general, and unless stated otherwise, 2 nm excitation and 5 nm emission slits were used for excitation spectra, and 5 nm excitation and 2 nm emission slits were used for emission spectra.

2.5.2 Perkin Elmer MPF-44E

A diagram of the principal components of the Perkin-Elmer MPF-44E is shown in Figure 2.2. The excitation source is an Oriel 150 W high-pressure xenon arc lamp, which emits a reasonably smooth continuous spectrum from the UV to the visible. A typical emission spectrum from the xenon arc lamp is shown in Figure 2.3. The grating monochromators are used to select a narrow band of wavelengths, from both the light source for excitation of the sample and from the fluorescence emitted by the sample. A fluorescence spectrum is then recorded by using the motor to change the angle of one of the diffraction gratings and thus select different wavelengths. The detector is a R928 Hamamatsu photomultiplier.

Measurements made are generally in the format of photomultiplier response (intensity) *vs.* wavelength. It was possible to use a filter before the emission monochromator on this instrument. In general the filters used were 350 nm, 390 nm or 430 nm. Measurements made using this instrument are uncorrected for instrument response.

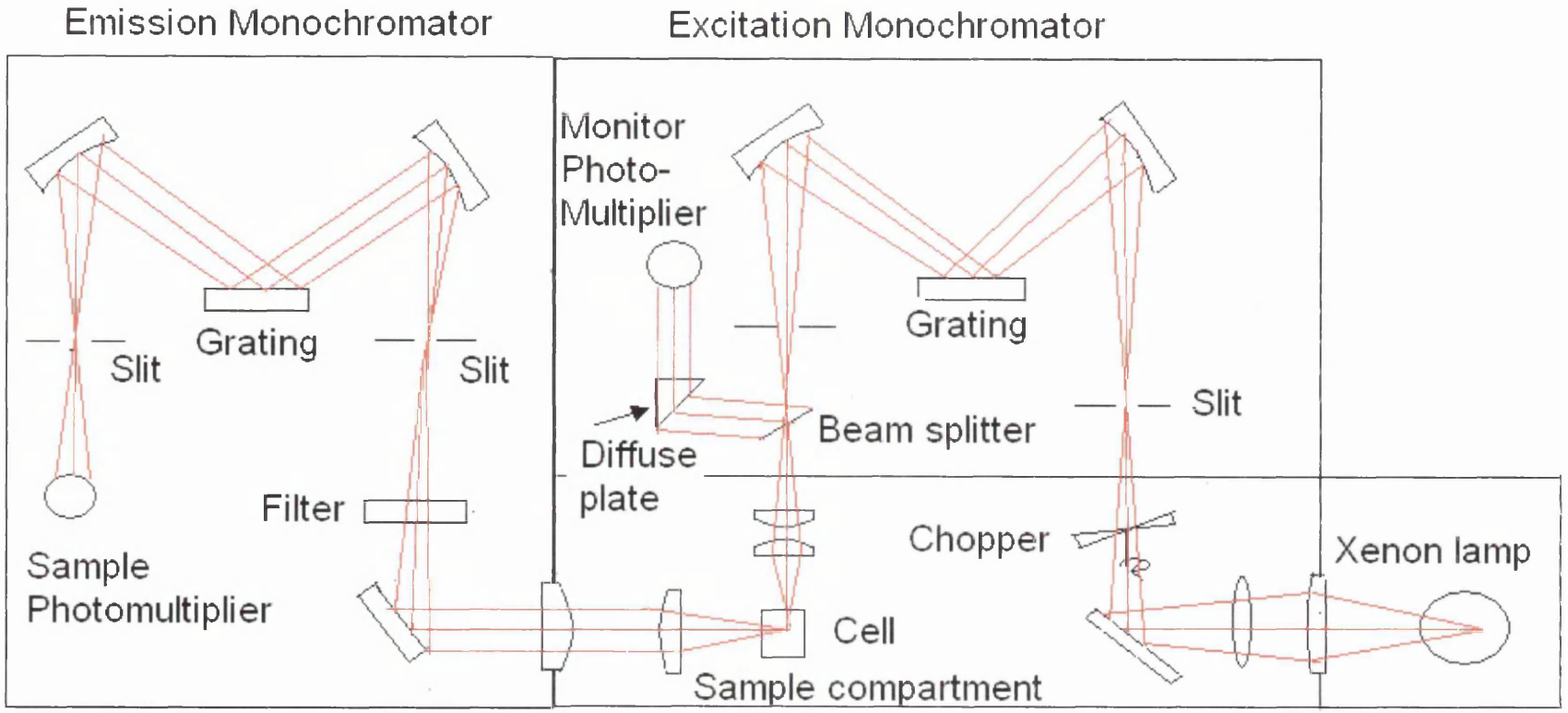

Figure 2.2: A diagram of the principal components of the Perkin-Elmer MPF-44E Fluorimeter [6]

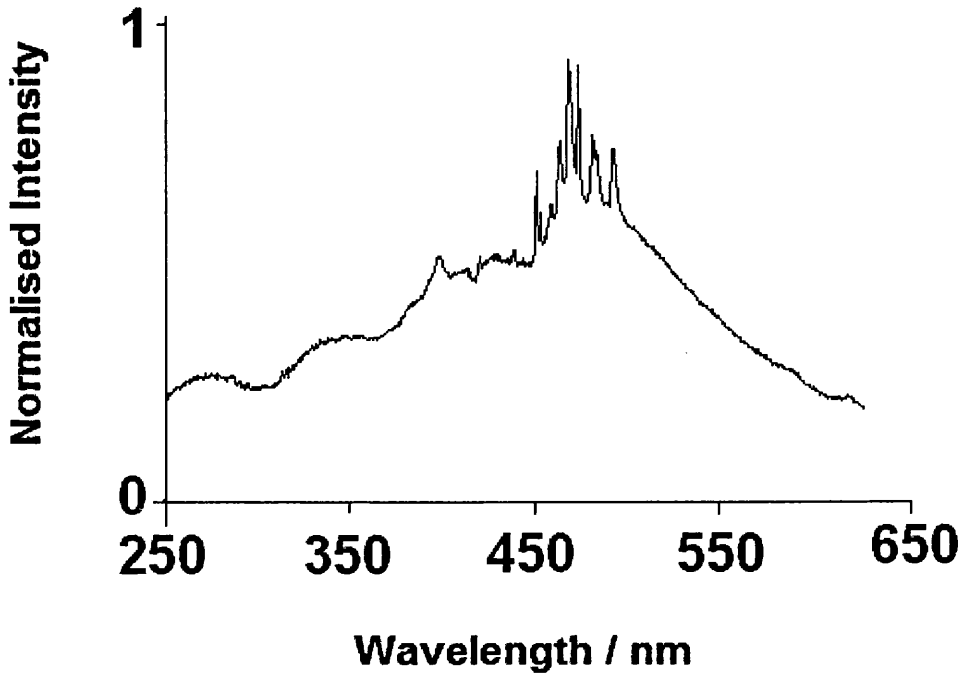

Figure 2.3: The emission spectrum of a 150 W xenon arc lamp.[5]

2.5.3 Horiba-Jobin-Yvon SPEX Fluorolog 3-22 spectrometer

This instrument uses a 450 W xenon arc lamp as an excitation source, and a SPEX monochromator with ruled plane gratings as the excitation wavelength selector. An additional SPEX monochromator is used to select the emitted luminescence from the sample and an R928P photomultiplier tube in photon counting mode is used as the detector. The instrument is self-calibrating and computer controlled. All control of slits, wavelengths, integration times, temperature can be accessed through the software. Fluorescence spectra measured using the SPEX Fluorolog 3-22 were automatically corrected for detector wavelength response using manufacturer's correction files.

The difference between the spectra obtained can be illustrated effectively by considering the Pd diselenolene **1** which is described in Chapter 3 (see Figure 2.4). It is dissolved in an ethanol:diethylether:toluene (1:2:1) glass. The temperature of the sample is 77 K. Emission spectrum (a) which is recorded on the Perkin Elmer MPF-44E is cut off before the spectrum (b) which is recorded on Horiba-Jobin-Ivon SPEX Fluorolog 3-22 spectrometer. This is due to the detector used for recording spectrum (b) being able to go right out until 850 nm.

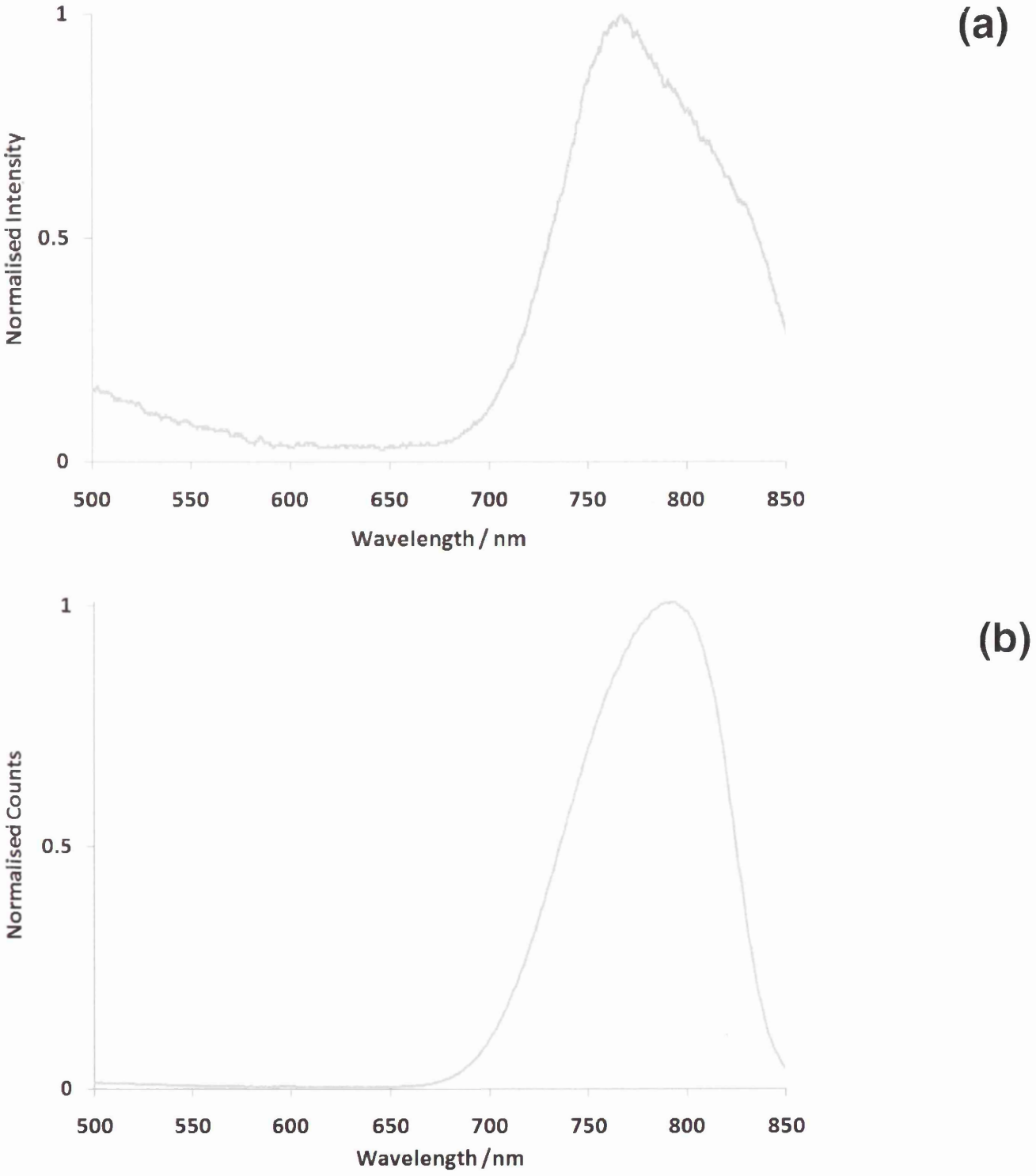

Figure 2.4: Emission spectrum of Pd diselenolene 1 (Chapter 3) in the solid state at 77 K on (a) Perkin Elmer MPF-44E and (b) Horiba-Jobin-Ivon SPEX Fluorolog 3-22 spectrometer. The excitation wavelength in both cases was 355nm.

2.5.4 Room temperature measurements

For room temperature solution measurements a sealed 1 cm × 1 cm quartz fluorescence cell was used. Where necessary, solutions were purged with dry nitrogen for *ca.* 30 mins before the measurements were taken. The absorbance of the solution was measured before and after purging. Low absorbances of *ca.* 0.1 at the excitation wavelengths were used in order to prevent self-absorption by the sample and the inner filter effect.

2.5.5 77 K measurements

For both frozen solution and solid state 77 K measurements the sample was held in an NMR tube, or quartz tube, of *ca.* 5 mm diameter and placed in liquid nitrogen in a phosphorescence dewar (see Figure 2.5). Two frozen organic glasses were used in this work (see chapters 3 and 4): ethanol:diethylether:toluene (1:2:1) (EDT), and methylcylohexane (MCH), as well as frozen toluene which gives a "snow". For all measurements done with the organic glasses it was essential that a glass was formed without any cracks and this was checked before each measurement was taken.

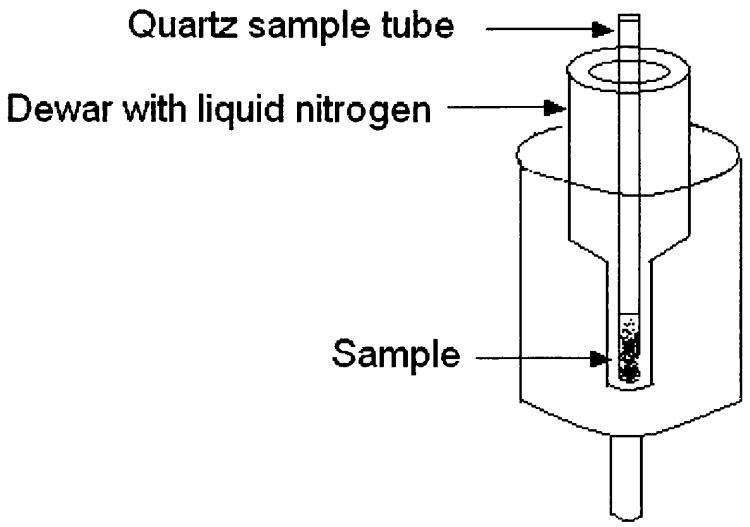

Figure 2.6: Dewar for luminescence measurements at 77 K

2.5.6 Solution phase emission quantum yields

The emission quantum yield, Φ_x, of sample x was calculated by reference to the standard R using Equation 2.1 below. A is the intensity of light absorbed at the excitation wavelength, I is the integrated emission intensity corrected for the instrument response, and n is the refractive index of the solvent.[7]

$$\Phi_x = \Phi_R(A_R/A_x)\,(I_x/I_R)(n_x/n_R)^2 \qquad \textbf{(eq. 2.1)}$$

Samples and reference were excited at the same wavelengths. Whenever possible sample and reference were prepared using the same solvent and if this was not the case the absorption of the sample and the reference were within 0.02 of each other at the excitation wavelength. Solutions were made optically dilute with an absorbance of *ca.* 0.1 in a 1 cm quartz cell. Each measurement was undertaken three times for both

the sample and the reference. The references used are detailed in Table 2.2 below and the absorption and emission spectrum for rhodamine-b and TPP in ethanol are given in Figures 2.6 and 2.7.

Standard	**Solvent**	**$\lambda_{max\ abs}$ /nm**	**$\lambda_{max\ emiss}$ /nm**	**Φ_{fl}**
Rhodamine-B	Ethanol	542	625	0.65[8]
TPP	Ethanol	420	649	0.15[9]
	Toluene	418	649	0.11[9]
Alpha-4	Benzene	392	437	0.18[10]

Table 2.2: Photochemical characteristics of standards used as references for quantum yields.

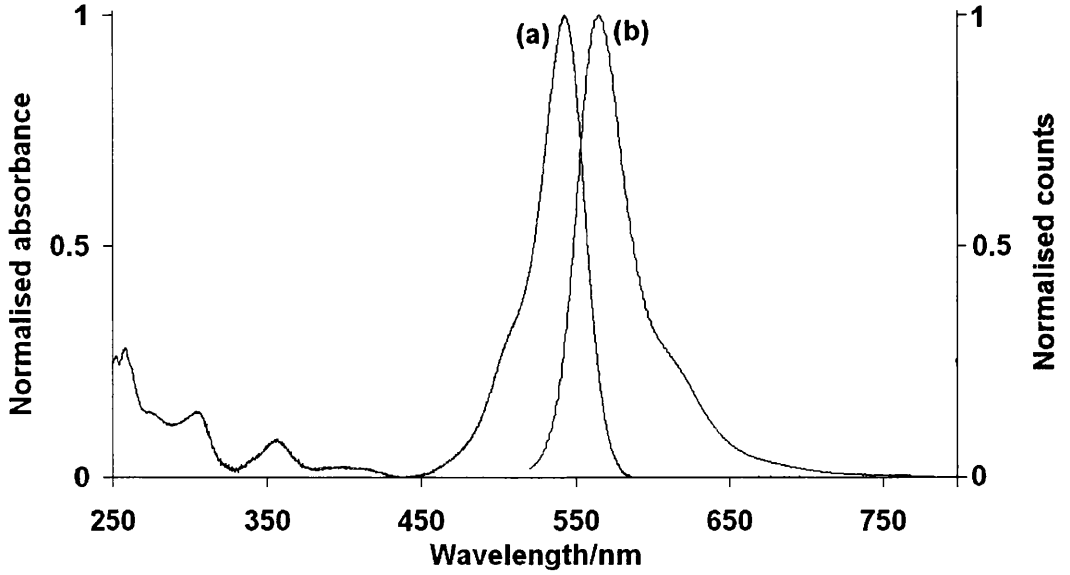

Figure 2.5: Absorption (a) and emission (b) of rhodamine-b in ethanol solution.

Excitation at 540 nm.

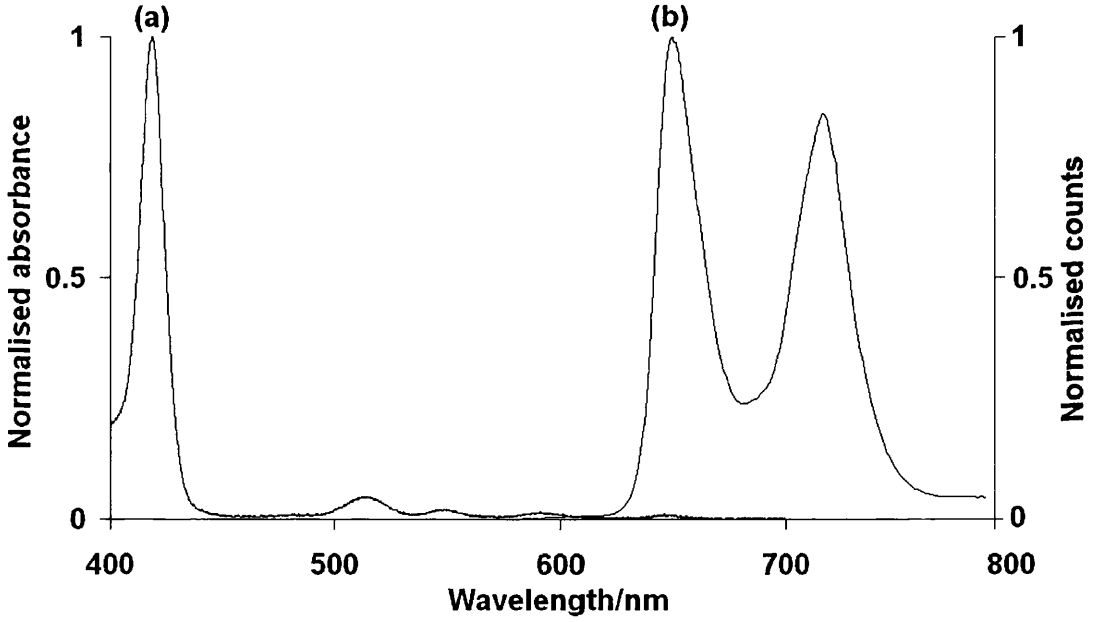

Figure 2.6: Absorption (a) and emission (b) of TPP in ethanol. Excitation at 420 nm.

2.5.7 Quantum yields at 77 K

Quantum yields for emission in 77 K EDT glasses were recorded for the palladium diselenolenes described in Chapter 3. These were measured with the SPEX Fluorolog 3-22 spectrometer using TPP in EDT as emission standard (Φ_{em} = 0.15 in ethanol;[8] Φ_{em} = 0.14 in EDT, at both 77 K and 298 K (this work see chapter 3)). The method of comparison used was as follows. Sample and reference solutions in EDT of comparable absorption were prepared and excitation wavelengths chosen where their absorbances were the same at *ca.* 0.3 in a 1 cm path length cell (these were 496 and 523 nm). The spectra of both the sample solution and the reference were then obtained at 77 K using these excitation wavelengths. The reference solution was then allowed to warm to RT and the emission spectrum recorded again. This gave four emission ratios: two with both sample and reference at 77 K; and two with sample at 77 K and reference at room temperature.

2.6 Time resolved studies

2.6.1 Phosphorescence lifetime measurements

Laser kinetic emission measurements were obtained using an Applied Photophysics laser kinetic spectrometer with either the second harmonic (355 nm) or the third harmonic (532 nm) emission from a Spectron Nd/YAG laser as excitation pulse. The emission monochromator was fitted with a grating blazed at 500 nm with a reciprocal dispersion of 4.65 nm m^{-1} and detection was made with a Hamamatsu R928 photomultiplier tube. Generally, and unless stated otherwise, emission slits of 19 nm were used, and where necessary a cut-off filter was used before the emission monochromator to minimise interference from scattered light and sample fluorescence. Either a 1 kΩ or 5 kΩ load terminator was used before the signal was passed to a LeCroy 9304AM digital storage oscilloscope. For 77 K glasses and 77 K

solids the averaged data from four decay curves were recorded; for RT solids, which gave a weaker signal, averaging was increased to sixteen shots and the laser amplifier used in order to improve the signal-to-noise ratio.

2.6.2 Jandel Table-Curve™

The kinetic data were analysed using Jandel Table-Curve™, and in those cases where a large pulse signal from scatter or adventitious fluorescence was apparent, curve fitting was carried out ignoring that initial distorted portion of the signal, which was typically the first 0.5 μs.

Jandel uses automated statistical methods to process x-y data to be best curve-fit equations. In total there are 58 equations available for fitting. In this thesis the decay equations, which will be used most regularly, will be: [11]

1. Decay (1st order);
2. Simple decay, hyperbolic forms (2nd order);
3. Simultaneous decay 1st, 2nd order (1+2).

2.6.3 Time correlated single photon counting (TCSPC)

TCSPC work on all polyfluorene polymers was all done at the Physics Department at the University of Durham. All picosecond (ps) work was done using the time correlated single photon counting (TSCPC) technique. A schematic of this technique is shown in Figure 2.7. The system uses a ps diode laser and Becker and Hickel electronics. It has an instrument response function (IRF) of *ca.* 90 ps. The ps excitation pulse from a Picoquant diode laser was used at 388 nm (a suitable wavelength for the polyfluorene absorption band). A liquid scatter was used to

measure the FWHM of the instrument response function (IRF). The fluorescence from the sample was detected by a micro-channel plate photomultiplier tube (MCP-PMT, Hamamatsu) after dispersion through the grating monochromator. For all decays the polariser in the emission slide was adjusted to be at 54.7° magic angle with respect to the polarisation axis of the excitation beam. The fluorescence decays were analysed on a pc using lobals software. Solutions with low absorbance (≤ 0.1) at the excitation wavelength were used.

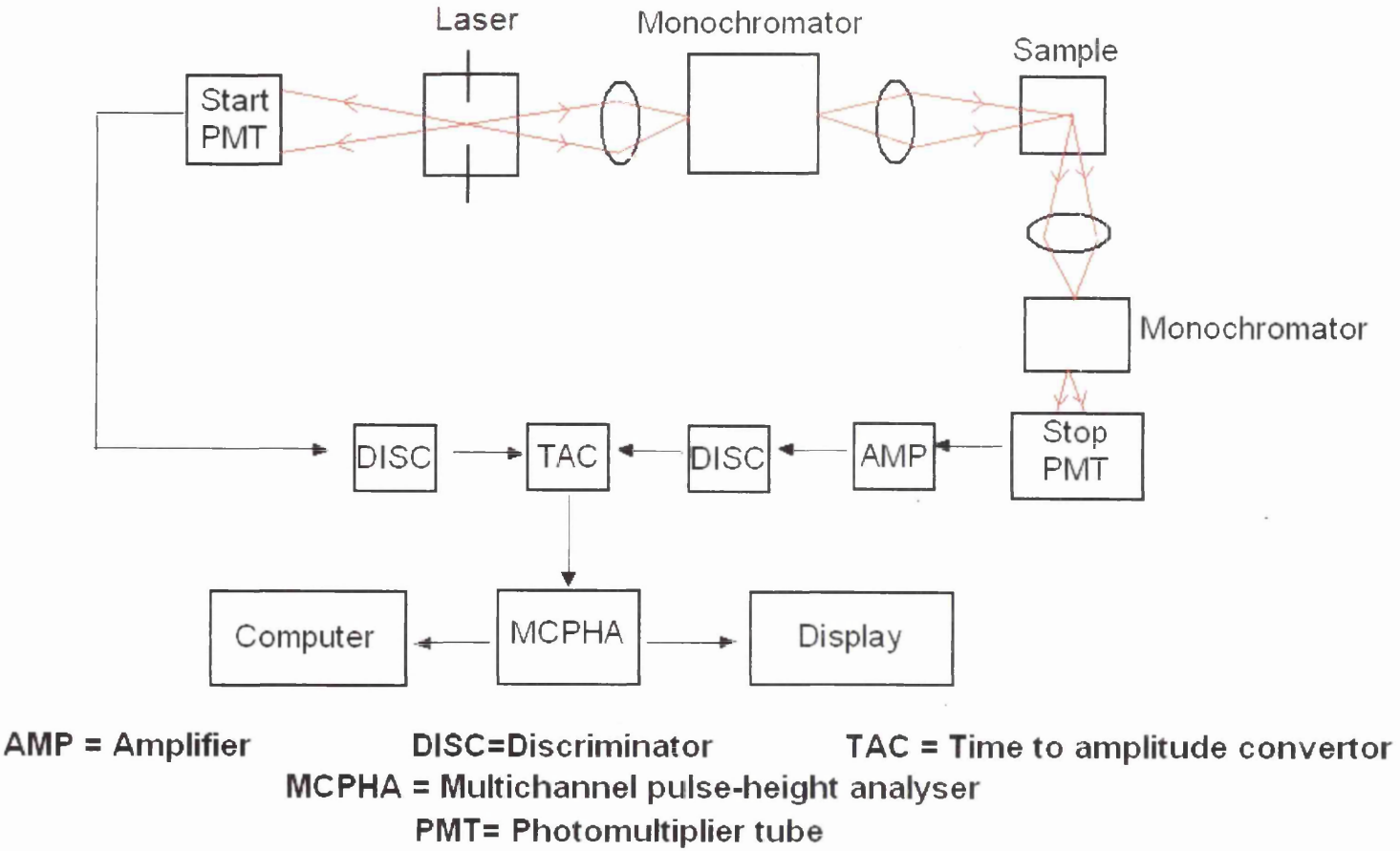

Figure 2.7: Schematic arrangement for TCSPC.[6]

2.6.4 Laser kinetic absorption spectroscopy

Laser kinetic absorption spectroscopy was carried out at the University of Coimbra Portugal.

Transient difference absorption spectra were obtained using an Applied Photophysics laser kinetic spectrometer with the third harmonic, 355 nm, of a Nd/YAG laser (Spectra Physics) as excitation source.

2.6.5 Singlet oxygen measurements

Singlet oxygen measurements were done at the University of Coimbra, Portugal. Measurement of singlet oxygen phosphorescence quantum yield was carried out using the SPEX Fluorolog 3-22 spectrometer with a 600-line diffraction grating monochromator, and a Hamamatsu R5509-42 photomultiplier cooled to 77 K in a liquid nitrogen chamber (Products for Research model PC176TSCE-005) with a Schott RG665 filter to eliminate all the first harmonic contributions from the sample emission in the 500-800 nm region from the infrared signal. 9*H*-Fluoren-9-one in ethanol was used as reference.[12]

2.7 Computational Techniques

2.7.1 DFT Calculations

DFT calculations were done at the University of Swansea with the assistance of Jeremie Pichereau. Compounds were drawn using Gaussview 3.0 and the Gaussian(R) 03W program, version 6.1 revision C-02. The program was run on a windows-NT operating system installed on a desktop having 128 Mb of RAM. The calculations were performed with one processor and the maximum available memory (128 Mb).

Geometry optimizations were carried out at the B3LYP/6-31G(d,p) level, with the LANL2DZ valence functions and effective core potentials for the Pd and Se atoms.

2.7.2 Intermolecular distances and angles

Crystal structure intermolecular distances and angles were measured using Mercury 1.3 (CCDC 2001-2004).

2.8 Error Analysis

Error estimates in this work have been calculated in two different ways.

Method 1

This method applies to the errors quoted on all quantum yield calculations.

Error estimates are quoted as ± one standard deviation (σ). This is the square root of the standard variance of n observations of the sample, which is shown in equation 2 below. $\bar{x}$ is the mean value.

$$\sigma = \sqrt{\sum_{i=1}^{n} \frac{(x_i - \bar{x})^2}{(n-1)}} \qquad \textbf{(eq. 2.2)}$$

When the error is associated with a calculated value (i.e. quantum yield calculations), all the uncertainties associated with the parameters involved in the calculation are taken into account. These can be determined from equation **(3)** for addition/subtraction and equation **(4)** for division/multiplication.

$$y = \sqrt{(a^2 + b^2)} \qquad \textbf{(eq.2.3)}$$

$$y = \sqrt{\left(\frac{a}{A}\right)^2 + \left(\frac{b}{B}\right)^2} \qquad \textbf{(eq.2.4)}$$

where y is the error of the calculated value and a and b are the errors related to the variables A and B respectively.

Method 2

This method applies to all errors associated with lifetime measurements.

When lifetimes have been recorded five values have been taken. The average of these values is the quoted lifetime with the errors calculated from the difference in the measurements. When it was not possible to record five values the error has been estimated from those obtained above. Typically lifetimes are precise to 5%.

2.9 References

1. Webster, C. A. *The Synthesis and Characterisation of Some Novel Compounds Containing Pt-Se Bonds*, PhD Thesis, University of Wales Swansea, 2006.
2. Ford S., *New Palladium Complexes Containing Organoselenium Ligands*, PhD Thesis, University of Wales Swansea, 2000.
3. www.ilpi.com/inorganic/glassware/vacline.html
4. Turro, N. J. *Modern Molecular Photochemistry*, University Science Books, Sausalito, California, 1999, p89.
5. Evans R. C. *Efficient Emitters for Technological Applications*, PhD Thesis, University of Wales Swansea, 2007.
6. Coyle, J. D.; Hill, R. R.; Roberts, D. R. *Light, Chemical Change and Life: a source book in photochemistry*, The Open University Press, Milton Keynes, UK, 1988.
7. Lakowicz. J. R. *Principles of Fluorescence Spectroscopy,* 2nd Ed, Kluwer Academic, New York, 1999.
8. Montalti, M.; Credi, A.; Prodi, L.; Gandolfi, M. T. *Handbook of Photochemistry*, 3rd Ed, CRC Press, New York, 2006, p146.
9. Montalti, M.; Credi, A.; Prodi, L.; Gandolfi, M. T. *Handbook of Photochemistry*, 3rd Ed, CRC Press, New York, 2006, p138.
10. Pina, J.; Burrows, H.D.; Becker, R.S.; Dias, F.B.; Macanita, A.L. *J. Phys. Chem. B* **2006**, *110*, 6495.
11. TableCurve 2D Automated Curve Fitting Software. User's Manual. Windows v2.0 software © Copyright 1994.

12. Martinez, C. G.; Neuner, A.; Marti, C.; Nonell, S.; Braun, A. M.; Oliveros, E.

Helv. Chim. Acta **2003,** *86*, 384.

Chapter 3

Palladium diselenolenes: a new group of near-infrared lumophores

3.1 Aim

The synthesis and structure of compounds $[Pd_2(Se_2C_8H_{12})_2(PBu_3)_2]$ (**1**) and $[Pd_2(Se_2C_8H_{12})_2(PPh_3)_2]$ (**2**) have been previously reported by Morley and Ford.[1] Upon further examination of these compounds by the author they were found to be luminescent, and the experiments described in this chapter deal with the photochemical characterisation of **1** and **2**.

3.2 Introduction

Over the past twenty-five years the optical properties of a number of transition metal compounds have been investigated due to their potential technological applications as visible and near-infrared absorbers and emitters in systems such as organic light-emitting diodes, molecular electronics, and sensors.[1-8] Much effort has concentrated on second and third row transition metals where heavy atom effects enhance both singlet to triplet intersystem crossing and radiative decay from the resulting triplet states.[8-20] For the group 10 elements most reports deal with the remarkable luminescent properties of Pt(II) complexes, and there are relatively few reports dealing with luminescent Ni(II) and Pd(II) complexes.[17-26] It has been suggested that the lack of luminescent Pd(II) complexes is a consequence of the low lying energy levels of the d-d excited states in Pd(II) in comparison to Pt(II).[21-25]

Several types of luminescent sulphur-containing transition metal compounds have been reported.[1,18,19] Eisenberg and co-workers have investigated many Pt(II) complexes possessing either a dithiolate or dithiocarbamate ligand, which show red emission in solution and in the solid state,[4] but related Pd(II) complexes have not

received much attention. Furthermore, studies of complexes of analogous ligands based on the heavier chalcogens with either Pt or Pd are rare, even though organoselenium compounds have a strong affinity towards the heavy transition metals, possibly because until recently there has been a lack of generally applicable preparative methods for such compounds.[1,27]

The reactions of 1,2,3-selenadiazoles with low-valent transition metal complexes have been used to prepare a wide range of selenium-containing compounds.[1] For example the preparation of cyclopentadienylcobalt diselenolenes using this route, shown in Figure 3.1, has been reported by Morley and co-workers.[25]

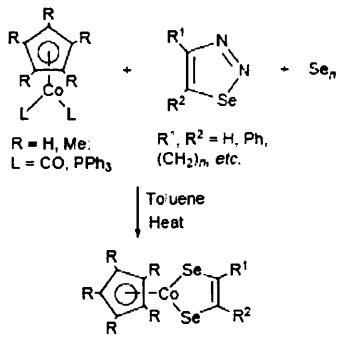

Figure 3.1: The reaction of 1,2,3 selenadiazoles with cyclopentadienylcobalt to give cyclopentadienylcobalt diselenolenes.[25b]

Morley and Ford reported the reaction of bis(cycloalkeno)-1,4-diselenins (which are prepared from 1,2,3-selenadiazoles) with a tributyl- or triphenyl-phosphinepalladium(0) precursor, which resulted in two novel palladium

diselenolenes, namely $[Pd_2(Se_2C_8H_{12})_2(PBu_3)_2]$ **1** and $[Pd_2(Se_2C_8H_{12})_2(PPh_3)_2]$ **2**, shown below in Figure 3.2.[25-27]

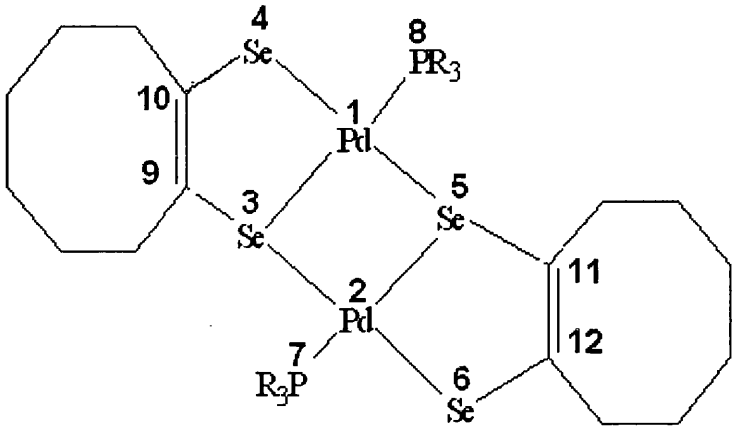

Figure 3.2: Structures of **1** (R = butyl) and **2** (R = phenyl). The atom numbering is that used in the text.

The reaction between cycloalkeno-1,2,3-selenadiazole and bis(triphenylphosphine) palladium(0) (see Figure 3.3) was chosen because bis(triphenylphosphine)palladium(0) is isoelectronic with cyclopentadienylcobalt(I) (shown in Figure 3.1). The resulting complex, **2,** was investigated via a range of analytical techniques such as single crystal X-ray diffraction, multinuclear NMR spectroscopy and mass spectrometry which all confirmed the dinuclear structure of the compound. This was the first example of both a palladium dinuclear dichalcogenolene and a palladium diselenolene.[25-27]

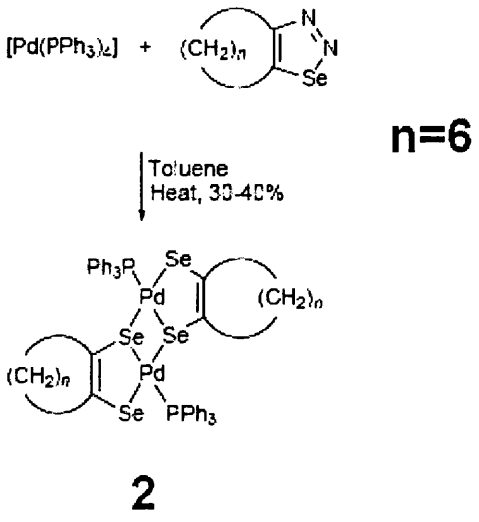

Figure 3.3: Synthetic route for **2**.[25-26]

The X-ray crystal structure obtained for **2** is shown in Figure 3.4.[25-26] Each palladium atom is approximately square planar coordinated with the maximum deviation from the least squares plane passing through the palladium atom and its four nearest neighbours being 0.2 Å. There is a relatively acute angle between the two square planes of 75.6°. This results in the two Pd atoms being relatively close together with a separation of 3.076 Å. This is less than the sum of their van der Waals radii (3.26 Å). This is however, considered to be longer than what would normally constitute a Pd-Pd bond,[25-26] and it was proposed that it arises as a result of geometric constraints and electrostatic interactions imposed by the ligands in the crystal packing. Geometric distortion also occurred due to the bridging ligands which causes a difference in the two Pd-Se lengths (2.485, 2.141 Å) in the Pd_2Se_2 unit, and the Pd-Se-Pd angles in the

bridge are 77.7°, which is less than the 90° which would be expected for a square planar complex.[25]

Analysis by multinuclear NMR spectroscopy, microanalysis and mass spectrometry indicated that the dinuclear structure was also maintained in solution. Even though the reaction mixture contained excess ligand the reaction favoured the dinuclear product over the mononuclear product, which would have contained two molecules of triphenylphosphine per palladium. This was attributed to the slightly lower basicity of PPh_3 in comparison to that of the Se atom.[25]

Prompted by these results, Morley and Ford then investigated the reactions of PBu_3 with bis(cycloalkeno)-1,4-diselenins and Pd(0) complexes, as shown in Figure 3.5 below. This resulted in the formation of a deep purple diselenolene product, **1.** Furthermore it was found that, by addition of either two or four moles of PBu_3 to the reaction mixture, the nature of the product could be controlled to give either a mononuclear or dinuclear complex. Both structures were confirmed by mass spectrometry and multinuclear NMR studies.[25a,b]

(a)

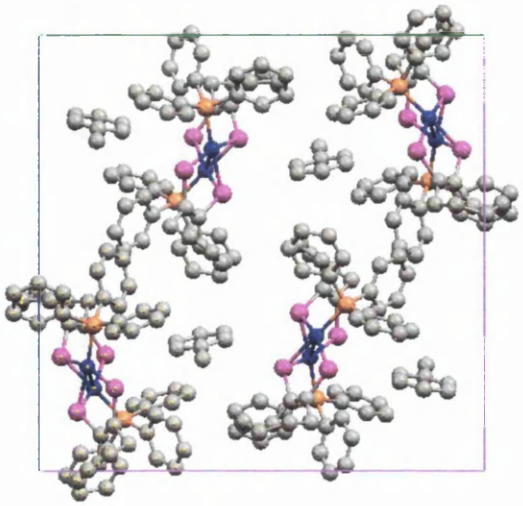

(b)

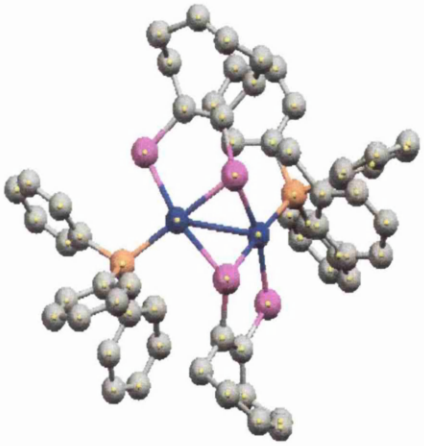

Figure 3.4: X-ray crystal structure of **2:** (a) crystal structure, (b) single molecule structure. Hydrogen atoms are omitted for clarity. Blue atoms = Pd, Pink = Se, Orange = P, Grey = C.[25]

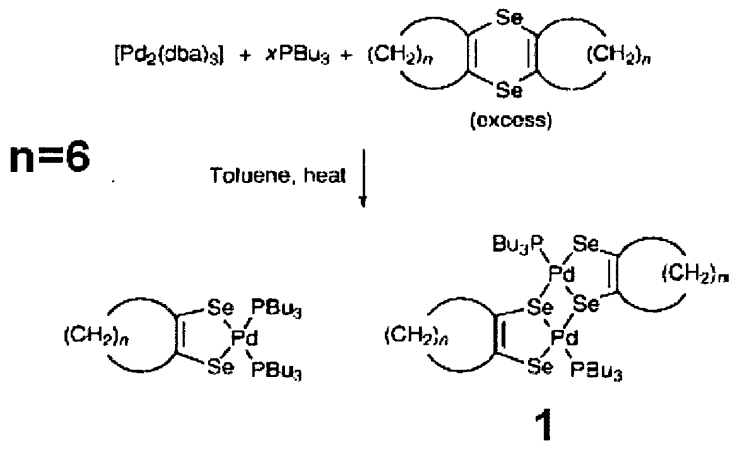

Figure 3.5: Synthetic route for **1**.[25]

The dinuclear species is analogous to **2** and in this case the increased basicity of the PBu_3 in comparison to PPh_3 allows the formation of the mononuclear complex, **3**, also. These were the first examples of diselenolenes which could be isolated in both the mononuclear and dinuclear forms. Although sulphur dinuclear complexes are well known,[25-26] mononuclear palladium diselenolenes and even dithiolenes containing ancillary ligands such as phosphines are not, even though their platinum analogues are well established in the literature.[25-26]

The structure of the mononuclear complex, **3**, has been determined by X-ray crystallography.[25] Unfortunately, a crystal suitable for structure determination of the dinuclear complex **1** could not be obtained, even after a number of attempts to do so by recrystallization.

It is possible to synthesise compounds **1** and **2** with C_6 and C_7 rings as well as the C_8 system shown above. The reaction was found to be most favourable for the C_8 system, possibly because in this case the formation of the cycloalkyne by-product is easier. However, for C_6 the ring strain in cyclohexyne is significant, which results in the reaction being less favourable.

Further examination of these compounds by the author showed them to be luminescent, and this chapter will focus on the photochemical characteristics of these compounds, which are, to the best of our knowledge, the first examples of luminescent Pd(II) selenium compounds in the literature.

3.3 Experimental

Compounds **1** and **2** were prepared as previously described,[26,27] and their structures confirmed by NMR spectroscopy and mass spectrometry. Compound **1** is a purple solid and gives red solutions; **2** is a dark green solid and gives green solutions. Mass spectrometry using ES (for compound **1**) or MALDI (for compound **2**) techniques was used to confirm the identity of both **1** and **2.** The mass spectra of both **1** and **2** are shown below, Figures 3.6 and 3.7. These are the same as the mass spectra for these compounds obtained by Morley and Ford.[25-27]

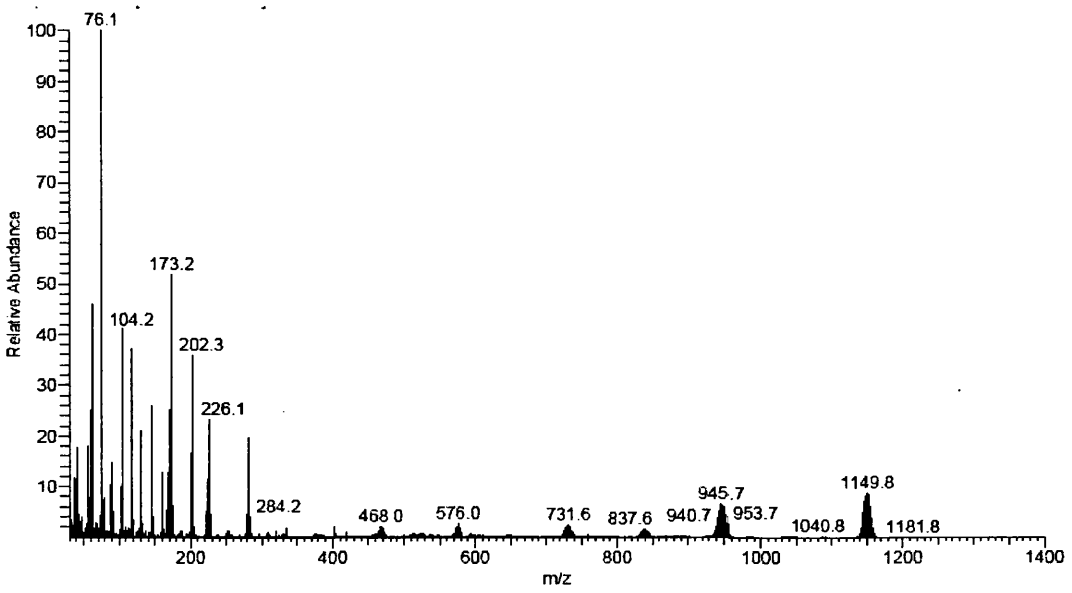

Figure 3.6: Mass spectrum of **1**.

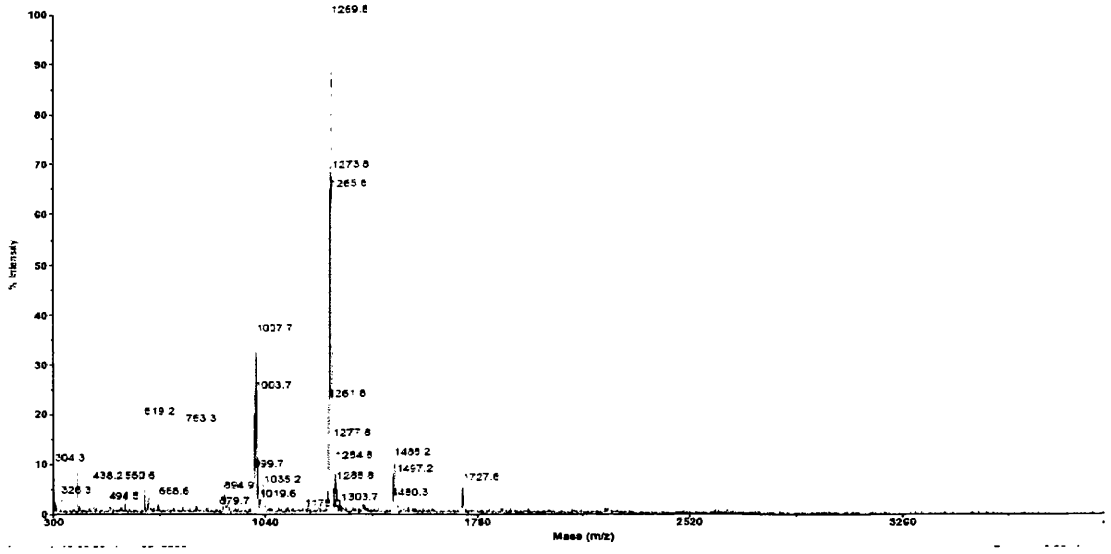

Figure 3.7: Mass spectrum of **2**.

3.3.1 Materials and general procedures

All the reactions involved in the preparations of **1** and **2** were performed using standard Schlenk techniques under an atmosphere of dry nitrogen. Acetonitrile (Fisher or Reidel-de Haen), diethylether (Fisher or BDH), ethanol (Fisher, or Jose Manuel Gomes Dos Santos LDA), methylcyclohexane (MCH) (Fisher spectroscopic grade),

and toluene (Fisher, or Merck spectroscopic grade) were used as supplied. Tetraphenylporphyrin (TPP) was obtained from Alfa Aesar and 9*H*-fluoren-9-one was a gift from J. Pina, Departmento de Quimica, Universidade de Coimbra, Portugal.

3.3.2 Methods

3.3.2.1 Absorption spectroscopy

UV-visible spectra were recorded using either a Unicam UV300 spectrometer or an HP 8452A diode array spectrophotometer. The molar extinction coefficients were obtained from absorption measurements using six solutions of different concentrations in quartz absorption cuvettes ranging from 1 mm to 10 cm pathlength. Experimental oscillator strengths, f_{exp}, were calculated from: $f_{exp} \equiv 4.3 \times 10^{-9} \int \varepsilon d\upsilon$, where $\int \varepsilon d\upsilon$ is the area under the curve of molecular extinction coefficient plotted against wavenumber.[26]

3.3.2.2.1 Emission spectroscopy

Room temperature and 77 K emission measurements were carried out using either a Perkin Elmer MPF-44E fluorescence spectrometer or a Horiba-Jobin-Ivon SPEX Fluorolog 3-22 spectrometer. 2 nm excitation and 5 nm emission slits were used for excitation spectra, and 5 nm excitation and 2 nm emission slits were used for emission spectra. For room temperature solution measurements a 1 cm × 1 cm quartz fluorescence cell was used. For 77 K measurements the sample was held in an NMR tube of *ca.* 3 mm diameter and placed in liquid nitrogen in a phosphorescence dewar. For measurements using frozen toluene the MPF-44E fluorimeter was used, while for all others the SPEX Fluorolog 3-22 spectrometer was used. Fluorescence spectra measured using the SPEX Fluorolog 3-22 were automatically corrected for detector wavelength response using manufacturer's correction files. Two organic glasses were

used: ethanol:diethylether:toluene (1:2:1) (EDT), which is relatively polar, and methylcylohexane (MCH), which is non-polar.[29]

Quantum yields for emission in 77 K EDT glasses were measured with the SPEX Fluorolog 3-22 spectrometer using TPP in EDT as emission standard (Φ_{em} = 0.15 in ethanol;[30] Φ_{em} = 0.14 in EDT, at both 77 K and 298 K (this work)). The method of comparison used was as follows. Sample and reference solutions in EDT of comparable absorption were prepared and excitation wavelengths chosen where their absorbances were the same at *ca.* 0.3 in a 1 cm path length cell (these were 496 and 523 nm). The spectra of both the sample solution and the reference were then obtained at 77 K using these excitation wavelengths. The reference solution was then allowed to warm to room temperature and the emission spectrum recorded again. This gave four emission ratios: two with both sample and reference at 77 K; and two with sample at 77 K and reference at room temperature. The emission quantum yield, Φ_x, of sample x was calculated by reference to the standard R using Equation 3.1 below. A is the intensity of light absorbed at the excitation wavelength, I is the integrated emission intensity corrected for the instrument response, and n is the refractive index of the solvent.[33]

$$\Phi_x = \Phi_R(A_R/A_x)\,(I_x/I_R)(n_x/n_R)^2 \qquad \textbf{(eq. 3.1)}$$

Samples and reference were excited at the same wavelengths. For the calculation of sample absorbances at 77 K from room temperature spectra, we have used a contraction value of 80% for EDT in going from RT to 77 K, which is typical for most organic glasses.[30] We also note that at the excitation wavelengths used the

solution phase absorption spectra and 77 K glass excitation spectra of **1** and **2** are quite flat and environment independent.

3.3.3.3 Laser kinetic emission spectroscopy

Laser kinetic emission measurements were obtained using an Applied Photophysics laser kinetic spectrometer with either the 355 nm or 532 nm emission from a Spectron Nd/YAG laser as excitation pulse. A Hamamatsu R928 photomultiplier, emission slits of 19 nm, a 644 nm wavelength cut-off filter and a 1 kΩ load terminator on the emission detection system were used for all measurements. For 77 K glasses and 77 K solids the averaged data from four decay curves were recorded using a LeCroy 9304AM oscilloscope. For RT solids, which gave a weaker signal, averaging was increased to sixteen shots and the laser amplifier used in order to improve the signal-to-noise ratio. The kinetic data were analysed using Jandel Table-Curve^{TM}, and in those cases where a large pulse signal from scatter or adventitious fluorescence was apparent, curve fitting was carried out ignoring that initial distorted portion of the signal, which was typically the first 0.5 - 1 μs.

3.3.3.4 Laser kinetic absorption spectroscopy

Transient difference absorption spectra were obtained using an Applied Photophysics laser kinetic spectrometer with the third harmonic, 355 nm, of a Nd/YAG laser (Spectra Physics) as excitation source.

3.3.3.5 Singlet oxygen measurements:

Attempts to measure room temperature singlet oxygen phosphorescence were carried out using the SPEX Fluorolog 3-22 spectrometer with a 600-line diffraction grating monochromator, and a Hamamatsu R5509-42 photomultiplier cooled to 77 K in a liquid nitrogen chamber (Products for Research model PC176TSCE-005) with a Schott RG665 filter to eliminate all the first harmonic contributions from the

sensitizer emission in the 500-800 nm region from the infrared signal. 9*H*-Fluoren-9-one in ethanol was used as reference.[32]

3.3.3.6 Computation

Calculations were performed with the Gaussian 03 suite of programs. Geometry optimizations were carried out at the B3LYP/6-31G(d,p) level, with the LANL2DZ valence functions and effective core potentials for the Pd and Se atoms. I would like to thank J. Pichereau who set up and ran these Gaussian calculations.

3.4 Results and Discussion

3.4.1 Absorption spectroscopy

Both compounds dissolve readily in MCH, acetonitrile, toluene, and EDT. Throughout this study no obvious signs of aggregation in solution were found. Both compounds gave linear Beer-Lambert plots in MCH across the concentration range 1.5×10^{-7} to 1×10^{-4} M. Absorption data are shown in Table 3.1, and Figures 3.8 and 3.9 give the absorption spectra of **1** and **2** in MCH. Absorption spectra in the visible and near-UV are characterized by three distinct transitions of decreasing intensity with increasing wavelength. The relatively high extinction coefficients indicate spin-allowed transitions. The two visible absorption maxima of **2** are shifted to longer wavelength by *ca.* 25-30 nm compared to those of **1**, consistent with transitions in which electron density is transferred onto the phosphine ligands.

The possibility of detecting weak, singlet-triplet, low energy absorption bands in the far-red/near-IR spectral region was investigated, since the measurement of such bands could help in the assignment of the emission. However, even at a concentration of 5.7×10^{-3} M in a 10 cm cell we could detect no additional absorption bands from **1** across

the wavelength range 700-1000 nm. Any absorption bands in this range, other than the tail of the visible band, must have very low extinction coefficients with ε less than *ca.* 1 M^{-1} cm^{-1}.

	EDT		MCH			Acetonitrile		Toluene	
	λ_{abs}/nm	ε /10^4 M^{-1} cm^{-1}	λ_{abs}/nm	ε /10^4 M^{-1} cm^{-1}	*f*	λ_{abs}/nm	ε /10^4 M^{-1} cm^{-1}	λ_{abs}/nm	ε /10^4 M^{-1} cm^{-1}
1	291	2.41 ± 0.09	285	2.34 ± 0.05		291	2.21 ± 0.03	292	2.31 ± 0.03
	326	1.43 ± 0.05	330	1.38 ± 0.03	0.228	327	1.32 ± 0.02	328	1.25 ± 0.02
	405 (409)[a]	0.71 ± 0.02	409 (403)[a]	0.68 ± 0.01	0.098	404	0.66 ± 0.02	406	0.66 ± 0.01
	574 (579)[a]	0.14 ± 0.01	573 (576)[a]	0.13 ± 0.01	0.018	583	0.12 ± 0.01	566	0.12 ± 0.01
2	334	2.61 ± 0.09	328	2.50 ± 0.02	0.700	341	2.24 ± 0.02	326	3.31 ± 0.02
	443 (449)[a]	2.52 ± 0.06	436	0.78 ± 0.01	0.117	427	0.61 ± 0.01	436	0.74 ± 0.01
	573 (578)[a]	1.48 ± 0.04	596	0.12 ± 0.01	0.019	591	0.11 ± 0.01	590	1.18 ± 0.01

Table 3.1. Absorption maxima, extinction coefficients and oscillator strengths for **1** and **2** in various solvents at room temperature.

[a]Wavelengths in brackets are corresponding maxima in excitation spectra.

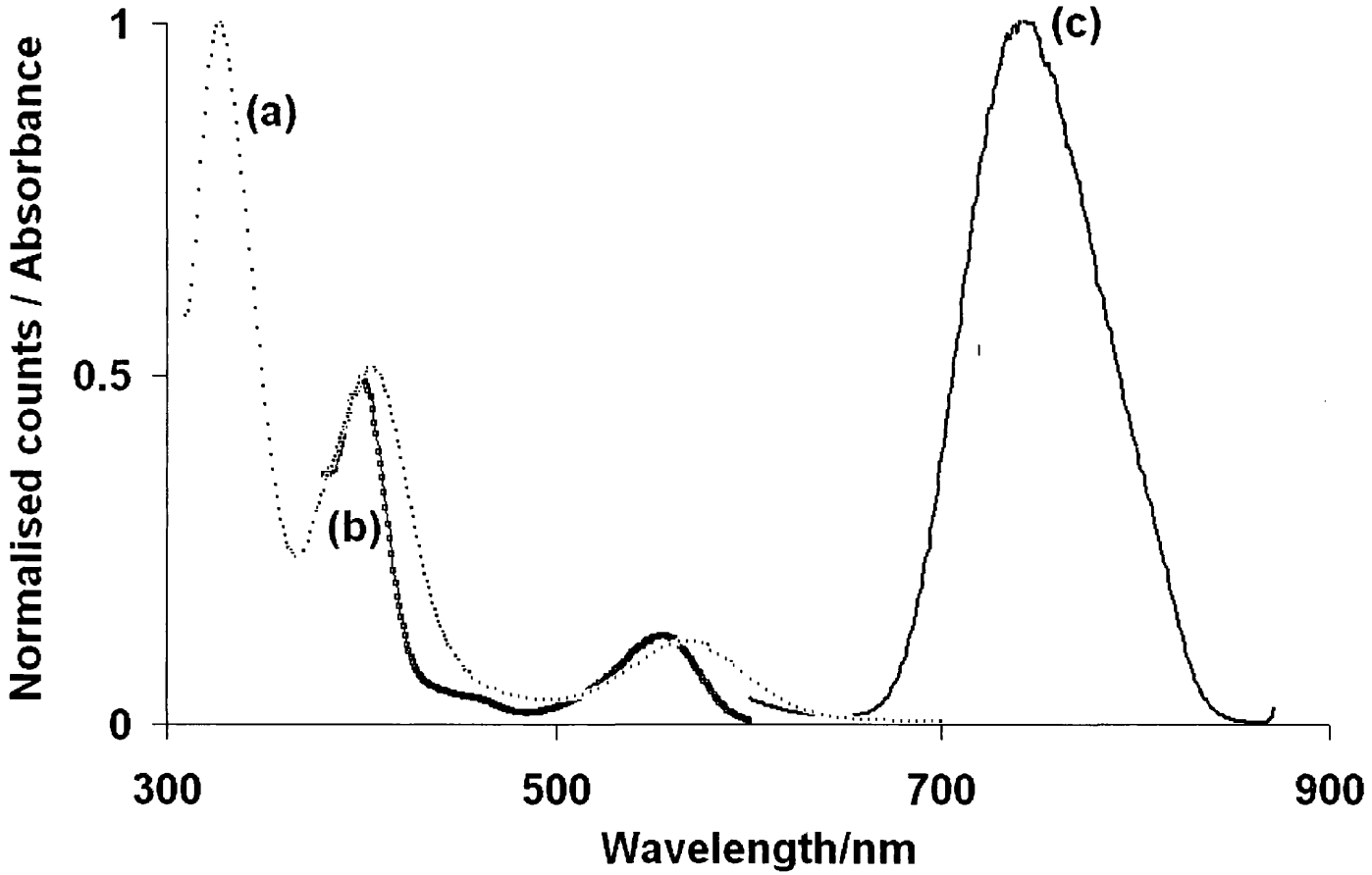

Figure 3.8: Spectra of **1** in MCH solution and 77 K glass. (a) absorption in RT solution; (b) excitation for 747 nm emission in 77 K glass; (c) emission for 445 nm excitation in 77 K glass.

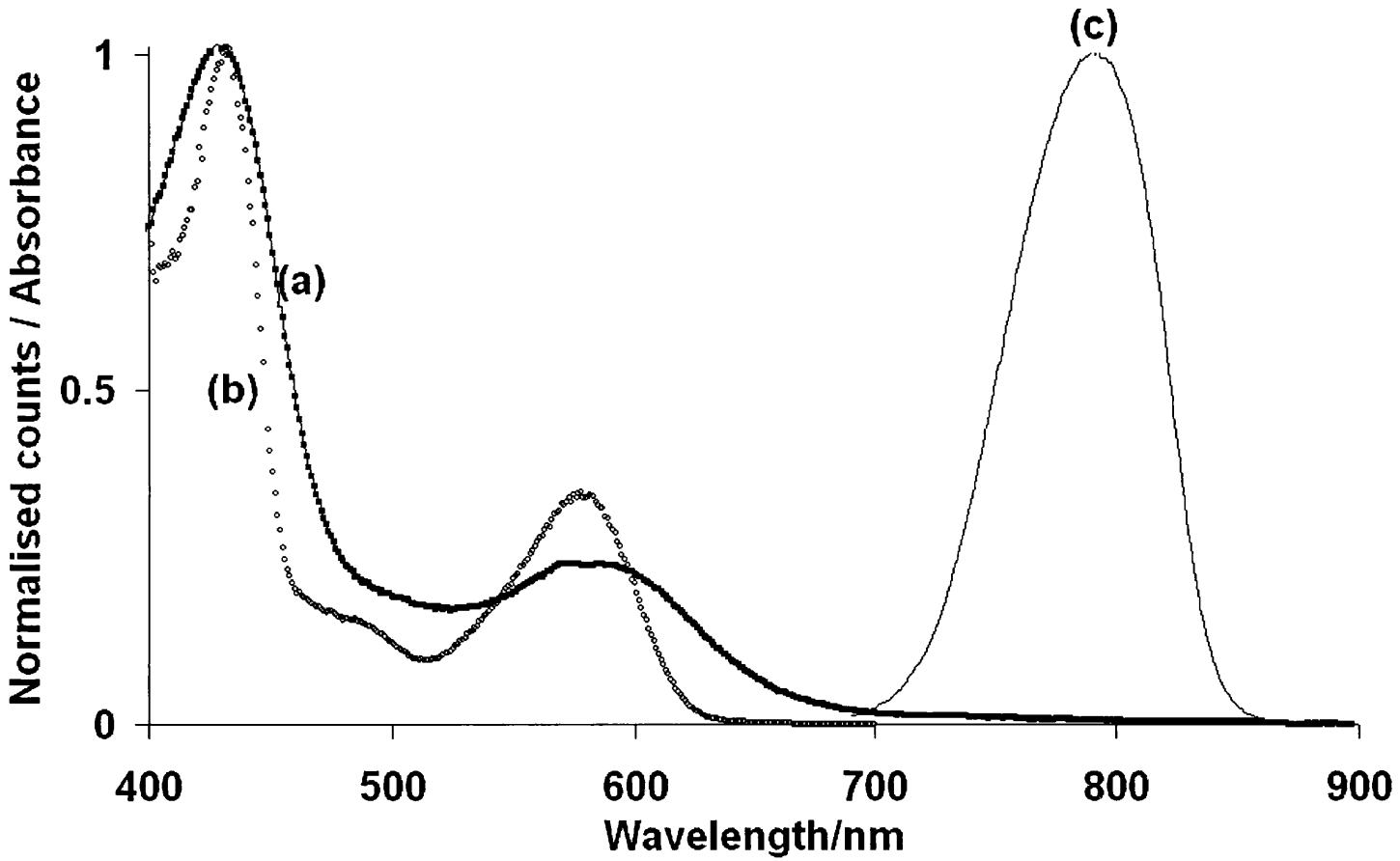

Figure 3.9: Spectra of **2** in MCH solution and 77 K glass. (a) absorption in RT solution; (b) excitation for 747 nm emission in 77 K glass; (c) emission for 445 nm excitation in 77 K glass.

3.4.2 Excitation and emission spectroscopy

Neither compound shows emission in either aerated or nitrogen-purged fluid solution but both show strong emission in the solid state and in organic glasses both at 77 K. While the bulk of the emission is in the near-infrared there is enough in the visible, particularly for **1,** for it to be seen as a cherry red glow. Figures 3.10 and 3.11 show emission and excitation spectra for solid state samples, while Figure 3.12 gives these for the compounds dissolved in EDT glass at 77 K. Table 3.2 collects excitation and emission data. For both compounds emission spectra are broad and asymmetric with the emission maximum of **2** generally shifted *ca.* 30 nm to the red compared to **1**, consistent with the relative positions of their absorption maxima, and with **1** showing asymmetry with a shoulder to the red of the main band which is at 750 nm while **2** shows a shoulder to the blue of the main band which is at 790 nm. It is interesting to note that in the solid state the emission maximum for **1** at 77 K is shifted *ca.* 30 nm to the red as compared to that at RT, while for **2** the shift is much smaller, *ca.* 7 nm, and in the opposite direction. In the solid state at 77 K excitation spectra show that excitation out to *ca.* 650 or 700 nm, for **1** and **2** respectively, is effective in inducing luminescence. The excitation spectrum of **1** also shows a very weak excitation band at *ca.* 620 nm for which a corresponding absorption band has not been detected in solution. As Figure 3.12 and Table 3.2 show, excitation spectra in a glass at 77 K are similar in shape to the RT absorption spectra but with excitation maxima shifted *ca.* 10 nm compared to RT absorption maxima. Emission spectra are very similar in both the MCH glass and the more polar EDT glass as seen in Figure 3.12.

Emission quantum yields for solid glasses at 77 K are difficult to determine precisely. Comparing emission intensities from **1** and **2** in EDT at 77 K with those from TPP as

emission standard in the same EDT solvent at both room temperature and 77 K, using two excitation wavelengths where their room temperature absorption spectra had identical absorbances gave emission yields of 0.12 (±0.01) for **1** and 0.13 (±0.01) for **2** in EDT glass at 77 K. There was no attempt made to measure solid state quantum yields but it is noted that for both compounds there is a *ca.* 3-5 fold increase in intensity as the solid is cooled from room temperature to 77 K. Furthermore, based simply on the size of the emission signals obtained, we estimate solid state quantum yields of **1** and **2** at 77 K to be of the same order of magnitude as those obtained in the low temperature glass.

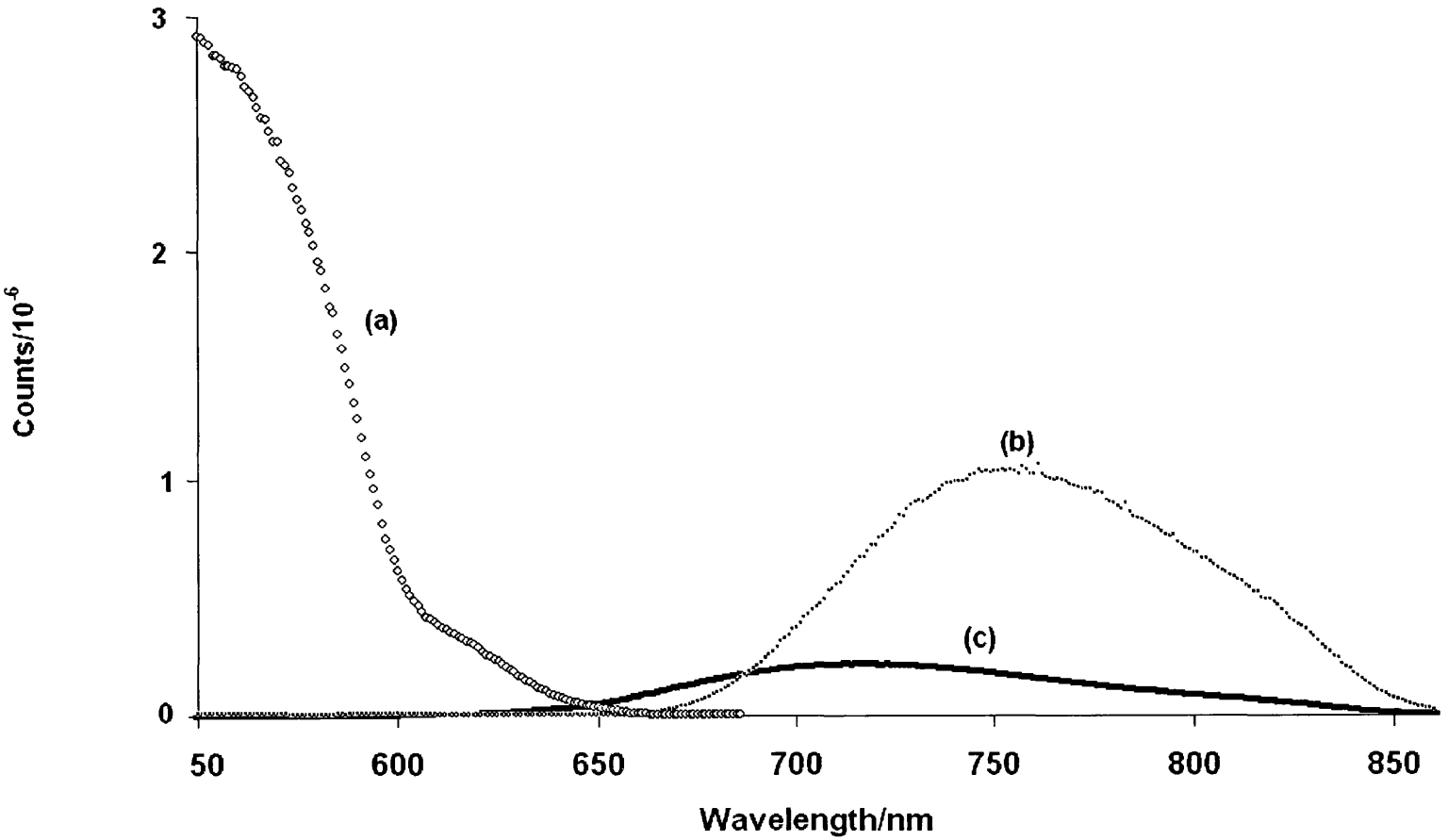

Figure 3.10: Spectra of **1** in the solid state. (a) excitation spectrum at 77 K for 717 nm emission; (b) emission at 77 K for 445 nm excitation, (c) emission at RT for 445 nm excitation.

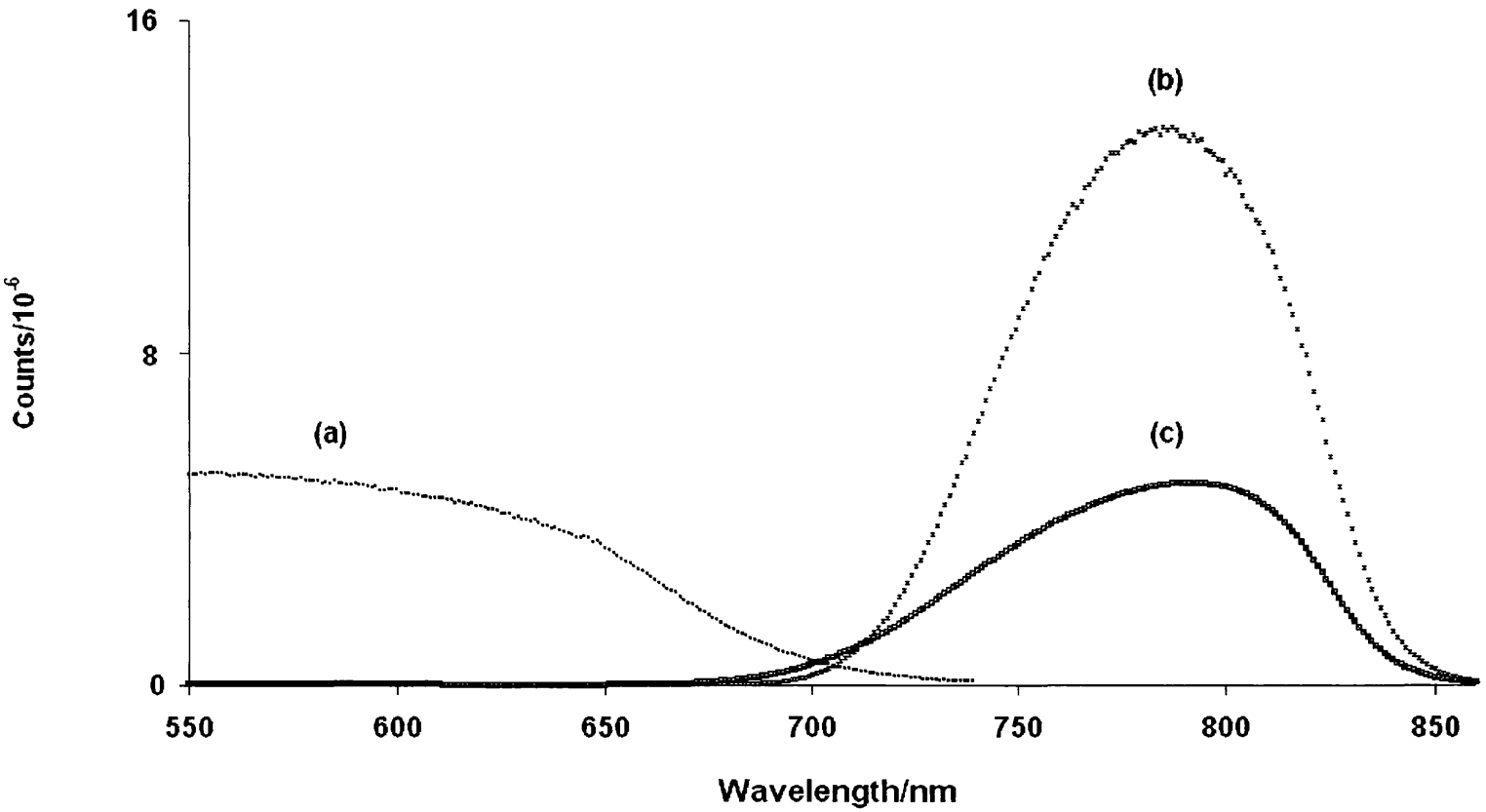

Figure 3.11: Spectra of **2** in the solid state. (a) excitation spectrum at 77 K for 785 nm emission; (b) emission at 77 K for 445 nm excitation, (c) emission at RT for 445 nm excitation.

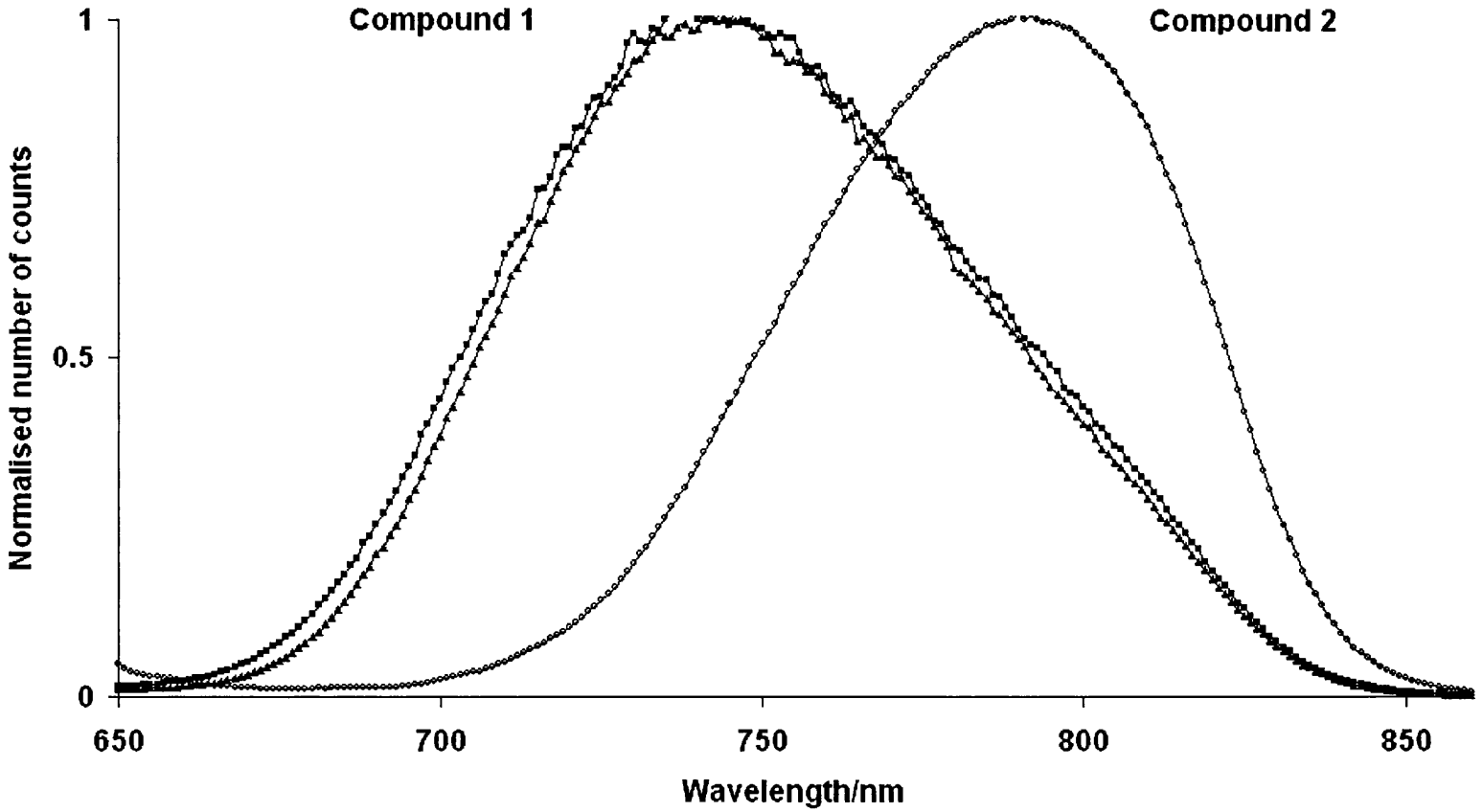

Figure 3.12: Emission spectra of **1** and **2** in organic glasses at 77 K for 445 nm excitation. (a) **1** in EDT; (b) **1** in MCH; (c) **2** in EDT.

3.4.3 Time resolved emission studies

Table 3.2 collects kinetic data. For each compound, decay kinetics are the same across the emission band and with either 355 or 532 nm excitation. While for both compounds a double exponential decay is statistically better than a single exponential the difference between the quality of the two fits for **1** is small and the single exponential fit is preferred for the kinetic analysis for **1**. In the case of **2** the difference in the quality of the fits is rather more significant, and the fitting parameters obtained by free fitting are generally constant for both excitation wavelengths, and emission bands. Figure 3.13 shows decay curves for **1** and **2** in EDT glass with residuals for single exponential and double exponential fits. Although there is no evidence for more than one chemical species present there may be a number of local environments or structural conformations in the solid or glass which give a number of lifetimes which together are modelled better by a double exponential than a single exponential decay. For completeness we include fitting parameters for both single and double exponential fits for both compounds in Table 3.2. For each compound, lifetimes at 77 K are the same whether in the solid state or the organic glasses with first order fit lifetimes of τ = 18.8 (±0.7) μs and 11.5 (±0.3) μs for **1** and **2** respectively (see Figure 3.14). Combination of these lifetimes with quantum yield data gives radiative lifetimes of 151 (±13) μs and 86 (±7) μs for compounds **1** and **2** respectively at 77 K in EDT glass. In the solid state at room temperature **1** has a lifetime of 1.83 (±0.02) μs while for **2** it is 7.0 (±0.3) μs.

Compound	λ_{exc}/nm	Solid state						Organic glass							
		298 K			77 K			EET				MCH		Toluene	
		λ_{emiss}/ nm	τ_o/μs 1st order	τ_o/μs 1+1 order	λ_{emiss}/ nm	τ_o/ μs 1st order	τ_o/μs 1+1 order	λ_{emiss} /nm	τ_o/μs 1st order	τ_o/μs 1+1 order	Φ_{emiss}	λ_{emiss} /nm	λ_{emiss} /nm	τ_o/μs 1st order	τ_o/μs 1+1 order
1	**355**	717	1.82 ± 0. 12	1.61 (90%) 3.55 (10%)	752	19.1 ± 0.38	19.5 (18%) 15.5 (82%)	742 789[a]	18.1 ± 0.14 18.2 ± 0.12	11.5 (27%) 20.1 (83%) 12.1 (29%) 21.2 (81%)	0.12	747	759	18.5 ± 0.11	15.1 (39%) 22.4 (61%)
	532	718	1.84 ± 0.13	1.12 (71%) 3.09 (29%)	752	19.5 ± 0.39	19.7 (20%) 15.6 (80%)	742 789[a]	18.5 ± 0.18 18.4 ± 0.14	17.1(87%) 28.1(13%) 17.9 (84%) 26.4 (16%)		747	759	18.3 ± 0.13	16.5 (82%) 28.9 (18%)
2	**355**	792	6.77 ± 0.25	2.75 (49%) 9.73 (51%)	785	11.6 ± 0.11	8.53 (38%) 13.7 (62%)	790 751[a]	11.2 ± 0.10 11.3 ± 0.13	9.11 (76%) 19.3 (24%) 9.23 (74%) 19.8 (26%)	0.13		798	11.6 ± 0.25	8.73 (68%) 18.7 (32%)
	532	792	7.29 ± 0.28	2.72 (47%) 10.2 (53%)	786	11.7 ± 0.12	9.89 (35%) 15.7 (65%)	791 751[a]	11.2 ± 0.10 11.3 ± 0.12	9.16 (78%) 19.1 (22%) 9.44 (75%) 19.6 (25%)			798	12.1 ± 0.26	8.65 (72%) 18.2 (28%)

Table 3.2: Lifetime and quantum yield data for **1** and **2** in various media. For double exponential (1+1) curve fits values in brackets are percentage contributions of each decay component. [a] Shoulder to the main peak.

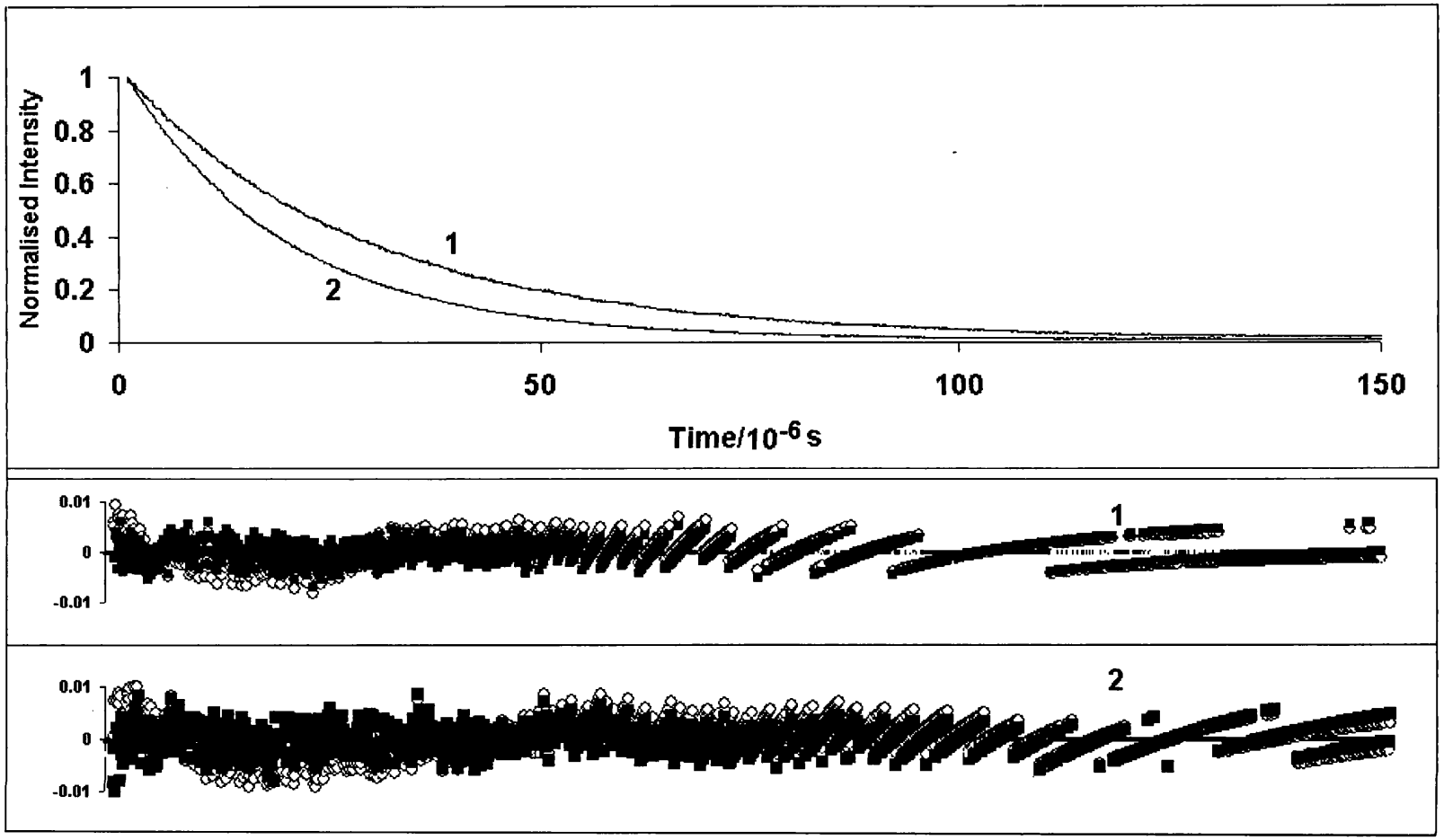
Normalised Intensity
1
0.8
0.6
0.4
0.2
0
1
2
0
50
100
150
Time/10-6 s
0.01
0
-0.01
1
0.01
0
-0.01
2

Figure 3.13: Emission decay curves for **1** and **2** in EDT glass, at 750 and 790 nm respectively, excitation at 355 nm, with residuals for single exponential (open circles) and double exponential (filled squares) fits. The aliasing which is apparent at long times in the residuals is a consequence of digitisation.

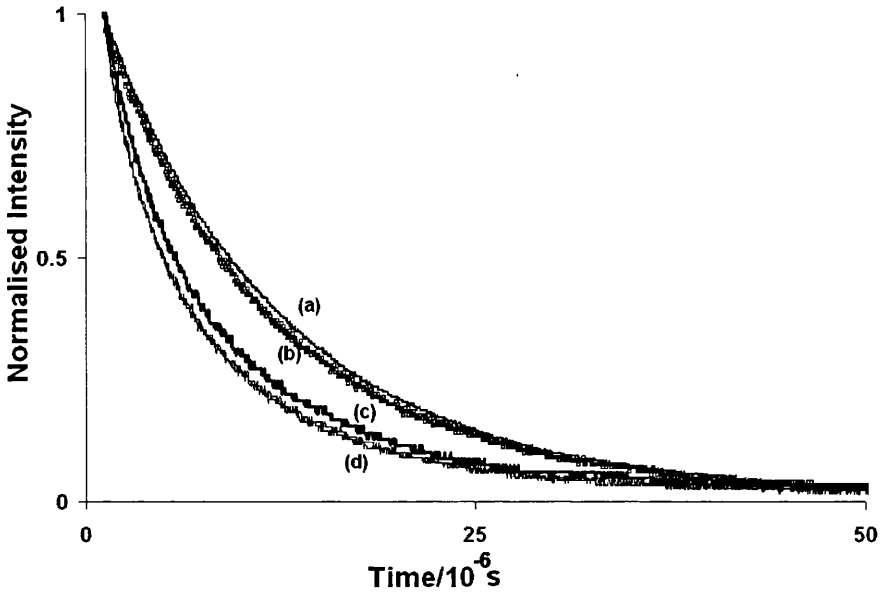

Figure 3.14: Normalised emission decay curves for **2**. (a) in EDT glass at 77 K (four indistinguishable overlying decay curves, for 750 nm and 790 nm emission wavelengths each with 532 and 355 nm excitation), (b) in solid state at 77 K: two overlying decay curves, for 532 nm and 355 nm excitation, and solid state at RT: two decay curves, for 532 nm (c) and 355 nm (d) excitation.

3.4.4 Nanosecond transient absorption and singlet oxygen studies

The long emission radiative lifetimes suggest a spin-forbidden transition. Because of this studies of ns transient absorption were carried out in the hope of detecting triplet-triplet absorption. For both compounds no transient absorbances greater than *ca.* 0.003 could be detected across the spectral range *ca.* 380-620 nm on the ns-ms timescale in either fluid EDT or toluene solution, in either the presence or absence of oxygen. However, both compounds do show weak transient absorptions in acetonitrile. For **2** in acetonitrile a very weak transient signal was detected showing a broad absorption across the visible with a maximum at *ca.* 420 nm. Both signal size and decay kinetics were oxygen dependent, and Figure 3.15 shows decay kinetics in the presence and absence of oxygen. In the absence of oxygen the data fit a single exponential decay with rate constant 2.8 ($\pm$0.1) $\times$ 10^6 s^{-1} and significant residual absorption, with relative amplitudes of 86% and 14%. In the presence of oxygen the decay curve fits a single exponential with k = 4.9 ($\pm$0.1) $\times$ 10^6 s^{-1} with no significant residual absorption. Compound **1** gives no significant signal in the presence of oxygen, but does give a very broad absorption across the visible with a maximum at *ca.* 420 nm in nitrogen-purged solution The curve obtained in the absence of oxygen can be fitted to a double exponential with: k_1 = 2.0 ($\pm$0.3) $\times$ 10^6 s^{-1}, 64%; and k_2 = 2.0 ($\pm$0.2) $\times$ 10^5 s^{-1}, 36%. It is difficult to assign these transients with any certainty, but the signals are not consistent with formation of an oxygen-quenched triplet because the signal amplitudes are oxygen dependent. Perhaps all we can say is that these compounds show some low yield photochemical activity in acetonitrile solution, with either excited state(s) or products which are long enough lived to interact with oxygen. Bearing in mind that these transients are observed in acetonitrile but not in toluene or EDT it is tempting to suggest they involve charge transfer species. As

further evidence, no emission could be detected which was assignable to singlet oxygen across the wavelength range 1200-1350 nm upon 550 nm excitation of either **1** or **2** in air-equilibrated acetonitrile solution. Based upon previous measurements with the system used we estimate the quantum yield of singlet oxygen formation, Φ_{Δ}, to be less than *ca.* 5×10^{-4} which we can also take as an upper limit for the quantum yield of any triplet states of significant lifetime.

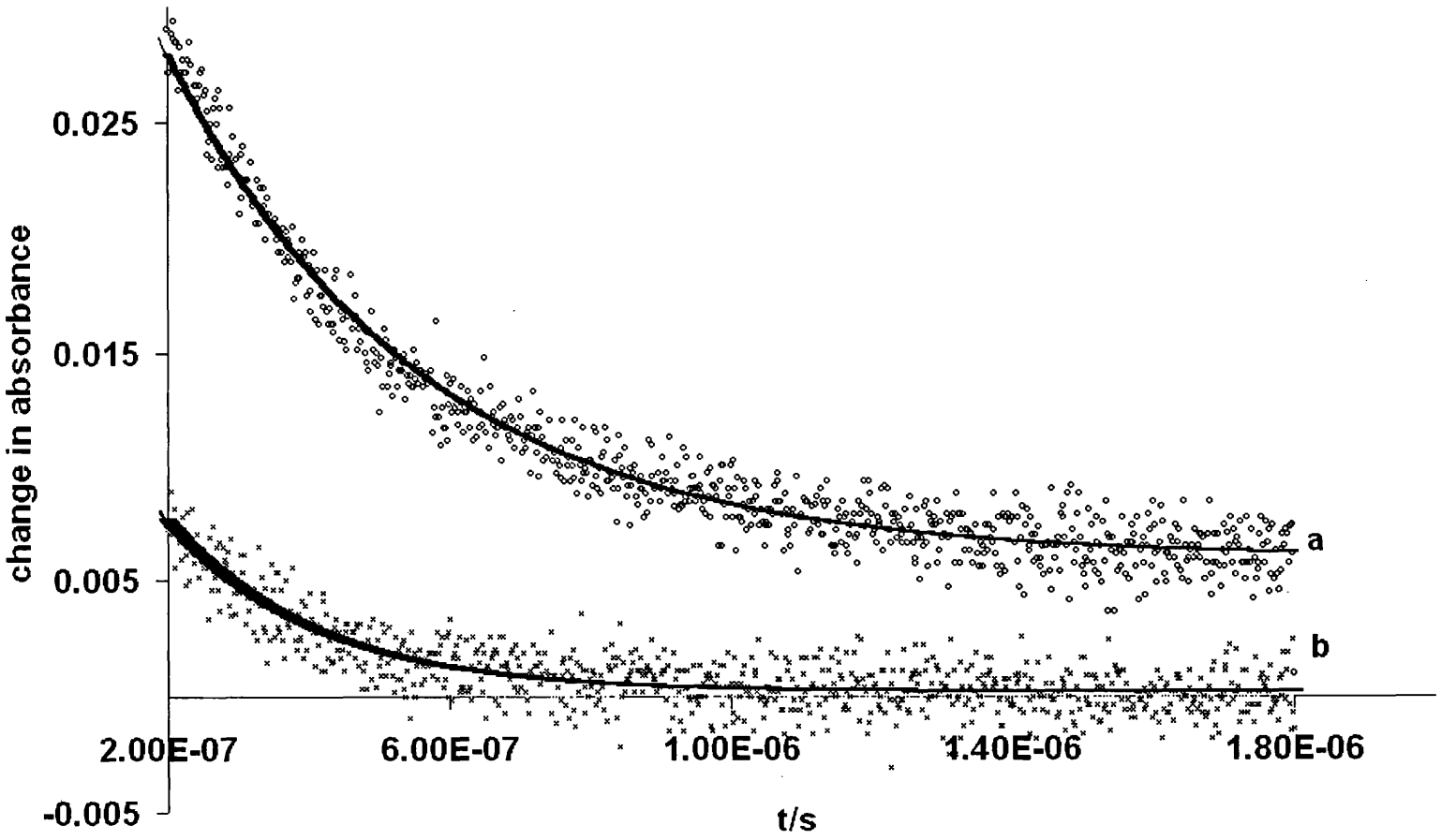

Figure 3.15: Transient absorbance of **2** at 420 nm following excitation at 355 nm. (a) nitrogen purged solution; (b) air-equilibrated solution.

3.5 DFT calculations

For the purpose of the initial calculations the substituents on the phosphine ligands were replaced by hydrogens. This, which is quite a general approach, has been shown previously by groups working on similar compounds not to make a significant difference to the resulting structure optimisation.[33] However, the crystal structure of **2** differs from that calculated by DFT optimization (shown in Figure 3.16) in that: the two planes formed by the ligands coordinated to the two Pd atoms are at an angle of *ca.* 110° and there is a relatively short Pd-Pd intramolecular distance (3.08 Å) in the crystal;[25] whereas in the DFT optimized structure all the Pd, Se, P atoms are essentially co-planar, the angle between the two Pd ligand planes is *ca.* 180°, and there is no short Pd-Pd distance.

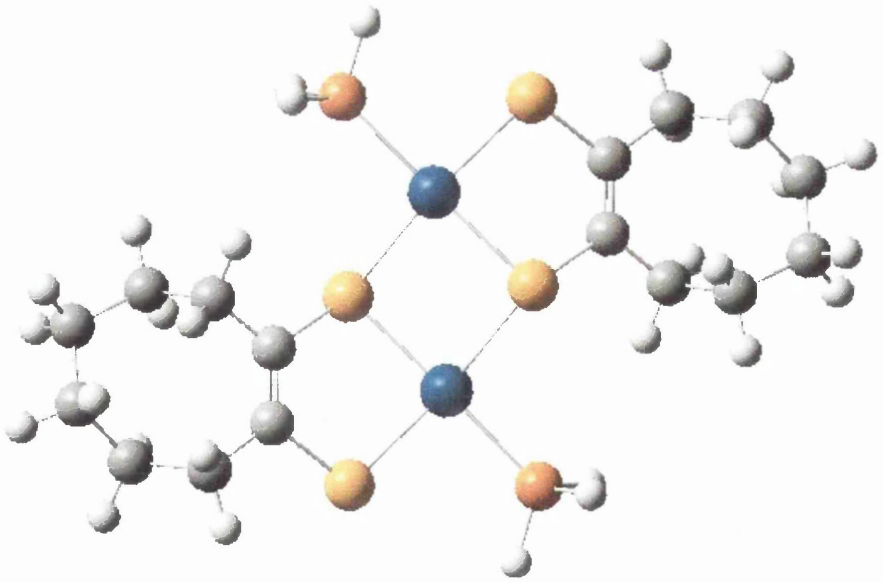

Figure 3.16: DFT optimized structure in which organic groups on the phosphorus atoms have been replaced by hydrogen atoms to facilitate the calculation.

The optimized DFT calculation described above gives a HOMO in which the main contributions are from Pd, Se, and cyclooctene π orbitals, with very little from the phosphines. In contrast, the LUMO has somewhat lower involvement of both Se and cyclooctene π orbitals, but includes significant contributions from the phosphines. Thus, DFT suggests a transition involving electron transfer from Se and carbon π orbitals onto the Pd phosphine ligands. The molecular orbitals are shown as isodensity plots in Figures 3.17, 3.18 and 3.19 below.

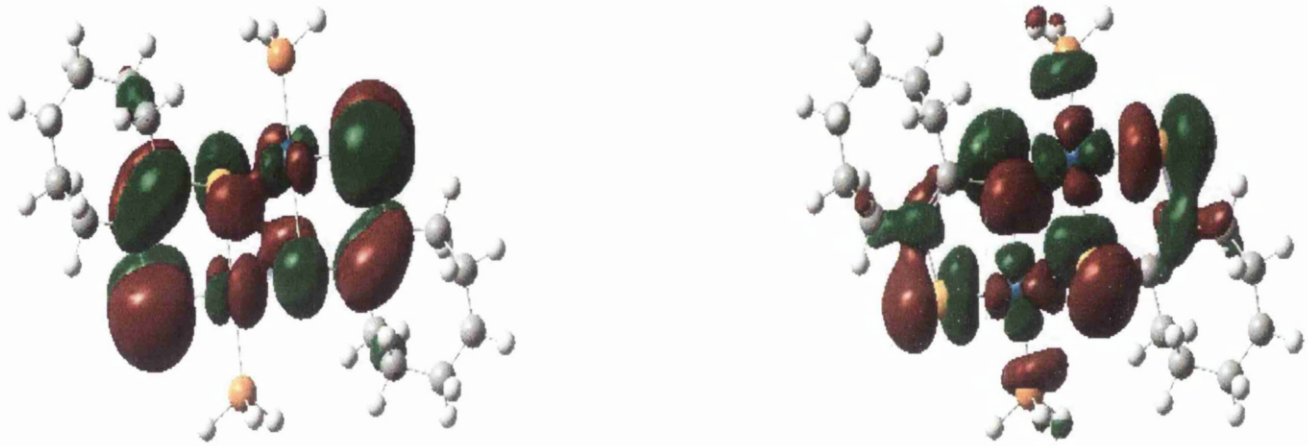

HOMO **LUMO**

Figure 3.17: DFT molecular orbital diagrams showing the HOMO and LUMO for the DFT optimized structure.

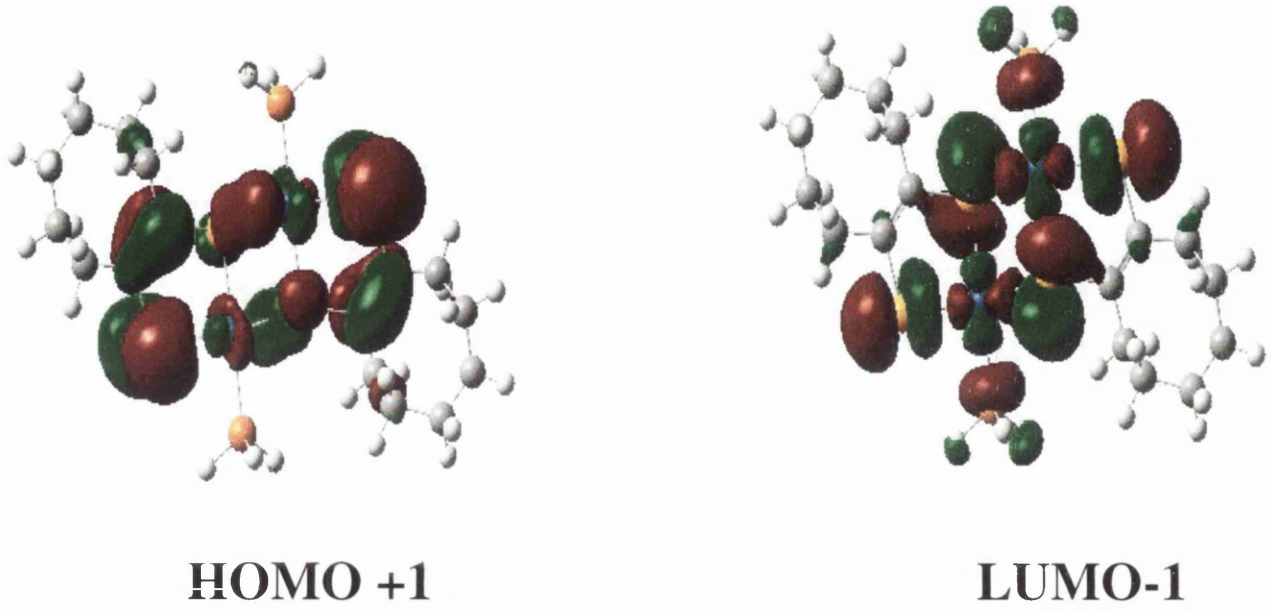

Figure 3.18: DFT molecular orbital diagrams showing the HOMO+1 and the LUMO-1 for the DFT optimized structure.

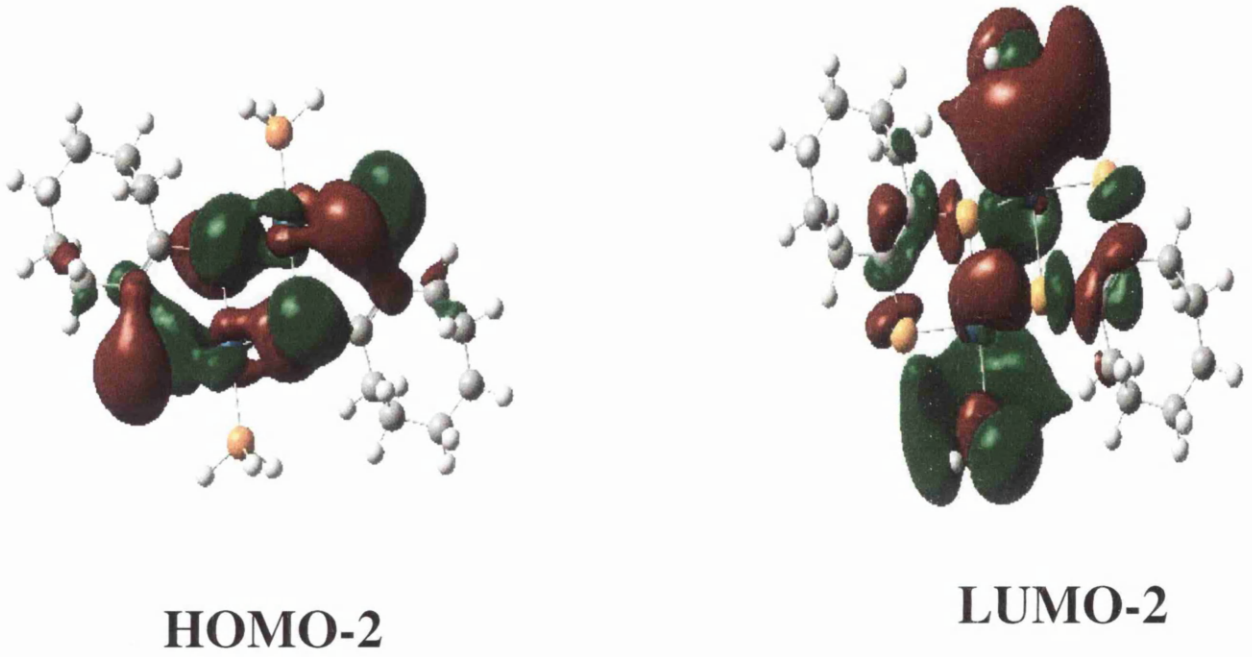

Figure 3.19: DFT molecular orbital diagrams for HOMO-2 and LUMO-2 for the DFT optimized structure.

The excited state calculations on the optimized structure gave a pair of closely lying singlet states at 877 and 885 nm, and a pair of closely lying triplet states at 1134 and 1127 nm. The calculated lowest allowed singlet-singlet transition is the 877 nm transition with oscillator strength of 0.021. The triplet/singlet energy ratio is 0.77. These can be compared to the experimental data where the lowest absorption energy level for **1** is at 573 nm and for **2** it is 596 nm with oscillator strengths of 0.018 and 0.019 respectively (Table 3.1); and the energy ratios of emission to lowest energy absorption are 0.74 and 0.73 for **1** and **2** respectively.

Although it is a generally accepted approach to replace the larger ligands on the phosphorus with hydrogen atoms,[33] it seemed appropriate, especially due to the discrepancies between the crystal structure and the DFT optimized structure to run the DFT calculation on the crystal structure. The molecular orbitals obtained from this calculation are given in Figures 3.20, and 3.21 below.

The crystal structure excited state calculations are collected in Tables 3.3 and 3.4, and Table 3.3 includes results for the DFT optimised structure for comparison. The calculations give: a pair of closely lying singlet states at 611 and 585 nm, which are blue shifted in comparison to the calculations made on the DFT optimised structure; a pair of closely lying triplet states at 684 and 629 nm, again blue shifted compared to those for the DFT structure; oscillator strengths which are greater for the crystal structure than the optimised structure; and a triplet/singlet energy ratio which, at 0.90, is larger than the 0.77 calculated for the optimised structure.

The results from calculations using the crystal structure are closer to those obtained experimentally.

Since the individual atomic orbitals of the Gaussian basis set are not orthogonal, the fractional atomic orbital electron character of the molecular orbital cannot be calculated simply from the square of the atomic orbital coefficient in the molecular orbital.[32] However, a measure of the relative contribution of an atomic orbital is given by the fractional contribution of the modulus of the coefficient in the molecular orbital, *i.e.* $F = |c_{(AO)}|/\Sigma|c_{(AO)}|$,[35] and summation of this term for any atom, F_{atom}, gives some indication of the importance of the atomic orbitals of that atom in the molecular orbital. Figure 3.22 gives a histogram of F_{atom} for the Pd, Se, P, and -ene C atoms in both HOMO and LUMO orbitals together with the difference F_{atom}(LUMO-HOMO). Both molecular orbitals are quite diffuse over Pd, Se and -ene C orbitals but the HOMO has little contribution from P atoms. In the HOMO the main atomic orbital contributions are from Pd, Se (notably Se4 and Se6, see Figure 3.2 for numbering), and -ene C atoms (notable C9 and C11), with little from P. In contrast, the LUMO has lower involvement of atomic orbitals on Se4 and Se6, and -ene carbons, C9 and C11, but increased contributions from atomic orbitals on P and Se3 and Se5.

Overall, the DFT calculations suggest a transition involving a shift in orbital character towards increasing P involvement and a reduction in -ene C involvement in the excited state, together with a significant shift in the distribution of involvement from Se4 and Se6 to Se3 and Se5. The increasing involvement of P atomic orbitals in the LUMO (and LUMO+1) orbital is consistent with the observation that the lowest energy absorption maxima of **2** are shifted to higher wavelength compared to those of **1** (Table 3.1).

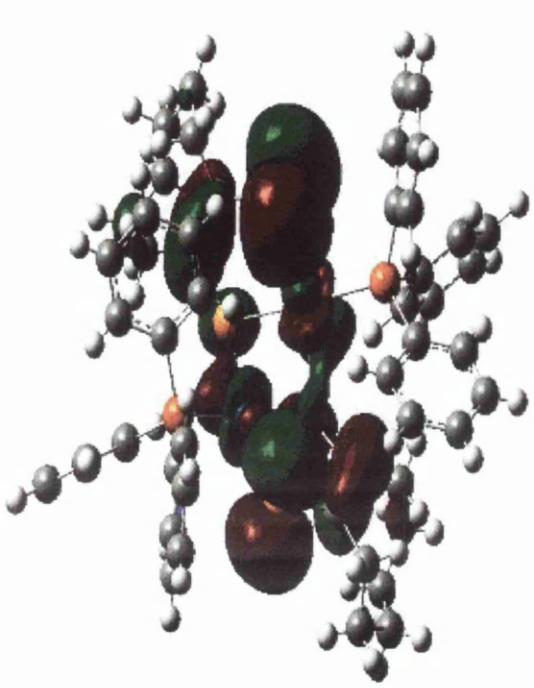

HOMO

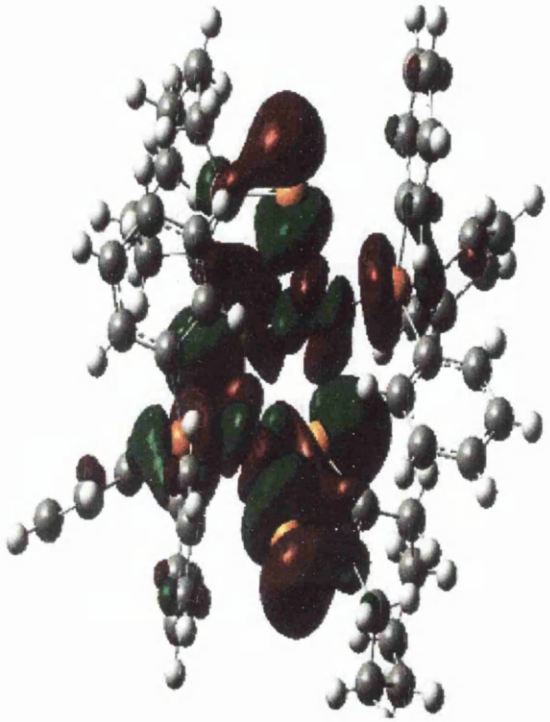

LUMO

Figure 3.20: Isodensity diagrams for the HOMO and LUMO of **2** obtained from DFT calculations on the crystal structure.

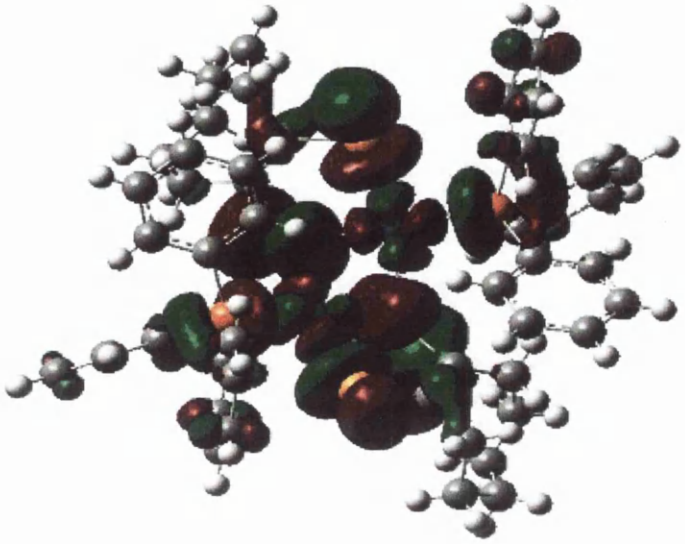

HOMO+1

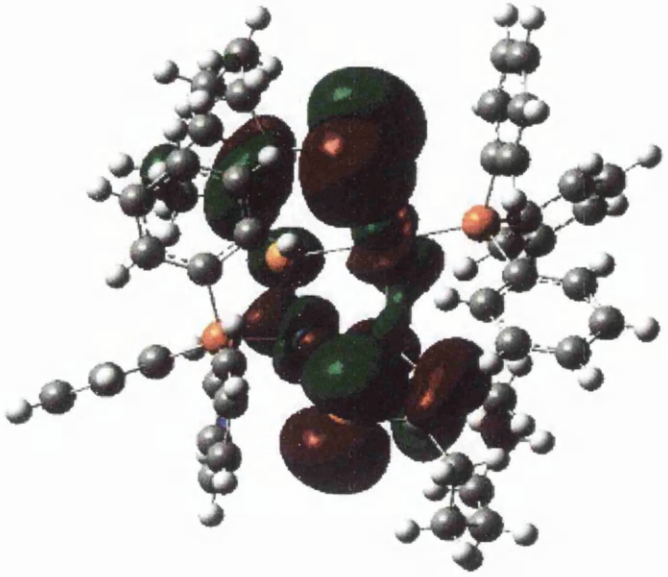

LUMO-1

Figure 3.21: The HOMO+1 and LUMO-1 of **2** obtained from DFT calculations on the crystal structure.

Energy level	DFT optimised structure			Crystal structure		
	State	*λ/nm*	*Oscillator strength*	*State*	*λ/nm*	*Oscillator strength*
1	Triplet	1134	0.00	Triplet	684	0.00
2	Triplet	1127	0.00	Triplet	629	0.00
3	Triplet	884	0.00	Singlet	611	0.016
4	Singlet	887	0.02	Singlet	585	0.0006
5	Triplet	790	0.00	Triplet	532	0.00
6	Singlet	762	0.00	Singlet	502	0.094

Table 3.3: Calculated transition properties of **2** for both the DFT optimized structure and the crystal structure.

Transition	Contribution	State	Wavelength/nm	Oscillator Strength
HOMO → LUMO (HOMO-1)→ (LUMO+1)	+0.694 -0.155	Triplet	684	0
(HOMO-1) → LUMO HOMO → (LUMO+1)	+0.632 -0.308	Triplet	629	0
HOMO → LUMO (HOMO-1)→ (LUMO+1)	+0.641 -0.213	Singlet	612	0.0156
(HOMO-1)→ LUMO HOMO → (LUMO+1)	+0.624 -0.274	Singlet	586	0.0006

Table 3.4: MO description, wavelengths, and oscillator strengths from DFT calculations for the transitions from S_0 to T_1, T_2, S_1 and S_2 for **2** in the crystal structure geometry.

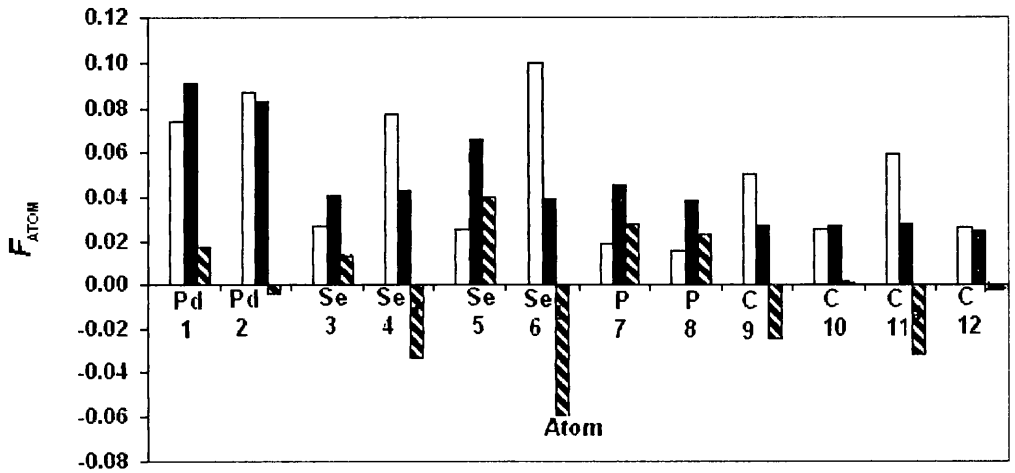

Figure 3.22: The fractional contribution of the sum of the modulii of the atomic orbital coefficients in the HOMO (open bars) and LUMO (filled bars) molecular orbitals, *i.e.* F_{atom} , for selected atoms. The difference, F_{atom}(LUMO) - F_{atom}(HOMO), is also shown (striped bars) The atomic numbering corresponds to that in Figure 3.2.

3.6 Origin of emission

The emission band is assigned to the molecular triplet because of the relatively long lifetime and the significant energy gap between emission and the lowest energy absorption band. The results of the DFT calculations also support this in that the calculations correlate well with the experimental data in terms of lowest singlet energy and transition oscillator strength, and a triplet in the far-red/near-IR. The structure in the emission bands is probably due to emission into two ground state vibrational levels separated by an energy difference of *ca.* 800 cm^{-1} rather than two distinct transitions, because the decay kinetics are the same for both bands.

The failure to detect any triplet-triplet absorption in solution on the ns timescale suggests that either the triplet lifetime is less than *ca.* 50 ns in fluid solution, or deactivation of the singlet state goes *via* a route in which the triplet state is not populated. Furthermore, assuming that any triplet formed can be quenched by oxygen to give singlet oxygen at about the diffusion controlled rate, then the failure to detect singlet oxygen indicates that $\Phi_T \times \tau \leq 50$ ns. Irrespective of whether it is rapid singlet state deactivation without triplet formation or rapid deactivation of the triplet state, the question is what is the nature of this very fast deactivation process; the detection of the triplet in the rigid environment of a glass or crystal suggests it involves molecular torsion.

3.7 Conclusions

Compounds **1** and **2** have been shown to give far-red/near-infrared phosphorescence when in the solid state or a rigid organic glass at 77 K. They are, to the best of our knowledge, the first examples of luminescent Pd-Se compounds in the literature. The complexes have radiative lifetimes of 2-7 μs in the solid state at 298 K. At 77 K in the solid state, and in frozen organic glasses, they have observed phosphorescence lifetimes of *ca.* 11-20 μs with

quantum yields of *ca.* 0.12, which gives radiative lifetimes of *ca.* 90-160 μs. No emission was detected from either **1** or **2** in fluid solution even when nitrogen-purged; in addition we could not detect any transient absorption which could be assigned to the triplet state, or any singlet oxygen generation in aerated solution ($\Phi_\Delta \leq 5 \times 10^{-4}$). The fact that this difference in behaviour occurs in going from fluid to rigid environments suggests molecular motion is an effective deactivation route for either the triplet state or its precursor.

DFT calculations give results in general agreement with those observed experimentally in terms of lowest singlet energy and transition oscillator strength, and a triplet state in the far-red/near-IR. The S_0 to S_1 and T_1 transitions show a shift in molecular orbital character from one with significant -ene π involvement but very little P involvement in the ground state to one with less -ene π but greater P involvement in the excited states; there is also a significant shift in the distribution of involvement of atomic orbitals on the four Se atoms.

3.8 *References*

(1) Ford, S.; Morley C. P.; Di Vaira, M. *Inorg. Chem.* **2004**, *43*, 7101.

(2) Lau, K. L.; Cheung, K. M.; Zhang, Q. F.; Song, Y.; Wong, W. K.; Williams, I. D.; Leung, W. A. *J. Organomet. Chem.* **2004**, *689*, 2401.

(3) Baldo, M. A.; Lamansky, S.; Thompson, M. E.; Forrest, S. R. *Appl. Phys. Lett.* **1999**, *75*, 4.

(4) McGarrah, J. E.; Kim, Y.; Hissler, M.; Eisenberg, R. *Inorg. Chem.* **2001**, *40*, 4510.

(5) Pyle, A. M.; Rehmann, J. P.; Meshoyer, R.; Kumar, C. V.; Turro, N. J.; Barton, J. K. *J. Am. Chem. Soc.* **1988**, *111*, 3051.

(6) Preininger, C.; Kilmant I.; Wolfbeis O. S. *Anal. Chem.* **1994**, *66*, 1841.

(7) Rosace, G.; Giuffrida, G.; Saitta, M.; Guglielmo, G.; Campanga, S.; Lanza, S. *Inorg. Chem.* **1996**, *35*, 6816.

(8) Evans, R. C.; Douglas, P.; Winscom, C. J. *Coord. Chem. Rev.* **2006**, *250*, 671.

(9) Miskowski, V. M.; Houlding V. H.; Che, C. M.; Wang, Y. *Inorg. Chem.* **1993**, *32*, 2518.

(10) Barigelletti, F.; Sandrini, D.; Maestri, M.; Balzani, V.; Zelewsky, A.; Chassot, L.; Jolliet, P.; Maeder, U. *Inorg. Chem.* **1998,** *27*, 3644.

(11) Graham, L. W.; Heath, G. A.; Krausz, E.; Moran, G. *Inorg. Chem.* **1991**, *30*, 347.

(12) Thomas, J.; Lin, J. T.; Lin, H.; Chang, C.; Chuen, C. *Organometallics* **2001**, *20* ,557.

(13) Laskar, I. R.; Hsu, S.; Chen, T. *Polyhedron* **2005**, *24*, 198.

(14) Gao, F. G.; Bard, A. J. *Chem. Mater.* **2002**, *14*, 3465.

(15) Colin, J.; Dixon, I. M.; Sauvage, J.; Williams, J. A. G.; Barigelletti, F.; Flamigni, L. *J. Am. Chem. Soc.* **1999**, *121*, 5009.

(16) Hao, L.; Lachicotte, R. J.; Gysling, H. J.; Eisenberg, R. *Inorg. Chem.* **1999**, *38*, 4616.

(17) Gellene, G. I.; Roundhill, D. M. *J. Phys. Chem. A*, **2002,** *106*, 7617.

(18) Bevilacqua, J. M.; Zuleta, J. A.; Eisenberg, R. *Inorg. Chem.* **1994**, 33,258.

(19) Paw, W.; Connick, W. B.; Eisenberg, R. *Inorg. Chem.*, **1998**, *37*, 3919.

(20) Carlson, B.; Phelan, G. D.; Kaminsky, W.; Dalton, L.; Jiang, X.; Liu, S.; Jen, A. *J. Am. Chem. Soc.* **2002**, *124*, 14162.

(21) Ma, Y.; Zhang, H.; Shen, J.; Che, C. *Synthetic Metals*, **1998**, 245.

(22) Zipp, A. P. *Coord. Chem. Rev.* **1988**, *84*, 47.

(23) Bevilacqua, J. M.; Eisenberg, R. *Inorg. Chem.* **1994**, *33*, 2913.

(24) Akawa, M.; Kanbara, T.; Fukumoto, H.; Yamamoto, T. *J. Organomet. Chem.* **2008**, *690*, 4192.

(25) a) Ford, S.; Khanna, P. K.; Morley, C. P.; Di Vaira, M. *J. Chem. Soc. Dalton Trans.* **1999**, 791-794. (Crystal structure CCDC ref. no. 186/1317)

b) Ford S., *New Palladium Complexes Containing Organoselenium Ligands*, PhD Thesis, University of Wales Swansea, 2000.

(26) Ford, S.; Lewtas, M. R.; Morley, C. P.; Di Vaira, M. *Eur. J. Inorg. Chem.* **2000**, 933-938.

(27) Ford, S.; Morley, C. P.; Di Vaira, M. *New J. Chem.* **1999**, *23*, 811-813.

(28) Turro, N. J. *Modern Molecular Photochemistry*; University Science Books: Sausalito, California, 1999, p89.

(29) Montalti, M.; Credi, A.; Prodi, L.; Gandolfi, M. T. *Handbook of Photochemistry*, 3rd Ed, CRC Press, New York, 2006, p138.

(30) Montalti, M.; Credi, A.; Prodi, L.; Gandolfi, M. T. *Handbook of Photochemistry*, 3rd Ed, CRC Press, New York, 2006, p552.

(31) Lakowicz, J. R. *Principles of Fluorescence Spectroscopy,* 2nd Ed, Kluwer Academic, New York, 1999.

(32) Martinez, C. G.; Neuner, A.; Marti, C.; Nonell, S.; Braun, A. M.; Oliveros, E. *Helv. Chim. Acta* **2003,** *86*, 384.

(33) Basque, R.; Maseras, F. *J. Comp. Chem.* **2002**, *21*, 562 .

(34) Clark, T. *A Handbook of Computational Chemistry*, Wiley-Interscience, New York, 1985.

(35) Foresman, J. B.; Frisch, A. *Exploring Chemistry with Electronic Structure Methods: a Guide to Using Gaussian*, Gaussian Inc., Pittsburgh, 1993.

Chapter 4:

The Photochemistry of a Novel Group of Luminescent Platinum Diselenones.

4.1 Introduction

It has been known that platinum(II) compounds have interesting chemical and physical properties for many centuries.[1] Much recent work on Pt(II) complexes has been driven by the discovery of the anti-cancer drug cisplatin.[2] In addition, due to the possible utilisation of inorganic compounds as dopants in organic light-emitting diodes, there has been a lot of recent interest in the luminescent properties of Pt(II) complexes.[3-7]

Luminescent transition metal complexes have fascinated photochemists for a long time. The luminescence from Pt(II) porphyrin complexes has been known since at least the 17th century.[1-7] One of the first reports was on the tetracyanoplatinates,[8] which were noted to be intensely luminescent in the solid state. This was later found to be due to a crystal structure in which the Pt atoms are stacked quite close together, and it is the molecular orbitals arising from the -Pt-Pt-Pt- stacking interaction which are involved in emission.[8] The colour of the emission in the tetracyanoplatinates can be tuned by altering the interatomic Pt-Pt separation, *e.g.* by varying the cation, which sits in between the stacks. When the stacking distance is reduced, the emission energy is reduced and the emission is red shifted.[6] The luminescence observed in the tetracyanoplatinates, like that of many complexes reported around this time, is a solid state property and is not present in solution.[9-10]

Prior to the 1970s however, reports of luminescence from Pt(II) square planar complexes in solution were uncommon.[11] Forrest and co-workers realised the potential of the unique properties of Pt(II) porphyrin complexes (Figure 4.1) as emitters in electroluminescent devices.[13-14] Pt(II) displays strong spin-orbit coupling that promotes the mixing of singlet and triplet states. This enhances the phosphorescent emission efficiency and shortens the triplet lifetime. The porphyrins are also thermally and chemically stable, and are sublimable.[13] These

properties made them particularly attractive candidates for organic light-emitting diodes and Pt(II) porphyrins were the first phosphorescent coordination compounds to be used as emitters in electroluminescent devices. Since then the use of phosphorescent platinum complexes has expanded to include; sensors, emissive probes for DNA, photosensitizers, singlet oxygen sensitizers, photo-oxidants and a range of photochemical devices.[13-15] The development of new, more efficient, luminescent Pt(II) complexes has attracted much attention from both academic and industrial research sectors.[16-24]

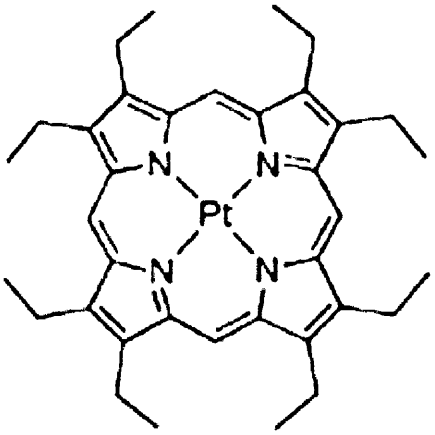

Figure 4.1: Structure of platinum porphyrin.[14]

Williams and co-workers have recently published a review which focuses on the advances that have been made over the past decade with regard to optimising the luminescent properties of square planar Pt(II) complexes.[14] The review highlights the progress that has been made in understanding the factors that govern the luminescence efficiency of Pt(II) compounds.

In order to achieve optimum luminescent efficiency it is necessary that the radiative rate constant of the emissive state be maximised whereas the non-radiative pathways must be minimised. When the metal oribitals contribute a lot to the excited states, particularly in simple Pt(II) complexes, the high spin-orbit coupling constant of Pt(II) (χ = 4481 cm^{-1})[25] promotes rapid intersystem crossing from the singlet to the triplet states at a rate of about 10^{1} s^{-1}.[14] This generally exceeds the radiative rate constant of the singlet excited state so intersystem crossing is efficient and emission typically comes from the triplet. The decay from the triplet state is also promoted by the relaxation of the spin selection rule due to the high spin-orbit coupling constant of Pt(II). The efficiency of this depends on the metal conribution to the lowest energy excited state. The radiative rate constants are greatest when the metal character of the lowest energy excited state is the greatest.[14]

There is a strong preference of Pt(II) complexes to be square planar. This results in the d_{x2-y2} orbial becoming antibonding. Population of this orbital is accompanied by elongation of the Pt-L bond. This elongation promotes the non-radiative decay of the metal-centred d-d excied states to the ground state. Excited states of different character, such as the MLCT or LC states may lie lower in energy than the d-d state, but if the d-d state is thermally accessible it can still exert an influence. Therefore, in order to promote emission in solution it is necessary to ensure that the lowest excited state is not d-d in nature and that the energy gap between the lowest-lying excited state and the higher-lying d-d state is large enough to prevent the d-d state becoming thermally active. This can be achieved by either lowering the energy of the emitting state, or raising the energy of the d-d state. This was presented by Willams and co-workers in the potential energy diagrams shown below.[14]

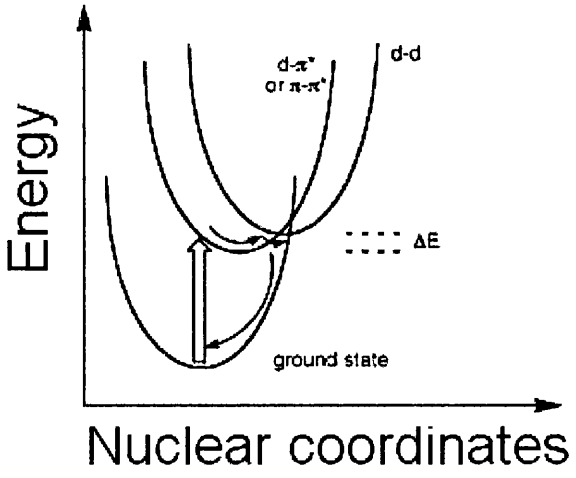

Figure 4.2: Potential energy surfaces for Pt(II) states. The excited state is displaced relative to the ground state, owing to the strongly antibonding character of the d_{x2-y2} orbital.[14]

Judicious selection of the ligand is also important in tuning the optical properties of the Pt (II) compounds; for example, strong field ligands or co-ligands can be introduced to raise the energy of the d-d state. Rigidity also favours luminescence over non-radiative decay.

4.1.1 Complexes of Pt(II) with chalcogens

The chemistry of the heavier chalcogens remains relatively unexplored, but shows a number of interesting features. Organoselenium-based ligands exhibit chemical and physical properties that include their strong affinity towards the heavier transition metals such as platinum and palladium.[1] However, unlike their sulphur analogues limited numbers of phosphorescent selenium compounds have been reported.

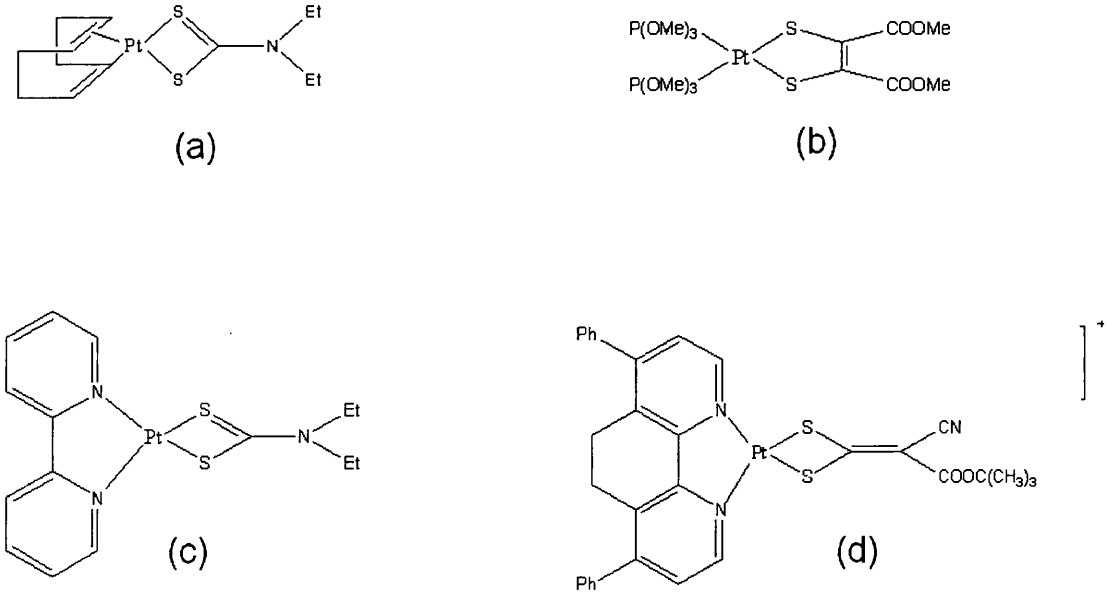

Figure 4.3: Examples of sulphur-platinum complexes presented by Eisenberg and co-workers.[28]

Pt(II) 1,1- and 1,2-dithiolates (dithiolenes) have received particular attention. Other examples of sulphur-containing ligands investigated include SCS-pincers, and dithiocarbamates (see Figure 4.3).[28]

Despite the interest in sulphur the other heavier chalogens remain relatively ignored, even though organoselenium ligands show an affinity towards Pt(II). [30]

The Pt(II) diselenolene $[Pt(Se_2C_8H_{12})(PPh_3)_2]$ (3) was first reported by Morley and Khanna,[31] and its structure has been recently reviewed.[32] Examination by the author showed that this compound gave a cherry red luminescence in the solid state under UV irradiation. The poor solubility of this compound precluded photochemical studies in solution. However from previous work it was known that Pt diselenolenes having different co-ligands could be

prepared from **3** and that these were soluble. It was considered that synthesis of the range of compounds shown in Figure 4.4 was worthwhile in order to study the photochemistry of this group of compounds in both solution and in the solid state, and it is this which is the subject of the work presented in this chapter.

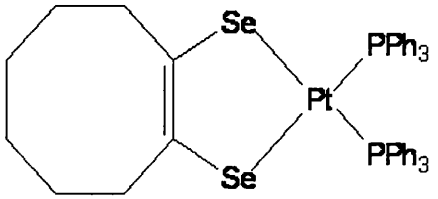

3

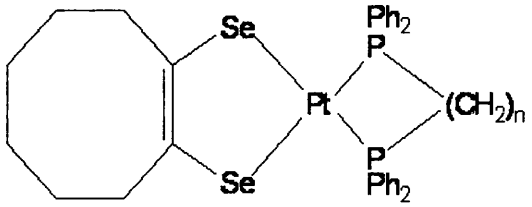

6,7,8

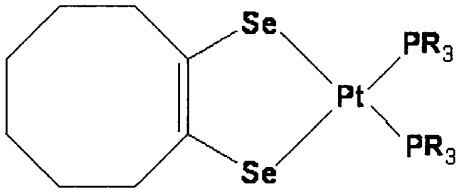

4,5

Figure 4.4: Structures of platinum diselenolenes; $[Pt(Se_2C_8H_{12})(PPh_3)_2]$, **3,** $[Pt(Se_2C_8H_{12})(PEt_3)_2]$, (R=Et) **4**, and $[Pt(Se_2C_8H_{12})(PBu_3)_2]$, (R=Bu) **5**, $[Pt(Se_2C_8H_{12})(dppm)]$ (n=1), **6**, $[Pt(Se_2C_8H_{12})(dppe)]$, (n=2) **,7**, $[Pt(Se_2C_8H_{12})(dppp)]$, (n=3), **8**

In particular this chapter will include:

1. A brief introduction to the previously reported synthesis and structural characterisation of Pt(II) diselenolenes of the general formula $[Pt(Se_2C_8H_{12})(PR_3)_2]$ where R is Et, Bu, or Ph and $[Pt(Se_2C_8H_{12})(L)]$ where L = dppm, dppe, or dppp.
2. A description of the photochemical characterisation of the Pt(II) diselenolenes. Due to the poor solubility of $[Pt(Se_2C_8H_{12})(PPh_3)_2]$, **3** in a range of solvents, it was

found that a full photochemical characterisation was not possible. However, **3** was used as a precursor to a range of other platinum diselenolenes which have good solubility. The majority of the studies were carried out using [Pt($Se_2C_8H_{12}$)(dppm)], **6**, the behaviour of which is representative of all these compounds, although some studies were completed using [Pt($Se_2C_8H_{12}$)(dppe)], **7**, [Pt($Se_2C_8H_{12}$)(dppp)], **8** [Pt($Se_2C_8H_{12}$)(PEt_3)$_2$], **4**, and [Pt($Se_2C_8H_{12}$)(PBu_3)$_2$], **5**, for comparison purposes. These were photochemically characterised in solution, organic glasses, and in the solid state.

A more in-depth analysis of the complicated photochemical behaviour observed, in order to evaluate the nature of the luminescence in all the different systems.

4.2 Experimental

All compounds were prepared as previously described,[31-32] and their structures confirmed by NMR spectroscopy and mass spectrometry. The compounds are all yellow solids which give yellow solutions.

4.2.1 Materials and general procedures

All the reactions involved in the preparations of **3**, **4**, **5**, **6**, **7**, **8**, **9** and **10** (see Figure 4.4) were performed using standard Schlenk techniques under an atmosphere of dry nitrogen. Acetonitrile (Fisher or Reidel-de Haen), diethylether (Fisher or BDH), ethanol (Fisher, or Jose Manuel Gomes Dos Santos LDA), and toluene (Fisher, or Merck spectroscopic grade) were used as supplied. Tetraphenylporphyrin (TPP) was obtained from Alfa Aesar and 9*H*-fluoren-9-one was a gift from J. Pina, University of Coimbra, Portugal.

4.2.2 Methods

4.2.2.1 Absorption spectroscopy

UV-visible spectra were recorded using either a Unicam UV300 spectrometer or an HP 8452A diode array spectrophotometer. The molar extinction coefficients were obtained from absorption measurements using five solutions of different concentrations in quartz absorption cuvettes ranging from 1 mm to 4 cm pathlength. Experimental oscillator strengths, f_{exp} were calculated from: $f_{exp} \equiv 4.3 \times 10^{-9} \int \varepsilon d\upsilon$, where $\int \varepsilon d\upsilon$ is the area under the curve of molecular extinction coefficient plotted against wavenumber.[33]

4.2.2.2 Emission spectroscopy

Room temperature and 77 K emission measurements were performed using either a Perkin Elmer MPF-44E fluorescence spectrometer or a Horiba-Jobin-Ivon SPEX Fluorolog 3-22 spectrometer. For room temperature solution measurements a 1 cm × 1 cm quartz fluorescence cell was used. For 77 K measurements the sample was held in a tube of *ca.* 3 mm diameter and placed in liquid nitrogen in a phosphorescence dewar. For measurements

using frozen toluene the MPF-44E fluorimeter was used while for all others the SPEX Fluorolog 3-22 spectrometer was used. Fluorescence spectra measured using the SPEX Fluorolog 3-22 were corrected for detector wavelength response using manufacturer's correction files. The organic glass used was ethanol:diethylether:toluene (1:2:1) (EDT).[34]

The quantum yields of fluorescence and phosphorescence of **6** in degassed toluene solutions were measured using the SPEX Fluorolog 3-22 spectrometer against TPP in ethanol as emission standard ($\Phi_{em} = 0.15$ in ethanol[35]) The method of comparison used was as follows. Sample and reference solutions of comparable absorption were prepared and excitation wavelengths chosen where their absorbances were the same at *ca.* 0.1 in a 1 cm path length cell. The quantum yield, Φ_x, was calculated by reference to the standard R using Equation 4.1 below. A is the intensity of light absorbed at the excitation wavelength, I is the integrated emission intensity corrected for the instrument response, and n is the refractive index of the solvent.[35]

$$\Phi_x = \Phi_R(A_R/A_x)\,(I_x/I_R)(n_x/n_R)^2 \qquad \textbf{(eq. 4.1)}$$

The sample and reference were excited at the same wavelengths: 353 nm; 377 nm, 420 nm, 424 nm to give four quantum yields and the average was taken. Quantum yields for **4**, **5**, **6**, **7**, **8**, **9** and **10** were obtained by comparison to **3** using uncorrected spectra obtained with the MPF-44E instrument. These quantum yields were calculated relative to that of tetraphenylporphyrin (TPP) in ethanol at 298 K ($\Phi_{em} = 0.15$).[35]

4.2.2.3 Laser kinetic emission spectroscopy

Laser kinetic emission measurements were obtained using an Applied Photophysics laser kinetic spectrometer with either the 355 nm or 532 nm emission from a Spectron Nd/YAG

laser as excitation pulse. A Hamamatsu R928 photomultiplier, emission slits of 19 nm, a wavelength cut-off filter and a 1 kΩ load terminator on the emission detection system were used for all measurements. The averaged data from four decay curves were recorded using a LeCroy 9304AM oscilloscope. The kinetic data were analysed using Jandel Table-Curve™, and in those cases where a large pulse signal from scatter or adventitious fluorescence was apparent, curve fitting was carried out ignoring that initial distorted portion of the signal, which was typically the first 0.5-1 μs.

4.2.2.4 Laser kinetic absorption spectroscopy

Transient difference absorption spectra were obtained using an Applied Photophysics laser kinetic spectrometer with the third harmonic, 355 nm, of a Nd/YAG laser (Spectra Physics) as excitation source, 4.6 nm slits, with data averaging across 16 excitation pulses.

4.2.2.5 Singlet oxygen measurements

Room temperature singlet oxygen phosphorescence measurements were carried out using the SPEX Fluorolog 3-22 spectrometer with a 600-line diffraction grating monochromator, and a Hamamatsu R5509-42 photomultiplier cooled to 77 K in a liquid nitrogen chamber (Products for Research model PC176TSCE-005) with a Schott RG665 filter to eliminate all the first harmonic contributions from the sensitizer emission in the 500-800 nm region from the infrared signal. 9*H*-Fluoren-9-one in ethanol was used as reference.[36]

4.2.2.6 Computation

Calculations were performed with the Gaussian 03 suite of programs. Geometry optimizations were carried out at the B3LYP/6-31G(d,p) level, with the LANL2DZ valence functions and effective core potentials for the Pt and Se atoms, and intermolecular distances were measured using Mercury 1.3 (CCDC 2001-2004).

4.2.3 Synthesis of Pt diselenolenes

The reaction of $[Pt(PPh_3)_4]$ with cycloocteno-1,2,3 selenadiazole in refluxing toluene was reported by Khanna and Morley in 1995. It was found to give two products, $[Pt(SeC_8H_{12})(PPh_3)_2]$ and the poorly soluble $[Pt(Se_2C_8H_{12})(PPh_3)_2]$. The compound $[Pt(Se_2C_8H_{12})(PPh_3)_2]$ also had a high melting point, which led to the initial belief that it was polymeric, $[Pt(Se_2C_8H_{12})(PPh_3)_2]_x$.[31-32]

Unfortunately, the poor solubility prevented a full spectral analysis of this compound. However, Webster and Morley later presented a MALDI mass spectrum of **3** which confirmed the mononuclear structure shown below in Figure 4.5.[32]

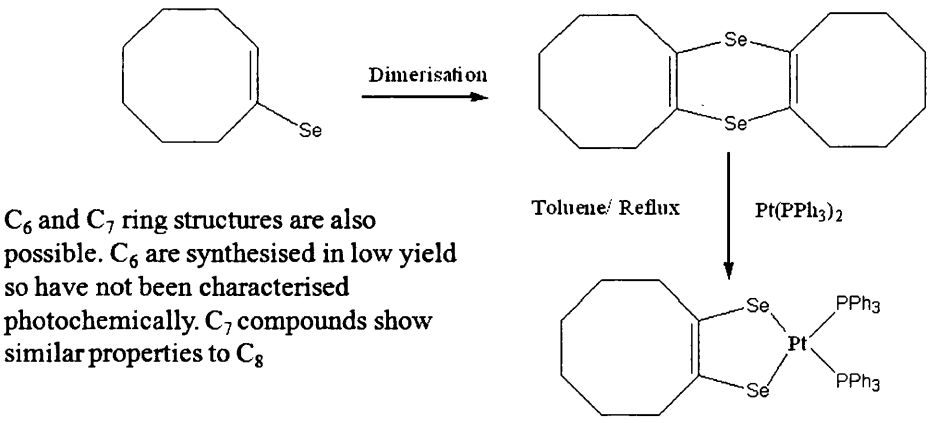

Figure 4.5: Structure and synthesis of $[Pt(Se_2C_8H_{12})(PPh_3)_2]$, **3**.[32]

Compound **3** can be used as a precursor for a range of other diselenolenes. Prolonged stirring of **3** with excess PR_3 (R = Et (**4**), or Bu (**5**)) in toluene at elevated temperatures yields diselenolenes of the type $[Pt(Se_2C_8H_{12})(PR_3)_2]$. The route for synthesis of $[Pt(Se_2C_8H_{12})(PEt_3)_2]$ is shown in Figure 4.6 below. The reactions of **3** with the chelating

phosphines, dppm, dppe, and dppm in toluene at 90 °C followed by column chromatography led to the isolation of the diselenolenes [Pt($Se_2C_8H_{12}$)(L)] (L = dppm (**6**), dppe (**7**), dppp (**8**)) shown in figure 4.7. Compounds incorporating chelating phosphines were of much greater stability than the complexes of trialkylphosphines. The trialkylphosphine diselenolenes (**4** and **5**) decomposed rapidly in $CHCl_3$, but not in acetonitrile or toluene. All compounds have been previously characterised via mass spectrometry, multinuclear NMR spectroscopy and where possible X-ray crystallography, and the identities of the compounds prepared for this work were confirmed by comparison of NMR and mass spectra with those previously described.

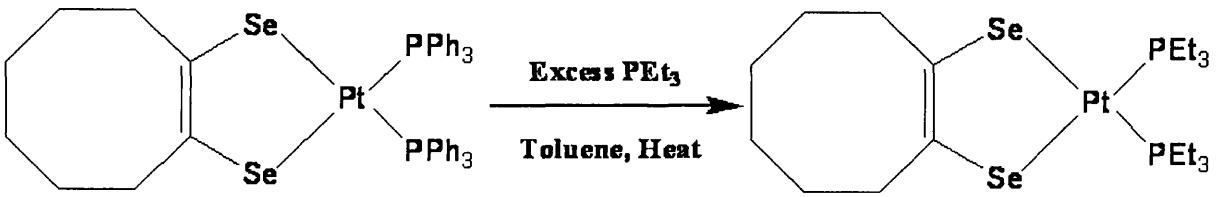

Figure 4.6: Synthesis of [Pt($Se_2C_8H_{12}$)(PEt_3)$_2$] (**4**) from **3**.

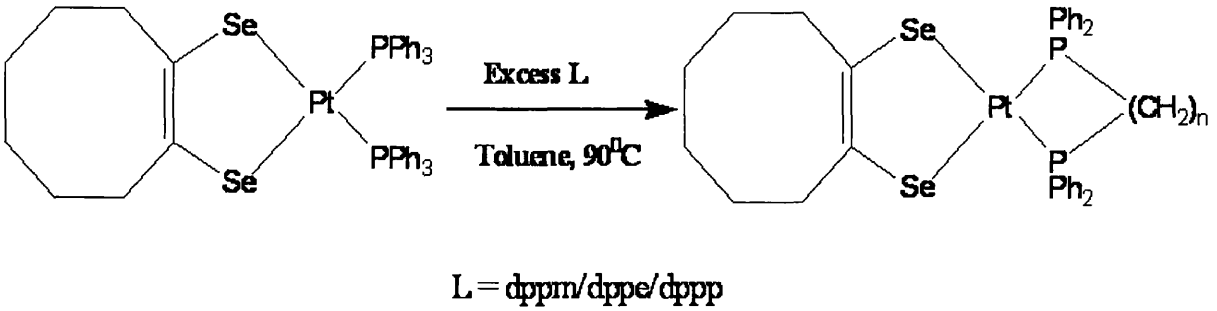

Figure 4.7: Synthesis of diselenolenes [Pt($Se_2C_8H_{12}$)(L)] (L = dppm (**6**), dppe (**7**), or dppp (**8**)).

The diselenolenes containing a cycloheptene ring have also been examined where possible. Data comparing compounds **3, 5, 6** and **10** ([$Pt(Se_2C_7H_{10})(PBu_3)_2$]) are collected in Table 4.2 and discussed further later in this chapter. Diselenolenes with a cyclohexene ring were synthesised in too small yield to be examined photochemically.

4.3 Results and Discussion

4.3.1 Photochemistry of 3 in the solid state

4.3.1.1 Steady state emission studies: emission and excitation

Compound **3** is strongly emissive in the solid state at both RT and 77 K as shown in Figures 4.8 and 4.9. The red emission is more intense, broader and slightly red shifted at 77 K compared to RT: λ_{max}(RT) = 700 nm; λ_{max}(77 K) = 710 nm. The RT excitation and emission spectra are shown in Figure 4.8. The excitation spectrum shows two main structured bands at 500 nm and 427 nm.

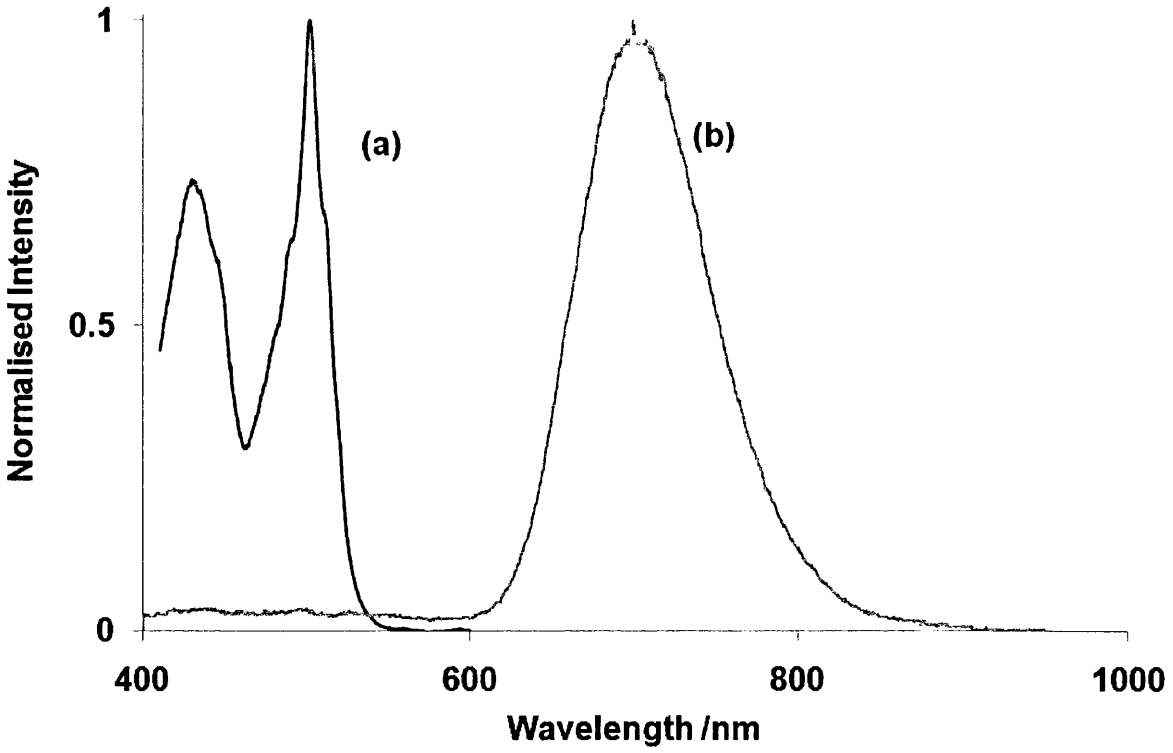

Figure 4.8: RT excitation and emission spectra of **3** in the solid state. (a) excitation, monitoring at an emission wavelength of 700 nm; (b) emission with 355 nm excitation.

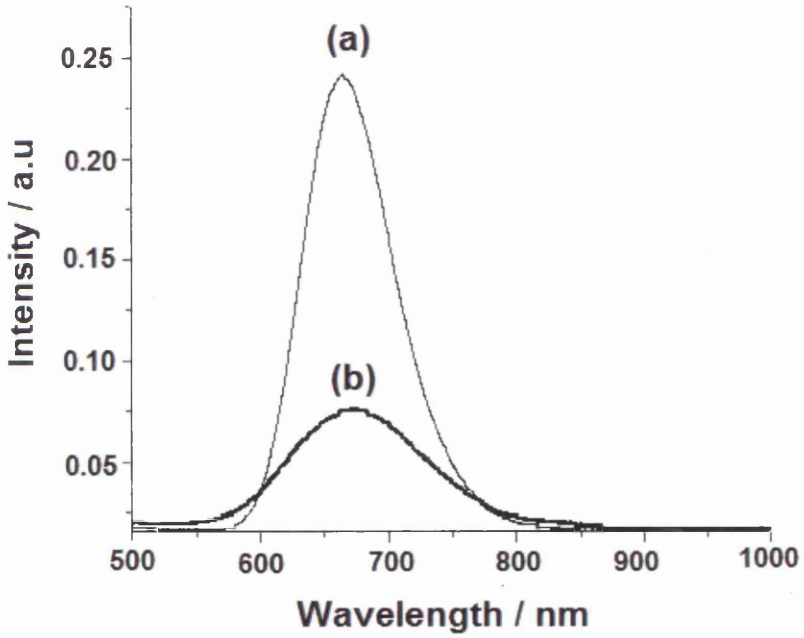

1

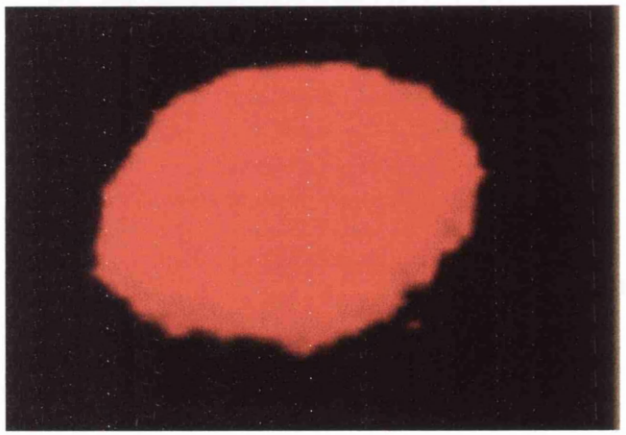

2

Figure 4.9: 1) Solid state (a) RT and (b) 77 K emission spectra of **3** with 355 nm excitation; 2) a photograph of the cherry red luminescence of complex **3** at RT with UV illumination.

4.3.1.2 Time resolved emission studies

Data from time resolved studies of **3** are collected in Table 4.3 At room temperature the decay kinetics of **3** using 355 nm excitation and collecting at emission wavelengths between 580-780 nm were analysed. The most intense signal was at 700 nm for which the decay fitted good first order kinetics from which the lifetime was calculated as 3.2×10^{-6} s. The kinetics of the decay were the same across the spectrum between the wavelengths investigated as shown in Figure 4.10. At 77 K the most intense signal was at *ca.* 710 nm (see Figure 4.11) for which a lifetime of 1.67×10^{-5} s was calculated when considering the decay to be first order.

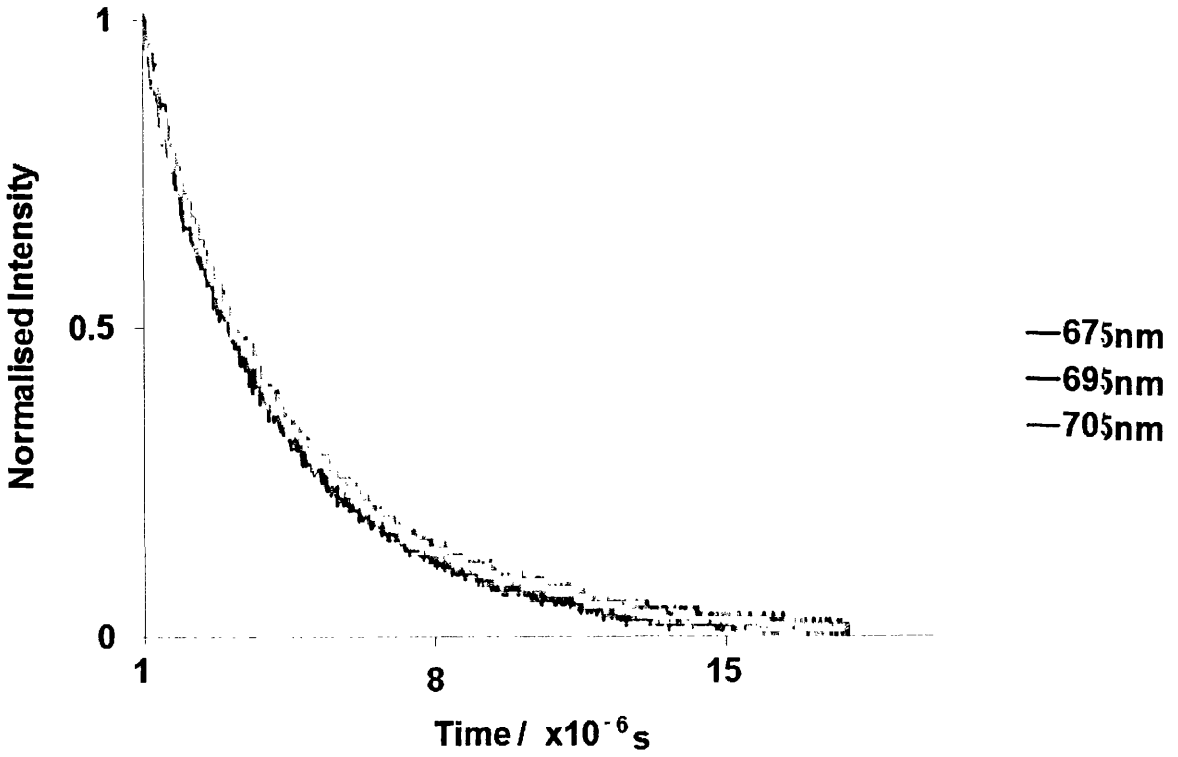

Figure 4.10: RT solid state decay curves for **3** at 675 nm, 695 nm and 705 nm. Excitation wavelength = 355 nm.

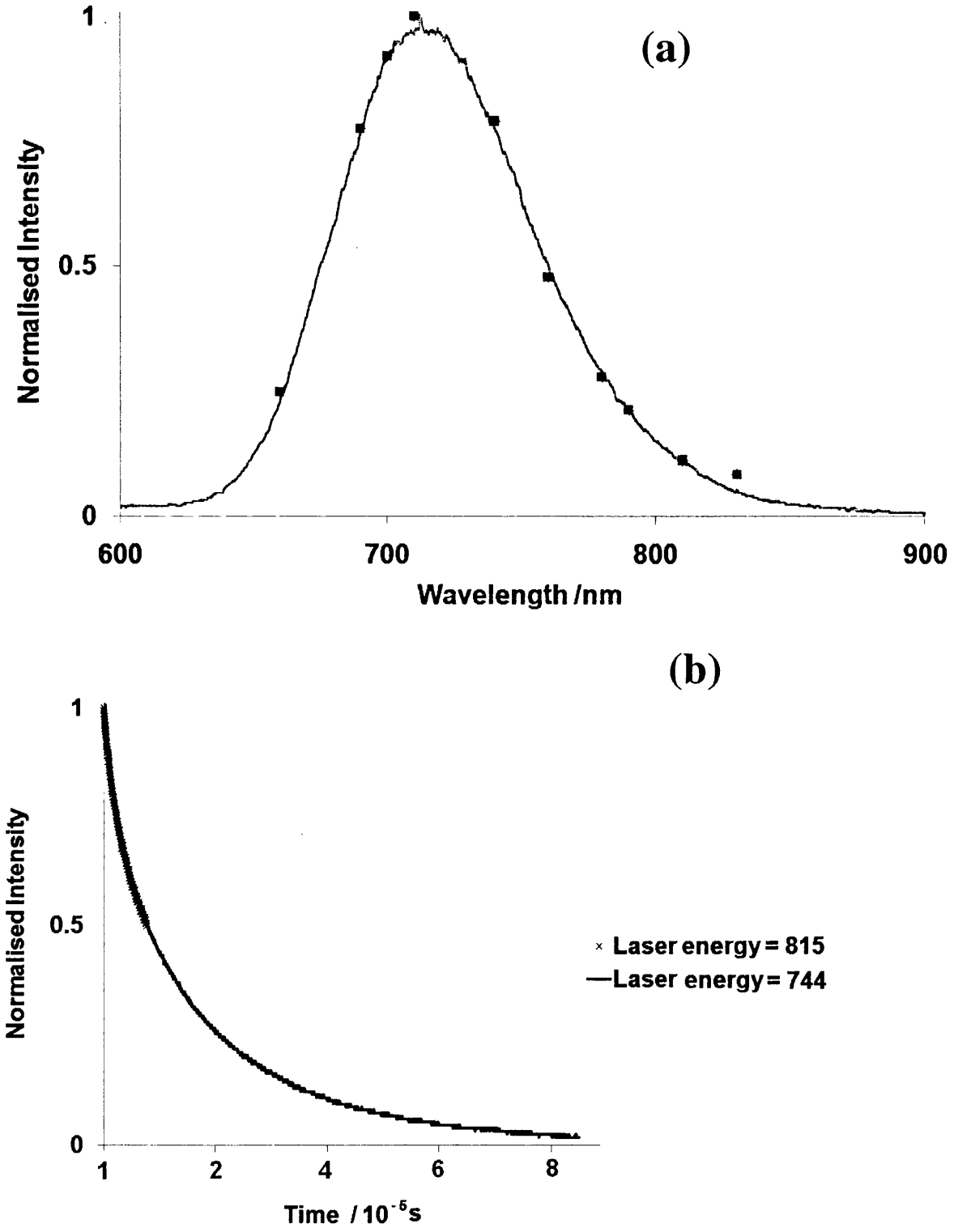

Figure 4.11: Emission spectrum and decay curves for compound **3** at 77 K. (a) Emission spectrum with points from the decay curve taken after 5×10^{-6} s at the corresponding emission wavelengths; (b) overlap of decays at different laser energies. In all cases 355 nm excitation was used.

4.3.1.3 Attempts to study ***3*** *in solution: emission from a suspension of microcrystallites?*

Due to the poor solubility of **3** at RT pure solution phase studies were not successful; all samples showed light scattering due to the presence of microcrystallites. However, we did examine the photochemistry of these samples in the hope that enough material would be dissolved to show some solution phase characteristics. Upon freezing the sample the emission spectrum shown in Figure 4.12 was obtained. The broad band emission has a λ_{max} of 628 nm. Upon freezing the solution the solid is seen to precipitate out upon the formation of the DCM snow

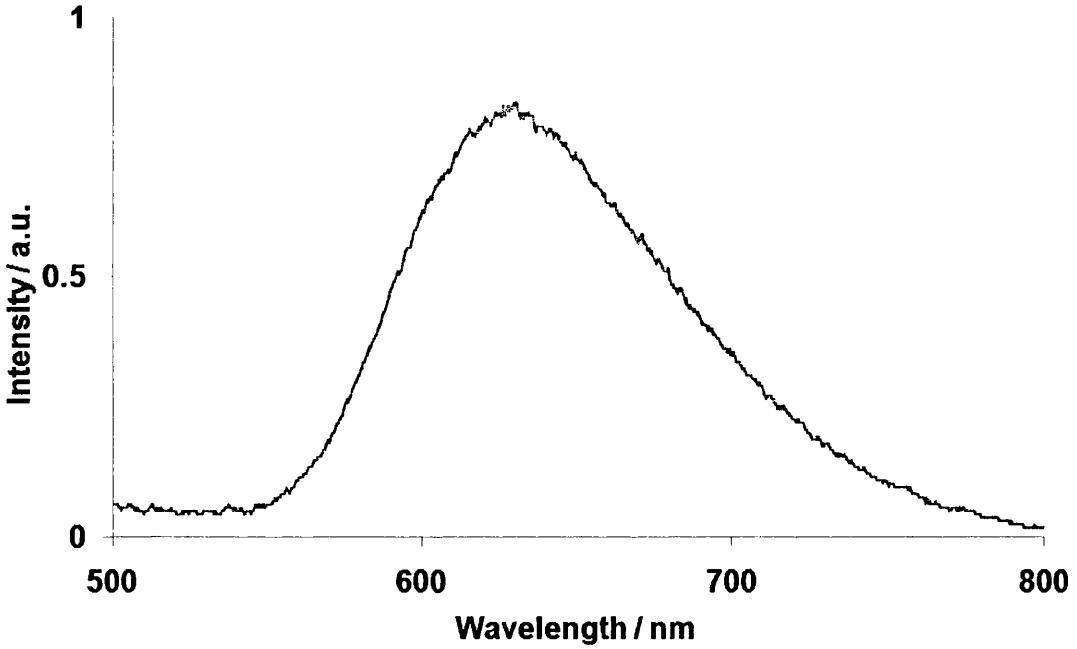

Figure 4.12: Emission spectrum of compound **3** at 77 K in frozen DCM solution. Excitation wavelength = 355 nm.

In addition to the broad band emission seen in the red region of the emission spectrum, there was also a structured emission in the blue region. This is shown in Figure 4.13 below: The emission consists of three definite bands at 431 nm (23,158 cm^{-1}) , 450 nm (22,212 cm^{-1}) and 471 nm (21,199 cm^{-1}). The energy spacings between the levels are 946 cm^{-1} and 658 cm^{-1}

respectively. It should be noted that Figures 4.12 and 4.13 are parts of the spectrum of the same compound. The red emission shown in Figure 4.12 is more intense than the blue emission shown in Figure 4.13. The two parts of the spectrum are presented separately in order to show both emissions more clearly.

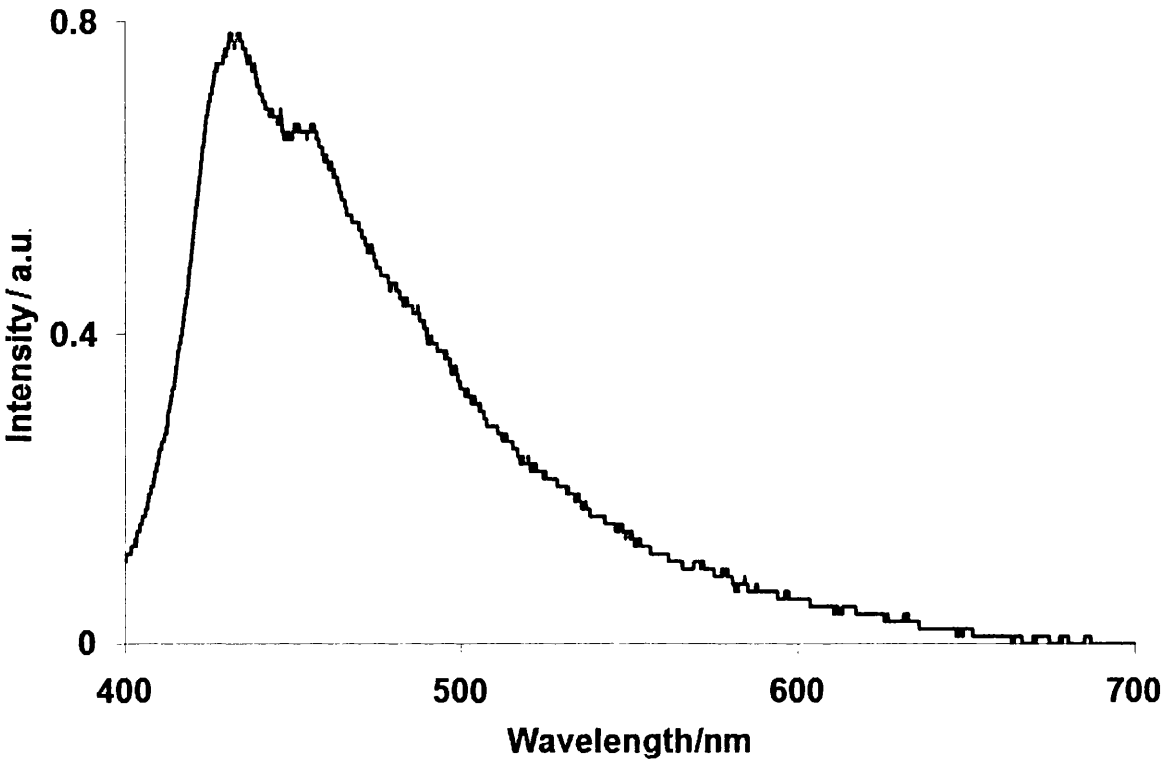

Figure 4.13: Emission spectrum of 1 in DCM at 77 K. Excitation wavelength = 385 nm.

4.3.1.4 Time Resolved Studies

The formation of aggregates in solution made a decay measurement of compound **3** difficult at RT in DCM solution. However, at 77 K a measurement was possible. The decay curve is shown in Figure 4.14. This fitted first order kinetics with a rate constant (k) of 37800 s^{-1} and a lifetime of 26 μs (a = 0.005 and b = 0.990)

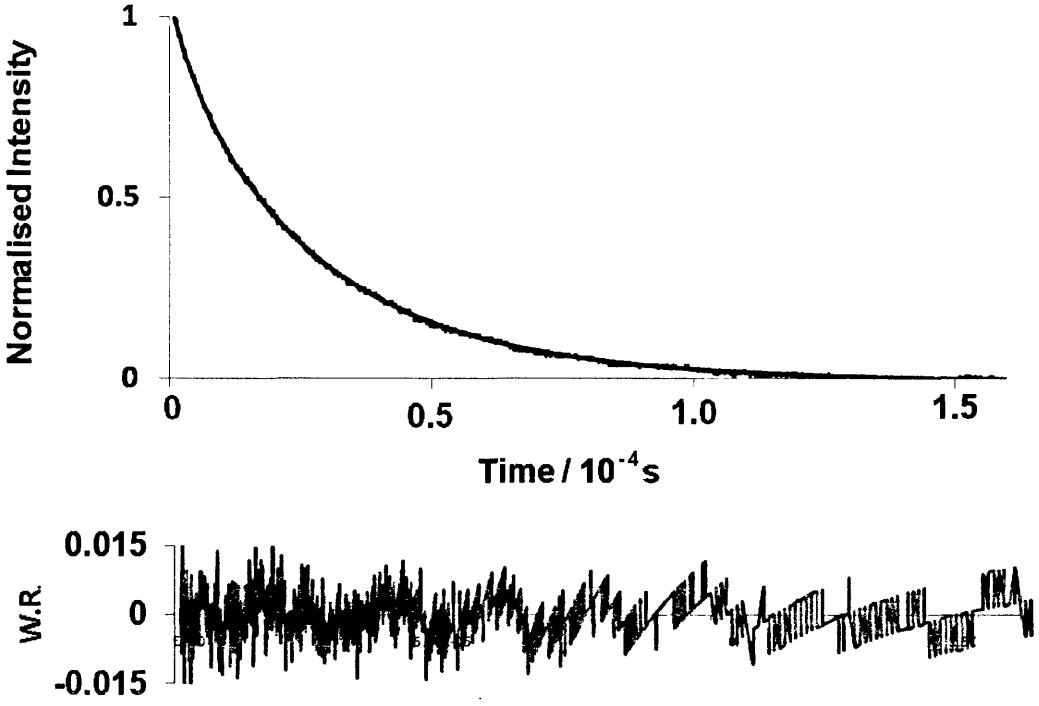

Figure 4.14: Normalised decay curve and residuals of a first order fit for compound **3** in DCM solution. Collecting at 650 nm with 355 nm excitation.

4.3.2 Solution Phase Studies

4.3.2.1 Absorption Spectroscopy

Absorption data for **4**, **5**, **6**, **7**, and **8** are collected in Table 4.1. All compounds are yellow in the solid state and form yellow solutions in acetonitrile, toluene and DCM.

All five compounds dissolve well in toluene and acetonitrile and show absorption bands in the UV and visible. No obvious signs of aggregation in solution were observed. Linear Beer-Lambert plots were obtained for compounds **4**, **5**, **6**, **7**, and **8** in toluene solution of concentration 1×10^{-4} M to 5×10^{-5} M in cells of path lengths 1 mm to 4 cm. In general the absorption spectra are made up of a strong absorption in the UV between 200-250 nm, with weaker UV bands between 250 and 350 nm, and then weaker absorptions tailing out into the

visible. The high oscillator strengths (*f*) of the 200-250 nm bands indicate fully spin-allowed transitions, whereas the weaker visible bands suggest moderately allowed to forbidden transitions. There is an interesting difference in absorption spectra between those complexes with chelating ligands, **6**, **7**, and **8**, and those with non-chelating ligands **4**, **5** and **10** in that the spectra of the latter show a very distinct absorption band at *ca.* 315 nm in MeCN.

As seen in Figure 4.15, there is a red shift in the lowest energy absorption band for compound **6** in comparison to **4** . This is perhaps a result of distortion at the Pt imposed by the chelating diphosphine. [32] Figure 4.16 shows the absorption of **4** and **6** in toluene solution.

As seen in Chapter 3 the palladium diselenolenes $[Pd_2(Se_2C_8H_{12})_2(PBu_3)_2]$ and $[Pd_2(Se_2C_8H_{12})_2(PPh_3)_2]$ show strong absorption bands in both the UV and visible regions; in comparison compounds **4**, **5**, **6**, **7** and **8** absorb relatively weakly in the visible region with the absorption maxima being in the UV region only. The assignment as LMCT for the low energy bands of both complexes was based on the positions of these absorption maxima. Since platinum is more difficult to reduce than palladium, a LMCT band would, all other factors being equal, be expected to be at higher energy (*i.e.* blue shifted) for a Pt complex compared to the Pd analogue. The assignment was also supported by the fact that the lowest excited state of a related series of bis(phosphine)platinum dithiolenes investigated by Eisenberg and co-workers has LMCT character.[37] There are some major differences between the two systems however: firstly the change from sulphur to selenium makes the ligand more electron rich; secondly, the dithiolenes concerned carry electron-withdrawing substituents, which make them better π-acceptors.[32] DFT calculations suggest the lowest energy states are, in fact, of LLCT character.

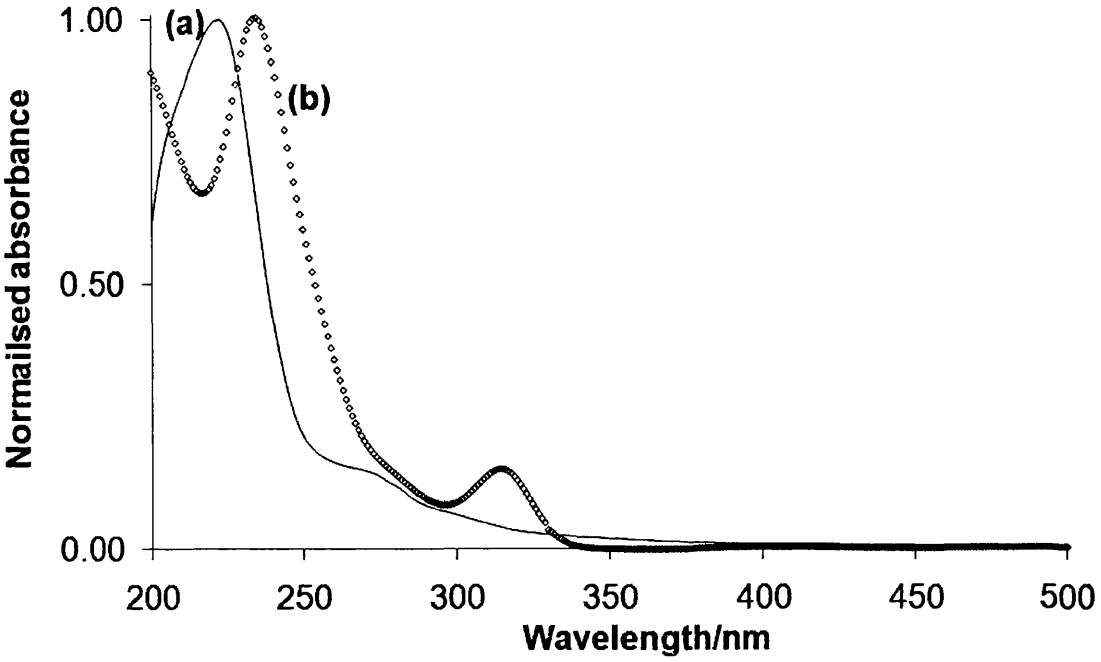

Figure 4.15: Absorption spectra of (a) **6** and (b) **4** in acetonitrile solution.

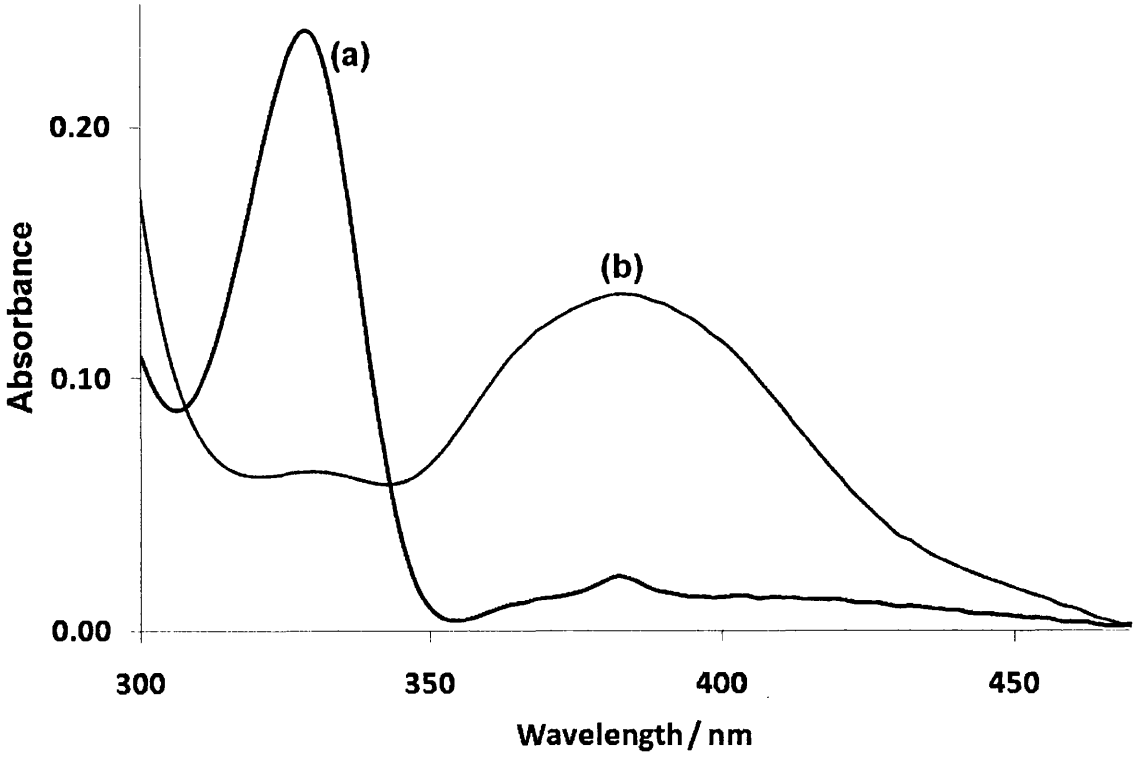

Figure 4.16: Absorption spectra of (a) **6** and (b) **4** in toluene solution.

solvent	*compound*											
	6 dppm				**7** dppe		**8** dppp		**4** PEt_3		**5** PBu_3	
	λ_{exc}/nm	λ_{abs}/nm	$\varepsilon/10^4 M^{-1}cm^{-1}$	*f*	λ_{abs}/nm	$\varepsilon/10^4 M^{-1}cm^{-1}$	λ_{abs}/nm	$\varepsilon/10^4 M^{-1}cm^{-1}$	λ_{abs}/nm	$\varepsilon/10^4 M^{-1}cm^{-1}$	λ_{abs}/nm	$\varepsilon/10^4 M^{-1}cm^{-1}$
toluene		286 330 384	5.17 ± 0.09 2.63 ± 0.01 1.33 ± 0.02	0.69 0.02 0.005	288 358 386	4.64 ± 0.06 1.06 ± 0.13 0123 ± 0.02	288 334 328	5.09 ± 0.08 1.59 ± 0.02 0.26 ± 0.001	286 328 382	5.12 ± 0.09 1.53 ± 0.001 0.65 ± 0.06	292 324 388	3.81 ± 0.04 1.81± 0.001 0.04 ± 0.001
acetonitrile [a]	377 418 497 532	223 276 313(sh) 382 420	5.12 ± 0.09 2.53 ± 0.08 1.65 ± 0.06 1.30 ± 0.001	0.64 0.09 0.05 0.001	224 286 305(sh) 422	5.42 ± 0.09 2.83 ± 0.001 1.11 ± 0.06 0.002 ± 0.001	220 276 307(sh) 420	5.11 ± 0.09 2.51 ± 0.001 0.006 ± 0.001	198 235 318 420	4.86 ± 0.09 2.93 ± 0.001 1.41 ± 0.06 0.05 ± 0.001	198 236 314 422	4.52 ± 0.09 1.32 ± 0.001 1.32 ± 0.06 0.04 ± 0.001
DCM[b]		365	1.37		350	1.35	325	1.41	320	1.47	320	1.55

(a) excitation spectrum of **6** was only recorded from 300 nm.

(b) not from this work. [32]

Table 4.2: Absorption data

4.3.2.2 Steady state emission studies

Emission data are collected in Tables 4.3 and 4.4 .Initial studies on all compounds were done using a 355 nm excitation wavelength. At this excitation wavelength in nitrogen-purged toluene solution all compounds showed narrow emission bands at *ca.* 650-660 nm. Representative spectra of **6** and **5** are shown in Figure 4.17. The emission is completely quenched by oxygen (see Table 4.3) and therefore can probably be assigned as molecular phosphorescence. It can be seen for **6** that there is also a weak shoulder present at *ca.* 700 nm, which is probably vibronic in origin.

In addition, structured bands superimposed on a broad tailing emission from the blue to green spectral region that do not disappear in aerated solution are also present. These are assigned to molecular fluorescence. This is shown in Figure 4.18.

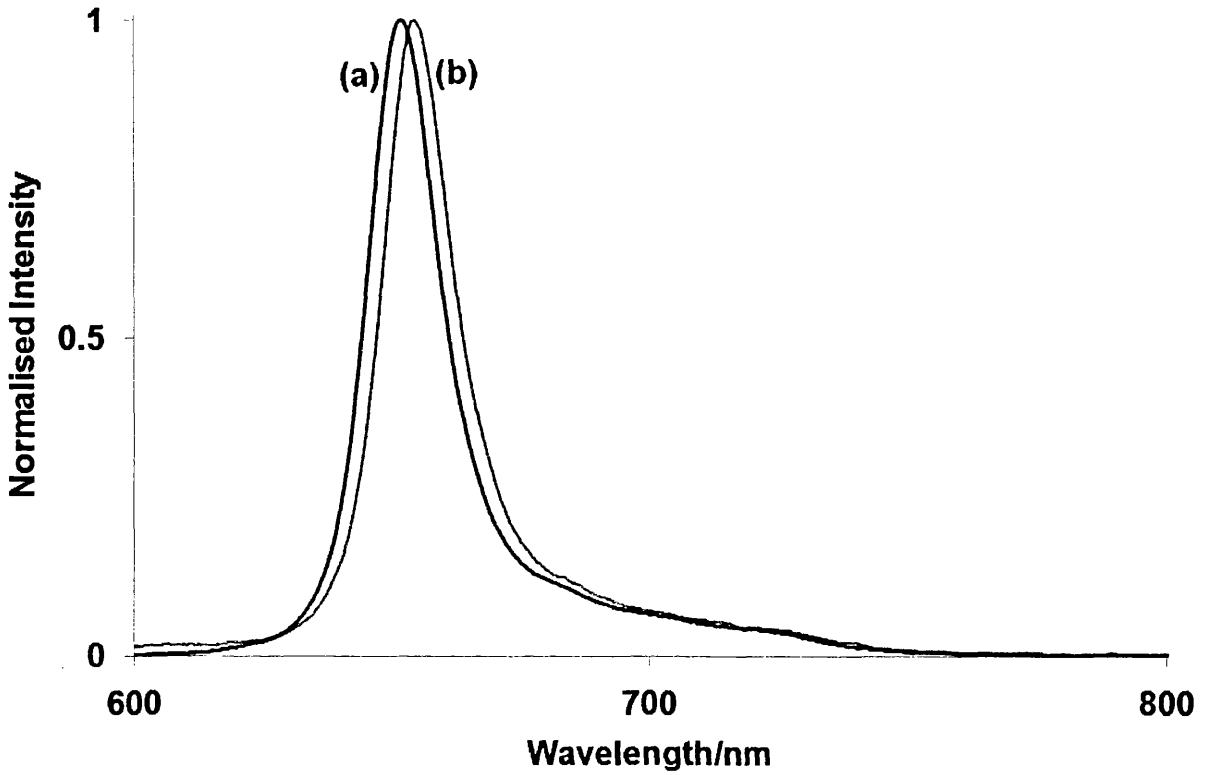

Figure 4.17: Emission spectrum of (a) **4** and (b) **6** at RT in nitrogen-purged toluene. solution. Excitation wavelength = 355 nm. Measurements were made using a 430 nm cut-off filter on the excitation monochromator. Both specrum are corrected.

In more detailed work another weak emission at *ca.* 550 nm which is *ca.* 75% quenched by oxygen was also observed. Figure 4.18 shows the full solution phase emission spectrum of **6**. Although the spectra from UV excitation are dominated by fluorescence for which the quantum yield is *ca.* 7%, it is possible to generate emission at the 550 nm and 650 nm bands using visible excitation (*ca.* 420 nm and 532 nm), and since the absorption of the sample in the visible is extremely small the quantum yield for visible excitation must be very high. By comparison with TPP as emission standard, and using either 355 or 347 nm excitation the emission quantum yield in toluene for **6** is calculated as 0.07 ± 0.001. Typical spectra of **6** using 355 and 532 nm excitation are shown in Figure 4.19. In addition, as seen in Table 4.3,

the position of the emission maximum of the sharp band does not change upon changing the ring size from C_8 to C_7 (*e.g.* compare **5** and $[Pt(Se_2C_7H_{10})(PBu_3)_2]$).

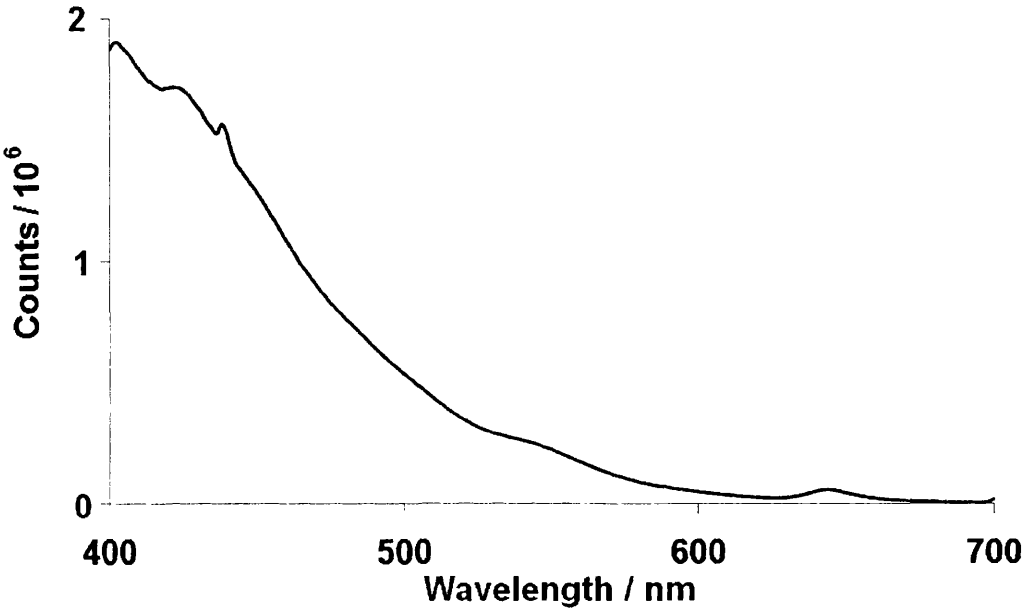

Figure 4.18: Emission spectrum of **6** at RT in nitrogen-purged acetonitrile solution. Excitation wavelength = 385 nm.

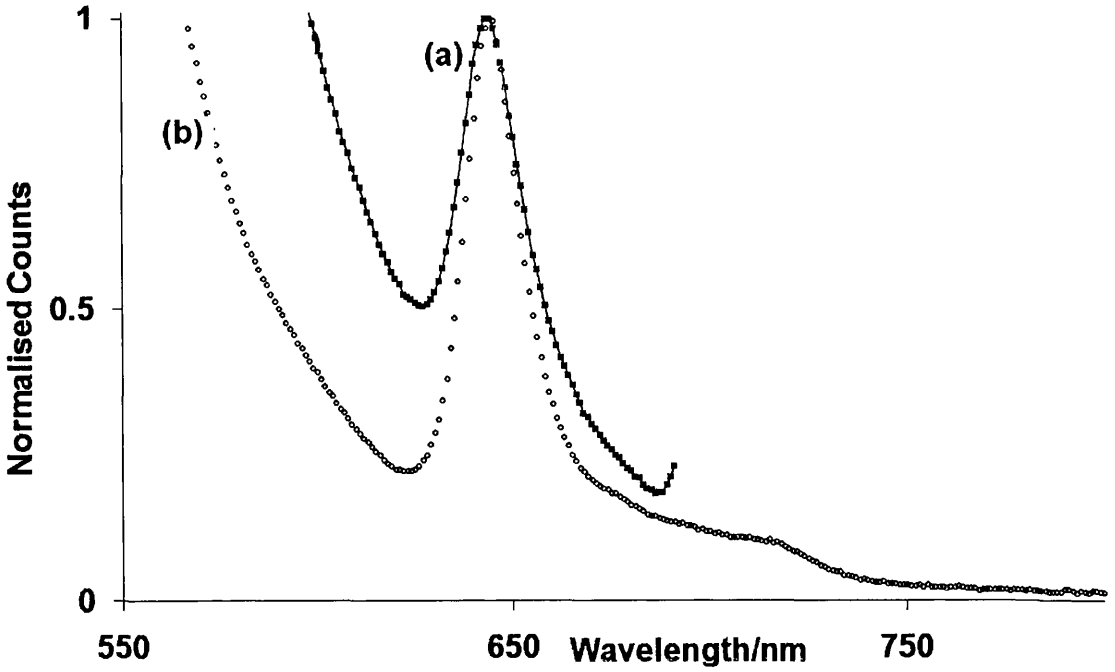

Figure 4.19: Emission spectrum of **6** in nitrogen-purged acetonitrile solution at (a) 355 nm excitation wavelength and (b) 532nm excitation wavelength.

compound	λ_{exc}/nm	emission in nitrogen-purged room temperature toluene					EDT glass		solid state			
									298 K		77 K	
		λ_{emi}/nm	$\tau_0/10^{-6}$s	Φ_{phos}	Φ_{flu}	Φ_{Δ}	λ_{emi}/nm	$\tau_0/10^{-6}$s	λ_{emi}/nm	$\tau_0/10^{-6}$s	λ_{emi}/nm	$\tau_0/10^{-6}$s
6 dppm	355	645	80 ± 0.2	0.0007	0.007	0.05	600(broad) 645(narrow)	11.8 ± 0.4 60.8 ± 0.7	640	1.89 ± 0.04	640	20.1 ± 0.5
	532	644	79 ± 0.2				650	60.1 ± 0.4	640	1.92 ± 0.01	640	23.4 ± 0.04
7 dppe	355	662	87 ± 0.3		0.005		581	22.8 ± 1.4			619	14.7 ± 0.90
	532	662	83 ± 0.3				580	25.1 ± 0.42			620	15.1 ± 0.14
8 dppp	355	649	55± 0.2		0.006		610	22.7 ± 2.5		1.51 ± 0.05	556	14.1 ± 0.90
	532	650	48 ± 0.2				610	26.1 ± 0.45		1.64 ± 0.03	560	15.0 ± 0.05
4 PEt_3	355	649	50 ±0.2		0.005		600	22.5 ± 1.1		3.45 ± 0.02	675	16.7 ± 0.7
	532	650	50 ± 0.3				600	27.4 ± 0.32		3.21 ± 0.02	675	17.4 ± 0.02

Table 4.3: Photochemical data for **4**,**6**, **7** and **8**.

compound	emission in nitrogen-purged room temperature toluene				emission in ethanol: diethylether:toluene (1:2:1) glass at 77 K		emission in the solid state			
							298 K		*77 K*	
	λ_{max}/nm	$\tau/10^{-6}$ s	$k_q/30^{30}$ M^{-1} s^{-1}‡	Φ_{phos}	λ_{max}/nm	$\tau/10^{-6}$ s	λ_{max}/nm	$\tau/10^{-6}$ s	λ_{max}/nm	$\tau/10^{-6}$ s
[$Pt(Se_2C_8H_{12})(PPh_3)_2$] (3)							675	3.21 ± 0.02	675	16.7 ± 0.7
[$Pt(Se_2C_8H_{12})$(dppm)] (6)	647	80 ± 2	1.08‡	0.094 ± 0.004	600 (broad) 645 (narrow)	11.8 ± 0.4 60.1 ± 0.7	630	1.89 ± 0.04	619	20.1 ± 0.5
[$Pt(Se_2C_7H_{10})(PBu_3)_2$] (10)	647	50 ± 1			614	18.3 ± 0.7			672*	14.2 ± 0.5
[$Pd(Se_2C_8H_{12})(PBu_3)]_2$ (5)	645	55 ± 2			758	18.5 ± 0.9	775†	1.85 ± 0.02	770	18.7 ± 0.4

‡ from a comparison of emission lifetimes in nitrogen-purged and air-equilibrated solutions.
* excitation at 470 nm.
† from emission spectrum recorded using 355 nm laser excitation.

Table 4.4: Photochemical data for compounds **3**, **6**, **10** and **5**.

4.3.2.3 Time-resolved emission studies

The assignment of emission as molecular phosphorescence was further confirmed by its long lifetime for all the compounds studied (see Table 4.2) and the observation that it is quenched by oxygen at the diffusion-controlled rate (see Table 4.3).

Either 355 nm or 532 nm laser excitation generates the *ca.* 650 nm emission band which decays over the 10^{-4} s timescale. The uncorrected point-by-point emission spectrum recorded 1 μs after the laser pulse is shown superimposed on the steady state emission in Figure 4.20.

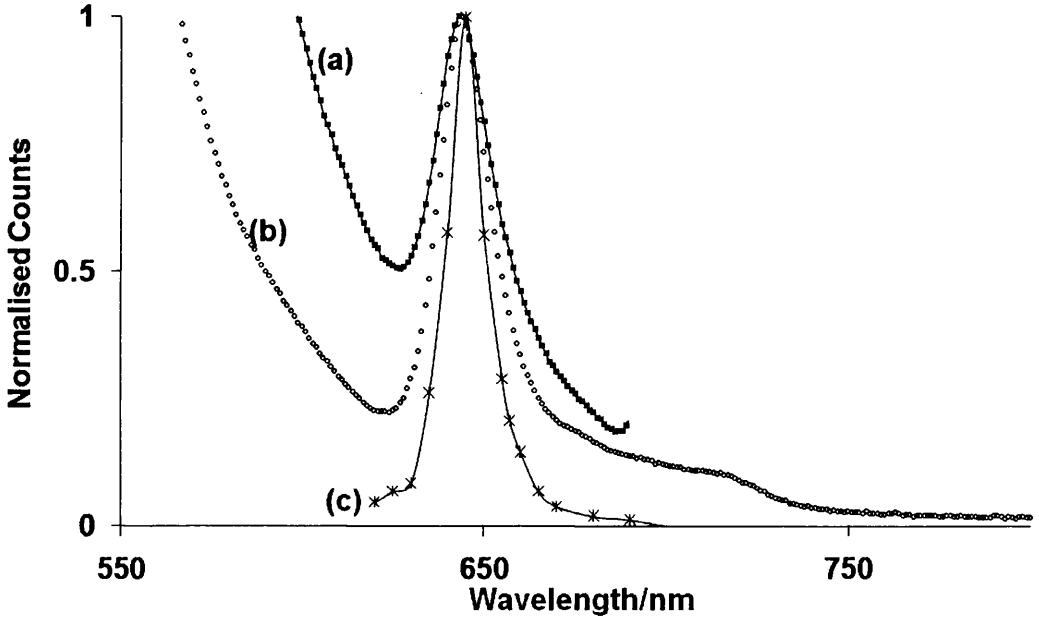

Figure 4.20: Steady state and time-resolved emission spectra of **6** in nitrogen purged toluene solution: (a) corrected steady state with 355 nm excitation; (b) corrected steady state with 532 nm excitation; (c) uncorrected point-by-point spectrum recorded with the laser using 355 nm excitation.

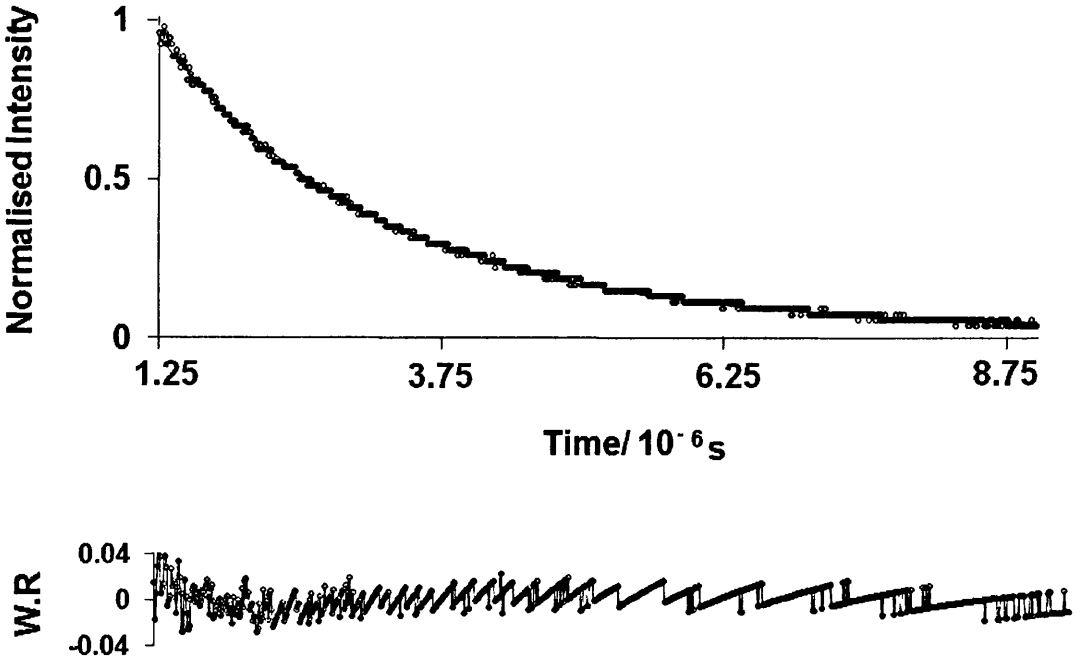

Figure 4.21: Decay curve and residuals for emission decay of **6**. Emission wavelength = 550 nm. Excitation wavelength = 355 nm.

The behaviour of **6** was examined in more detail than that of the other compounds. For **6** the decay kinetics of the band at 550 nm (Figure 4.21) gave an emission curve with a best fit first order lifetime of *ca.* 2 μs, but a statistically better fit to a double exponential with lifetimes of 0.5 μs and 2 μs, and relative contributions of 45% and 55% respectively. The emission in the 420-500 nm region is much shorter lived, and too fast for the detection limits of the ns laser equipment used, *i.e. ca.* 50 ns.

Table 4.2 collects kinetic and emission data recorded at *ca.* 650 nm. For all compounds, decay kinetics are single exponential, the same across the emission band, and the same with either 355 or 532 nm excitation. The lifetimes range from *ca.* 50 μs (**7** and **8**) to *ca.* 80 μs (**6** and **5**). Combination of these lifetimes with the quantum yield data gives radiative lifetimes for phosphorescence of *ca.* 1-2 ms (see Table 4.2).

4.3.2.4 *Steady state excitation spectra*

The complexity of the emission spectra prompted a more detailed analysis. As shown in Figures 4.22 and 4.23 the excitation spectra are very significantly different for detection at the different emission wavelengths corresponding to fluorescence (437 nm detection) or phosphorescence (650 nm detection), and at 550 nm. The excited state which is the origin of the 650 nm emission is populated by absorption into two groups of bands: (i) bands across the 500-600 nm range with a maximum at 532 nm and a very weak band at 595 nm (see Figure 4.25), and (ii) two bands at 380 and 420 nm, which may well be vibrational levels (ΔE = 2061 cm^{-1}) of one electronic transition.

The state from which *ca.* 550 nm emission occurs is predominantly populated from bands in the 500-550 nm range. Our first thoughts were that these were the same as those of group (i) above. However this is not the case because, while the two excitation spectra in this region are similar, they are not identical: that for 550 nm emission shows a maximum at 525 nm compared to 532 nm for the excitation spectrum of the 650 nm band (see Figure 26) Furthermore they differ in shape, with much less separation between the main band and the secondary band/shoulder at 485 nm in the 550 nm excitation spectrum.

Fluorescence at *ca.* 440 nm is generated from the state(s) populated by the broad but structured band across the 300-400 nm range. It is perhaps worth noting that the excitation spectrum across the 300-450 nm region, for detection at 437 nm, is the same whether the solution is nitrogen-purged or air-equilibrated.

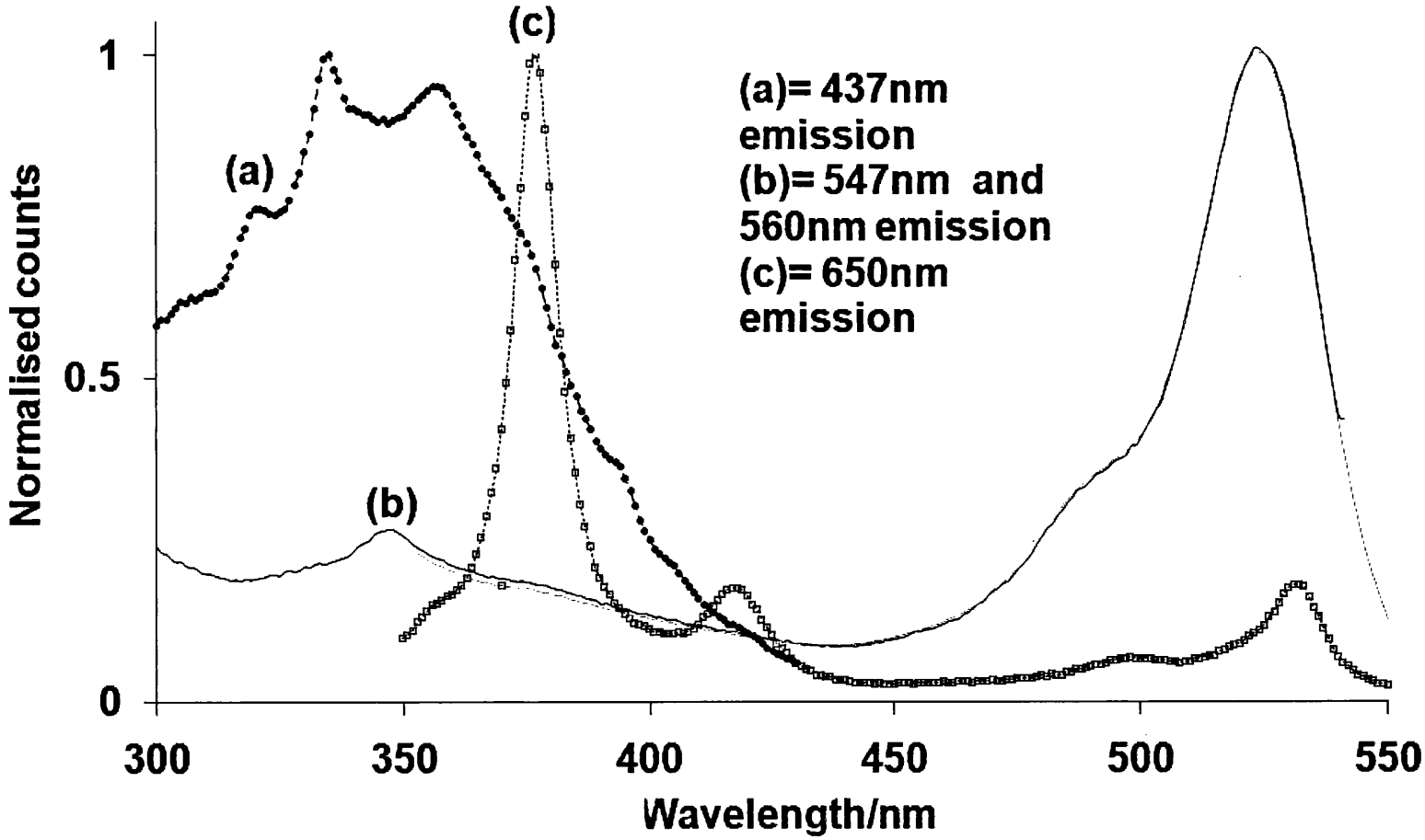

Figure 4.22: Excitation spectra of **6** at RT in degassed acetonitrile solution at different emission wavelengths.

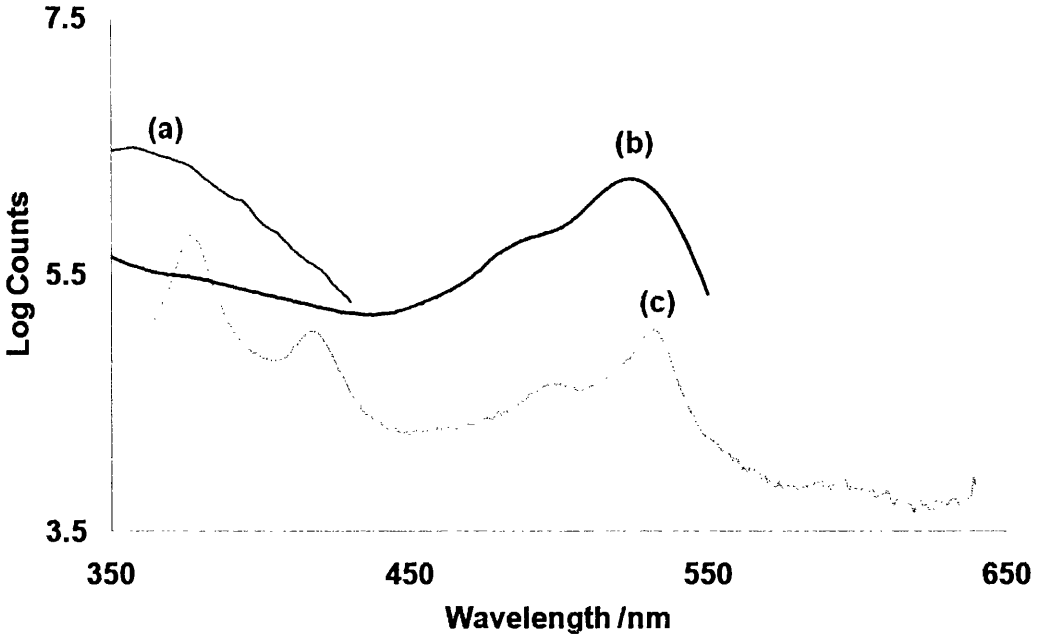

Figure 4.23: Excitation spectra of **6** at RT in degassed acetonitrile solution for detection at different emission wavelengths: (a) 437 nm; (b) 547 nm; (c) 650 nm. The emission intensity is given in logarithmic scale to facilitate comparison of emission bands of very different intensity.

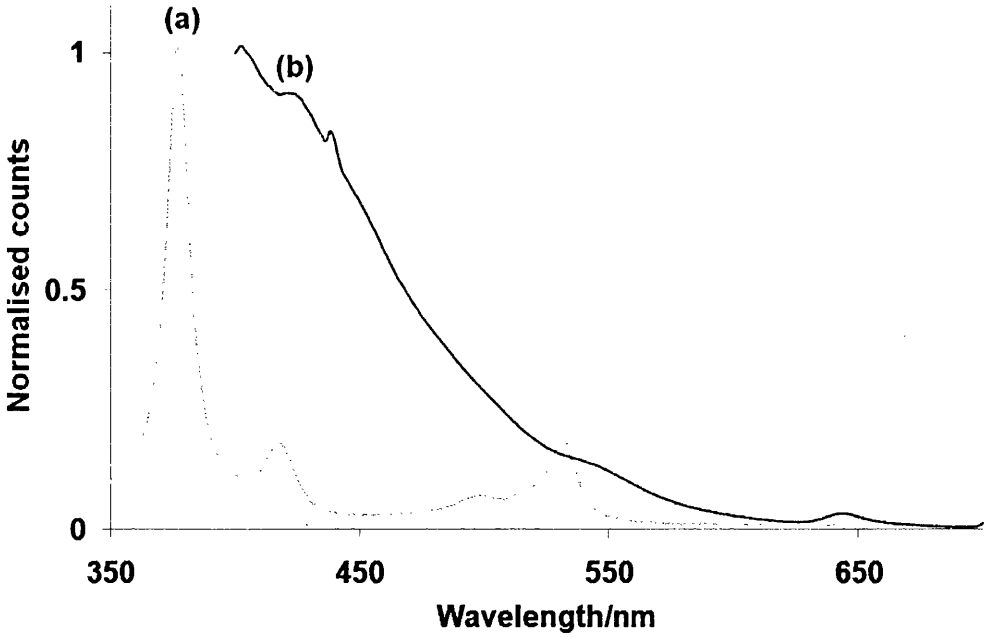

Figure 4.24: Spectra of **6** at RT in degassed acetonitrile solution: (a) excitation spectrum monitored at 650 nm emission wavelength; (b) emission spectrum for 355 nm excitation.

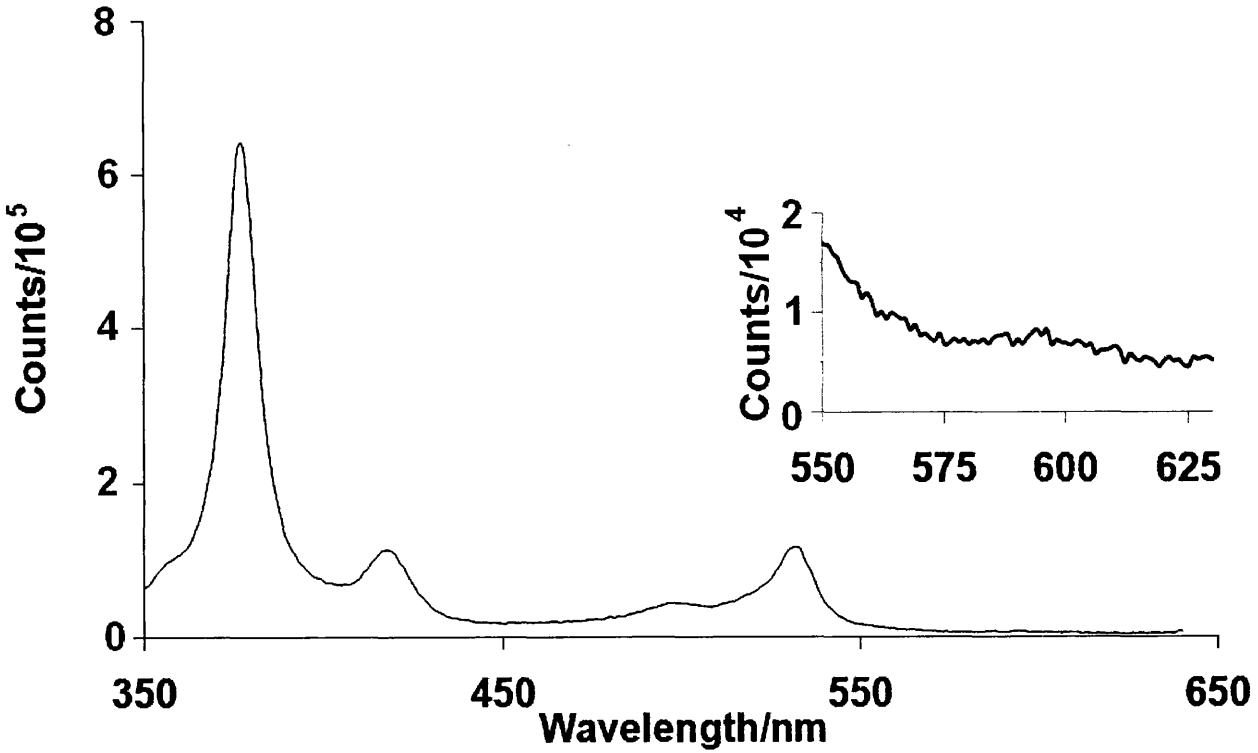

Figure 4.25: Excitation spectrum of **6** in degassed acetonitrile solution for detection at an emission wavelength of 650 nm. The inset shows, highly magnified, the response in the 550-650 nm region which shows the possibility of an additional band at *ca.* 595 nm.

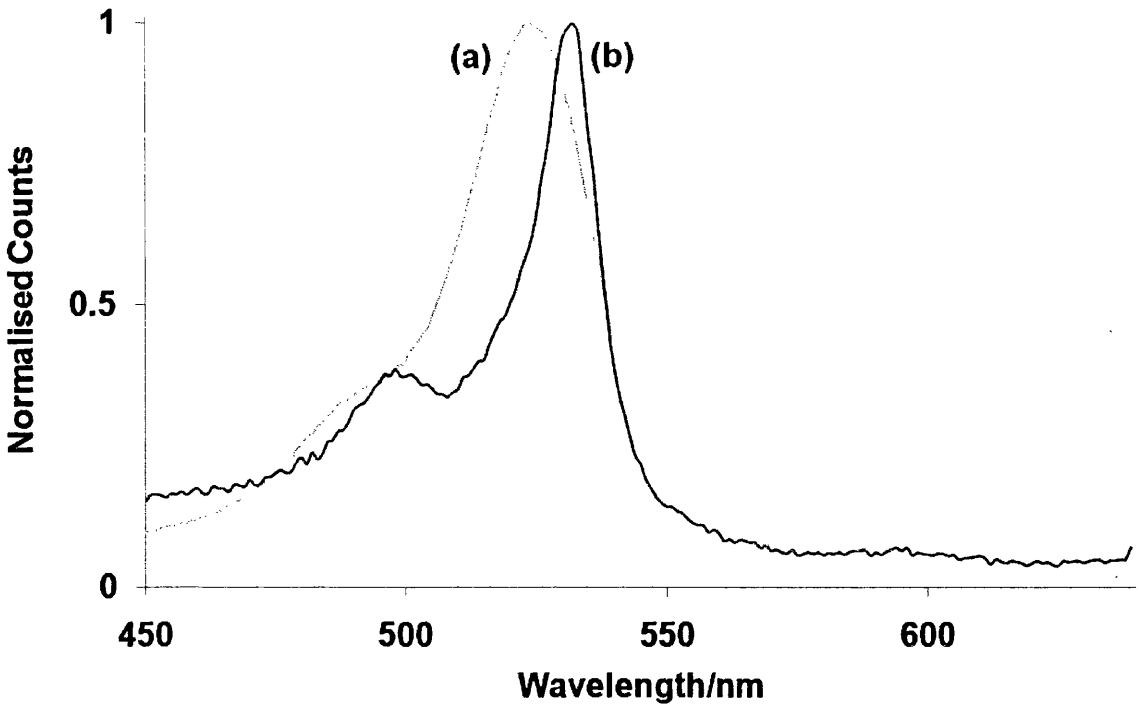

Figure 4.26: Normalised excitation spectra of **6** at RT in nitrogen-purged acetonitrile solution for: (a) 547 nm; (b) 650 nm emission wavelengths.

4.3.2.5 Transient absorption studies

In nitrogen-purged acetonitrile, **6** gives weak transient absorption changes ($\Delta A \leq \approx 0.01$) between 400-600 nm, with the strongest signal at 420 nm. As shown in Figure 4.27, this arises from two distinct transients: one short-lived and one long-lived. The quality of the data precludes the distinction between two independent processes and two processes in which the faster component is the precursor of the slower. A double exponential fit gives lifetimes of 1.42 ± 0.13 μs (α_1 = 0.023 ± 0.002) and 76 ±2 μs (α_2 = 0.01 ± 0.0002). The lifetime of the long-lived species is the same as that of phosphorescence emission within experimental error, and this transient is absent in air-equilibrated solution. There remains a weaker and shorter lived (τ = 0.64 μs) species even in air-equilibrated solution. It is tempting to associate this

and the shorter lifetime species observed under nitrogen with that responsible for the partially oxygen-quenched emission band at 550 nm.

In addition, a signal at 520 nm was detected. This is shown in Figure 4.28. This unlike the absorbance detected at 420 nm has no long-lived component just a short-lived component with a lifetime of *ca.* 0.70 ± 0.01 μs. This also disappears in aerated solution.

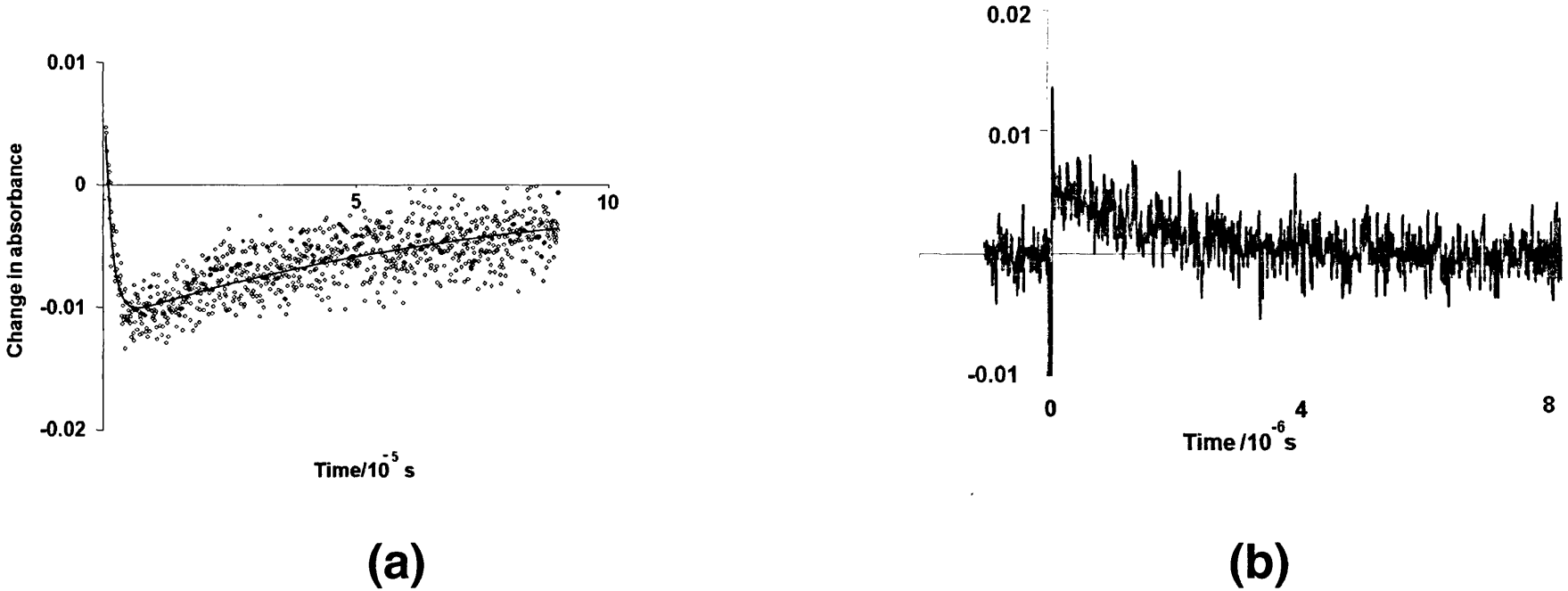

Figure 4.27: Transient absorbance of **6** in (a) nitrogen-purged, and (b) air-equilibrated acetonitrile solution at 355 nm excitation and 420 nm absorption. Note the difference in timescale for the two curves.

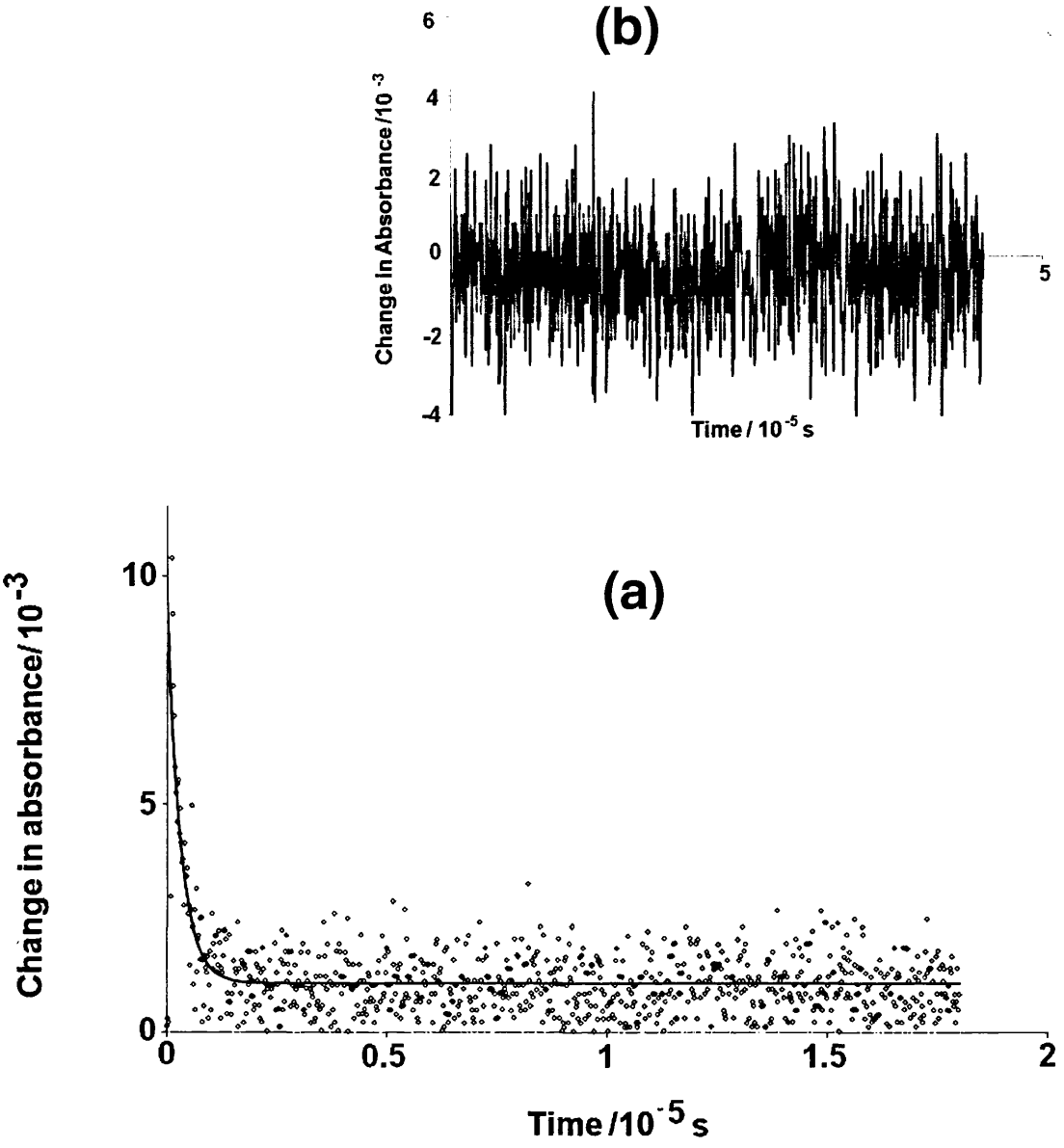

Figure 4.28: Transient absorbance of **6** at RT in (a) nitrogen-purged, and (b) air-equlibrated acetonitrile solution at 355 nm excitation and 520 nm absorption.

4.3.2.6 *Singlet oxygen studies*

Due to the long emission radiative lifetime it was thought worthwhile to investigate whether or not there is singlet oxygen formation upon photoexcitation, since this would help confirm the triplet character of the emission. For **6,** in air-equilibrated acetonitrile with 550 nm excitation, an emission across the wavelength range 1200-1350 nm was detected which was absent in nitrogen purged solutions, and which can therefore be reliably assigned to singlet oxygen (Figure 4.29 below). Comparison with emission from 9*H*-fluoren-9-one as standard (Φ_Δ = 0.42 in acetonitrile)[36] gives Φ_Δ = 0.005 for **6**, which is, as expected for such a long-lived phosphor, comparable to the phosphorescence yield (Φ_{phos} = 0.007).

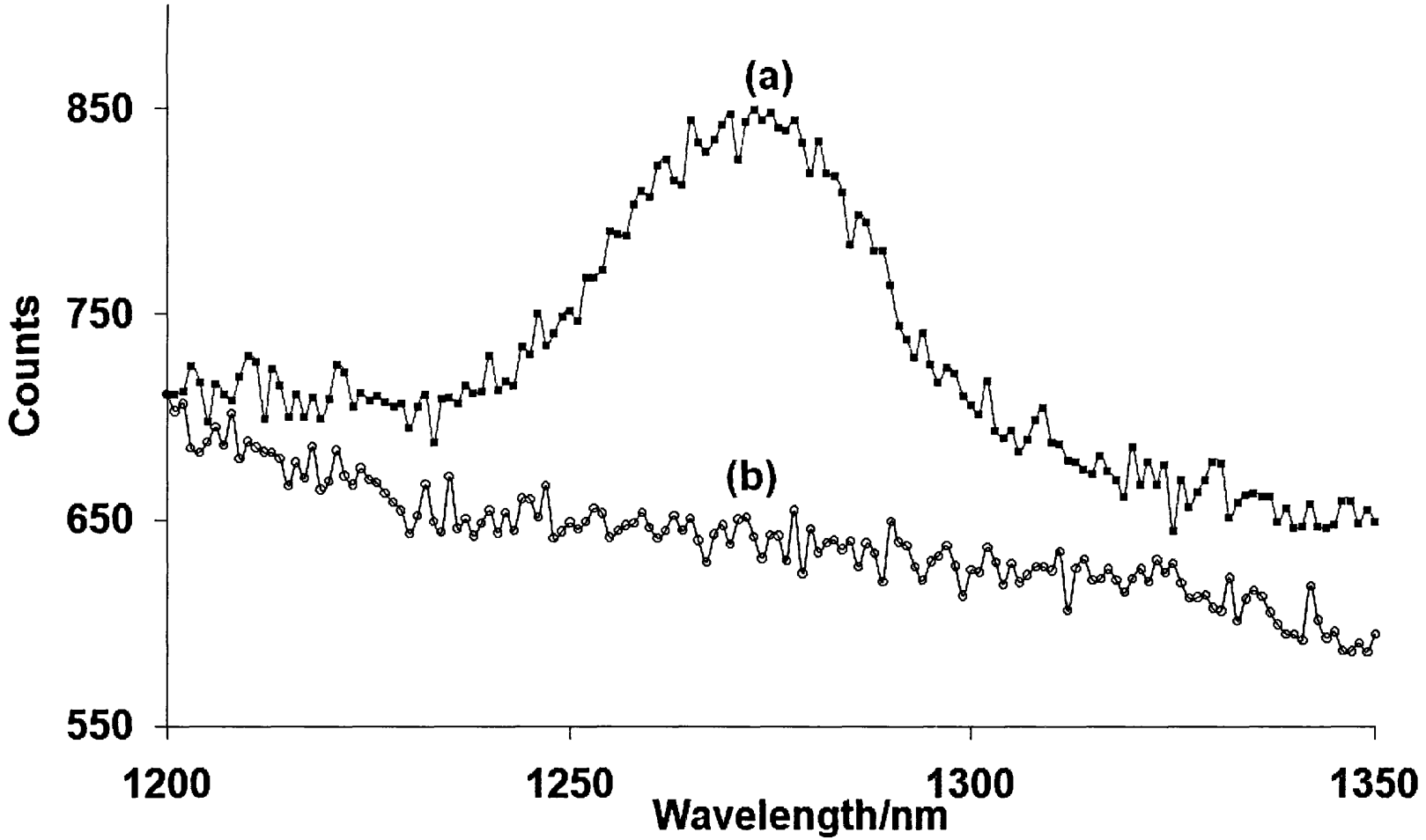

Figure 4.29: Near-IR emission spectra from irradiation of **6** at RT in (a) air-equilibrated acetonitrile solution, and (b) nitrogen-purged solution. Excitation wavelength = 532 nm.

4.3.3 Solid state studies

4.3.3.1 Steady state emission studies

Emission data for all compounds studied are collected in Tables 4.2 and 4.3. All compounds were examined for luminescence under steady state and pulsed laser UV (355 nm) and visible (532 nm) excitation in the pure solid state at RT and at 77 K, and also in EDT glass at 77 K.

In EDT glass, and in the pure solid, all compounds show structured fluorescence in the 420-480 nm range. This is shown for **6** in Figure 4.30 and 4.31, and **4** in Figure 4.32. In Figure 4.30 four bands are seen, at 421 nm (23,800 cm^{-1}), 442 nm (22,600 cm^{-1}), 454 nm (22,000 cm^{-1}) and 474 nm (21,100 cm^{-1}). The energies of the bands are not equally spaced so cannot be considered as a vibrational progression. Similar but not identical bands can be observed, with varying degrees of structure, even when the broad orange/red emission is absent. The short lifetime and position suggest this feature is S_n to S_0 fluorescence.

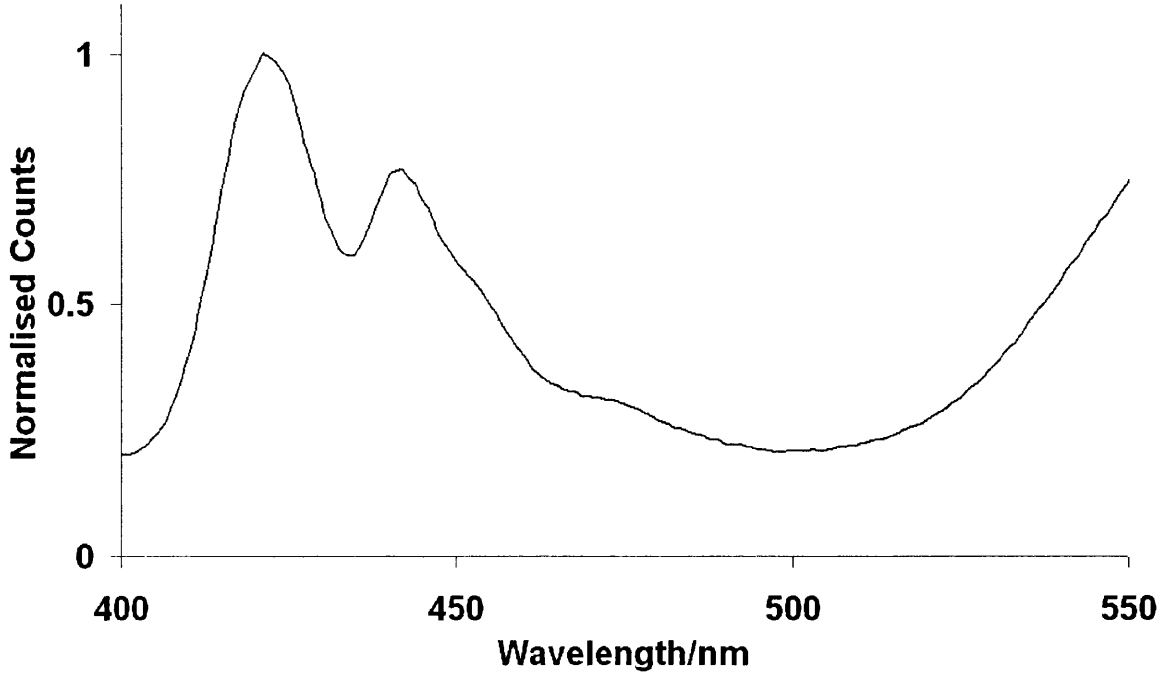

Figure 4.30: Fluorescence spectrum of **6** in an EDT glass at 77 K. Excitation wavelength = 355 nm.

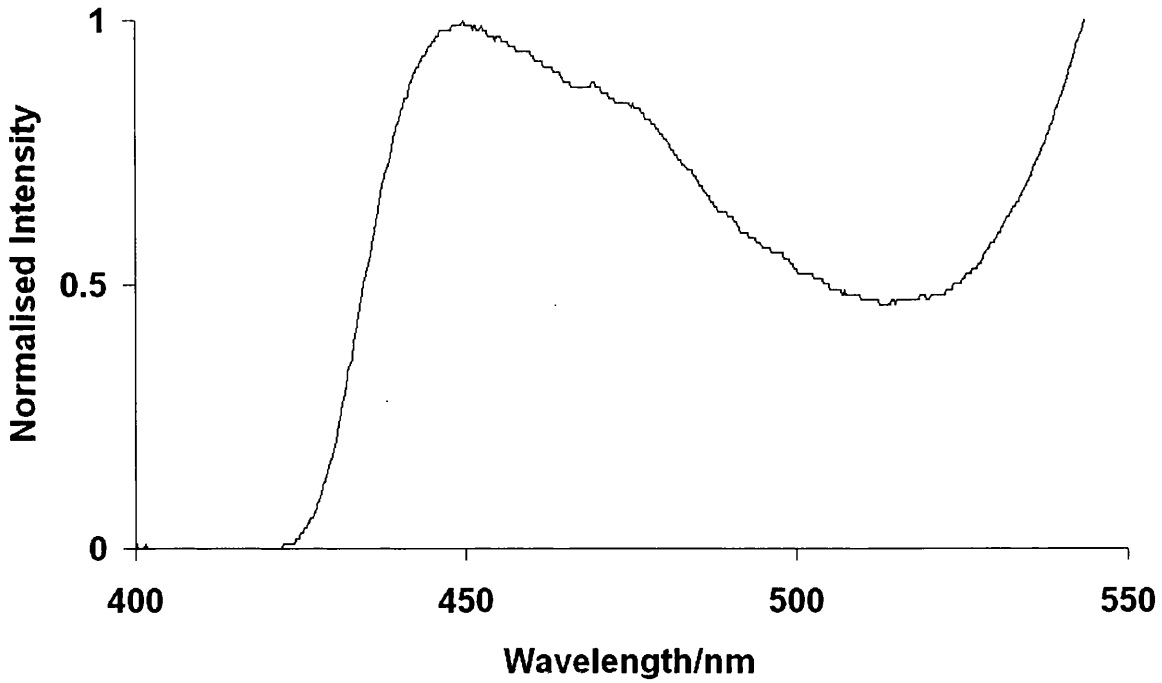

Figure 4.31: Fluorescence spectrum of **6** in the solid state at 77 K. Excitation wavelength = 355 nm.

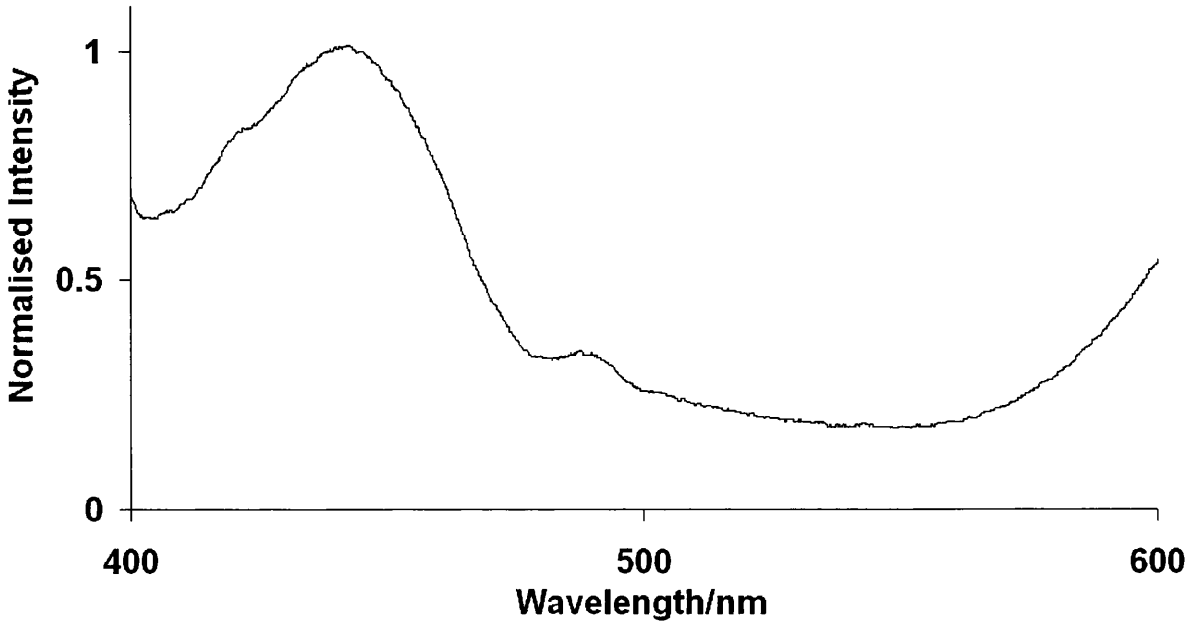

Figure 4.32: Solid state RT fluorescence spectrum of **4**. Excitation wavelength = 355 nm.

In the solid state at 77 K all the complexes exhibit long-lived intense emission in the 550-750 nm range. Emission decays are acceptable fits to single exponentials with lifetimes of *ca.* 14-20 μs. The emission spectra are all broad and structure-less (Figure 4.33) but show emission maxima ranging from *ca.* 550-680 nm depending upon the ligands. Only **5** and **6** show strong emission in the solid state at RT, which is even broader than that at 77 K and is somewhat reduced in intensity.

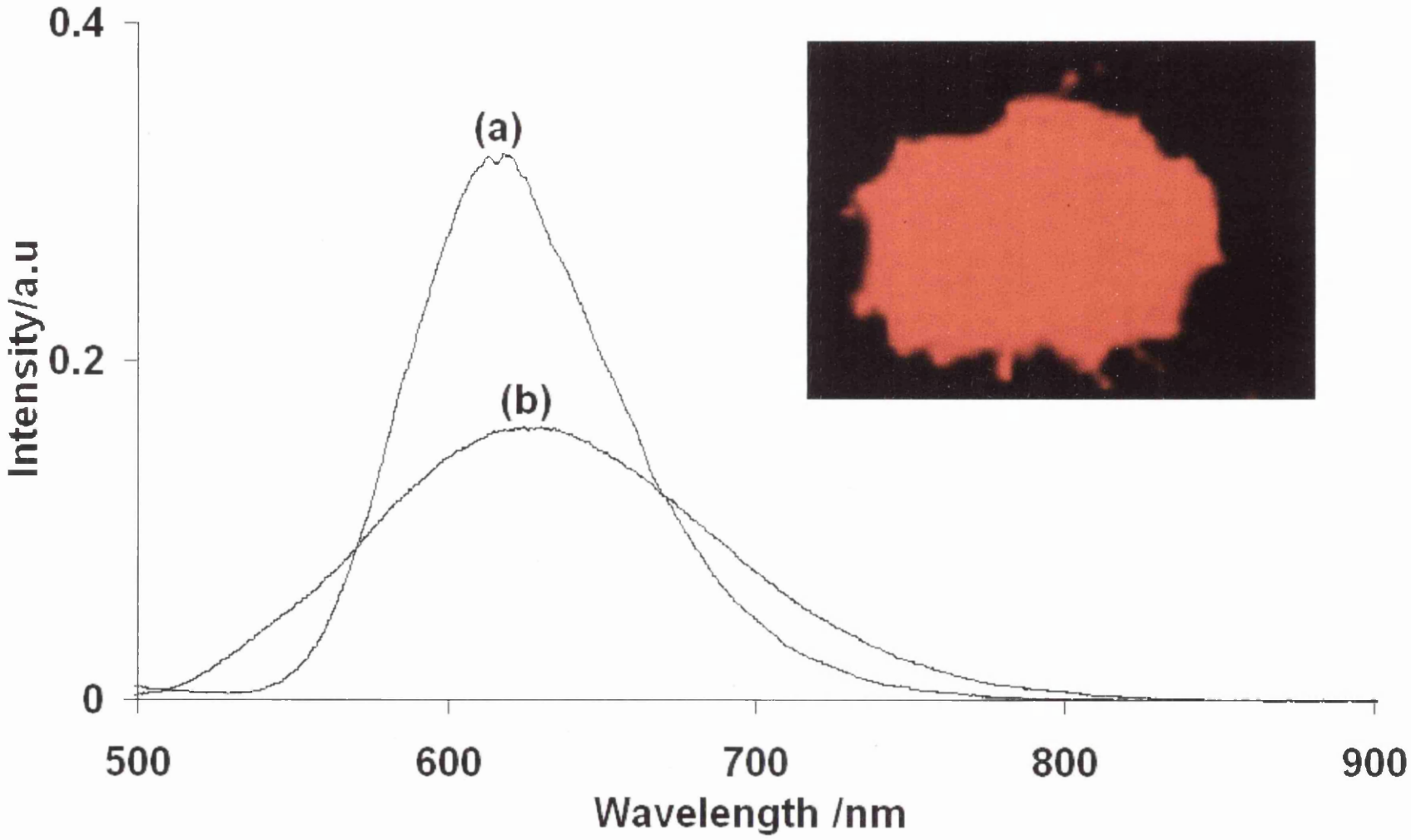

Figure 4.33: Solid state emission of pure **6** at (a) 77 K and (b) RT. Excitation wavelength = 355 nm.

When examined at 77 K in an EDT glass the general behaviour of all the compounds is similar in that an intense broad emission band with emission maximum in the 610-680 nm range is observed (see Figure 4.34 for a typical spectrum). However for **6** (Figure 4.35) there is also a distinct feature at 645 nm, which, by comparison with the solution phase emission spectra, we assign to molecular phosphorescence.

Although the compounds are soluble in EDT at room temperature, cooling to 77 K gives a glass with a translucent appearance, indicative of formation of micro-crystallites. We might expect that the photochemical behaviour in EDT glass at 77 K will be more like that seen in the solid than that in solution and all compounds give broad band emission with some broad structure in EDT glass at 77 K. However, the emission spectra, while broad and in the same spectral region, are not exactly the same as those seen in the solid state.

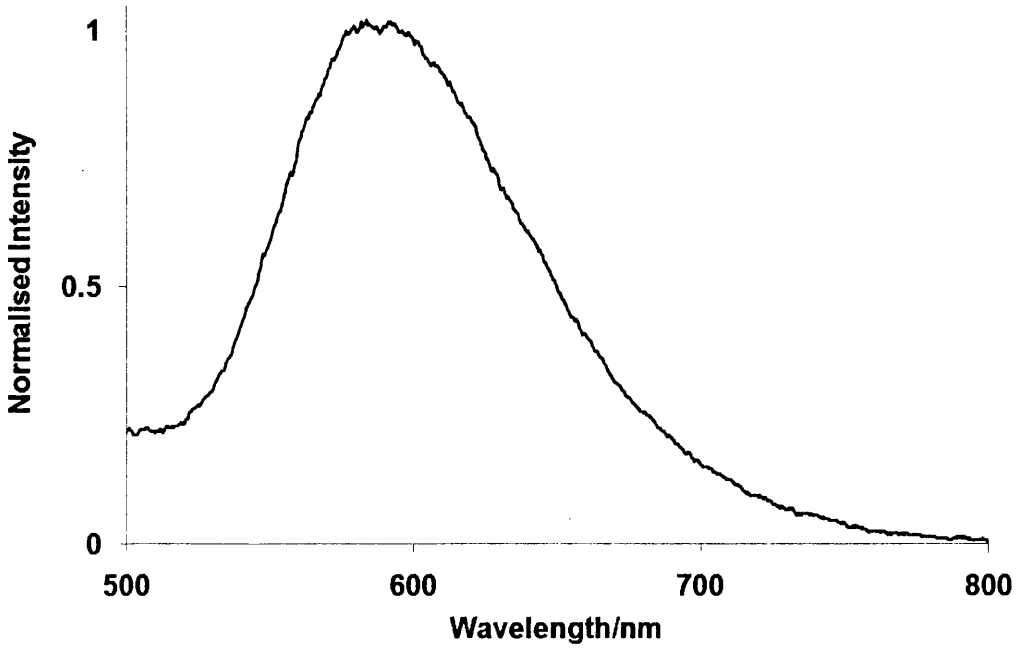

Figure 4.34: Emission spectrum of **8** in EDT glass at 77 K. Excitation wavelength = 355 nm.

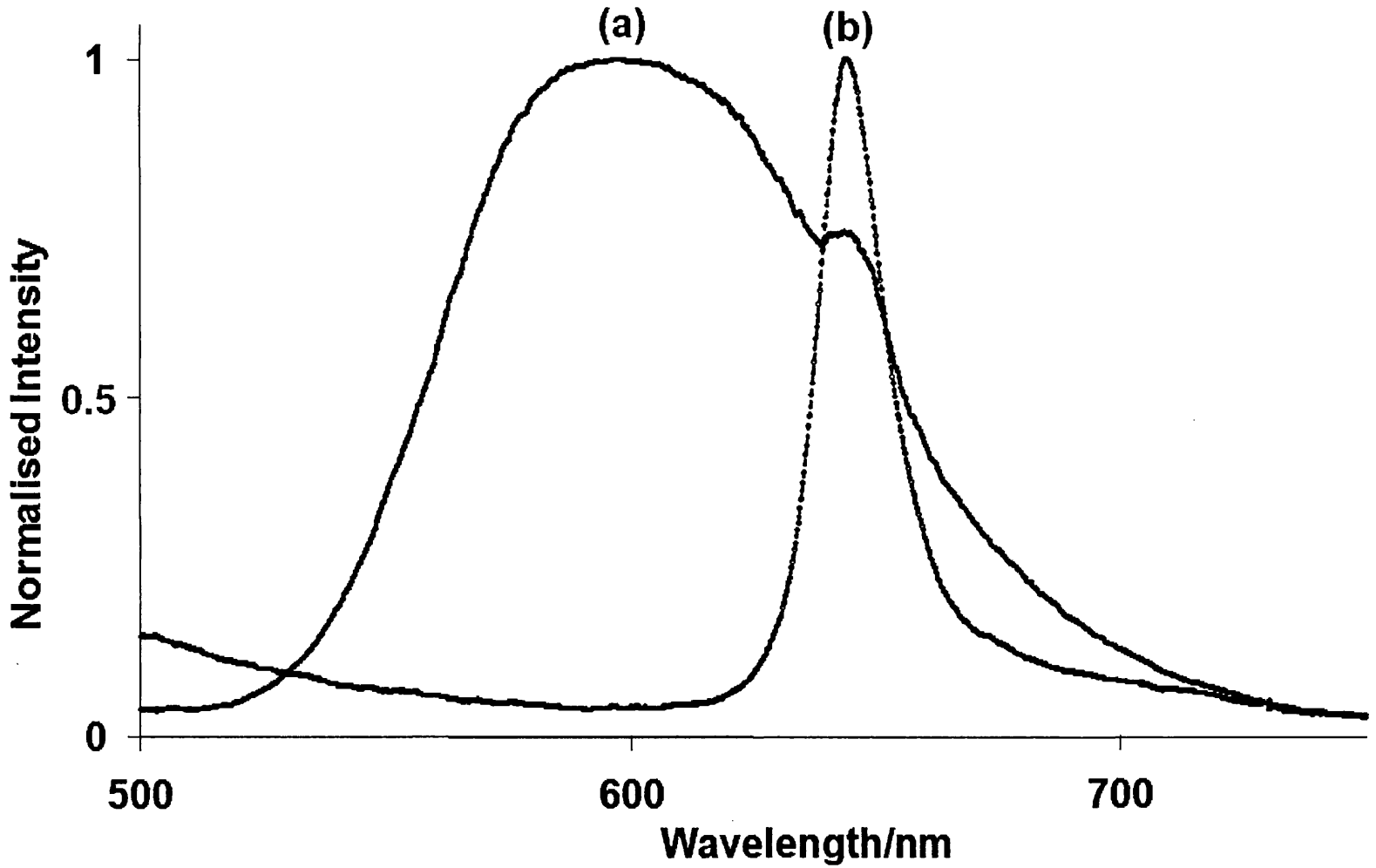

Figure 4.35: Uncorrected normalised emission spectrum of **6** in (a) EDT glass, and (b) nitrogen-purged toluene solution. Excitation wavelength = 355 nm.

For **4** with 377 nm excitation there is no change in emission spectrum with concentration over the range *ca.* 1×10^{-4} M to 1×10^{-6} M which suggests specific concentration-dependent aggregation is not the cause of emission.

Excitation spectra are detection wavelength dependent (see Figure 4.36 below), with emission at 658 nm showing an additional excitation band at 474 nm which is absent for detection at either 554 or 638 nm.

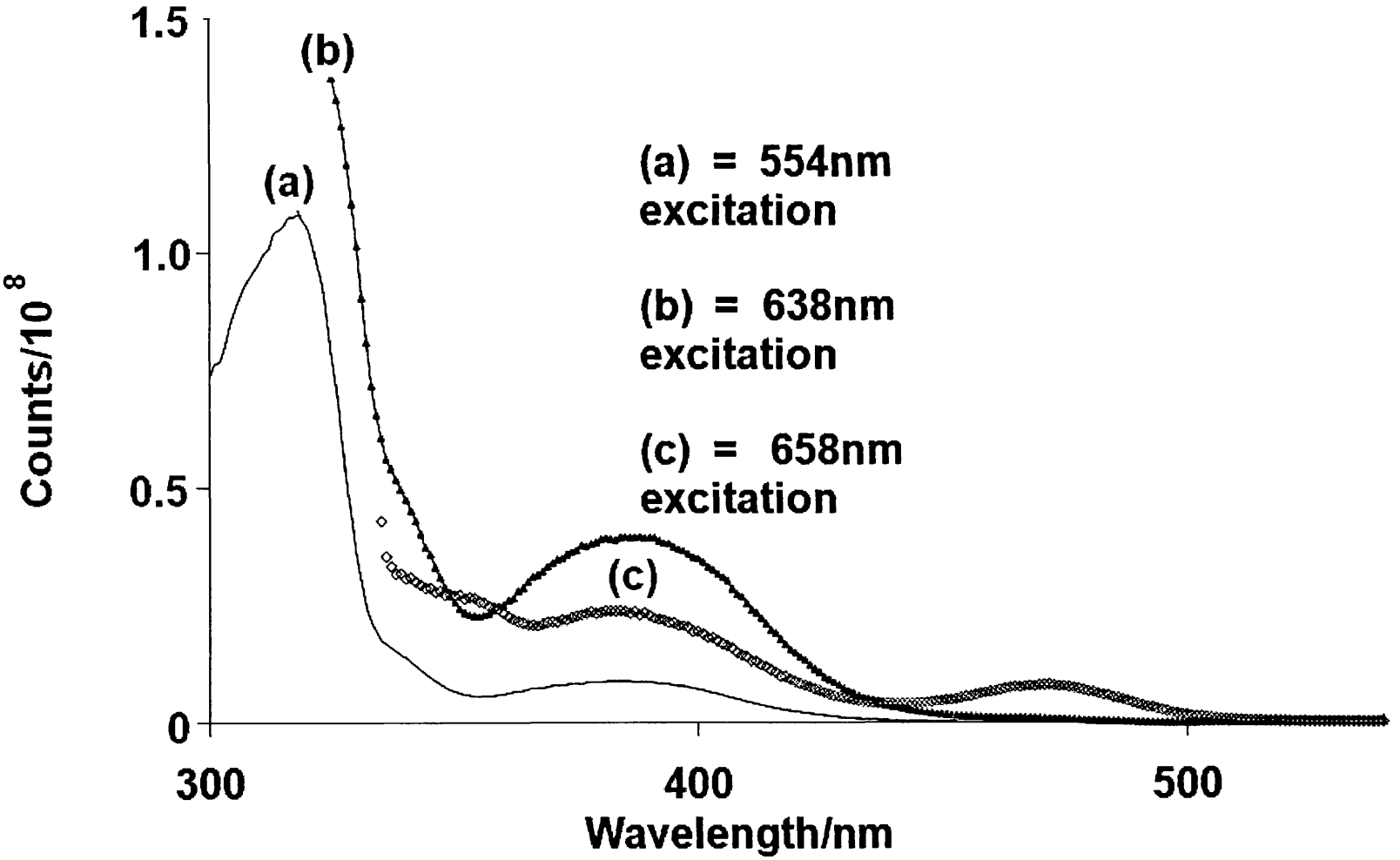

Figure

Figure 4.36: Excitation spectra of **6** in EDT glass at various emission wavelengths.

4.3.3.2 Time-resolved emission studies

In the solid state, for all compounds the emission decay kinetics are exponential, the same across the emission band, and the same with either 355 nm or 532 nm excitation (see Figure 4.37).

Examination of the emission decay kinetics across the emission bands for two compounds, *i.e.* **4** and **6,** showed no wavelength dependence of emission decay at either 77 K or RT (see Figures 4.37, 4.38 and 4.39 for decay kinetics and residuals). For all compounds solid state room temperature decay lifetimes are *ca.* 1.4-3.2 μs, which are significantly shorter than those at 77 K. It is interesting to note that while the emission quantum yield for **6** increases by perhaps only a factor of 1.5 in going from RT to 77 K the lifetime increases by a factor of 10.

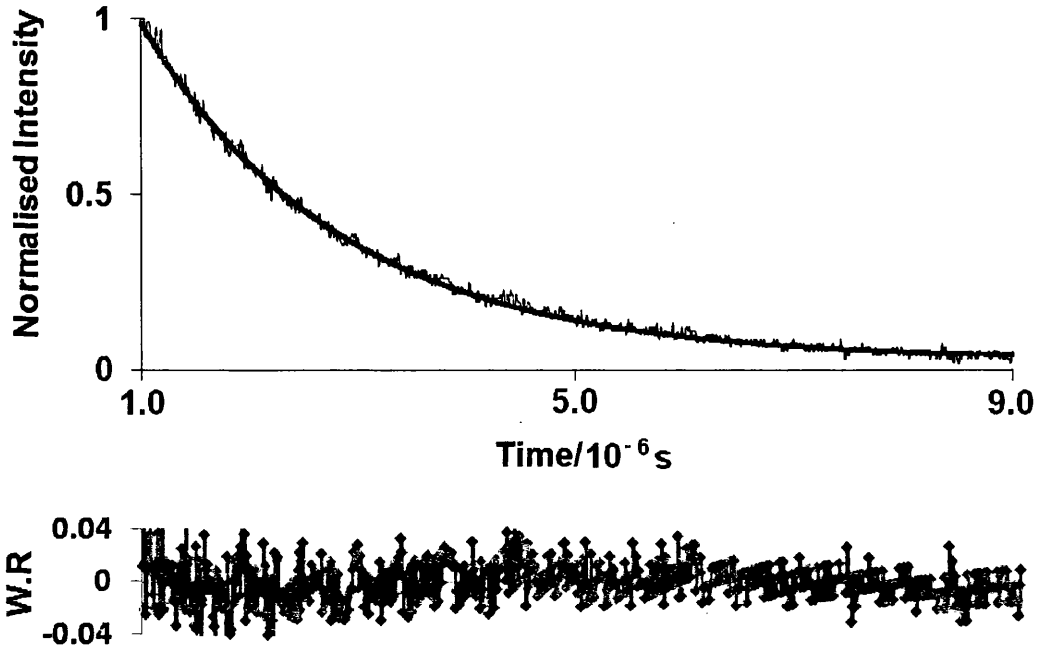

Figure 4.37: Decay curve and corresponding residuals for **6** at RT. Emission wavelength = 650 nm. Excitation wavelength = 355nm.

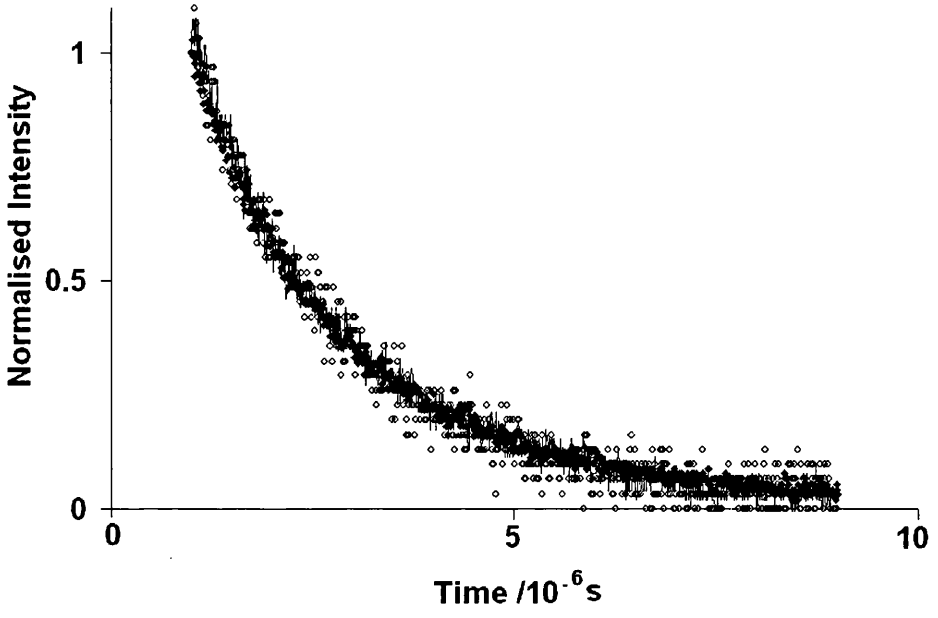

Figure 4.38: Overlap of decays of **6** in the solid state at RT. Excitation wavelengths = 355 nm (open circles) and 532 nm (closed, joined squares).

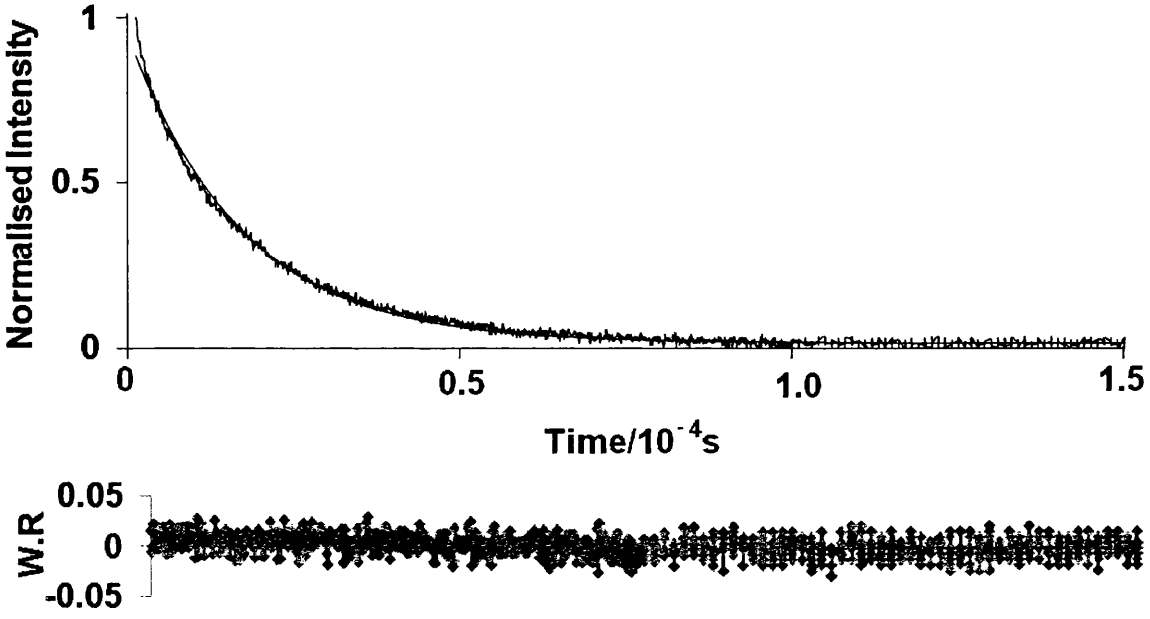

Figure 4.39: Solid state decay and corresponding residuals of **6** at 77 K. Emission wavelength = 650 nm Excitation wavelength = 355 nm.

The emission spectrum of **6** in an EDT glass is useful because it shows an additional distinct sharp feature at 645 nm. Furthermore the decay kinetics for the broad emission, measured at 580 nm (lifetime = 25 μs), and the sharp band at 645 nm (lifetime = 80 μs), are different (Figures 4.40, 4.41 and 4.42). It is certain then that the emission from **6** in the glass involves two species and by comparison with the solution phase emission spectra we assign the feature at 645 nm to molecular phosphorescence. If this is correct then the broad band emission cannot also be molecular phosphorescence and it is tentatively suggested that both the broad emission component seen in glasses at 77 K and the broad band solid state emission have a similar origin in that they are due to some intermolecular interactions, in the solid state or in aggregates formed in the low temperature glass. This will be more thoroughly discussed in the next section.

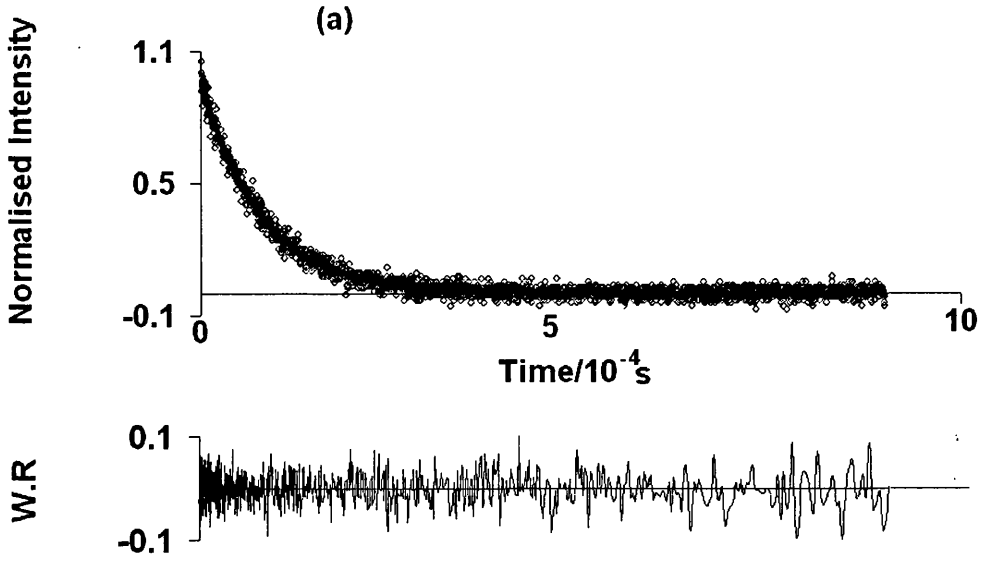

Figure 4.40: Decay of **6** in nitrogen-purged degassed toluene solution. Excitation wavelength = 355 nm. Emission wavelength = 650 nm.

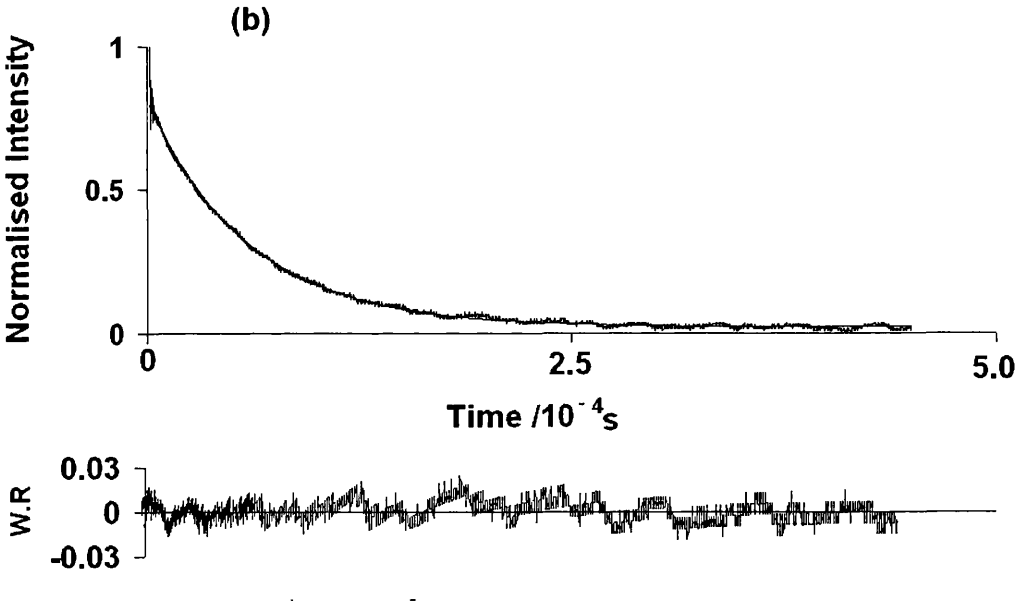

Figure 4.41: Decay curve of **6** in EDT glass at 77 K. Excitation wavelength = 355 nm. Emission wavelength = 650 nm.

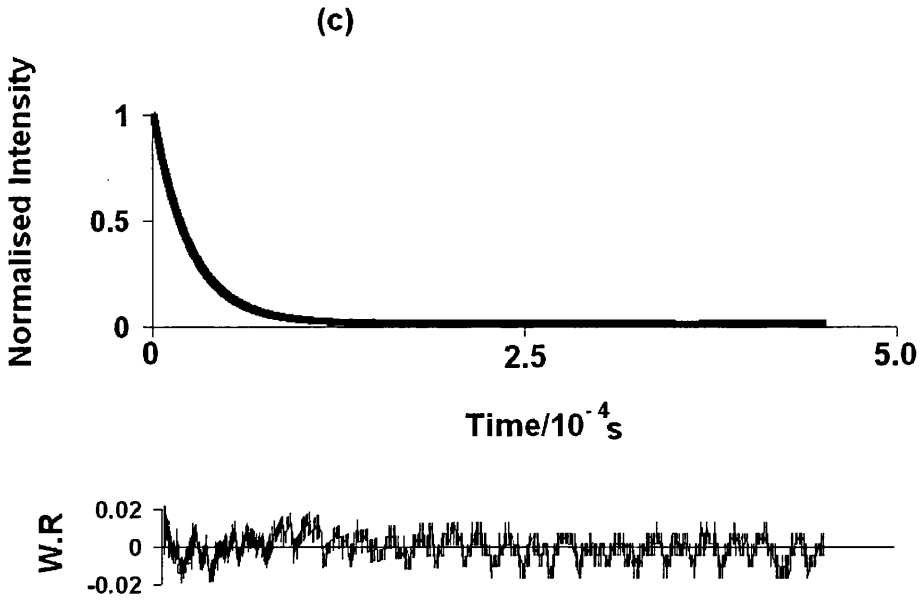

Figure 4.42: Decay curve of **6** in EDT glass at 77 K. Excitation wavelength = 355 nm. Emission wavelength = 580 nm.

4.3.4 Density Functional Theory

Density functional theory calculations were completed on the crystal structure of **5**. These give a HOMO-LUMO transition which lies at 690 nm, close in position to the molecular phosphorescence observed for the complexes in solution. However, the transition involves electron density being transferred from platinum and selenium onto phosphorus. If this is the case then the HOMO-LUMO transition would be indicative of the phosphine ligand and would change accordingly as the phosphorus ligand changed. This is not what is observed in solution as changing the phosphorus ligand has no effect on the position of the molecular phosphorescence which is always at 650 nm. The results from the DFT calculations are presented below.

Excited state data from DFT calculations are collected in Table 4.4. The calculated first excited state triplet arises from the HOMO-LUMO transition and lies at 690 nm, which is comparable to the molecular phosphorescence of these compounds at 640-650 nm. The calculated first excited singlet arises from the HOMO-LUMO transition and lies at 575 nm with a very weak oscillator strength of 0.003. The next highest energy singlet transition is at 476 nm again with a weak oscillator strength 0.006 arising from a HOMO-1 to LUMO transition, and this is followed by a transition at 369 nm with $f = 0.03$ from a mixed state transition. Figures 4.43 and 4.44 show the HOMO and LUMO. In the HOMO much of the electron density is situated on the p orbitals of the selenium with some involvement of the Pt d orbitals. The LUMO shows electron density which is more diffuse around the whole molecule, with electron density being distributed around all atoms apart from the cyclooctene ring. The electron shift in the transition is therefore predominantly from Se p-orbitals to P p-orbitals, *i.e.* an LLCT transition. Experimentally the triplet/singlet ratio is 0.87 while that from calculation is 0.82.

In terms of molecular absorption the agreement between experiment and calculation is reasorable with weak visible transitions both calculated and observed. The molecular phosphorescence at *ca.* 650 nm matches reasonably well the calculated value of 690 nm. However the observed fluorescence does not match what would be expected for a simple photophysical system in that the experimental fluorescence lies in the 420-480 nm region whereas the calculated singlet energies are 575 nm, 476 nm and 369 nm.

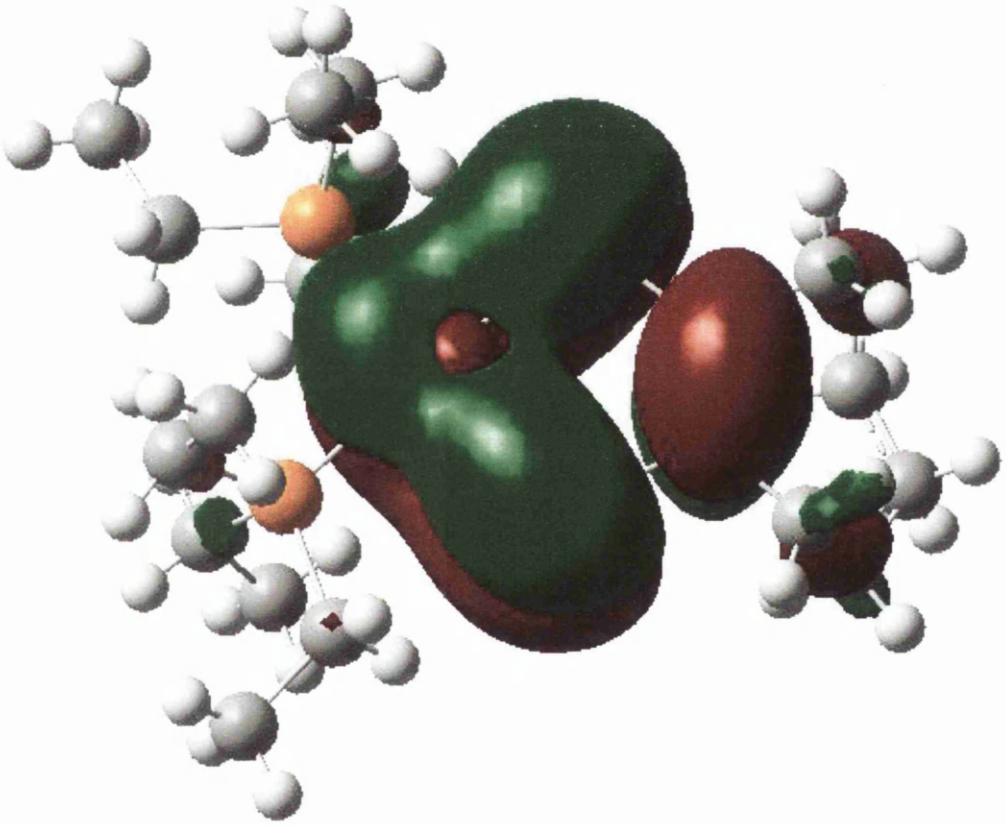

Figure 4.43: DFT calculated HOMO from the crystal structure of **5**.

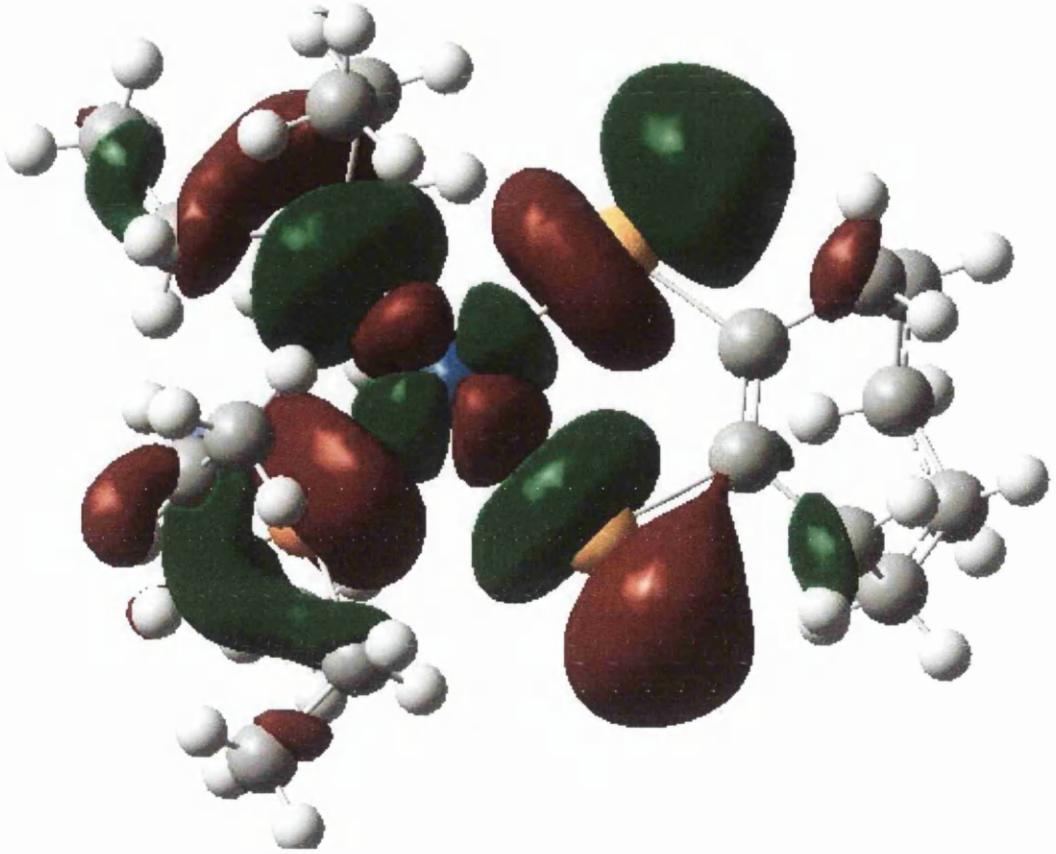

Figure 4.44: DFT calculated LUMO from the crystal structure of **5**.

Excited State	**Spin**	***Wavelength /nm***	**Oscillator Strength (*f*)**
1	Triplet	690.26	0.0000
2	Singlet	575.72	0.0003
3	Triplet	549.33	0.0000
4	Singlet	476.13	0.0006
5	Triplet	423.95	0.0000
6	Singlet	369.29	0.0030
7	Triplet	356.01	0.0000
8	Triplet	348.04	0.0000
9	Triplet	342.01	0.0000
10	Singlet	338.23	0.0010
11	Singlet	336.02	0.0020
12	Singlet	326.18	0.0008

Table 4.4: Excited state energies calculated by DFT

4.3.5 Origin of Emission

4.3.5.1 Origin of solution luminescence

The energy level diagram and Jablonski diagram in Figures 4.45 and 4.46 bring all the experimental data together in a proposed model.

The totally oxygen-quenched emission at 650 nm and the long lived transient at 420 nm under nitrogen can be confidently assigned to the lowest triplet state.

The most obvious candidate for the emission at *ca.* 550 nm is the S_1 state since there is no oxygen quenching of 550 nm emission when using excitation across the 500-600 nm range. The excitation spectra show this state to be populated by direct excitation at 533 nm, but not by excitation into the bands associated with emission at 650 nm. It is therefore suggested that the excitation spectrum for 650 nm emission corresponds to direct excitation into the triplet manifold, *i.e.* S_0 to T_n excitation, and we therefore place the triplet energies as follows: T_1 at ca. 640 nm from the onset of phosphorescence; T_2 at 498 nm from the lowest energy of the pair of bands in the 650 nm excitation spectrum at 498 nm and 532 nm, the pair being separated by a vibrational level of 1300 cm^{-1}; and T_3 at 418 nm from the lowest energy of the pair of bands in the 650 nm excitation spectrum, the pair being separated by a vibrational level of 2610 cm^{-1}.

The emission bands in the 400-500 nm region we assign to fluorescence, specifically $S_2 \rightarrow S_0$ fluorescence. The singlet energies are placed as follows: S_1 at 525 nm from the lowest energy band in the 550 nm excitation spectrum, which also shows a vibrational shoulder at 485 nm; S_2 at 427 nm from the highest energy emission bands in the 400-500 nm region.

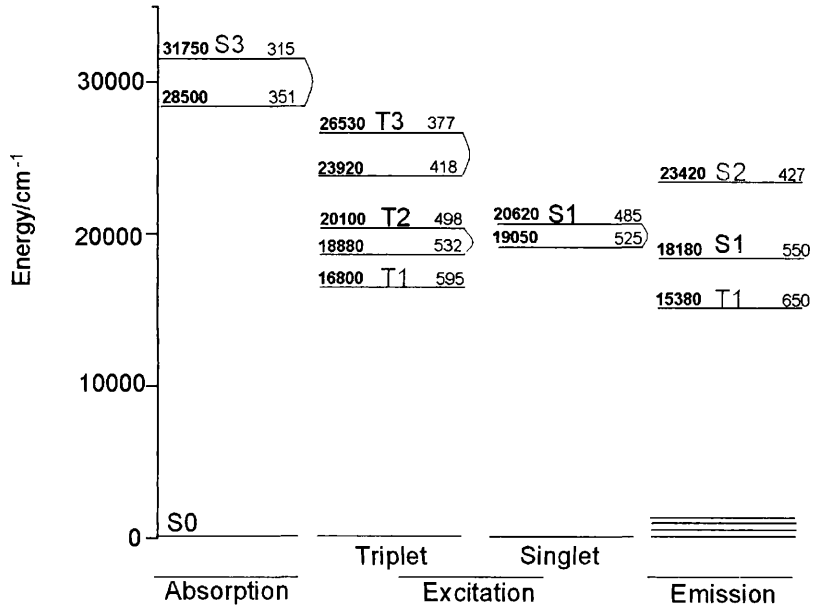

Figure 4.45: Proposed energy level diagram for the platinum diselenolenes in solution incorporating data from absorption, excitation and emission studies. Numbers in bold are energies in cm^{-1}, number in normal font to the right are wavelengths in nm. Transitions which are thought to be vibrational levels of the same electronic transitions are connected.

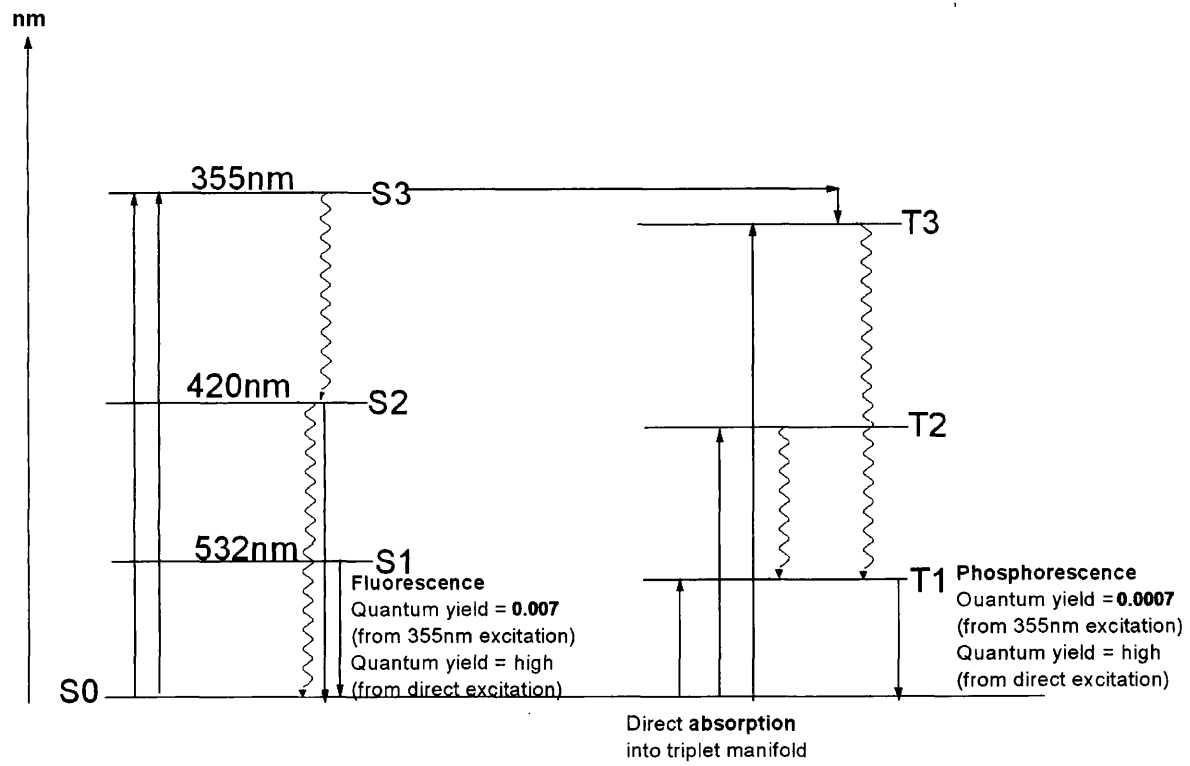

Figure 4.46: Jablonski diagram for the platinum diselenolenes in solution incorporating data from absorption, excitation and emission studies.

Because the excitation spectra of either the 550 nm or 650 nm bands do not show excitation into the S_2 levels as being an efficient population route it is proposed that deactivation of the S_2 level is predominantly via $S_2 \rightarrow S_0$ fluorescence and non-radiative processes.

With 355 nm excitation $S_2 \rightarrow S_0$ fluorescence has a quantum yield of *ca.* 0.07 and $T_1 \rightarrow S_0$ phosphorescence a quantum yield of 0.007.

4.3.5.2 Origin of the broad band emission in the solid state and EDT glass

The very broad emission bands in the solid state and as microcrystallites in EDT glass suggest states arising from intermolecular interactions. Given the size and shape of the HOMO and LUMO and the predominantly selenium to phosphine LLCT nature of the lowest energy transition we examined the crystal structures available to consider the possibility of solid state intermolecular excited state interactions

4.3.5.3 Crystal structure

The crystal structures for these compounds have been previously reported,[32] and there are no significant ground state intermolecular contacts. Initially we thought that the emissions might have a similar origin to the broad band emission seen in stacked platinum complexes such as the tetracyanoplatinates, but the X-ray diffraction data for **9**, $[Pt(Se_2C_7H_{10})(PEt_3)_2]$ and **6** show the closest intermolecular distances to be greater than 500 pm which is too large for this to be the case.

Given that the DFT calculations showed that the HOMO-LUMO transition involved electron density moving from the selenium p orbitals onto the phosphorus p orbitals we investigated the intermolecular contacts between these two atoms in adjacent molecules in the crystal. Although it was already clear that there were no interactions

which could be considered to be significant in the ground state, we were interested to see if any could be important in the excited state where the molecular orbitals become more diffuse. For example, Dexter exchange energy transfer, which involves the overlap of ground state and excited state wavefunctions between the donor and acceptor molecule, can occur at distances between the donor and acceptor of up to approximately 10 Å.[40]

The distances between the Se1---P1 and Se2---P2, and the in-plane Se-P1-P2 angles are reported for all available crystal structures of the diselenolenes in Table 4.5. It can be seen that for all three examples the phosphorus and selenium atoms are between 5-6 Å apart. It should be also noted that the phosphorus atoms on one molecule and selenium atoms on an adjacent molecule are positioned similarly in the crystal structures. The best guess at the minute is that an intermolecular charge-transfer interaction between the large Se p orbitals on one molecule and the P orbitals of an adjacent molecule is responsible for broad-band solid state emission as well as that observed from microcystallites in organic glass/snow at 77 K.

Figures 4.47 to 4.53 show the crystal packing structures for compounds **4**, **6** and **9**. The intermolecular arrangements seen in these structures will be discussed further when outlining the origin of the emission.

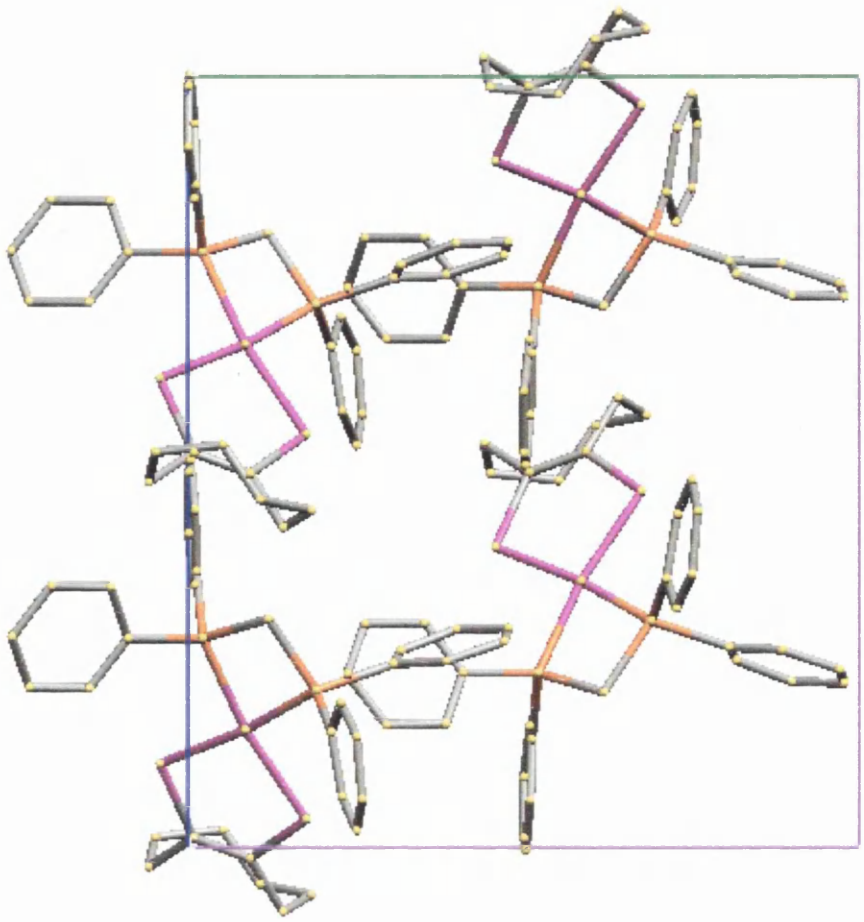

Figure 4.47: Crystal structure of **6.** [32] Pink = selenium and platinum; orange = phosphorus; grey = carbon. Hydrogens are removed for clarity.

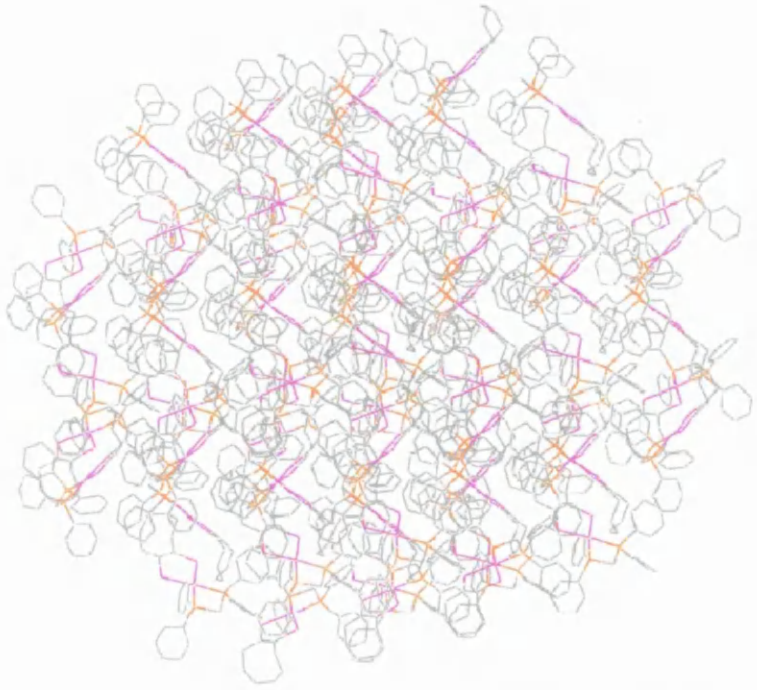

Figure 4.48: Pattern observed in the crystal of **6**.[32] Pink = selenium and platinum; orange = phosphorus; grey = carbon. Hydrogens are removed for clarity.

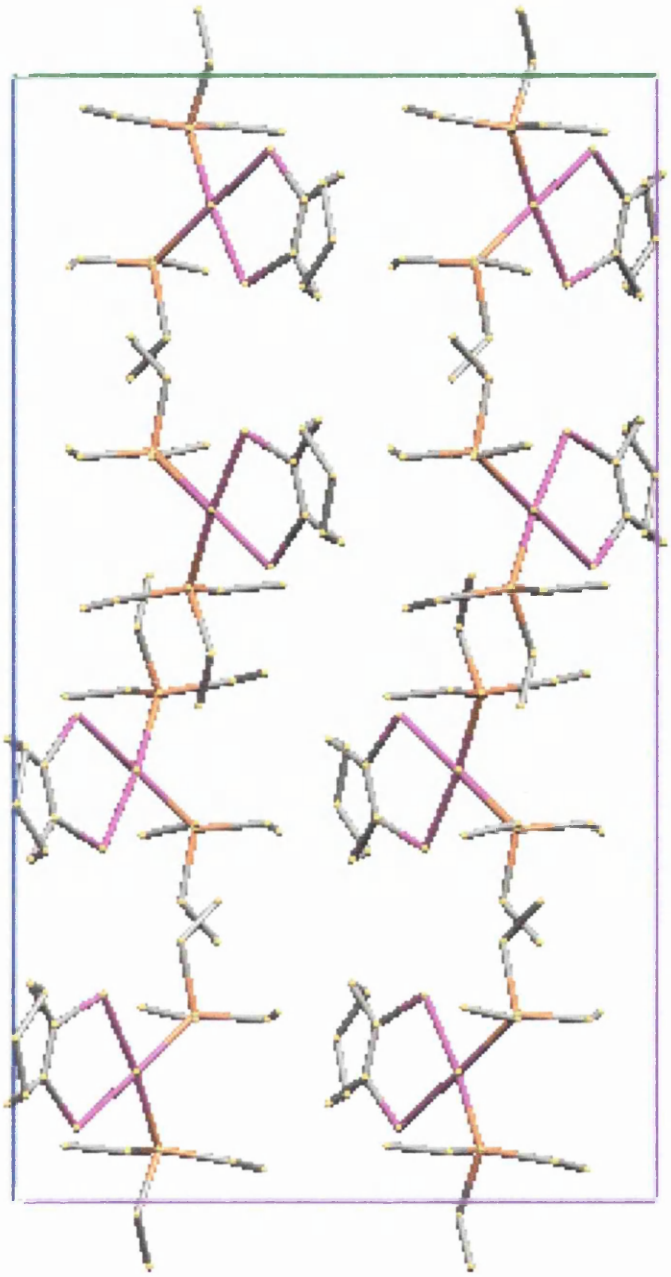

Figure 4.49: Crystal structure of **9**.[32] Pink = Selenium and platinum; orange = phosphorus; grey = carbon. Hydrogens are removed for clarity.

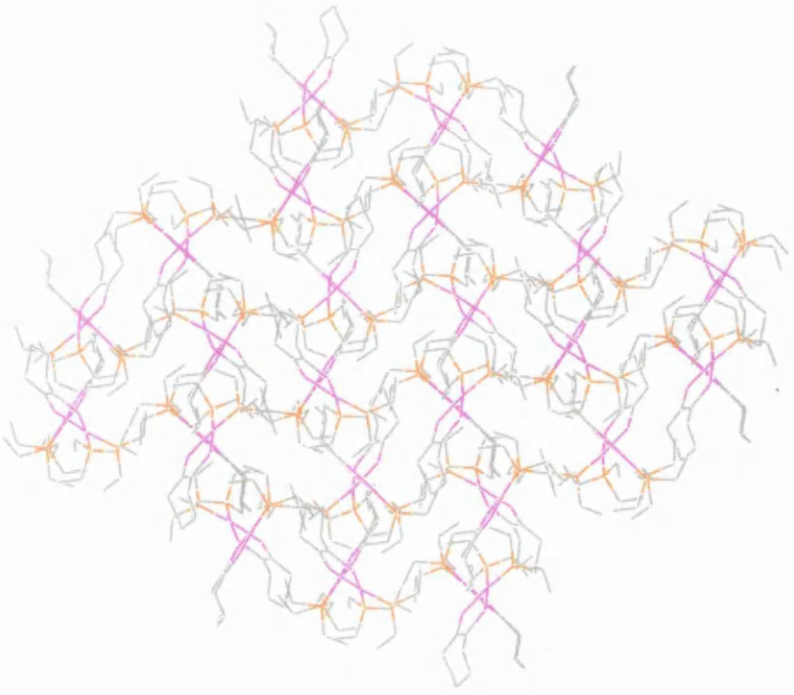

Figure 4.50: Pattern observed in the crystal of **9**.[32] Pink = selenium and platinum; orange = phosphorus; grey = carbon. Hydrogens are removed for clarity.

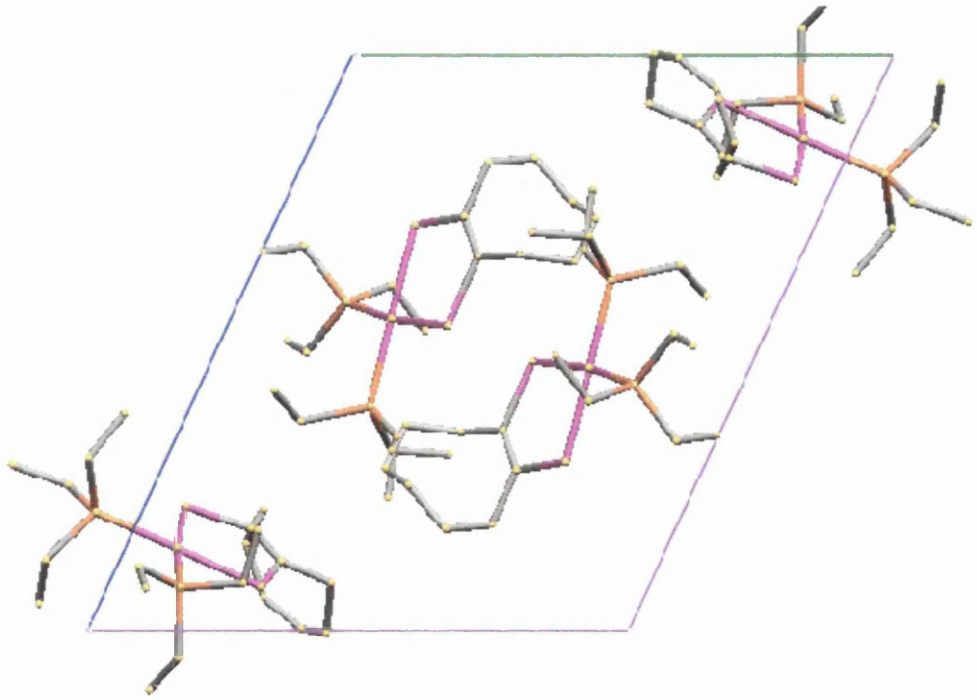

Figure 4.51: Crystal structure of **4**.[32] Pink = selenium and platinum; orange = phosphorus; grey = carbon. Hydrogens are removed for clarity.

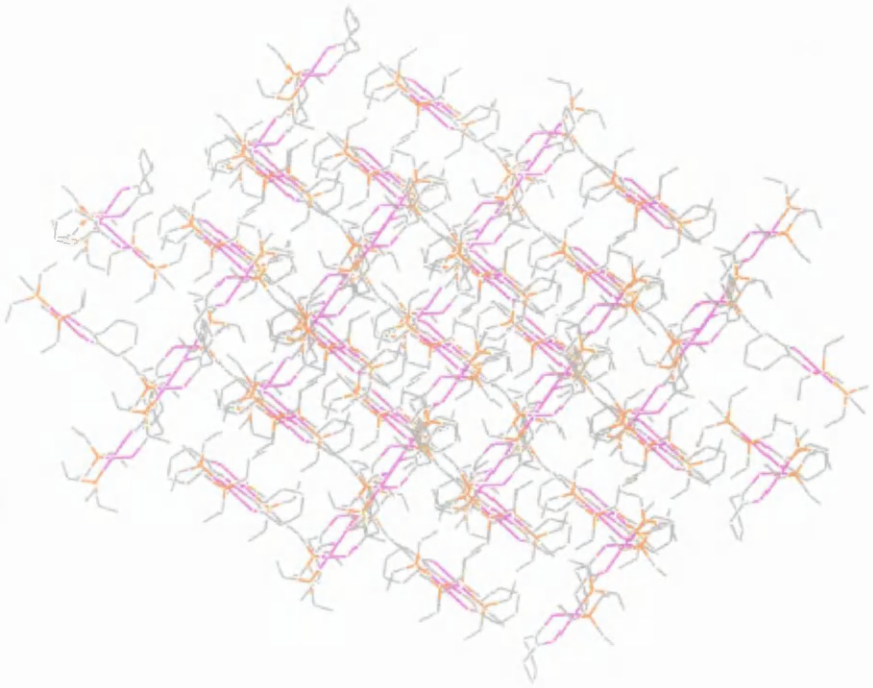

Figure 4.52: Pattern observed in the crystal of **4**.[32] Pink = selenium and platinum; orange = phosphorus; grey = carbon. Hydrogens are removed for clarity.

Compound	Crystal structure	Intermolecular distance		Angle of the plane of interaction
		Se(3)----P(3) Å	Se(2)----P(2) Å	Se-P-P angle(°)
$[Pt(Se_2C_8H_{12})(dppm)]$ (**6**)	Orthorhombic	6.191	5.544	109.88
$[Pt(Se_2C_7H_{10})(PEt_3)_2]$ (**9**)	Orthorhombic	5.663	5.919	114.04
$[Pt(Se_2C_8H_{12})(PEt_3)_2]$ (**4**)	Monoclinic	5.904	5.419	85.05

Table 4.5: Se-P intermolecular distances and angles. [32]

In both **6** and **9** there are infinite linear arrays of alternating Pt coordinating planes at *ca.* 100° to each other in a zigzag arrangement, whereas in **4** the molecules are arranged such that the Pt coordinating planes form stacks of slightly distorted squares with angles alternating between 113 and 85°. The common arrangement in all three crystals is one in which Pt coordinating planes lie at *ca.* 90-110° to each other with alternating Se and P in a ---Se---P---Se---P---Se---chain or ring. It is tentatively suggested that it is this structural arrangement and the resulting excited state intermolecular interactions, which are responsible for the solid emission. Although the facilities are not available in Swansea it would be of some interest to study the angular dependence of absorption and emission characteristics of these compounds in single crystal studies.

4.4 Conclusion

The purpose of this chapter was to investigate and establish further the origin of the luminescence in platinum diselenolenes .The emission upon 355 nm excitation in fluid solution was identified to be molecular phosphorescence. In addition to this it was seen that molecular phosphorescence occurred from the systems upon excitation at 420 nm or 532 nm. Although the 532 nm band was prominent in the excitation spectrum it was not until we carried out an in-depth investigation that we discovered a small absorption band at 550 nm. Because of the very small amount of absorption at this wavelength the emission is considered to have a quantum yield of very close to 1. Also the triplet character of the long-lived excited state has been confirmed by the detection of singlet oxygen and the possibility of triplet-triplet absorption.

The molecule exhibits fluorescent emission bands in the blue region of the spectrum. These are not a result of vibrational progression. The quantum yield of fluorescence

for **6** was calculated as *ca.* 7%. In addition to this there is a partially oxygen-quenched band at 530 nm. The complex excitation spectrum has also been resolved and a Jablonski and energy level diagram has been presented.

The origin of the solid state emission has also been identified. Like in solution it is also possible to excite the molecule at 532 nm and observe solid state emission. However, in an EDT glass we only observe the sharp solution peak at this excitation wavelength. DFT calculations show that during the HOMO-LUMO transition electron density moves from the selenium onto the phosphorus. Upon consideration of the crystal structure, the selenium and phosphorus are close enough together for these orbitals to interact in the excited state. The distance between the phosphorus and selenium is consistent in all crystal structures, which were available for analysis. A pattern that occurs between and throughout the crystal structures has been identified. From this it can be concluded that the intermolecular patterns and the distances observed in the crystal structure are the cause of the broad emission observed from both the pure solid at RT and 77 K and also in an EDT glass at 77 K.

4.5 References

1. Morley, C.P.; Ford, S, Di Vaira, M. *Polyhedron*, **2004**, *23*, 2967.

2. Rosenberg, B, Van Camp, L. Trosko, J.E, Mansour, V.H. *Nature*, **1969**, 22, 285.

3. Yam, V.W.W. *Acc.Chem Res.* **2002**, *35*, 555-563.

4. Evans, R.C.; Douglas, P.; Winscom, C. *Coord. Chem. Rev.* **2006**, *250*, 2093

5. Sacksteder, L.; Baralt, E.; DeGraff, B.A.; Lukrhard, C. M.; Demas, J. N. *Inorg. Chem.* **1991**, *30*, 2468-2476.

6. Crosby, G. A. *Acc. Chem. Res.* **1975,** *8*,2384.

7. Roundhill, D. M.; Gray. H. B.; Che, C. *Acc. Chem. Res.* **1989**, *22*, 55.

8. Gliemann, G.; Yersin H. *Struct. Bond.* **1985**, *62*, 87

9. Yersin, H.; Glieman, G. *Ann. N. Y. Acad. Sci.* **1978**, *313*, 539.

10. Glieman, G. *Comments Inorg. Chem.* **1986**, *5*, 263

11. Ballardini, R.; Varani, G.; Indelli, M. T.; Scandola, F. *Inorg. Chem.* **1986**, *25*, 3858.

12. Zipp, A. P. *Coord. Chem. Rev.* **1998**, *84*, 47.

13. Baldo, M. A.; O'Brian, D. F.; You, Y.; Shoustikov, A.; Sibley, S.; Thompson, M. E.; Forrest, S. R. *Nature* **1998**, *395*, 151.

14. Williams. J. A. G. *Coord. Chem. Rev.* **2008**, *252*. 2596

15. Lamansky, S.; Djurovich, P.; Murphy, D.; Abdel-Razzaq, F.; Lee H. E.; Adachi, C.; Burrows, P. E.; Forrest, S. R.; Thompson, M. E. *J. Am. Chem. Soc.* **2003**, *123*, 4304-4312.

16. Aiello, I.; Dattiilo, D.; Ghedini, M.; Golemme, A. *J. Am. Chem. Soc.*, **2003**,123, 5598.

17. Bevillacqua, J. M.; Eisenberg. R. *Inorg. Chem.* **1994**, *33*, 2913-2923.

18. Ghedini, M.; Pucci, D.; Scaramuzza, N.; Komitov, L.; Lagerwall, S. T. *Adv. Mater.* **1995**, *7*, 659.

19. Omnes, L.; Timini, B.A.; Ghedini, M.; Gollemme, A. *J. Am. Chem. Soc.* **2003**, 123, 5598.

20. Tang, C. W.; Van Slyke, S. A. *Appl. Phys. Lett.* **1987**, *51*, 193-195.

21. Lu, W.; Mi, B.; Chan, M. C. W.; Hui, Z.; Che, C.; Zhu, N.; Lee, S. *J. Am. Chem. Soc.* **2004**, *126*, 4958-4971.

22. Arena. G.; Calogero, G.; Campagna, S.; Scolaro, L. M.; Ricevuto, V.; Romeo, R. *Inorg. Chem.* **1998,** *37*, 3763-3769.

23. Peyratout, C. S.; Aldridge, T. K.; Crites, D. K.; McMillin, D. R. *Inorg. Chem.* **1995**, *34*, 4484-4489.

24. Cummings, S. D.; Eisenberg R. *J. Am Chem. Soc.* **1989**, *111*, 8916-8917

25. Montalti, M.; Credi, A.; Prodi, L.; Gandolf, M. T. *Handbook of Photochemistry*, 3rd Ed, Taylor and Francis, **2006.**

26. Younus, M.; Kohler, A.; Cron, S.; Chawdhury, N.; Al-Mandhary, M. R.; Khan, M.,S.; Lewis, J.; Long, N. J.; Friend, R. H.; Raithby, P. R. *Angew. Chem. Int. Ed. Engl.* **1998**, *37*, 3036.

27. Huertas, S.; Hissler, M.; McGarrah, J. E.; Lachicotte, R. J.; Eisenberg, R. *Inorg. Chem.* **2003**, *40*, 1183.

28. Bevilacqua, J. M.; Eisenberg, R. *Inorg. Chem.*, **1994**, *33*, 2913.

29. Miskowski, V. M.; Houlding, V. H.; Wang, C. M. *Inorg. Chem.* **1989**, *29*, 1529.

30. Ford, S.; Morley, C. P.; Di Vaira, M *New. J. Chem* **1999**, *23*, 811.

31. Khanna, P. K.; Morley, C. P. *J. Chem. Res. (S)* **1995,** 64

32. Webster, C. A. *The Synthesis and Characterisation of Some Novel Compounds Containing Pt-Se Bonds*, PhD Thesis, University of Wales Swansea, 2006.

33. Turro, N. J. *Modern Molecular Photochemistry*, University Science Books, Sausalito, California, 1999, p89.

34. Montalti, M.; Credi, A.; Prodi, L.; Gandolfi, M. T. Handbook of Photochemistry, 3rd Ed, CRC Press, New York, 2006, p138.

35. Montalti, M.; Credi, A.; Prodi, L.; Gandolfi, M. T. *Handbook of Photochemistry*, 3rd Ed, CRC Press, New York, 2006, p552.

36. Martinez, C. G.; Neuner, A.; Marti, C.; Nonell, S.; Braun, A. M.; Oliveros, E. *Helv. Chim. Acta* **2003,** *86*, 384-397.

37. Bevilacqua, J. M.; Zwelta, J. A.; Eisenberg, R. *Inorg. Chem.* **1994**, *33*, 258-266.

38. Turro, N. J. *Modern Molecular Photochemistry*, University Science Books, Sausalito, California, 1999, p5.

39. Parr, R.G. Yang, W. *Ann .Rev. Phys. Chem,* **1995**,46,701

40. Dexter, D. L. *J. Chem. Phys.* **1953**, *21*, 836.

Chapter 5:

A study of the photophysics of some polyfluorenes with ketone defects

5.1 Chapter aim

There is much focus towards the synthesis and characterisation of polymer based compounds which can be used as blue emitters in Organic Light Emitting Diodes (OLEDs). The work presented in this chapter was completed when I had the opportunity of a four month research ERASMUS placement working with Professor Hugh Burrows and the Photochemistry group at the University of Coimbra, Portugal. One of the main interests of the group is the photochemical and photophysical properties of polyfluorene compounds.

The work detailed in this chapter is an extension of the work of Ana Teresa Marques,[1] a fellow member of the photochemistry group. One of the problems with using polyfluorenes in OLEDs is the fact that they degrade to produce defects which emit in the green spectral region, which results in a loss of colour purity and efficiency from the device. There is much debate into the origin of these defects and much research has been focused towards finding methods to prevent their formation. In this chapter, photophysical measurements on ketone-defect polymers will be presented. The photochemistry group in Portugal have a long standing collaboration with Professor Ulli Scherf at the University of Wuppertal, Germany, whose group specialises in polymer synthesis, and all polymers used in this chapter have been synthesised by the Scherf group unless stated otherwise. I would like to thank the ERASMUS scheme for the funding which made this collaboration possible.

5.2 Introduction

5.2.1 Conjugated Polymers

Conjugated polymers have been known to be electroluminescent since the 1960's.[2] Polyacetylene (shown in figure 5.1) was the subject of initial interest. However, polyacetylene is not easy to process and for this reason investigations then shifted towards the development of new conjugated polymers.[3-4] These included polythiophene (PT), polyaniline (PANI) , polypyrrole (PPy) and poly(p-phenylene) (PPP), as well as many others (see figure 5.1).[5,6] The significance of these classes of polymer was recognised in 2002 by the Nobel Prize in chemistry being awarded to H. Shirakawa, A.G MacDiarmid, and A.J.Heeger who are considered to be the pioneers in this type of materials research.[7] These materials, which have been most specifically studied for application in OLED technology, can also be used in polymer lasers [8-12] photodiodes, [13] sensors,[14] and solar cells.[15-18]

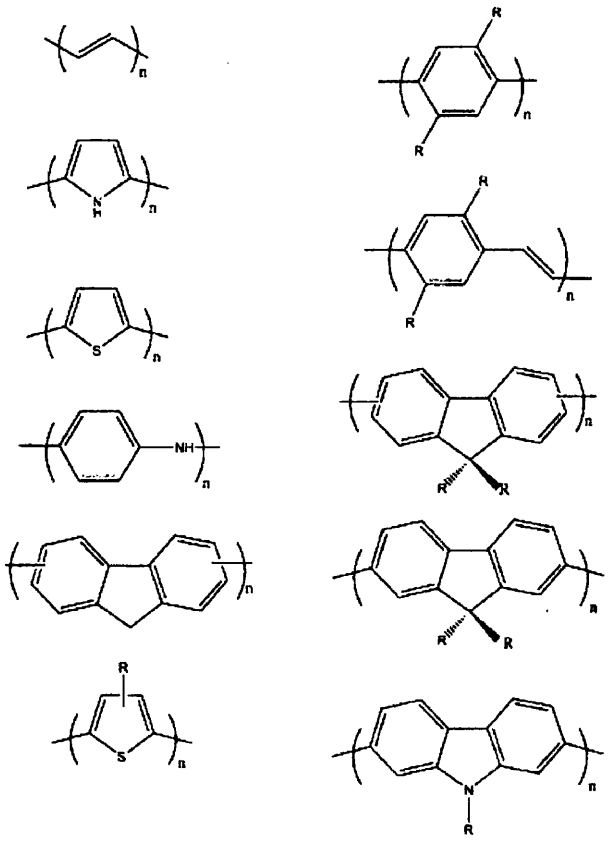

Figure 5.1: Typical un-substituted π- and σ – conjugated polymers.[6]

5.2.2 Polyfluorenes

The electroluminescence of polyfluorenes (PFs, Figure 5.2) was noted in 1991 by the Yoshimo group.[19] Their use in OLED applications advanced considerably within 10 years, and in 2001 when reviewed by Leclerc, they were described as having 'exceptional electrical and optical properties for application in light emitting diodes'.[6] Since then interest in polyfluorenes specifically as blue emitters in OLEDs has rapidly increased[20-21] because of their advantageous properties which include:

1. high solid state quantum efficiencies; [23-24]
2. exceptional thermal and chemical stability in inert environments (PF has a decomposition temperature of greater than 400 °C); [25,27]

3. the addition of long alkyl (or other) substituents at the C9 position makes PFs soluble in a range of organic solvents;[18,27]
4. via co-polymerisation the band gap and energy levels can be readily manipulated over the whole visible range of the spectrum. [28]

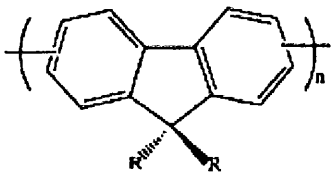

Figure 5.2: Structure of polyfluorene.[6]

The first synthesis of PF's was published by Yoshino and co-workers in 1989 who made the polymer via the oxidative coupling of fluorene monomers using $FeCl_3$ as a coupling agent.[29] Since then many other synthetic techniques have been developed and now there are many possible synthetic routes towards PFs. The most common techniques include: A) Yamamoto, B) Suzuki, and C) Stille, coupling reactions, which are shown in figure 3.[6] Most homo and co-polymers so far described in literature have been synthesised via the Yamamoto route however, the preferred route now seems to be Suzuki coupling.[6]

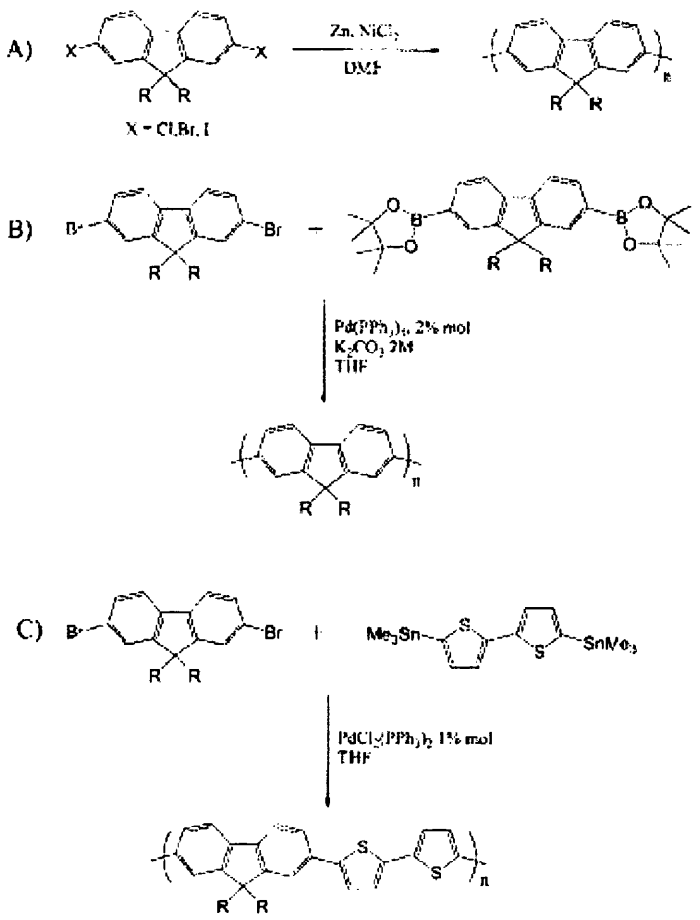

Figure 5.3. Synthetic routes towards the preparation of polyfluorenes [6]

Despite the range of PF polymers and oligomers available, only PF8 (dioctyl), sometimes referred to as PFO, PF6 (dihexyl) and PF2/6 [di(2-ethylhexyl)] are commonly used. This focus is mainly due to the mesomorphic properties of these polymers, which are known to demonstrate many crystalline phases.[29]

PF8 (PFO) shown in figure 5 has two distinct backbone conformations, referred to as the α or β phase. The β form is more planar and less disordered than the α form, and can be identified as a separate longer wavelength feature in both the absorption and emission spectrum, which results in enhanced vibronic structure and reduced Stokes shift but at the same time retains a high quantum yield. [30-32]

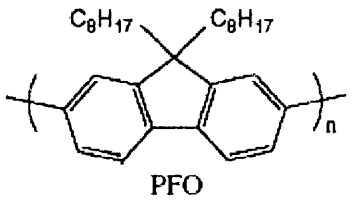

PFO

Figure 5.4. Structure of PFO[32]

PF2/6 has a chiral centre on each repeat unit in the chain and is a racemic mixture of (S) and (R) enantiomers. It has a simple structure and high stability, which makes it a good candidate for use as a model molecule for phase behaviour studies. The emissive properties of PF2/6 in both solid state and solution are the same. [32-35]

5.2.3 The origin of the defect emission

Unfortunately PF2/6 and PF2/8 generally show some green defect emission (the g-band with emission located between 525 and 540 nm) in solution and the solid state.[36-43] The origin of this emission has evoked much debate. Some groups have taken advantage of the g-band as a possible route for creating materials with a stable green emission.[43] Problems in determining the origin of the green band have arisen due to the PF samples being subjected to different synthesis, processing and handling protocols.[42] This band has variously been attributed to: fluorene/fluorene excimer emission,[41] fluorenone oxidation product emission[44], unspecified aggregate emission[44], and the presence of cross-linked units.[46] The g-band has generally been seen to be intensified by heating, UV exposure in air and/or by passing an electrical current through polymer solutions to initiate electro-generated chemiluminescence.[43,47]

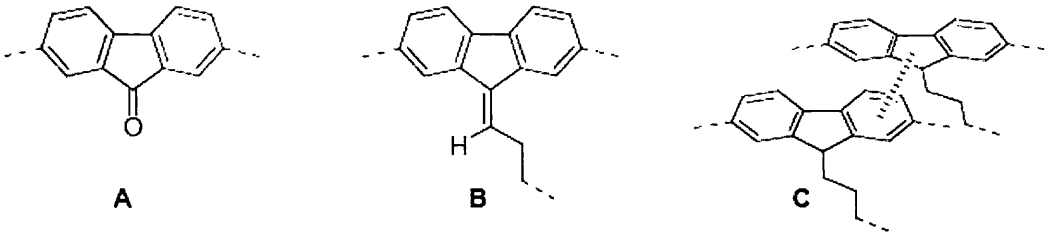

Figure 5.5: Possible causes of the g-band: a) ketone defects; b) alkyline defects; c) cross-linked units. [25]

5.2.3.1 Excimer formation

Fluorene/fluorene excimer emission was initially considered the most probable cause of the g-band emission. (An excimer is an excited state complex, which is formed by the interaction of an excited state chromophore with a ground state chromophore.[48-49]) One theory is that excimers form between 2 polyfluorene chains. Another, suggested by Sims and co-workers, is that g-band emission is due to excimer formation between two fluorenone defects located at adjacent chains or chain segments.[47]

The argument for excimer formation is usually substantiated by the lack of significant changes in the UV-Vis absorption spectrum with increased emission intensity of the g-band. In addition the absence of the band in dilute solution fluorescence spectrum supports the theory, since dilution leads to increased inter-chain distances. This however does make the assumption that inter-chain interactions due to chain coiling or folding are not effective.[42] There are, however, many reports in which authors strongly disagree with excimer formation as the predominant cause of the g-band. [50-51]

5.2.3.2 *Aggregates*

One report suggested that the growth of aggregates could act as exciton traps, with the g-band forming from the excimers in the aggregated region. As well as the structural reorganisation associated with excimer formation there is also the possibility that the excimer could mediate the growth of the aggregate regions. The evidence, which supports this, includes the lack of measurable change in the absorption spectrum and the common fluorescence excitation spectrum for the emission and the g-band.[43, 52-55]

5.2.3.3 *Formation of ketone defects*

List, Scherf and co-workers [56] suggested a link between the formation of a ketone group at the C-9 site (to give keto-defects, shown in figure 5.6) and the evolution of the g-band emission during the oxidation process. They argue that the g-band emission originates directly from an emissive state of the fluorenone. Zojer and co-workers created a model whereby fluorenone defects, created following or accompanying scissions of the mono alkyl/or dialkyl side chains, act as low-energy trap sites for excitons. Dipole-dipole Förster transfer or energy migration assisted processes populate the fluorenone sites which then emit with what is considered the characteristic fluorenone spectrum. 9 fluorenes units are more planar that 9,9 dialkylfluorene units and for this reason, 9 fluorenone containing polyfluorenes may be more prone to aggregation and excimer formation than 9,9 polyfluorenes.[56]

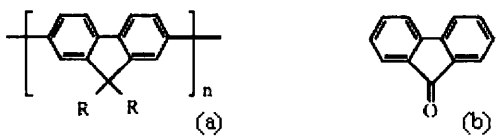

Figure 5.6: Chemical structures of (a) a polyfluorene, and (b) a polyfluorenone (PF0). [56]

Many reports support this theory. Lupton and co-workers for example, reported that direct excitation of keto-defects produce the g-band emission.[57] In 2006 Scherf and co-workers also suggested the additional possibility of alkylidene defects.[58]

5.2.4 Energy transfer from polyfluorene into ketone defects

Recent theoretical studies on model fluorenone containing oligomers suggest that the green emission originates from the fluorenone parts due to very efficient energy transfer and strong localisation (i.e. trapping) of the excitons on the low-energy fluorenone units. [60-62] It has been suggested that 'competition' occurs after photo-excitation between the blue band PF luminescence and energy transfer to the green fluorenone via a Förster dipole-dipole energy transfer interaction since the spectral overlap between the fluorescence spectrum of PF and the absorption spectrum of the ketone defect is large.[61] At low acceptor percentages, i.e 1 and 0.5%, the emission is typically dominated by polyfluorene blue emission presumably due to inefficient energy transfer between the polyfluorene donor and fluorenone acceptor. However, at higher defect concentrations the emission is dominated by the fluorenone acceptor, indicating perhaps more effective energy transfer.[63] Heeger, Moses and co-workers, working with a poly(9,9-dioctylfluorene-co-flurenone) with 1% fluorenone (PFO-F(1%)) (shown in figure 7), reported that Förster ET to, and charge carrier trapping on, the fluorenone defects (with subsequent fluorenone emission) was responsible for the colour degradation of the PF emission.[63]

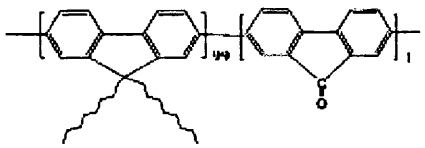

PFO-F (1%)

Figure 5.7: Molecular structure of PFO-F (1%).[63]

5.2.5 Previous Studies on PF2/6 and polyfluorenes with defects

Initial photochemical studies were completed by A.T. Marques from the University of Coimbra on a sample of PF2/6 with a number average molecular mass 210 kg mol^{-1} [1] The 2-D structure is shown in figure 5.8. This compound dissolves readily in a range of hydrocarbons, and some of the photochemical data already available in literature is summarised in table 1.[1] In all solvents investigated by Marques the PF2/6 has an absorption λ_{max} of ca. 390 nm and an emission λ_{max} of ca. 420 nm with a quantum yield ranging from 0.25 to 0.50 with a lifetime of 420-430 ps measured by time correlated single photon counting (TCSPC).[1]

Solvent	λabs / nm	λemi / nm	Φ_f	τf / ps	χ^2
Cyclohexane	389	414	0.250	420	1.31
Toluene	391	416	0.420	420	1.20
Dichloromethane	392	414	0.450	440	1.30
Chloroform	391	417	0.325	430	1.85
Chlorobenzene	392	416	0.496	420	1.42

Table 5.1: Absorption and emission behaviour of **1** in a range of solvents. [1]

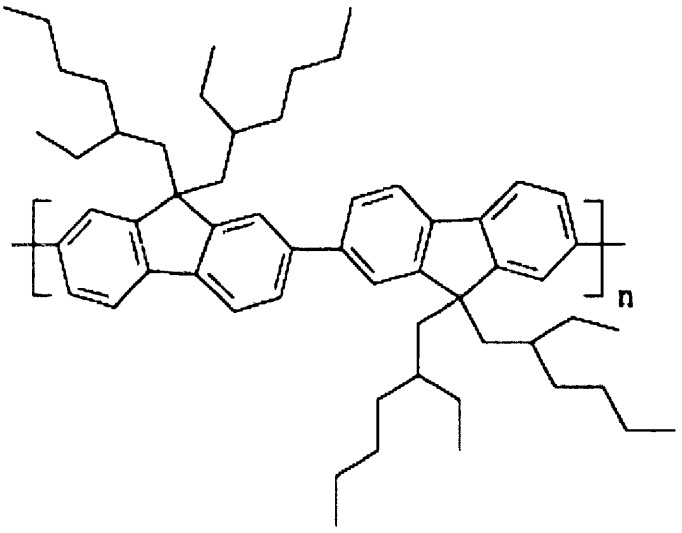

Figure 5.8: 2-D structure of **PF2/6** [1]

A.T.Marques also investigated the absorption and emission spectroscopy of the PF2/6 defect polymers that will be used in this chapter.[1] Figures 5.9 and 5.10 show the absorption and emission spectra as a function of defect concentrations.

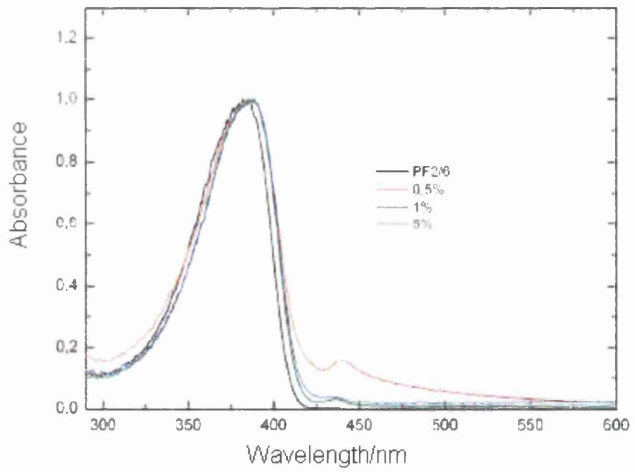

Figure 5.9: Absorption spectrum of PF2/6 and PF2/6 with different percentages of ketone defects.[1]

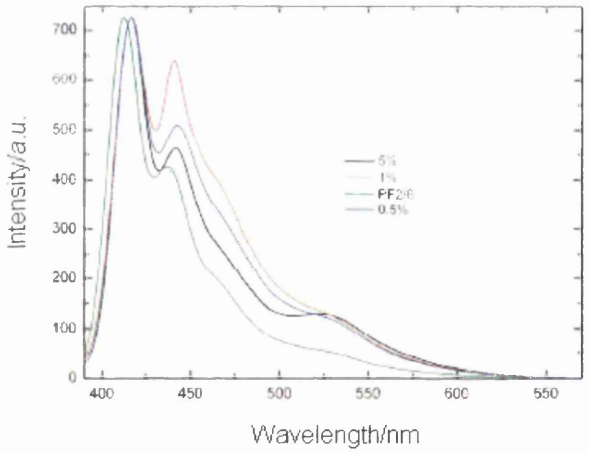

Figure 5.10: Emission spectrum of PF2/6 (green) and PF2/6 in the presence of different percentages of ketone defects; 5 % (black), 1 % (red), 0.5 % (blue) (λ_{ex} = 380 nm).[1]

5.3 Experimental

5.3.1 Instrumentation and computational techniques

5.3.1.1 Absorption studies

UV-visible spectra were recorded at Swansea University using either a Unicam UV300 spectrometer or a Hewlett Packard HP 8452A single beam diode array spectrophotometer. The Shimadzu 2100 spectrometer at the Chemistry Department at the University of Coimbra, Portugal was also used to make some measurements.

5.3.1.2 Steady state emission and excitation measurements

Room temperature and 77 K emission measurements were carried out using either a Perkin Elmer MPF-44E fluorescence spectrometer or a Horiba-Jobin-Ivon SPEX Fluorog 3-22 spectrometer.

5.3.1.3 Quantum yields

Quantum yields were measured against alpha-4 dissolved in ethanol as standard. The solutions of the polymer and references were made up to have an absorbance of ca. 0.1. The quantum yield, Φ_x, was calculated by reference to the standard R using Equation 5.1 below. A is the intensity of light absorbed at the excitation wavelength, I is the integrated emission intensity corrected for the instrument response, and n is the refractive index of the solvent.[36]

$$\Phi_x = \Phi_R(A_R/A_x)\,(I_x/I_R)(n_x/n_R)^2 \qquad \textbf{(eq. 5.1)}$$

5.3.1.4 Time correlated single photon counting (TCSPC)

All picosecond (ps) work was done using time correlated single photon counting (TSCPC) at the Physics Department, University of Durham. Decay curves were recorded using 385 nm

excitation and collecting data at either the polyfluorene emission maximum of 420 nm or the defect emission maximum of 550 nm. Decay curves for each sample were collected over a time period of 30 minutes. Decay kinetics were analysed using Globals Programme.

5.3.2 Chemicals

5.3.2.1 Solvents

HPLC fluorescence grade (without stabiliser) >99.995% Tetrahydrofuran (THF) was purchased from Fisher scientific and was used as received. THF did not exhibit any detectable emission under the conditions used.

5.3.2.2 Polymers

All polymers were a gift from Professor Ullrich Scherf at the University of Wuppertal, Germany. Table 5.2 gives details of the polymers used. The codes refer to the numbers used by the Scherf group to identify the polymer. Where available M_n and M_w are also given.

Code	Defect (%)	M_n	M_w	Average Number of Repeat Units per Chain
PF2/6	0	22.3	56.8	59
Fgp5.6	2.0	58.9	115.2	155
Fgp5.7	5.0	58.2	108.9	154

Table 5.2: Molar mass characteristics of the polymers used.[1]

5.4 Results and discussion

5.4.1 Optical studies of PF2/6 without any defects, in THF solution

5.4.1.1 Absorption

PF2/6 dissolves readily in THF to give a clear solution which appears blue in reflected light. The broadband absorption has an absorption λ_{max} at 386 nm. [1,25]

5.4.1.2 Emission

The emission spectrum is typical for a polyfluorene (figure 5.14). Dialkylated PFs typically emit blue light at a wavelength region of 415-420 nm as well as two additional vibronic side bands at 439-445 nm and 470-475 nm. These have been assigned to 0-0, 0-1, and 0-2 intrachain singlet transitions. The behaviour of PF2/6 in THF is comparable to its behaviour in halogenated solvents as shown in table 1.[63] The emission λ_{max} is at 414 nm with additional bands at 438 nm and 470 nm. Φ_f in THF is 0.35, which is similar to its quantum yield in chloroform solution (0.325). [1]

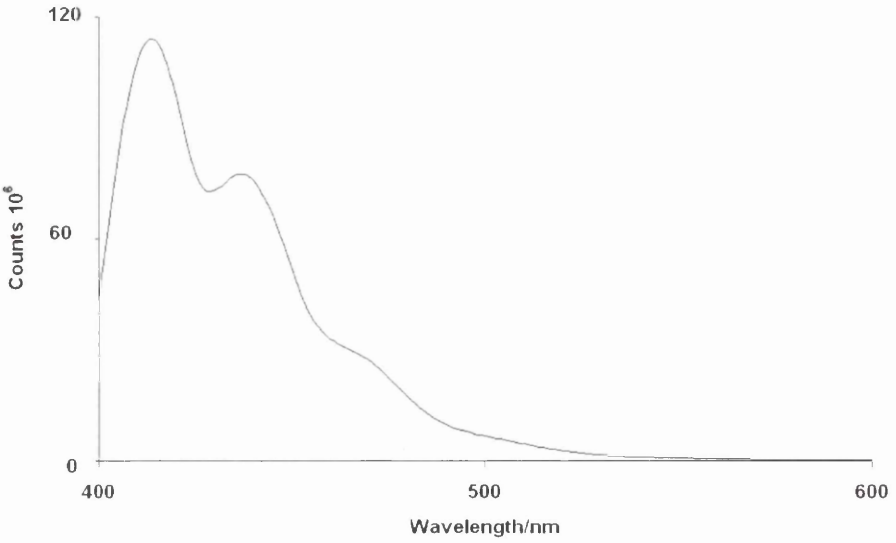

Figure 5.14: Emission spectrum of PF2/6 in THF solution. Excitation wavelength = 385 nm.

5.4.2 Optical studies on polyfluorenes with 0%, 2% and 5% ketone defects

5.4.2.1 Time correlated single photon counting studies

In this section of work, the interest is focused towards examining energy transfer between fluorene-fluorene and fluorene-fluorenone units. Decays were recorded using a 385 nm excitation pulse and collecting at either the polyfluorene emission maximum of 420 nm or the defect emission maximum of 550 nm. Each sample was made up to give approximately the same absorbance of 0.10 at the excitation wavelength and, to get some idea of relative emission yields, each decay was collected over the same time i.e. 30 minutes so that each sample absorbed approximately the same number of excitation photons.

5.4.2.2 Fluorene emission with and without defects, collected at the fluorene emission maximum, 420 nm

The emission decay curve of PF2/6 with no defects is presented in figure 5.15, and the decays of the polyfluorenes Fgp5.6 and Fgp5.7 (see Table 5.2) which have 2 % and 5 % defects respectively, are presented in figures 5.16 (a) and (b). Upon increasing the defect concentration both the overall emission yield and emission lifetime decreases. The decay curves have been fitted to 2 exponentials using the Globals programme, although it is important to recognise that Globals is only a fitting programme, and the values obtained may have no physical significance. Fitting parameters are shown in table 5.3.

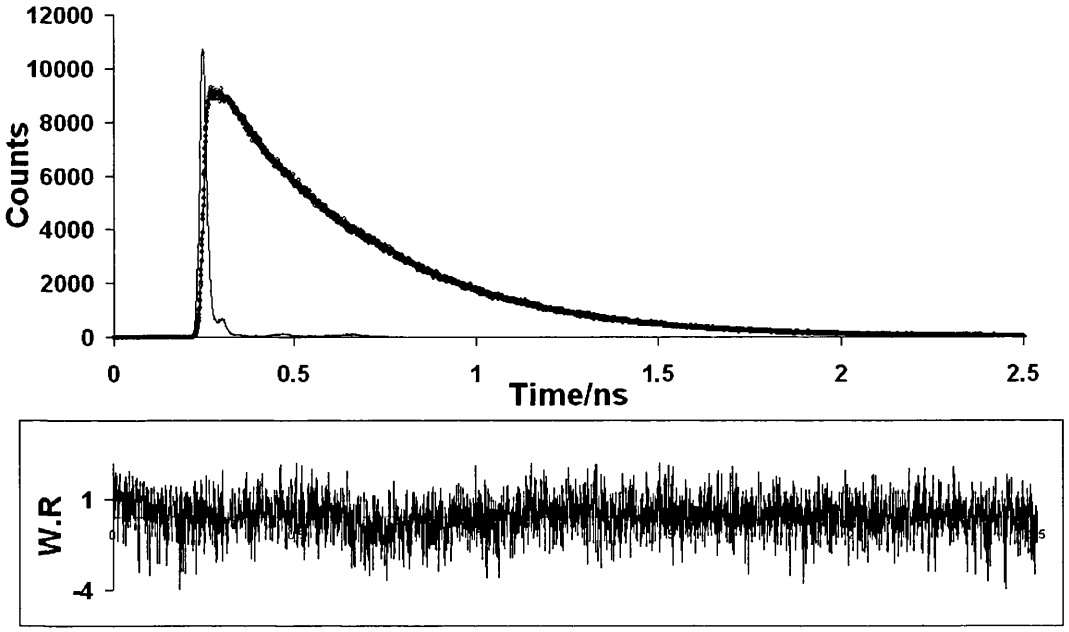

Figure 5.15: TCSPC measurement and residuals for PF2/6 in THF solution. The excitation wavelength was 385 nm, the emission wavelength was 420 nm, and the decay was recorded over 30 minutes.

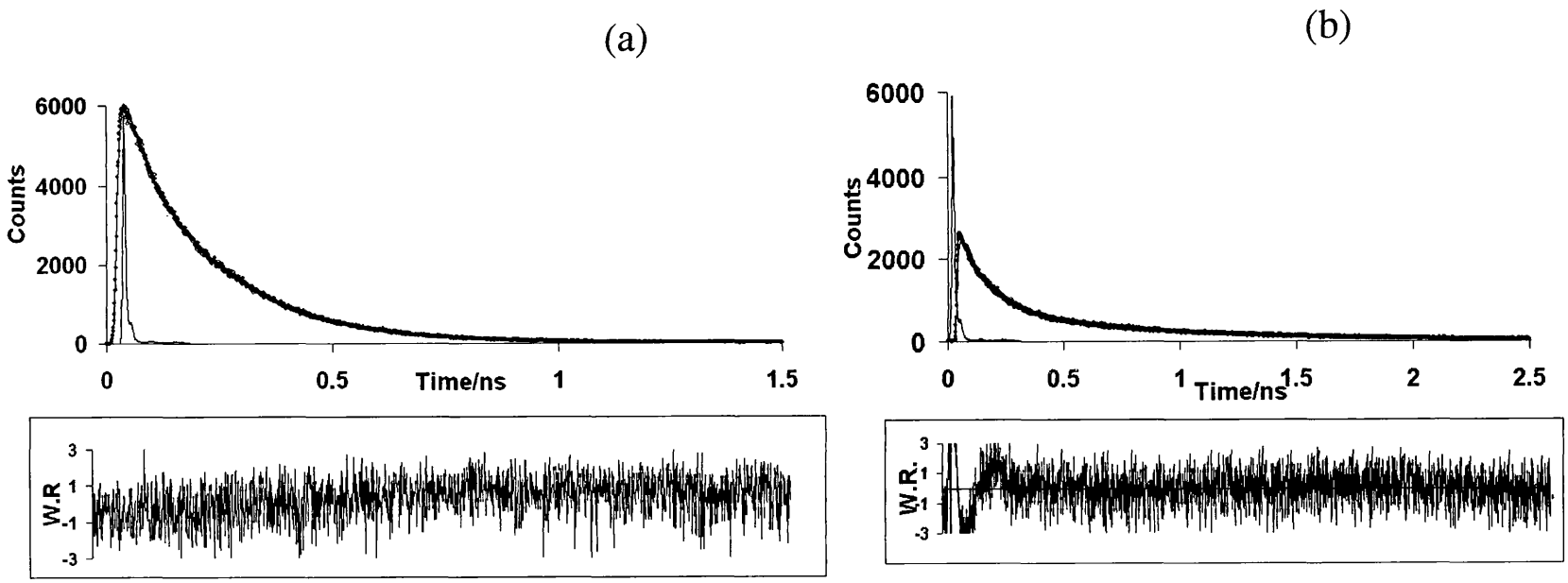

Figure 5.16: TCSPC decays and residuals of the polyfluorenes Fpg5.6 (a) and Fpg5.7 (b) which carry 2 % and 5 % ketone defect respectively. The decays were measured with 385 nm excitation wavelength. Decay curves are collected at 420 nm emission wavelength. The decays were measured over 30 minutes. Please note the longer timescale on figure (b).

Defect	λ emission /nm	α_1	τ_1	α_2	τ_2	χ^2
0%	420	2.70	0.369	0.501	0.584	1.14
2%	420	0.591	0.290	4.68	0.162	1.13
5%	420	0.113	0.271	4.51	0.165	1.17

Table 5.3: Table of fitting parameters obtained for polyfluorenes with 0%, 2% and 5% defects, (PF2/6, Fpg5.6 and Fpg5.7), using 385 nm excitation and 420 nm emission wavelengths.

5.4.3 Description of the Polymer

As shown in table 5.2 both polymers with defects have essentially the same molecular weight characteristics. In order to understand the energy transfer kinetics within a polydisperse sample such as these it is useful to consider the polymer chain length distributions. These can be calculated using standard statistical arguments.[64] For statistical step growth polymerisation the probability of a chain with **n** repeat units between end groups, P_n, is given by:

$$P_n = (1-f)^n.f \qquad \textbf{(eq. 5.2)}$$

Where **f** is the ratio of end groups to repeat units.

Since each chain of length **n** contains **n** repeat units, the relative number of repeat unit units in chains of length **n**, $\mathbf{R_N}$ is given by:

$$\mathbf{R_N = P_n.n} \qquad \textbf{(eq.5.3)}$$

The probability of a chain of length **n** having no defects, $\mathbf{P_{nd}}$, in a polymer containing **x**% defects is given by;

$$\mathbf{P_{nd}} = (100-\mathbf{x})/100)^{\mathbf{n}} \qquad \textbf{(eq.5.4)}$$

Then the relative number of repeat units in chains of length **n** without any defects, $\mathbf{R_{Nnd}}$, is given by:

$$\mathbf{R_{Nnd} = R_N.\ P_{nd}} \qquad \textbf{(eq.5.5)}$$

.

Figures 5.17 and 5.18 show these distributions for polymers carrying 2% and 5% defects respectively. As expected the distribution of chains with no defects is shifted to the short chain side of the overall distribution while that for chains with defects it is shifted to the long chain side.

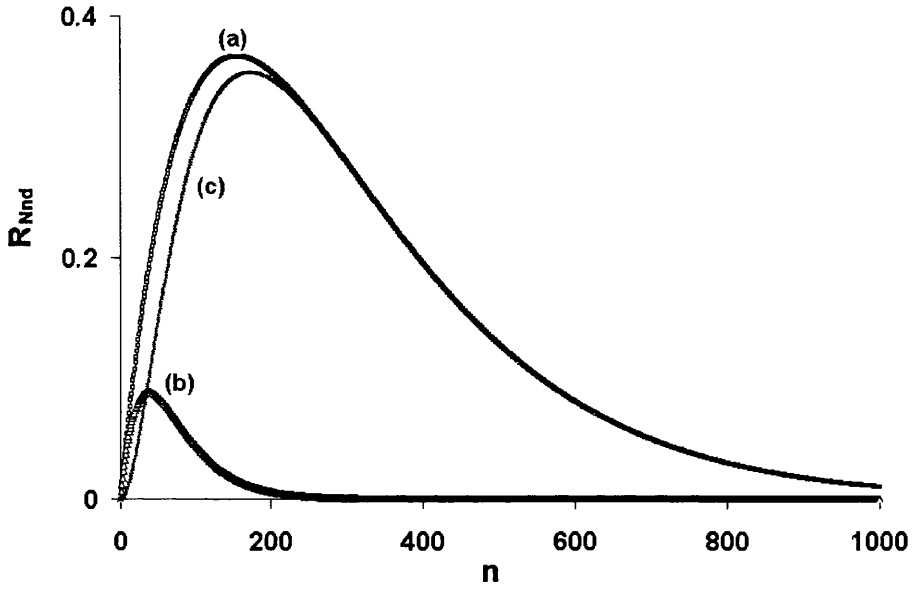

Figure 5.17: Chain length distributions for a polymer of average length **n** = 154 carrying 2 % defects. (a) is the overall distribution for the polymer, (b) the distribution of chains carrying no defects, and (c) the distribution of chains carrying at least one defect. (The distribution is normalised such that the area beneath the curve is equal to **n**.)

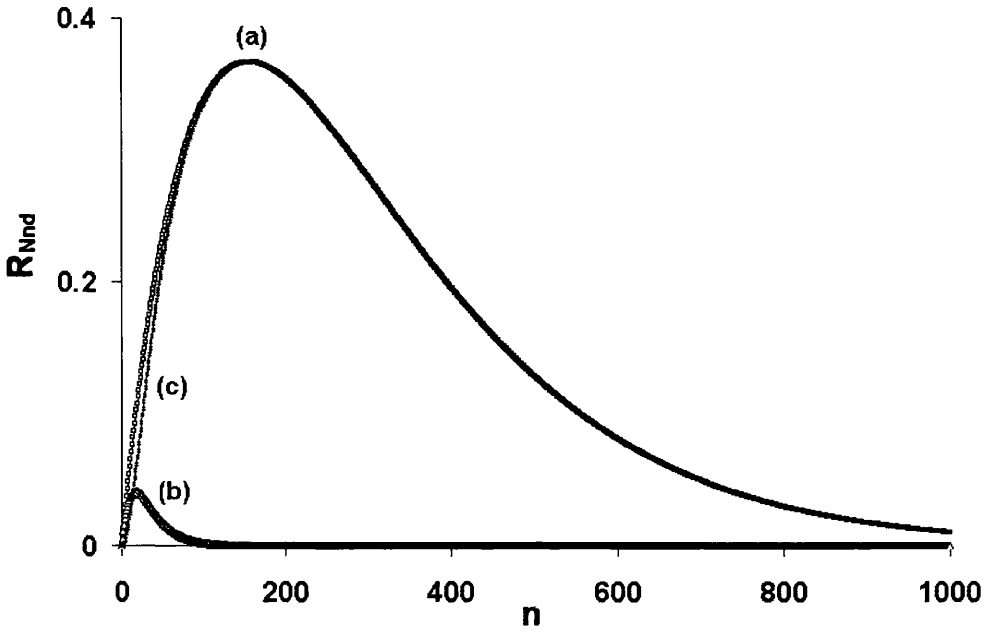

Figure 5.18: Chain length distributions for a polymer of average length **n**=154 carrying 5 % defects. (a) is the overall distribution for the polymer, (b) the distribution of chains carrying no defects, and (c) the distribution of chains carrying at least one defect. (The distribution is normalised such that the area beneath the curve is equal to **n**.)

5.4.4 Förster resonance energy transfer

Both intra and intermolecular energy transfer in a conjugated polymer system is generally modelled by the Förster theory, whereby the rate is determined by the spectral overlap between the donor and acceptor groups. Förster is a long range (~40-100Å) coulombic interaction whereby direct contact of the donor and acceptor groups is not required; instead energy transfer occurs via the electromagnetic field. Förster showed that the rate of energy transfer between D* and A for a dipole-dipole interaction is given by:[59]

$$k_{DA} = k^2 J.\ 8.8\times10^{-28}\ mol / R_i^{\ 4} \tau_{rad} R^6 \qquad - \qquad \textbf{(eq. 5.6)}$$

where: **k** is an orientation factor which is a reflection of the angle of interaction between 2 dipoles; **J** is the spectral overlap integral between the donor and acceptor (see equation 5.7); **R** is the distance between **D** and **A**; $\mathbf{R_i}$ is the refractive index; and τ_{rad} the radiative lifetime of D.

The Förster distance, $\mathbf{R_0}$, which is that distance at which the rate of FRET is equal to the radiative rate constant, and hence FRET is 50% efficient, can then be calculated via:[59]

$$\mathbf{R_0 = 0.2108[\kappa^2 \Phi_0 D R_i^{-4} \int I_D(\lambda) E_a(\lambda) \lambda^4 d\lambda]^{1/6}} \qquad \textbf{(eq. 5.7)}$$

Where $\mathbf{\Phi_0 D}$ is the donor emission quantum yield, and $\mathbf{I_D(\lambda) E_a(\lambda) \lambda^4 d\lambda}$ is the spectral overlap between donor emission spectrum, $\mathbf{I_D(\lambda)}$, and acceptor absorption spectrum, $\mathbf{E_a(\lambda)}$.

The spectral overlap for PF-PF energy transfer is shown in figure 5.19 from which the Förster energy transfer distance for PF-PF FRET was calculated as 27.9Å, which compares well with other values for polyfluorenes in the literature,[65] The calculated rate constant for FRET at the PF-PF distance of 8.5Å is 1.47 x 10^{12} s^{-1}. This calculation shows that nearest neighbour PF-PF energy transfer is very fast. However the high efficiency of quenching by a relatively small fraction of defects requires energy migration across many repeat units. Examination of the approximate relative quantum yields given by the integrated areas beneath the emission curves of the three polymers used in this study, Figure 5.20, indicate that with 2% defects energy migration is such that each defect has access to ca. 40 repeat units while for 5% the number is ca 20. Since the efficiency of FRET falls as the sixth power of the distance separating donor and acceptor, energy transfer migration along a chain is faster by a series of single energy transfers "hops" than by a single "jump" across a longer distance.

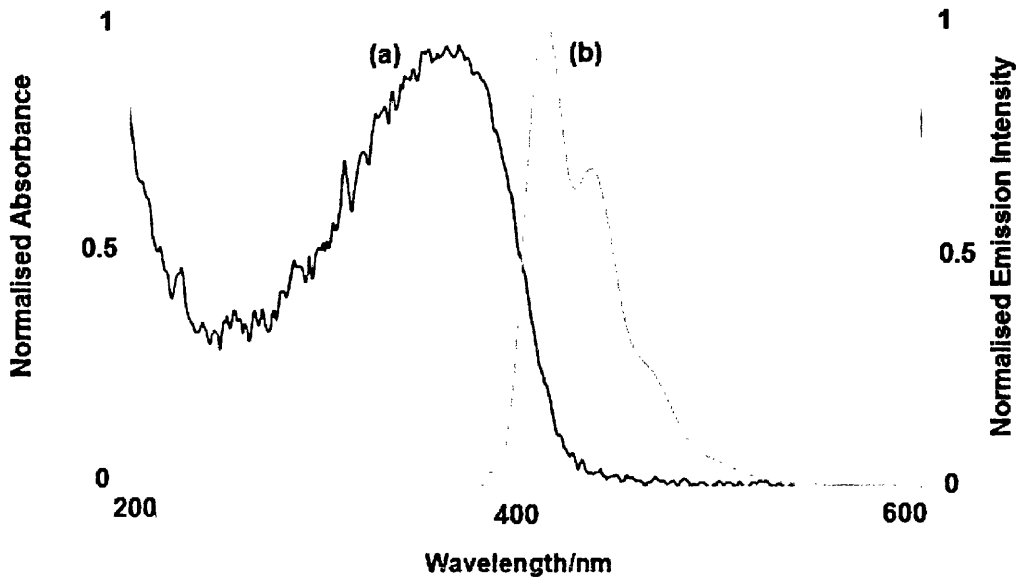

Figure 5.19: Overlap of the absorption spectrum (a) and emission spectrum (b) of PF2/6. Excitation wavelength = 385 nm.

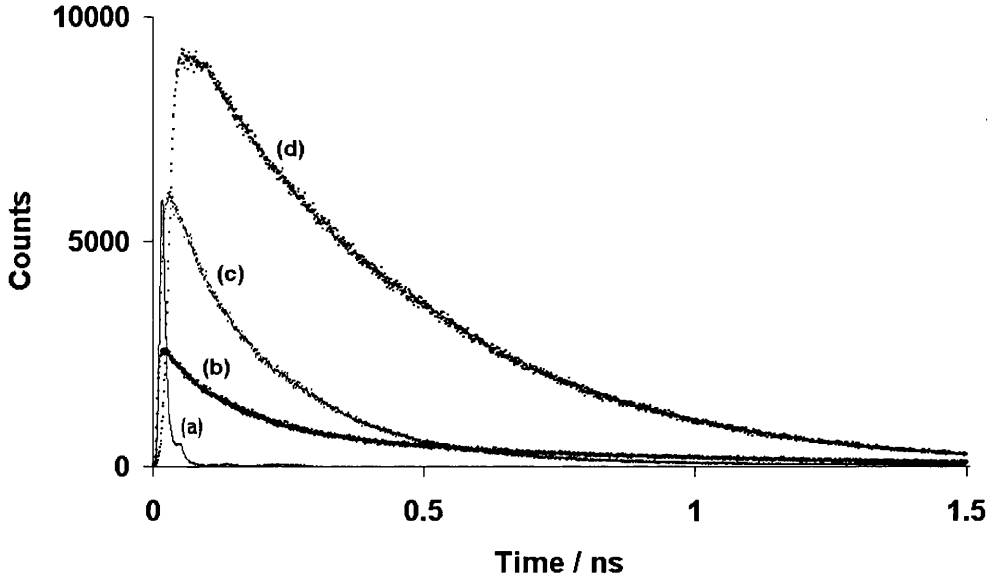

Figure 5.20: Experimental decay curves obtained from TCSPC. (a) Instrument response pulse; (b) 5 % defects; (c) 2 % defects; and (d) no defects. Emission wavelength = 420 nm. Excitation wavelength = 385 nm.

5.4.5 Energy Transfer Migration

Figure 5.21 show the kinetics of energy migration into a defect trap from a single repeat unit adjacent to an end group, which acts as a blocking unit such that energy transfer past it in the direction away from the defect is not possible, (see figure 5.22). The curves are for distances of 2 to 18 repeat units from the trap, with energy migration as a one dimensional random walk with both the repeat unit-repeat unit and repeat unit-defect "step" time equal to $1/k_{DA}$ for PF-PF FRET (1.47×10^{12} s^{-1}), and 100% energy loss within the defect trap. As can be seen, FRET from any site within about 10 repeat units of a defect occurs with high efficiency within about 100 ps. For repeat units further away energy migration into the defect trap occurs on a somewhat longer timescale.

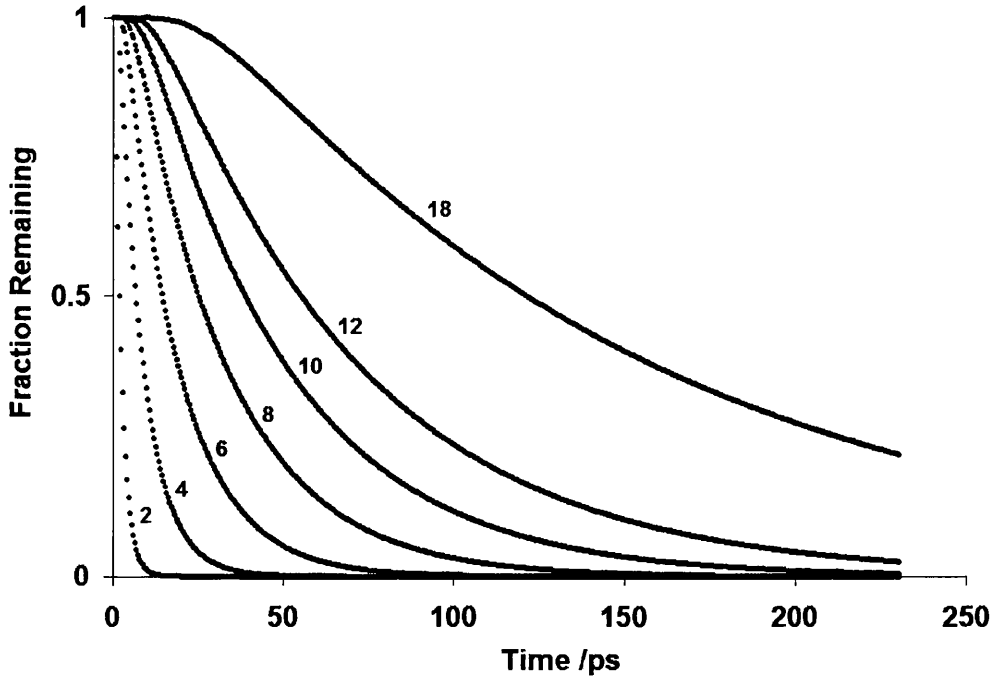

Figure 5.21: The kinetics of energy migration into a defect trap from a repeat unit at distances of: 2,4,5,8,10,12 and 18 repeat unit units from the trap.

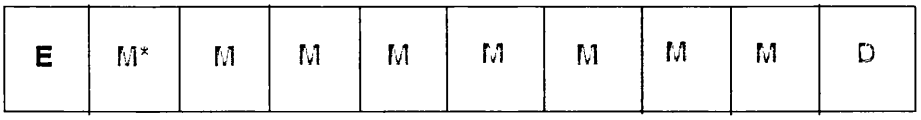

Figure 5.22: Arrangement for energy migration kinetics shown in Figure 21. Migration is a one dimensional random walk with both the repeat unit-repeat unit and repeat unit-defect "step" time equal to $1/k_{DA}$ for PF-PF FRET. **E**, is an end group which acts as a blocking site, **D** is a defect trap, **M*** is the initially excited repeat unit and **M** is a repeat unit.

5.4.6 Modelling Decay Curves

While Figure 5.21 gives an idea of individual energy transfer kinetics what is required is an integration across all possible excitation sites within the polymer; i.e. each repeat unit. Within the group in Swansea there is available a computer modelling program, *Program Clusters,* which can be used to model energy migration of this type. This program, designed by Alastair Douglas, was initially designed for modelling energy transfer dynamics in systems with unusual dimensionality and has been successfully used by Evans and co-workers to model energy transfer between lanthanides in silicates.[66] We have, by suitable choice of input parameters, adapted this program for use in the modelling of energy transfer in linear polymers containing defect traps.

Assumptions used in the model

1. Each repeat unit is equally excited by the excitation pulse.

2. Energy transfer rates are the same between PF-PF and PF-defect trap.

3. Once energy migrates into a defect it is trapped there and lost from the system.

4. The end group is considered as a block to energy migration and is not a quencher.

5. Energy migrates in a one dimensional random walk.

The program creates a random distribution of polymer chains and defects in a 10x100000 array. Energy is then allowed to transfer between nearest neighbour repeat units in a series of "steps" in which a fixed fraction (in this case 0.25) of the excitation energy at any repeat unit is transferred to any neighbouring repeat unit or defect trap. The total amount of energy remaining within the array after each step is calculated to give a decay curve for energy migration into traps alone. To account for the natural decay of excitation this curve is then adjusted with an exponential decay term corresponding to the decay in the absence of trapping. The step time, ***s***, is a variable, and the intensity after a number of steps, **z**, $\mathbf{I_z}$ is then given by:

$$\mathbf{I_z = R_z \times e^{-k(zs)}} \qquad \textbf{(eq. 5.8)}$$

Where $\mathbf{R_z}$ is the response from the clusters program at step number **z**; **zs** is the total time from t=0, and **k** is the decay rate in the absence of energy trapping.

Both the step time and natural decay rate are then variables for curve fitting to the observed decay. In addition, since energy migration is so fast a significant fraction can occur with the instrument response time, we introduce another normalisation variable to allow for this, i.e. the emission maximum does not correspond to the array population at t=0.

Figures 5.23 and 5.34 show the curve fit using *program clusters* for 2% and 5% defects respectively. The fits are very good. Furthermore, the best fit step times are very similar for both curve fits at 2.7 $\times 10^{-13}$ s and 3.4 $\times 10^{-13}$ s, which correspond to ET rate constants of 1.01

$x10^{12}$ s^{-1} and 0.85 x 10^{12} s^{-1} , for 2 % and 5 % defects respectively. These values compare very well to the calculated FRET rate constant of 1.47 x 10^{12} s^{-1}.

It must, however, be emphasised that unlike TCSPC curve fitting programs, our fits have not be obtained by a rigorous statistical analysis. Rather we have varied all three variables about a series of small incremental steps. What is more important is that, while TCSPC programs involve deconvolution of the instrument response profile we are not yet in a position to easily do this in our analysis. Because of these factors the quality of the curve fits should be taken as an indication of the potential usefulness of the approach taken here rather than a definitive statement of some statistical quality of fit. However, we note that using a 2 exponential fit from Globals requires essentially 4 variables to fit the data, whereas the approach presented here only requires 3. Furthermore, while it is very difficult to assign any physical significance to the values obtained from Globals, those obtained from the approach present here have some clear physical meaning.

It should also be noted that while the best fit natural rate constant for 2 % defects was 3.7 x 10^9 s^{-1} that for 5% defects was much lower at 6.9 x 10^8 s^{-1}. (The longer lifetime "tail" of the 5% defect curve is obvious in the raw data (Figures 5.16 a and b). The reason for this difference is not clear. However, it is worth noting that the decay curve in the absence of defects is not itself exponential and is rather complex, and it is possible that the addition of 5% defects is a significant enough change in overall polymer structure that the "natural" repeat unit decay kinetics are different. In addition, with a higher defect concentration, and therefore higher defect emission, it is perhaps possible that there is contribution from the broad defect band emission, even at 420 nm. In this regard, it is worth pointing out that with 5% defects the emission decay at the defect maximum of 550 nm (see below) also shows a long emission "tail".

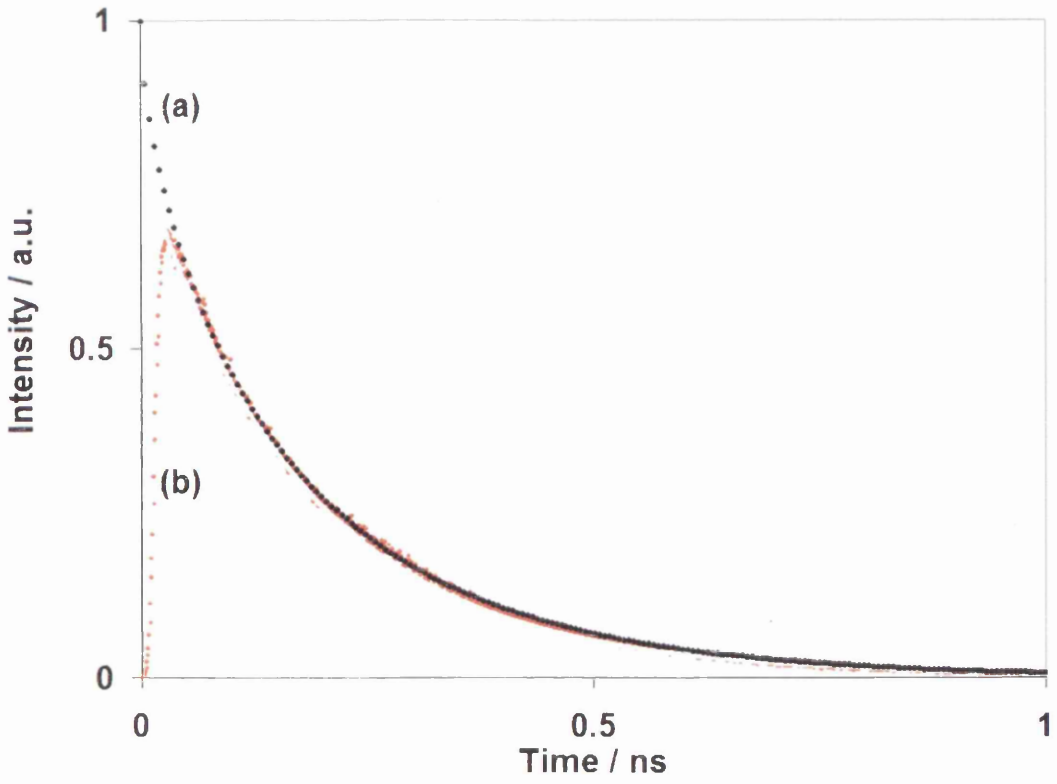

Figure 5.23: Comparison of experimentally obtained decay curve from TCSPC (red) and the fitted curve obtained from *program clusters* (black) for the polyfluorene carrying 2 % defects (Fpg5.6).

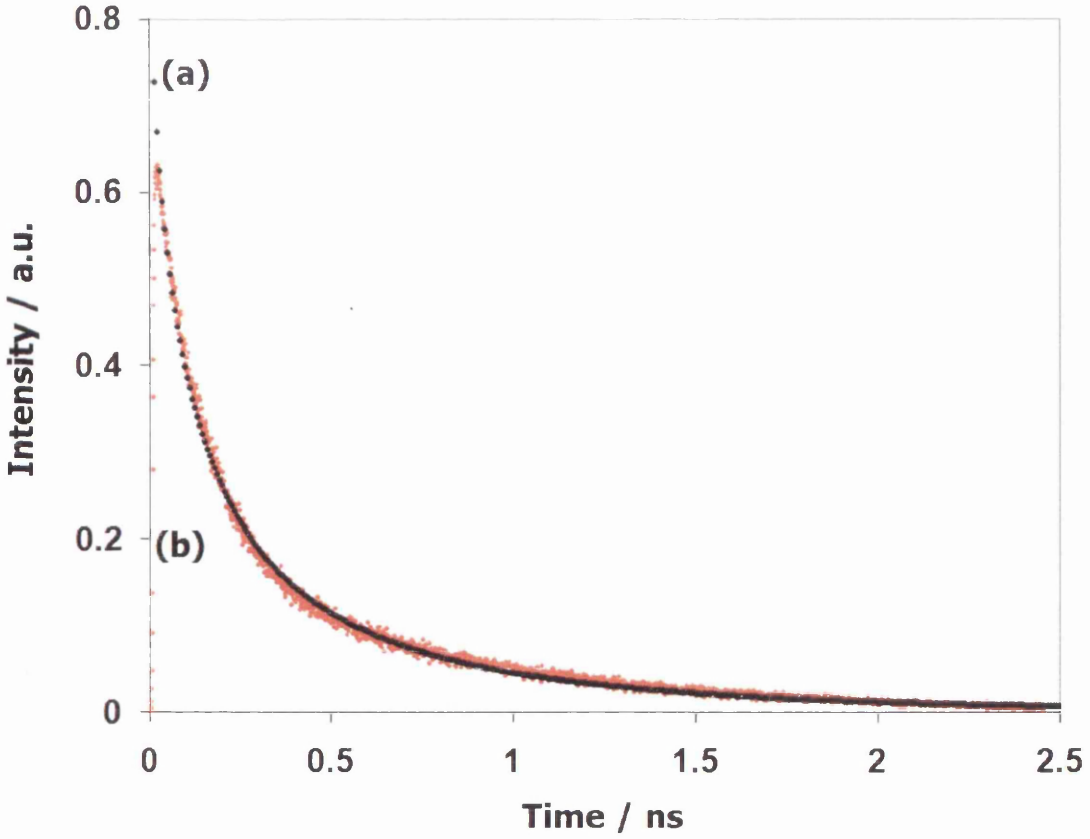

Figure 5.24: Comparison of experimentally obtained decay curve from TCSPC (red) and the fitted curve obtained from *program clusters* (black) for the polyfluorene carrying 5 % defects, Fpg5.6.

5.4.7 Defect decays collected at 550 nm emission, the defect maximum

The decays of the polyfluorenes with 2% and 5% defects, using 385 nm excitation and 550 nm emission wavelengths, are reported in figure 5.24 and table 5.4. Again the decays were fitted by the Globals software to two exponentials with good χ^2 values and residuals. The emission observed for polymers carrying 2% and 5 % defects at 550 nm is expected to be complex, since in addition to emission from the defect site there will also be a contribution from PF emission. However we can make the following observations.

a) The emission yields from the integrated decay curves show that the emission intensity from the 5% defect sample is higher.

b) In both cases the curve fit gives a significant very fast grow-in, which is faster for 5% than 2%, although the timescale for this is so fast it is difficult to be confident in the assignment.

c) For the sample carrying 5% defects the lifetime of the dominant long lived emission is 1.01 ns which is not too dissimilar to that from the program clusters fit of, 6.9×10^{8} s^{-1} suggesting that both decays might correspond to the same species.

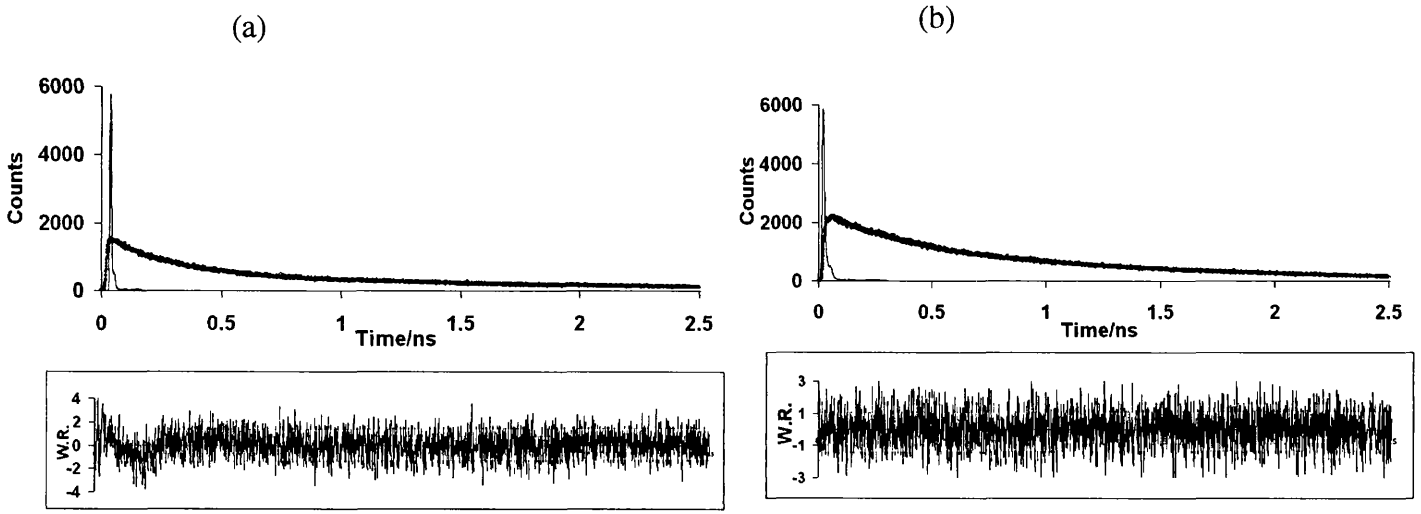

Figure 5.24: TCSPC decays of polyfluorene polymers with (a) 2 % and (b) 5 % ketone defect. The decays are measured with a 385 nm excitation wavelength. Decay curves are collected at a 550 nm emission wavelength. The decays were measured over 30 minutes.

Defect	λ emission /nm	α_1	τ_1	α_2	τ_2	χ^2
2%	550	1.14	0.21	-1.611	0.003	1.12
5%	550	0.960	1.01	-1.26	0.001	1.20

Table 5.4: Table of fitting parameters obtained for emission from polyfluorenes with 2% and 5% PF defects, obtained using 385 nm excitation and 550 nm emission wavelengths.

5.5 Conclusions

The purpose of this study was to use the TCSPC to examine the emission kinetics of polyfluorenes which have ketone defects built into the polymer chain. For emission at the 420 nm polyfluorene maximum, both the emission lifetime and the emission yield decreased upon increasing the defect concentration. For emission at 550 nm, the defect maximum, the emission yield increased with defect concentration. This provides strong evidence for energy transfer between the PF and the defect unit. FRET calculations showed that energy transfer between two PF-PF units is rapid, with a rate constant of 1.47×10^{12} s^{-1} at the PF-PF distance of 8.5Å. Due to the polydispersity of the polymer system the energy transfer kinetics and mechanism are complex. Modelling was used to show the individual energy transfer kinetics into a defect trap from a repeat unit. This demonstrated that for repeat units close to the trap energy migration into the trap is very fast.

To better understand the energy transfer kinetics the chain length distributions were considered *Program Clusters* was used to integrate across all the possible excitation sites

within the polymer to give an integrated decay curve which could be curve fitted to the experimental data to obtain both the energy transfer rate constant and the rate constant for decay in the absence of energy transfer. The very good agreement between the curved fitted energy transfer rate constants: 1.01 $x10^{12}$ s^{-1} and 0.85 x 10^{12} s^{-1} , for 2 % and 5 % defects respectively, and that calculated by FRET theory, 1.47 x 10^{12} s^{-1}, provides very strong support for the validity of the interpretation of the energy transfer kinetics and the modelling approach taken.

5.6 References

1. Marques, A.T.; *A Photophysical and Photochemical Study of the Degradation of Polyfluorenes*, Dissertation, **2006**. University of Coimbra, Portugal.
2. Bernanose , A,; Vouaux, P.; Chim, *J.Chem.Phys*, **1953**, 50, 261
3. Shirakawa, H.; Louis, E.J.; MacDiarmid, A.G.; Chiang. C.K.; Heeger, A.J. *Chem. Commun,* **1997**, 578
4. Burroughes, J.H.; Bradley, D.D.C.; Brown. A.R.; Burn, P.L.; Mackey, K.; Friend, R.H.; Holmes A.B. *Nature*, **1990**, 347, 539
5. Winokur, M.J.; Chunwachirasiri, W. *Journal of Polymer Science. Part B: Polymer Physics,* **2003**, 41, 2690
6. Leclerc, M. *Journal of Polymer Science. Part A: Polymer Chemistry*, 2001, 39, 2867
7. Burroughs, J.H.; Bradley, D.D.C.; Brown, A.R.; Burn, P.L.; Marks, R.N.; Mackey, K, Friend, R.H.; Holmes, A.B. *Nature*, **1990**, 347, 539
8. Kallinger,C.; Hilmer, M.; Haugeneder, A.; Perner,M.; Spirke, W.; Lemmer. U.; Feldman. J.; Scherf. U.; Mullen. K.; Gombert. A.; Wittwer. V. *Adv. Mater,* **1998**,10, 920

9. McGehee, M.D.; Heeger, A.J. *Adv.Mater*, **2000**, 12, 1655

10. Kozloz, V.G.; Forrest, S.R. *Curr.Opin.Solid.State.Mater.Sci.*, **1999**, 4, 2003

11. Scherf, U.; Riechel, S.; Lemmer, U.; Mahrt, R. *Curr.Opin.Solid.State.Mater.Sci,* 2001, 5, 143

12. Tessler, N.; Denton, G.L.; Friend, R.H. *Nature*, **1996**, 382, 695

13. Imahori, H.; Fukuzumi, S. *Adv.Funct.Mater*, **2004**, 14, 525

14. McQuade, D.T.; Pullen, A.E.; Swager. T.M. *Chem.Rev*, **2000,** 100, 2537

15. Hoppe, N.; Saricftci, N.S. *J.Mater.Res,* **2004**, 19, 1924

16. Brabec, C.J.; Saricftci, N.S. *Adv. Func.Mater*, **2001**, 11, 15

17. Halls, J.J.M.; Arias, A.C.; Mackenzie, J.D.; Wu, W.S.; Inbasekaran, M.; Woo, E.P.; Friend, R.H. *Adv. Mater*, **2000**, 12, 498

18. Grell, M.; Bradley, D.D.; Ungar, G.; Hill, J.; Whitehead, K.S. *Macromolecules*, **1999**, 32, 5810

19. Fukuda, M.; Sawada. K.; Yoshimo, K. *Jpn.J.Appl.Phys. Part 2*, **1989**, 28, L1433

20. Liu, J.; Tu, G.L.; Zhou, Q.G.; Cheng, Y.X.; Geng, Y.H.; Wang, C.X.; Ma.,D.G.; Jing, X.B.; Wang, F.S. *J.Mater.Chem*, **2006**, 16, 1431

21. Tu, G.L. ; Zhou, Q.G. ; Cheng, Y.X. ; Geng, Y.H. ; Wang, L.X. ; Ma, D.G. ; Jing, X.B. ; Wang, F.S. *J.Mater.Chem*, **2006**, 16, 1431

22. Pei, Q.B. ; Yang, Y. *J.Am.Chem.Soc*, **1996**, 118, 7416

23. Dieter, N. *Marcromol.Rapid.Commun*, **2001**, 22, 1365

24. Scherf, U.; List, E.J.W. *Adv.Mater*, **2002**, 14, 477

25. Galbrecht, .;, *PhD Thesis: Novel Polyfluorene Base Co-polymers for Opto Electronic Applications*, **2008**, University of Wuppertal, Germany.

26. Heliots, G.; Xia, R.; Bradley. D.D.C. *Appl.Phys.Lett,* 2003, 83, 2118

27. a) List, E.J.W.; Gunter, R.; Scandiucci di Freitas, P.; Scherf, U. *Adv.Mater*, **2002**, 14, 374. b) *ibid* 26

28. Halls, J.J.M.; Arias, A.C.; Mackenzie, J.D.; Wu, W.; Inbasekaran, M.; Woo,E.P.; Friend, R.H. *Adv.Mater*, **2000,** 12, 7

29. Chunwaschirasiri, W.; Tanto, B.; Huber, D.L.; Winokur, M. *J.Phys.Rev.Lett,* **2005**, 94,107402

30. Moilton, A.; Hiorns, R.C. *Polym.Int*, **2004,** 53, 1397

31. Gamerith, S.; Gadermaier, C.; Scherf.,U. *Phys.Status Solidi A*, **2004**, 201, 1132

32. Grell, M.; Bradley, D.D.C.; Ungar, G.; Hill, J.; Whitehead, K.S.; *Macromolecules*, **1999**, 32, 5810

33. Lieser,G.; Oda, M, Miteva.; O.Y, Meisal A.; Nothofer. H.G.; Scherf. U.; *Macromolecules*, **2004**, 37, 9438

34. Tanto, B.; Guha, S.; Martin, C.M.; Scherg, U.; Winokur. M.J.; *Macromolecules*, **2004**, 37, 9438

35. Knarapila, M.; Stepanyan, R.; Lyons. B.P.; Torkkelu, M.; Hase, T.P.A.; Serimaa, R.; Gauntner, R.; Seek. O.H.; Scherf. U.; Monkman, A.P. *Macromolecules*, **2005**, 38, 2744

36. Bradley, D.D.C.; Grell, M.; Long, X.; Mellor, H.; Grice, A. *SPIE proc. Int.Soc.Opt.Eng,* **1997**, 3145, 254

37. Long, X.; Grell, M.; Malinowski, A.; Bradley, D.D.C.; Inbasekaran, M.; Woo, E.P. *Opt. Mater*, **1998**, 9, 70

38. Pei, Q. ; Yang, Y. *J.Am.Chem.Soc*, **1996**, 118, 7416

39. Kreyenschmidt, M.; Klarner, G.; Fuhrer, T.; Ashenhurst, J.; Karg, S.; Chen, W.D.; Lee, V.H.; Scott, J.C.; Miller, R.D.; *Macromolecules*, **1998**, 31, 1099

40. Lee, J.I.; Klamer, G.; Miller, R.D.; *Synth.Met*, **1999**, 101, 126

41. Palson, L-O.; Wang. C.; Monkman. A.; Bryce, M.R.; Rumbles, G.; Samual, I.D.W. *Synth.Met*, **2001,** 119, 627.

42. Blinxnyuk, V.N.; Carter, S.A.; Scott, J.C.; Klamer, G.; Miller, R.D. ; Miller, D.C. ; *Macromolecules*, **1999**, 32, 361

43. Sims, M.; Bradley, D.D.C.; Ariu, M, Koeberg.; M, Asimakis. A.; Grell, M.; Lidzey, D.G. *Adv.Funct.Mater*, **2004**, 14, 76

44. List, E.J.W.; Guentner, R.; De Freitas, P.S.; Scherf, U.; *Adv.Funct.Mater*, **2002**, 12, 374

45. Silva, C.; Russel, D.M.; Dhoot, A.S.; Herz, L.M.; Daniel, C.; Greenham, N.C.; Arias, A.C.; Setayesh.; S, Mullen.; K, Friend, R.H. *J.Phys.Condens.Matter*, **2002**, 14, 9803

46. Scherf, U.; List, E.J.W. Adv.Mater.2002, 14, 472

47. Sims, M.; Bradley, D.D.C.; Aria, M.; Koeberg, M. *Adv.Funct.Mater.* **2004**, 14, 766

48. Stevens, B.; Hutton, E.; *Nature*, **1960**, 186, 1045

49. Conwell, E.M. *Synth.Met*, **1997**, 85,995

50. Bliznyuk, V.N.; Carter, S.A.; Scott, J.C.; Klamer, G.; Miller, R.D. ; Miller,D.C. *Macromolecules*, **1999**, 32, 361

51. Yan, M. ; Rothberg, L.J. ; Papadimitrakopoulos, F.; Galvin, M.E.; Miller, T.M, *Phys.Letts*, **1994**, 73, 744

52. Herz, L.M.; Phillips, R.T.; *Phys.Chem.Rev.B,* **2000**, 61, 13691

53. Teetsov, J.; Fox, M.A.; *J.Mater.Chem*, 1999, 9, 2117

54. Teetsov, J.; Van den Bout, D.A. *J.Phys.Chem.B*, **2000**, 104, 9378

55. Teetsov, J.; Van den Bout, D.A.; *Macromol.Symp*, **2001**, 167, 153

56. Scherf, U.; *Adv.Funct.Mater*, **2004**, 14, 8

57. Lupton, J.M.; Craig, M.R.; Meijer, E.W. *Appl.Phys.Lett*, **2002,** 80, 4489

58. Becker, K.; Lupton, J.M.; Feldman, J.; Nehls, B.S.; Galbrecht, F.; Gao, D.Q.; Scherf. U. *Adv.Funct.Mater*, **2006**, 16, 364

59. Forster, T. *Disc FaradaySoc*, **1959**, 27,7

60. Dexter, D.L. *J.Chem.Phys*, **1953**, 21, 836

61. Grigalevicius, S.; Forster, M.; Elinger, S.; Landfester, K.; Scherf, U. *Macromol. Rapid. Commun.* **2006**, 27, 200

62. Wiesenhofer, H.; Zojer, E.; List, E.J.W.; Scherf, U.; Bredas. J.L.; Beljonne. D. *Adv.Mater*, **2006**, 18, 310

63. Gong, X.; Moses, D.; Heeger, J. *J.Phys.Chem.B*, **2004**, 4, 8601

64. Cowey, J.M.G. *Polymers: Chemistry and Physics of Modern Materials,* Intertext Books, Buck, UK, 1973

65. Montilla, F.; Frutos, L. M.; Mateo,C.R.; Mallavia, R. *J.Phys.Chem.C,* **2007**,111,18405

66. Evans, R. C. *Efficient Emitters for Technological Applications*, PhD Thesis, University of Wales Swansea, 2007.

Chapter 6:

A photochemical and photophysical investigation of a polyfluorene-polythiophene co-block polymer

6.1 Chapter Aim

The work presented in this chapter was completed during a four month research ERASMUS placement working with Professor Hugh Burrows and the photochemistry group at the University of Coimbra, Portugal. The photochemistry group in Portugal have a long standing collaboration with Professor Ulli Scherf at the University of Wuppertal, Germany. In 2007 Scherf and co-workers reported the synthesis and solvent- selective photoluminescence quenching of a novel amphilic co-diblock polyfluorene- polythiophene polymer, specifically, poly (9,9, dialkylfluorene) poly(3-diethylphosphonato-hexyl thiophene) which has poly (3-(6-bromo hexyl) thiophene) polymeric end cap groups.[1] This will be referred to as PFPT throughout this chapter. It was shown that the optical properties of the polymer are strongly influenced by solvent properties, such that in THF:water mixtures the emission intensity was significantly reduced as the fraction of water was increased.[1] The purpose of the work presented here was to investigate the photochemistry and photophysics of the PFPT system further in a range of different solvent systems.

6.2 Introduction

6.2.1 Copolymerisation

Compolymerisation can be used as a method to suppress "green-band" formation in polyfluorenes (PF) (as described in chapter 5).[2-5] However, co-polymerisation is more commonly used as a way of synthesising modified PF co-polymers which open up the opportunity of a polymer-system which emits light across a wide range of the visible spectrum. This is generally achieved by incorporation of blocks of repeat units with a lower HOMO/LUMO energy gap than that of the blue emitting polyfluorene.[6]

6.2.2 Polythiophenes

Polythiophenes are generally synthesised either by electroxidative polymerisation or by transition metal catalysed coupling reactions of suitable monomers.[7-8] Poly(3-alkyl thiophene) (PAT) was the first example of a soluble, fusible conducting polymer and it also demonstrated novel characteristics such as thermochromism and solvatachromism. It is soluble in a range of solvents and exhibits good chemical stability. [9-13] The solvatachromic properties have been attributed to the variety of structures which oligothiophenes and polythiothenes can adopt, as shown in figure 6.1 below. Rotation of the planes of the thiophene rings along a polymer chain can change the energy at which it absorbs or emits, and there is also the possibility of interchain interactions and aggregated well-ordered states.[13] Polythiophenes have a relatively low HOMO-LUMO energy gap and as a result generally emit in the red region. However, since this gap is relatively sensitive to the torsion angle between consecutive thiophene units it is possible to tune the emission of the polythiophene from the UV to the IR by judicious selection of the substituent.[13]

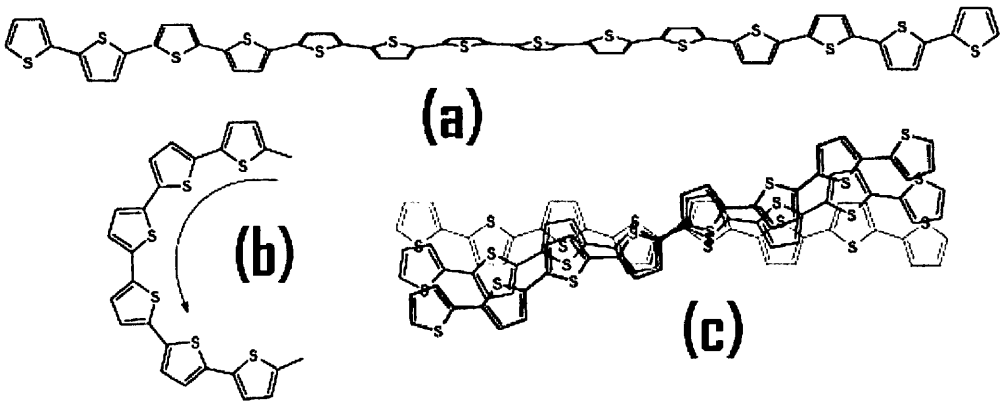

Figure 6.1: Variations on the helical organisation of polythiophenes. (a) Helical transoid (large pitch) (b) Helical cisoid (small pitch) (c) Helical packing of predominantly planar chains.[14]

Ohmori and co-workers were the first to report the electroluminescent properties of PTs [15-16] and this has since been intensively studied by groups such as Heeger and co-workers.[17]

6.2.3 Properties of PFPT

PFPT (shown in figure 6.2) is a rod-coil block polymer. Previous to its synthesis all polymers of this type consisted of 2 or more hydrophobic blocks. [1]

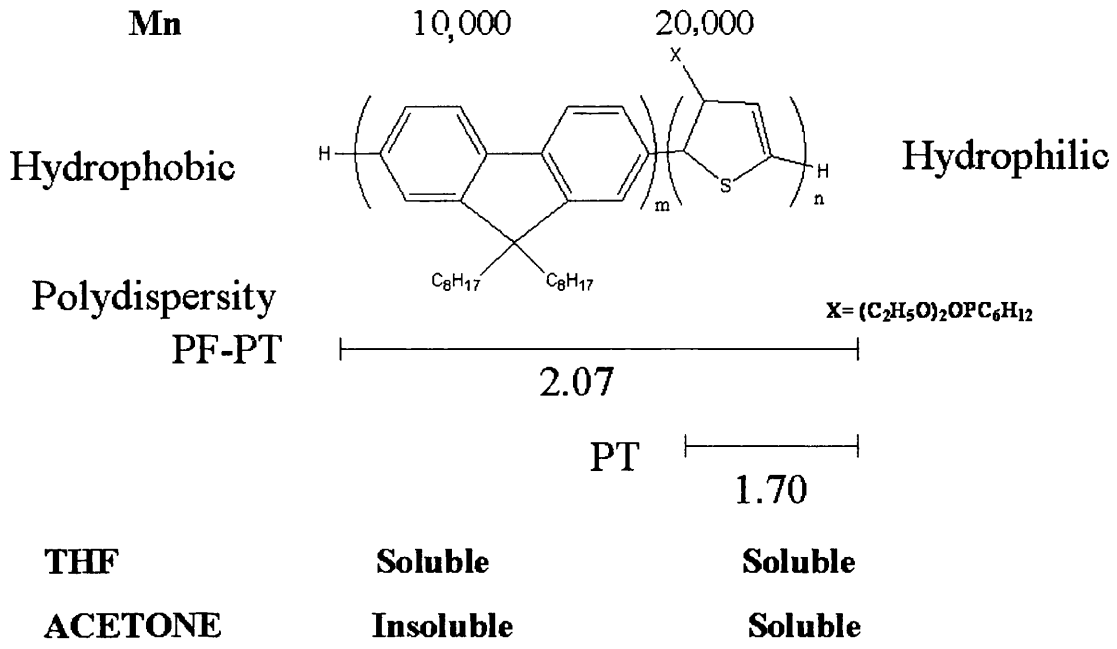

Figure 6.2. Summary and chemical properties of the properties of the PFPT co-block polymer.

The PFPT co-diblock polymer has both hydrophilic and hydrophobic component blocks. The hydrophilic PT part consists of a regioregular poly [3-(6-diethylphosphanato-hexyl) thiophene. The polar phosphanate side groups were chosen by Scherf and co-workers to be the hydrophilic group because they have good solubility in mixtures of organic solvents as well as water. The PF part is hydrophobic. It was chosen for ease of synthesis and its high HOMO-LUMO energy gap which could allow energy transfer from PF to PT. The alkyl side chains enhance the solubility of the polymer.[17] The resulting PFPT polymer is soluble in solvents such as THF; the PT part is soluble in acetone and water/polar solvent mixtures.

In rod-coil polymers such as PFPT the self assembly behaviour has been reported to also be dominated by the aggregation/crystallisation of the different rigid rod blocks. These

aggregation properties have been seen to influence the absorption and emission properties of the polymer and the polarity of the solvent has strong influence on the PFPT absorption and emission spectrum as shown in figure 6.3 and figure 6.4:

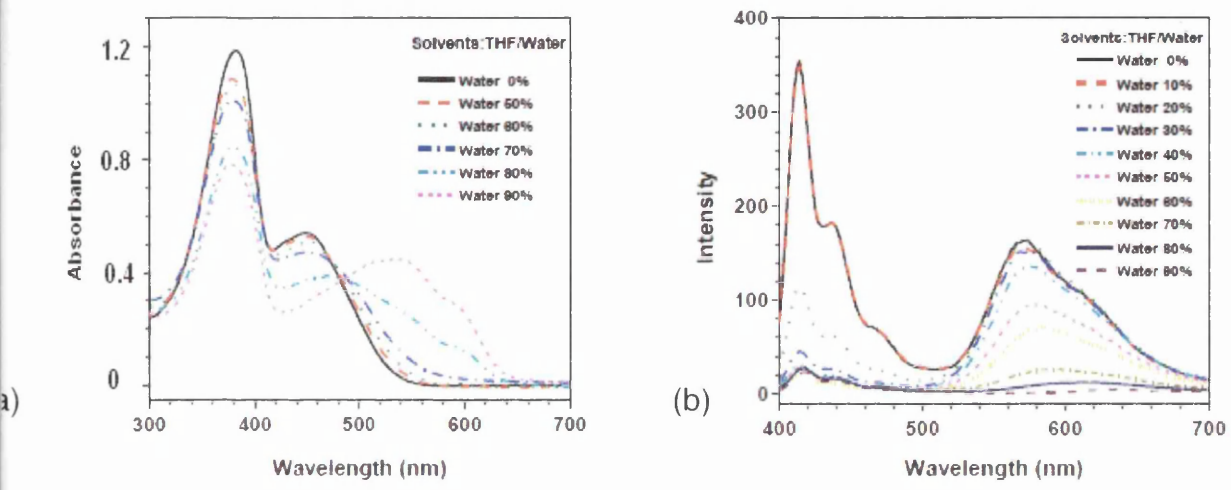

Figure 6.3: Effects of increased water content in THF: water mixtures on the absorption and emission spectra of PFPT. UV- Vis spectrum (a), emission spectrum (b).[1]

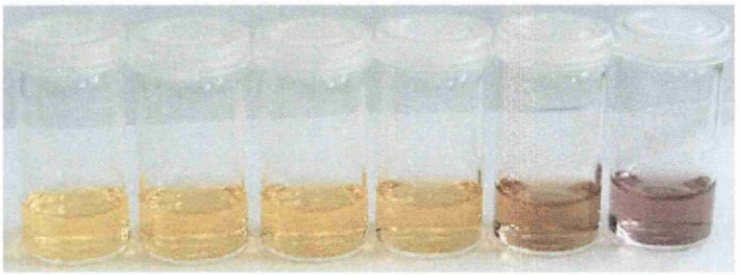

Figure 6.4: Solvatochromism of PFPT in water:THF mixtures[1] the absorption λ_{max} shifts from 420 nm to 540 nm with increasing water content (fig 6.3b).

Since the copolymer has hydrophobic PF and hydrophilic PT parts, increasing the amount of water in a water/organic mixture will make the solvent system more selective for the PT

block and cause the PF block to aggregate since the solubility of PF is distinctly reduced as water content increased. The aggregates initially consist of associated PF2/6 blocks and isolated "hairy" dissolved PT blocks. Emission from the PF block is quenched significantly by aggregation as water content is increased, while emission from PT is not reduced much as water content goes from 0-30%. While THF:water mixtures with low water content, up to ca.30%, are selective solvents for the hydrophilic PT blocks, increasing the water content even further causes the PT chains to associate also. The formation of these "compact" aggregates in solvent mixtures with high water contents (up to 70%) leads to luminescence quenching of PT emission as well (see Fig 6.3). A schematic of these aggregation processes is given in figure 6.5 below.[1]

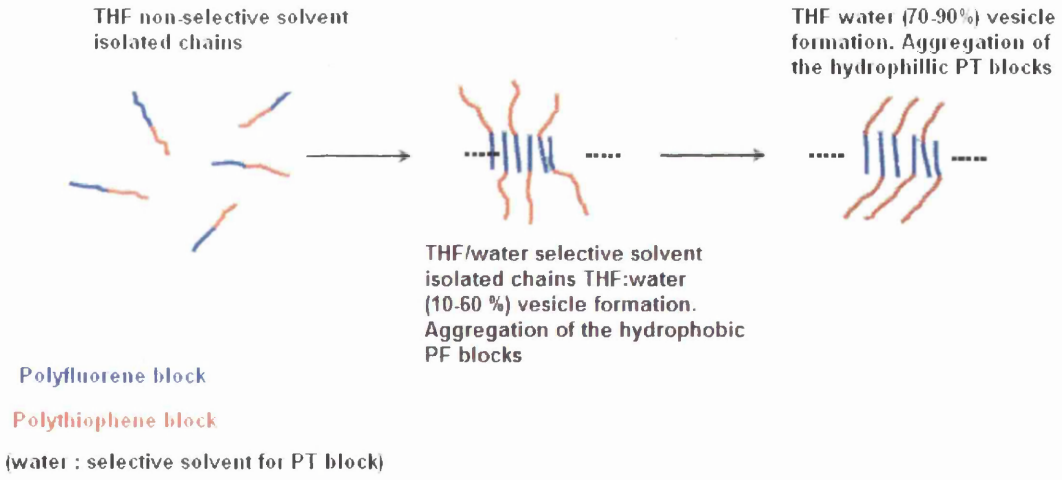

Figure 6.5: Two step aggregation of the PFPT polymer as water content is increased in water/THF mixtures.[1]

6.3 Experimental

6.3.1 Instrumentation and computational methods

6.3.1.1 UV-vis absorption spectroscopy

UV-visible spectra were recorded at Swansea University using either a Unicam UV300 spectrometer or a Hewett Packard HP 8452A single beam diode array spectrophotometer. The Shimadzu 2100 spectrometer at the Chemistry Department, University of Coimbra, Portugal was also used to make some measurements.

6.3.1.2 Steady state emission and excitation measurements

Room temperature and 77 K emission measurements were carried out using either a Perkin Elmer MPF-44E fluorescence spectrometer or a Horiba-Jobin-Ivon SPEX Fluorog 3-22 spectrometer. All experiments used 1 cm x 1 cm quartz cells. For the light scattering experiment the sample was excited at 600 nm and the emission was measured between 580 nm to 620 nm.

6.3.1.3 Quantum yields

Quantum yields were measured against PT-α-4 dissolved in ethanol. The solutions of the polymer and references were made up to have an absorbance of ca. 0.1 at the excitation wavelength and yields were corrected for any difference in solvent refractive index between sample and reference.

6.3.1.4 Time correlated single photon counting (TCSPC)

All pico-second (ps) measurements were made using the time correlated single photon counting (TSCPC) technique. This was done at the Physics Department, University of Durham (see experimental, section 2). Decay curves were recorded using 385 nm excitation, and emission collected at either the polyfluorene emission maximum of 420 nm or the polythiophene emission maximum of 520 nm.

6.3.1.5 Curve fitting

The "Globals" kinetic fitting programme was used for the analysis of all fluorescence decays.

6.3.2 Materials

6.3.2.1 Solvents

Tetrahydrofuran (THF): HPLC fluorescence grade THF without stabiliser and guaranteed analysis of >99.995% was purchased from Fisher and used as received.

Acetone and water: Reagents were the purest grade available (>99.5%), and were used without further treatment.

None of the solvents exhibited any detectable emission under the conditions used.

6.3.2.2 Polymers

PF2/6: PF2/6 was synthesised by the Scherf group via *Yamamoto* cross coupling. The M_n value for the polymer is 22.3 kg mol^{-1} and the M_w value is 56.8 kg mol^{-1}.

Oligothiophenes: PT-α4 was a gift from J.Pina, University of Coimbra, Portugal.[18]

Polyfluorene-polythiophene (PFPT) co-block polymer: Poly-((bis)-octyl)fluorene-polythiophene. This was synthesised by the Scherf group via a Suzuki cross coupling reaction.[88] (See figure 6.2 for details of average molar masses).

6.4 Results and Discussion

6.4.1 PFPT and PF2/6 in 100% THF

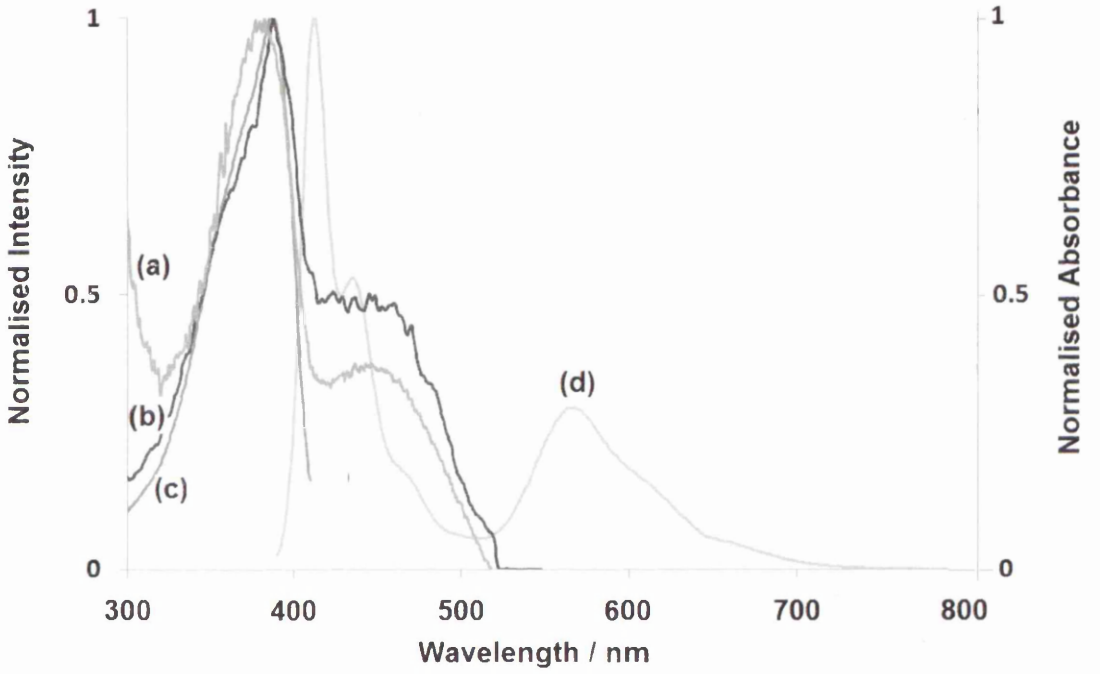

Figure 6.6: Normalised absorption, emission and excitation spectra for PFPT in THF. a) absorption; b) excitation for 565 nm emission; c) excitation for 420 nm emission, and d) emission spectrum for 385 nm excitation.

Figure 6.6 shows the normalised absorption, emission, and excitation spectra of PFPT in THF. The structured emission in the 400-500 nm range is due to PF emission while the broader band from ca 500-700 nm is PT emission. The band at ca. 385 nm in the absorption spectrum is due to PF absorption while the broad band around 440 nm is due to PT absorption. The presence of the strong excitation band at 385 nm while monitoring at the PT

emission maximum is conclusive evidence for energy transfer from the PF block into the PT block.

Figures 6.7 and 6.8 give TCSPC emission curves for PF2/6 and PFPT using 385 nm excitation and measuring at the PF emission maximum of 420 nm.

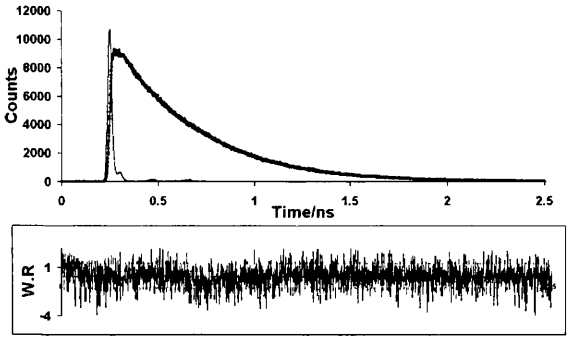

Figure 6.7 : Fluorescence decay curve for PFPT in THF from TCSPC. Emission was collected at the maximum of the PF emission, 420 nm, with an excitation wavelength of 385 nm.

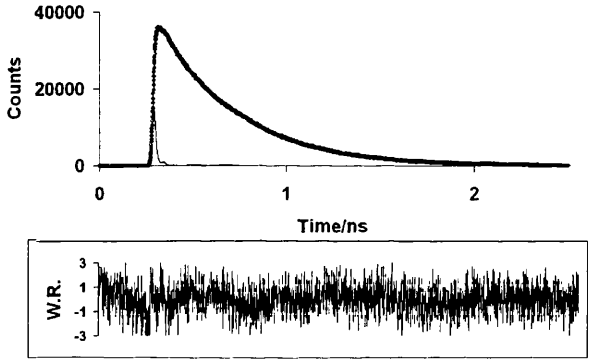

Figure 6.8: Fluorescence decay curve for PF2/6 in THF from TCSPC. Emission was collected at the maximum of the PF emission, 420 nm, using an excitation wavelength of 385 nm.

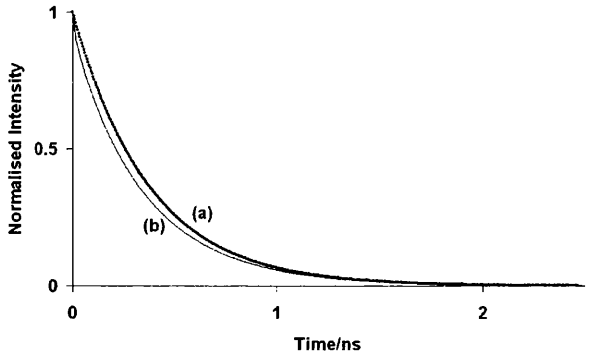

Figure 6.9: Comparison of normalised simulated decay curves from Globals analysis of Figures 6.7 and 6.8: (a) PF2/6 and (b) PFPT.

Curve fitting decay parameters are given in tables 6.2 and 6.3 (along with those measured in different solvent mixtures) and figure 6.9 makes a comparison of the normalised emission curves reconstructed using these parameters. Comparison of the decay kinetics for PFPT and PF at 100% THF suggests that up to ca 10% of the PF groups may be energy transferring into PT by what is, on the ps timescale, a dynamic process. Examination of figure 6.6, and the intensities of the TCSPC curves 6.7 and 6.8, however, suggests a much higher ET efficiency than 10% and this must be occurring on a timescale faster than the detection response of the TCSPC instrument i.e. "static" energy transfer.

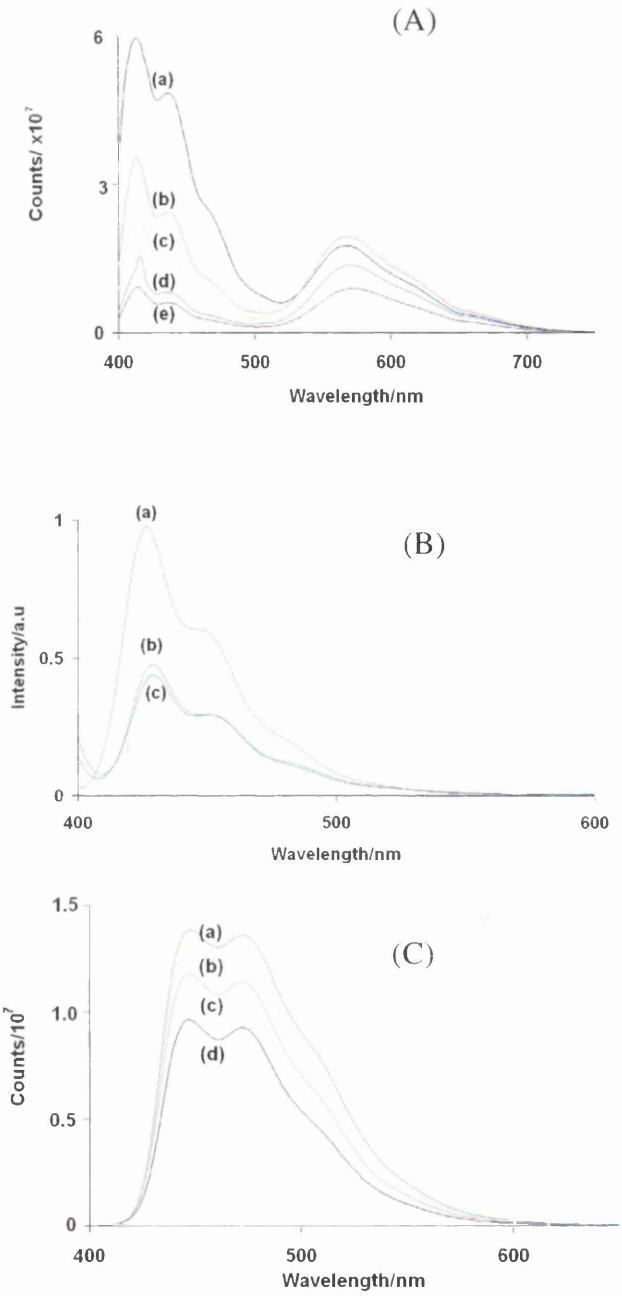

Figure 6.10: Effect of water content of THF:water mixtures on emission spectra of A)PFPT, B) PF2/6 and C) α4- PT. The excitation wavelength is 385nm for all samples.
(A) Emission spectra of PFPT in (a) 100:0: (b) 80:20: (c) 60:40; (d) 40:60; (e) 20:80, THF:water mixtures.
(B) Emission spectra of PF2/6 in: (a) 75:25; (b) 50:50: (c) 25:75, THF:water mixtures.
(C) Emission spectra of α4 in: (a) 25:75; (b) 50:50; (c) 75%:25%; (d) 100:0 THF:water mixtures.

6.4.2. Steady-state emission

Figure 6.10:(A), (B) and (C), show the variation in emission spectrum with solvent composition for PFPT, PF2/6 and α4-PT. The most notable feature is the major reduction in PF emission upon increasing water content even though emission from PT remains essentially unchanged. If energy transfer from PF is an important population route for PT emission, as figure 6.6 suggests, then we would expect the ratio to remain constant unless the population of PF repeat units which energy transfer into PT are not the same as those which are responsible for generating the PF emission. (Although we must also allow the, albeit unlikely, possibility that an increase in emission quantum yield for PT in the THF:water mixture fortuitously compensates for a decrease in population formed by energy transfer from PF.)

6.4.3. Time correlated single photon counting (TCSPC)

Fluorescence decay curves for PFPT and PF 2/6 in different THF:water solvent ratios, using excitation at 385 nm, which is into both the PF and PT absorption bands, and measured at the PF emission maximum, are shown in figures 6.11 and 6.12 respectively. Both sets of data show a decrease in emission intensity with increasing water content.

The fitting parameters obtained from the Globals Programme for PFPT and PF2/6 are given in tables 6.1 and 6.2 respectively. Figure 6.13 shows normalised decay curves which have been reconstructed from these parameters. Irrespective of the detailed kinetics these decay curves show that while the lifetime of PF in PFPT decreases significantly with increasing water content the lifetime of PF2/6 does not.

We tentatively interpret this solvent dependent steady-state emission and time-resolved behaviour as follows.

PF2/6 - For PF2/6 it is known that increasing water content leads to an increase in aggregation.[1,2] The steady-state data shows a decrease in quantum yield upon aggregation. The kinetic data shows that this is not due to a general decrease in lifetime, but rather a complete loss of emission from aggregates, with, what are presumably, free polymer chains, contributing a much lower intensity, but similar lifetime, emission to that found in 100% THF.

PFPT - We suggest there are two essentially distinct populations of PF repeat units in the chain – a) those for which energy transfer into PT is very rapid and which are not influenced much by solvent variation, and b) those which do not energy transfer into PT and which have a solvent dependent lifetime and hence solvent dependent emission quantum yield. The nature of the PF quenching process is unknown, but it is not unreasonable to suggest this also may be due to aggregation, although the fact that the lifetime behaviour is different for PF2/6 and PFPT indicates that the nature of the aggregation in PF2/6 which quenches fluorescence completely is not the same as that in PFPT which causes a reduction in lifetime.

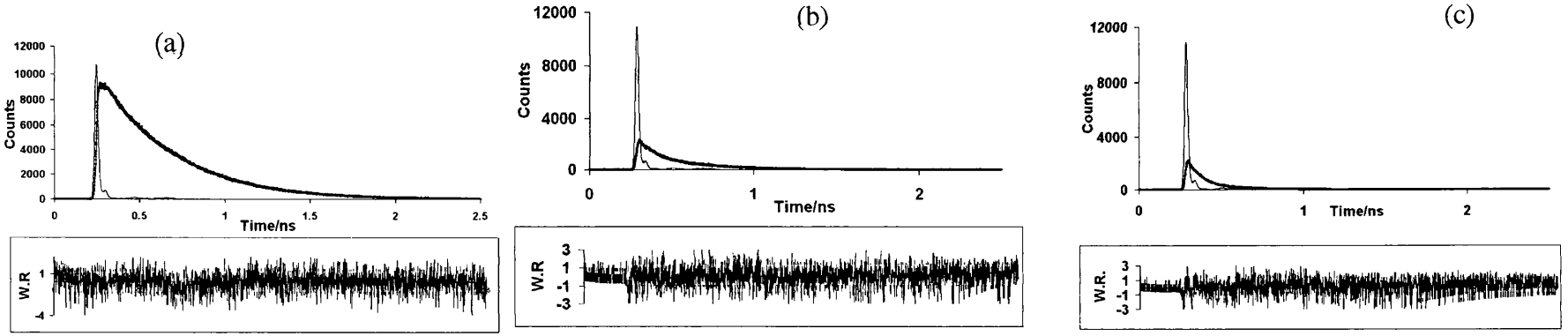

Figure 6.11. Fluorescence decay curves from TCSPC experiments with PFPT in THF:water mixtures: (a) 100:0, (b) 75:25; (c) 50:50. Emission collected at the maximum of the PF emission, 420 nm, using an excitation wavelength of 385 nm.

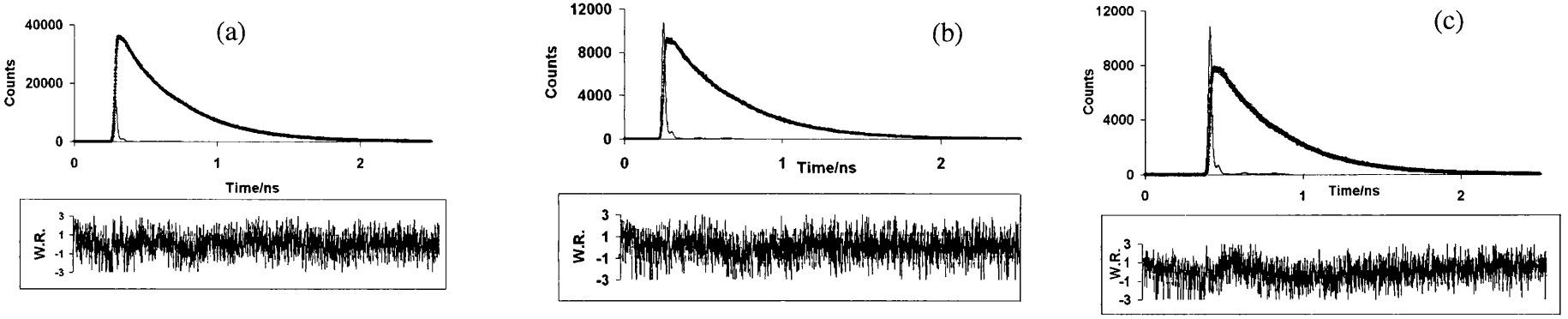

Figure 6.12. Fluorescence decay curves from TCSPC experiments with PF2/6 in THF:water mixtures: (a) 100:0, (b) 75:25; (c) 50:50. Emission collected at the maximum of the PF emission, 420 nm, with an excitation wavelength of 385 nm.

THF:Water	α_1	τ_1	α_2	τ_2	α_3	τ_3	χ^2
100:0	0.426	0.184	2.41	0.382	0.315	0.0135	1.13
75:25	3.67	0.134	1.22	0.368	3.03	0.001	1.07
50:50	8.242	0.101	0.13	0.454	5.99	0.015	1.01

Table 6.1. Kinetic parameters obtained from TCSPC for PFPT in a range of THF:water mixtures. Measured at the PF emission maximum of 420 nm with 385 nm excitation.

THF:Water	α_1	τ_1	α_2	τ_2	χ^2
100:0	2.70	0.37	0.50	0.58	1.14
75:25	2.69	0.37	0.006	0.59	1.12
50:50	2.79	0.36	0.002	0.50	1.22

Table 6.3: Kinetic parameters obtained from TCSPC for PF2/6 in a range of THF:water ratios. Measured at the PF emission maximum of 420 nm with 385 nm excitation.

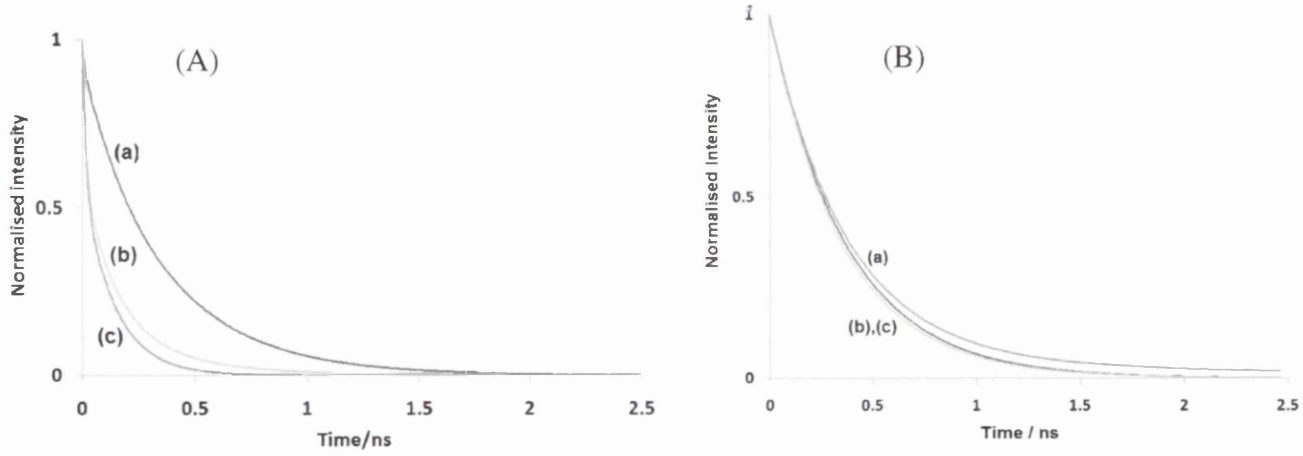

Figure 6.13: Normalised decay curves reconstructed from the parameters in table 6.2 and 6.3. (A) PFPT in THF:water mixtures as follows: (a) 100:0; (b) 75:25; (c) 50:50. (B) PF2/6 in THF water mixtures as follows: (a) 100:0; (b) 75:25; (c) 50:50.

6.4.4 Light scattering

Upon the addition of water both solutions became more turbid, due to the formation of aggregates in the solution; see Figure 6.14A. Figure 6.14B shows the variation in light scattering vs the emission intensity for PFPT at the maximum of the PF emission. The emission intensity decreases monotonically with increasing light scattering, presumably because of aggregate quenching. The situation for emission intensity measured at the maximum of the PT emission, Figure 6.14C shows an initial slight increase in intensity as water content, and also scattering, increases, up to a water content of 60%, but after this emission from the PT unit decreases. These results correlate in a general sense with the two stage aggregation process proposed by Scherf and co-workers,[1] with aggregation quenching of the PF block preceding aggregation quenching of the PT block as water content is increased.

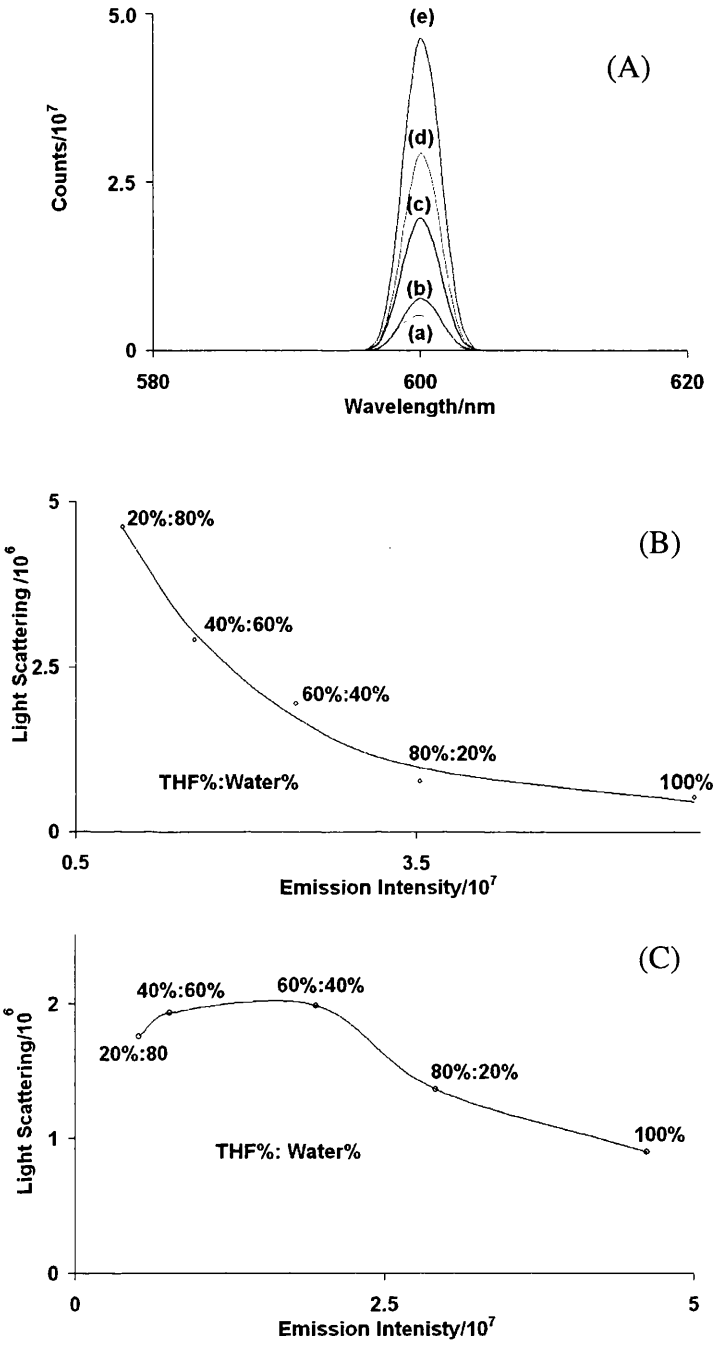

Figure 6.14:

(A) Light scattering from PFPT solution at different THF:water ratios (a) 100:0; (b) 80:20; (c) 60:40; (d) 40:60; (e) 20:80; (600 nm excitation).

(B) Illustrates how the light scattering increases and the emission intensity of the PF decreases upon the addition of water to THF solutions of the PFPT polymer.

(C) Illustrates how the light scattering increases and the emission intensity of the PT unit initially increases then decreases upon the addition of water to THF solutions of the PFPT polymer.

6.4.5 Förster resonance energy transfer from PF to PT in 100% THF solution

FRET between PF-PF units has been described in chapter 5 section 4.4. In order for FRET to occur there must be spectral overlap between the absorption of the acceptor unit and the emission of the donor.[21] As seen in figure 6.15 below this is the case for PF and PT units also. The Forster distance R_0 between the PF donor (D) and PT acceptor (A) was calculated as 47.9Å. The separation between a PF and PT unit where the two polymer blocks meet, R(D-A), is 6.9 Å, and at this distance the FRET rate constant is 8.3×10^{-13} s^{-1}. However, in order to calculate the energy transfer efficiency from the PF block as a whole to the PT block it is also necessary to consider energy migration through the polymer chain between PF-PF units, as already discussed in chapter 5 section 4.4.

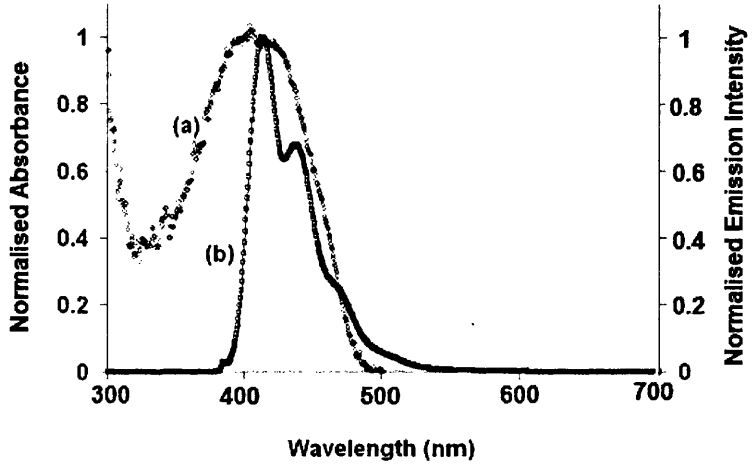

Figure 6.15: Spectral overlap between the emission from the donor (PF) and absorption of the acceptor (PT) for PF to PT energy transfer in THF. (a) Absorption spectrum of PT; (b) emission spectrum of PF.

The PF chain length distribution in the PFPT polymer is illustrated in figure 6.16.

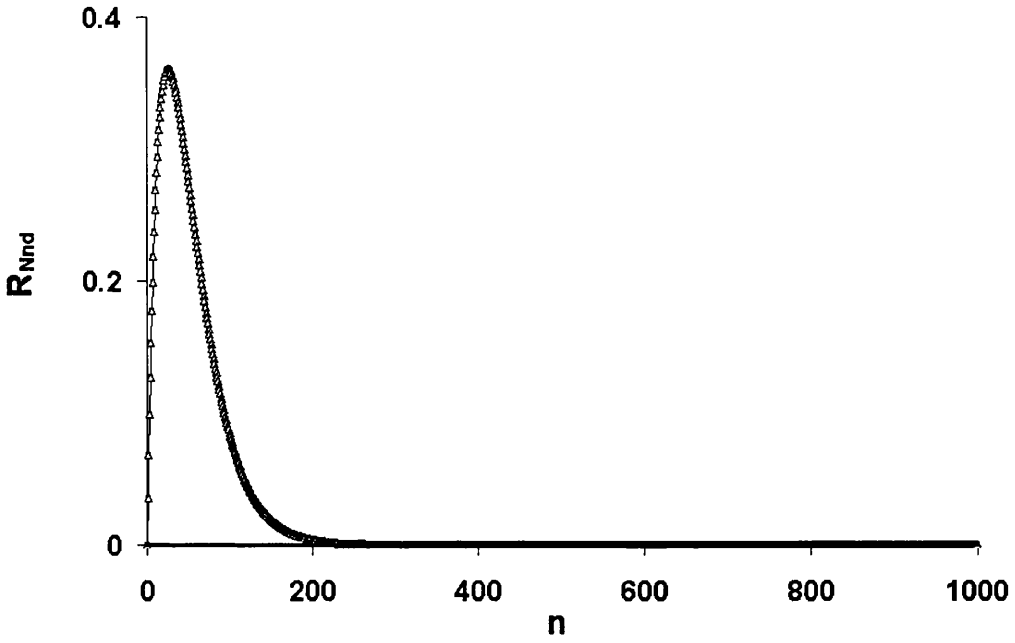

Figure 6.16: The polymer chain length distributions for the PFPT co-block polymer.

Every chain has at least one repeat unit next to the PT block. Every chain length longer than 2 has one repeat unit 2 units away from the PT block and one repeat unit next to the PT block etc. This means that the number of repeat units adjacent to a PT block is equal to the total number of chains, and the number of repeat units at a separation of n repeat units away from the PT block is the sum of the populations of all chains longer than **n**. The probability of a PF unit being a separation **n** units away from the PT block decreases exponentially with increasing chain length as shown in figure 6.17.

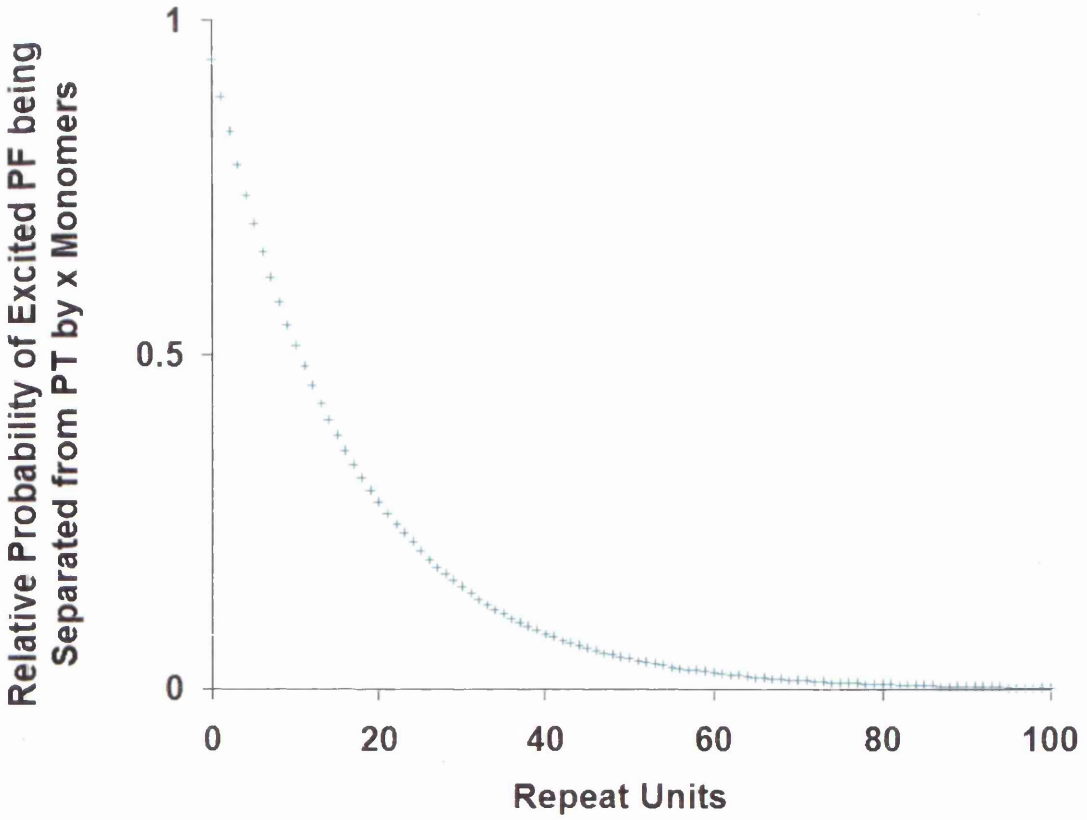

Figure 6.17: Relative probability of a PF-PT distance for different PF chain lengths (normalised to a probability of one for adjacent PF PT units).

6.4.6. Fluorescence quenching upon increasing the water content in the solvent composition

PF-PF energy transfer from excited PF repeat units close to a PT unit will occur very quickly, within a few tens of ps, while for excitation energy initially absorbed at the end of a long PF chain energy migration will take so long that defect quenching will not reduce either quantum yield or emission lifetime. These two extremes could represent the two distinct populations of PF units – those which do energy transfer very quickly, and those which cannot energy transfer. However as figure 6.16 shows we would also expect a very significant fraction of PF repeat units to be in the intermediate region in which energy transfer quenching might not

be the exclusive deactivation route but for which it is still important. It is this intermediate section of the PF population which does not seem to feature significantly in either our steady-state or time-resolved studies. Perhaps the only definite conclusion that can be reached from these studies is that neither the steady-state, nor time-resolved experiments effectively probe the PF-PT energy transfer process. Although the reasons why this should be the case are far from clear.

We can, however, suggest the following very general picture of what might be happening to PFPT as the water content of the solvent mixture is increased. When water, which is a poor solvent for PF, is initially added to the solution in THF (75:25 THF:water) the PF sections of the polymer begin to aggregate. Upon aggregation, the PF units get closer together and energy is able to migrate between adjacent PF chains. This energy is mostly that lost radiatively, and aggregation quenching results in a quenched PF emission and shorter lifetime. Upon the addition of more water (50-75% water) the shorter chain PF units also begin to aggregate. More energy is transferred between PF chains and is lost, which means less is transferred to the PT unit. This results in less energy transfer between the PF and PT and hence, a reduced emission from both units, which is seen in both the TCSPC and steady-state emission data. Aggregation initially occurs between PF repeat units that are furthest away from PT on polymers carrying long PF chains. As the energy from these PF units is mainly lost radiatively this will not initially have much effect on the amount of energy transferred to PT, but will affect the PF lifetime. Upon increased aggregation, all PFs begin to aggregate and this means that emission from both PF and PT is quenched.

6.4.7 Optical studies of PFPT in acetone/ water solutions

The behaviour of PFPT in a range of acetone:water mixtures was also very briefly examined and the results from this study are included here for the sake of completeness, and for others who may work in the field. It was found that polymer aggregation occurred with much lower water content than was the case in THF:water mixtures.

6.4.7.1 Absorption

Solvatochromic behaviour is also shown in these solvent mixtures, as seen in figure 6.17 below. In pure acetone the colour of the solution is orange. In 10% water 90% acetone the colour of the solution is deep purple.

Figure 6.18: Photograph of the solvatochromic behaviour of PFPT in acetone/water mixtures: Solvent composition from left to right acetone:water; 90:10, 80:20, 60:40, 50:50, 40:60, 20:80, 10:90.

6.4.7.2 Emission

Figure 6.19 shows variation in the emission spectrum with solvent composition. Upon the addition of water both bands decrease in intensity, with emission from the PF group initially decreasing rather more quickly with increasing water content than that from the PT group. However as the water content is increased from ca. 50% upwards the PF emission spectrum remains essentially constant in both shape and intensity, while that of the PT groups continues to decrease.

There is also a marked red shift in the emission spectrum of the PT group as water content is increased; behaviour which is not observed in THF:water mixtures. This shift can probably be attributed to the formation of aggregates with a linear arrangement of thiophene rings, which pushes both the absorption and emission spectra towards the red.[14]

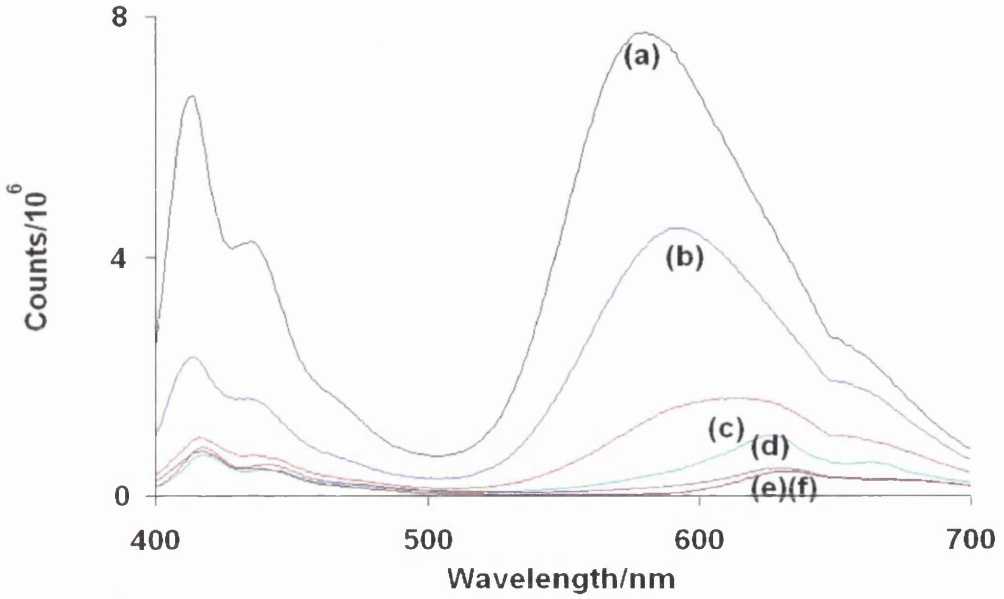

Figure 6.19: Emission spectrum of PFPT in different acetone/water mixtures: (a) 100:0; (b) 80:20; (c) 60:40; (d) 40:60; (e) 20:80; (f) 10:90..

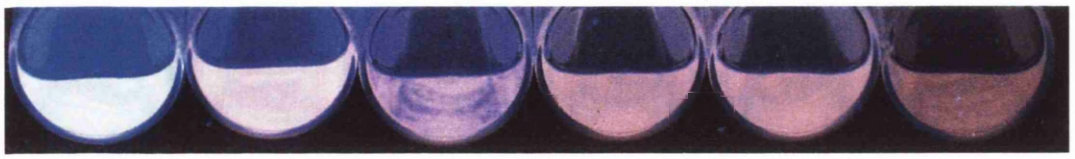

Figure 6.20: Photograph of the solvatochromic emission behaviour of PFPT in acetone:water mixtures. Solvent composition from left to right acetone:water; 90:10, 80:20, 60:40, 50:50, 40:60, 20:80, 10:90.

6.5 Conclusions

The purpose of this work was to examine some of the photochemical and photophysical processes which occur in the novel PFPT co-block polymer synthesised by Scherf and co-workers. In this chapter the possibility of FRET between the PF and PT unit is considered. Evidence for energy transfer was seen from the excitation spectrum of PFPT recorded at the PT emission maximum. Decay curves of both the PF2/6 oligomer and the PFPT in 100% THF also provide further evidence of energy transfer, both dynamic and static. The decay kinetics suggested that up to 10 % of the PF groups may be energy transferring into the PT, on the ps time scale of the experiment i.e. the dynamic process. Examination of the steady-state emission data however, suggested that the energy transfer efficiency is in fact greater than 10 %. This must be on a time scale which is faster than the detection response of the instrument and is therefore considered to be a static process.

The optical properties of PFPT are solvent dependent with a major reduction in the PF emission upon increasing the water content even thought the emission from the PT group remains essentially unchanged. From this evidence it is concluded that there are two essentially distinct populations of the PF repeat units into the chain; those which are close enough to the PT for efficient energy transfer and those which are so far away that no energy transfer is possible within the natural emission lifetime.

The data are generally consistent with the two stage aggregation process proposed by Scherf and co-workers, in which aggregation quenching of the PF block precedes aggregation quenching of the PT block, as water content is increased.

A brief study of PFPT in a range of acetone:water solutions has also been presented. The polymer is solvatachromic in these solutions with a shift observed in both the absorption and emission spectrum with increased water content. Although the studies on these systems were brief, it is expected that any further measurements made will be limited by aggregation which occured even at very low concentrations.

6.6 References

1. Tu, G.; Li, H.; Forster, M.; Heiderhoff, R.; Balk, L.J.; Sigel, R.; Scherf, U. *Small*, **2007**, 6, 1001
2. Suh, Y.S.; Won, Ko.; S, Jung.; B-J, Shim.; H-K, *Optical Materials*, **2002**, 21, 109
3. Klaerner, G.; Davey, M.H.; Chen. W.D.; Scott, J.C.; Miller, R.D. *Adv.Mater*, **1998**, 10, 993
4. Lee, J-IK.; Klaerner, G.; Miller, R.D. *Chem.Mater*, **1999**, 11, 1083
5. Klaerner, G.; Miller, R.D. *Macromolecules*, **1998**, 31, 2007
6. Ma, Z. ; Lu, S. ; Fan, Q-L. ; Qing, C-Y. ; Wang, Y-Y. ; Wang, P.; Huang, W.; Polymer, 47, 21, 7382
7. Yamamoto, T.; Sanechika, K.; Yamamoto, A. *J, Polym. Sci. Polym. Ed*, **1980**, 18, 9
8. Lin, J.W.P.; Dudek, L.P. *J.Polym.Sci. Polym.chem.Ed*, **1980**, 18, 2869
9. Yamamoto, T.; Sanechika, K.; Yamamoto, A.; *Bull.Chem.Soc. Jpn*, **1983**, 56 , 1497
10. Yamamoto, T.; Sanechika, K.; *Chem. Ind (London),* **1982**, 301
11. Kaneto, K.; Yoshino, K.; Inuishi, Y. *Solid State.Commun*, **1983**, 46, 389
12. Amer, A.; Zimmer, H.; Mulligan, K.J.; Mark, H.B.; Pons, S.; McAleer, J.F. J. *Polym. Sci. Poly Lett.Ed*, **1984**, 22, 77
13. McCullough, R.D. *Adv.Mater,* **1998**, 10, 93
14. Langeveld-Voss, B.M.W.; Janssen, R.A.J.; Meijer, E.W. *Journal of Molecular Structure*, **2000**, 521, 285
15. Ohmori, Y. ; Uchida, M. ; Muro, K. ;Yoshino. K. *Jpn.J.Appl.Phys. Part 2*, **1991**, 30, L1838
16. Ohmori, Y. ; Uchida, M. ; Muro, K. ; Yoshino, K. *Solid. State. Commun*, **1991**, 8, 605
17. Braun, D.; Gustaffson, G.; McBranch, D.; Heeger, A.J. *J. Appl. Phys*, **1992**, 72, 564

18. Pina, J.; Burrows, H.D.; Becker, R.S.; Dias, F.B.; Macanita, A.C.*J. Phys. Chem. B*, **2006**, 100, 6499

19. Forster, T. *Disc. Faraday. Soc*, **1959**, 27,7

20. Murov, S.L.; Carmichael, I.; Hug, G.L. *Handbook of Photochemistry*, 2nd Ed, New York, **1993**

21. Dexter, D.L. *J.Chem.Phys*, **1953**, 21, 836

Chapter 7:

Conclusions

7.0 Conclusions

In this work several novel and known luminescent systems have been investigated, namely (i) palladium diselenones, (ii) platinum diselenones and (iii) polyfluorenes. Particular attention has been paid to understanding the photochemical processes that occur upon photoexcitation of these systems. In addition to the photochemical techniques used, Density Functional Theory (DFT) was used, as described in chapter 3 and 4, to obtain a better understanding of the excited state characteristics of both the palladium and platinum diselenones. When considering the polyfluorene (PF) systems discussed in chapters 5 and 6 a new kinetic modelling approach has been used which, unlike most multiexponential fitting methods used to-date, leads to parameters which have physical significance.

7.1 Palladium diselenones

The synthesis and structural characterisation of the palladium diselenones **1** and **2** described in chapter 3 had already been reported. The photochemistry of these systems had however, not been investigated. Initially the luminescence from these compounds was not immediately apparent, but after an in depth investigation both **1** and **2** were identified as far infra-red lumphores. These are believed to be the first example of luminescent Pd-Se compounds in the literature. The complexes show a radiative lifetime of 2-7 μs in the solid state at 298 K. At 77 K both in the solid state and in frozen organic glass the complexes have phosphorescence lifetimes of ca. 11-20 μs. No emission was seen for either compound in fluid solution when nitrogen-purged; in addition we could not detect any transient absorption which could be assigned to the triplet state, or any singlet oxygen generation in aerated solution ($\Phi_\Delta \leq 5 \times 10^{-4}$). The fact that this difference in behaviour occurs in going from fluid to rigid environments suggests molecular motion is an effective deactivation route for either the triplet state or its precursor.

DFT calculations gave ground state and excited state results which were in general agreement with the data observed experimentally. This showed that there was involvement from the –ene group in the ground state which was absent in the excited state and also involvement from the phosphorus group in the excited state which was absent in the ground state.

7.2 Platinum diselenones

The aim of the work presented in Chapter 4 was to investigate, and establish further, the origin of the luminescence of platinum diselenones. The emission observed upon excitation at 355 nm in fluid solution was identified as molecular phosphorescence. Close examination also showed a 532 nm band in the phosphorescence excitation spectrum, a band which is not obvious in the absorption spectrum, and for which a quantum yield of close to 1 is inferred. In addition to phosphorescence these compounds also fluorescence with emission in the blue. The origins of the emission observed for these compounds in fluid solution is described in Chapter 4 by means of an energy level and Jablonski diagram which brings together data from absorption, emission, excitation and theoretical studies.

No definitive explanation of the origin of the orange/red emission observed for these compounds in the solid state was possible. However it is tentatively attributed to an intermolecular charge transfer transition in the solid state. A suggestion supported by a characteristic solid state structural arrangement involving selenium and phosphorus atoms close enough together to possibly interact in the excited state and a HOMO-LUMO transition involving significant electron density transfer from selenium onto phosphorus atoms.

7.3 Polyfluorene emission

Polyfluorenes (PFs) are a group of conjugated polymers with applications in OLED devices due to their photochemical properties which include a high quantum yield and intense blue emission. One problem with PFs is that after time they degrade to form a green band which results in reduction of colour purity. Many theories exist in literature as to why this happens. One suggested by Scherf and co-workers is that ketone defects form within the polymer chain which result in the green emission.

The results presented in Chapter 5 are an extension of work completed by A.T.Marques at the University of Coimbra on PFs carrying ketone defects. TCSPC measurements on these systems showed that upon increasing the defect concentration both the overall emission yield and emission lifetime decreased. The purpose of this study was to use the TCSPC to examine the emission kinetics of polyfluorenes which have ketone defects built into the polymer chain. For emission at the 420 nm polyfluorene maximum, both the emission lifetime and the emission yield decreased upon increasing the defect concentration. For emission at 550 nm, the defect maximum, the emission yield increased with defect concentration. This provides strong evidence for energy transfer between the PF and the defect unit.

FRET calculations showed that energy transfer between two PF units was feasible with the energy transfer rate constant being calculated as 1.47×10^{12} s^{-1} at the PF-PF distance of 8.5Å. To better understand the energy transfer kinetics the polymer chain length distributions were considered, *Program Clusters* was used to integrate across all the possible excitation sites within the polymer to give an integrated decay curve which could be fitted to the experimental data to obtain both the energy transfer rate constant and the rate constant for decay in the absence of energy transfer. The very good agreement between the curve-fitted energy transfer rate constants and that calculated by FRET theory provides very strong support for the validity of the interpretation of the energy transfer kinetics and the novel

modelling approach taken. A particular success of this modelling approach is that the parameters obtained have physical meaning unlike those obtained from standard multiexponential fitting programs most often used.

7.4 Photochemistry of a PFPT co-block polymer

Co-polymerisation can be used as a method to suppress "green-band" formation in polyfluorenes (PF) (as described in chapter 5). It can also be used to produce co-polymer systems which emit light across a wide range of the visible spectrum. PFPT is such a wide band emissive block copolymer. In Chapter 6 we looked at whether FRET occurs between the PF and PT blocks within the polymer chain. The excitation spectrum recorded at the PT emission maximum provided initial proof for energy transfer. TCSPC decays were obtained and the kinetics for PFPT emission decay were compared to those of a PF2/6 oligomer. The results showed that up to ca. 10 % of the PF groups may be energy transferring into the PT block on the timescale of the experiment, ps-ns, and as such is considered to be a dynamic process. However, the steady state emission data suggest that the efficiency of energy transfer is greater than this, with most occurring on a timescale which is faster than the detection response of the TCSPC instrument.

The optical properties of PFPT are solvent dependent. The most notable feature being that upon increasing the water content the emission from PF decreases, even though that from the PT remains almost constant. This was considered to be due to two distinct populations of the PF repeat unit into the chain. Those which are close enough to the PT for efficient energy transfer to occur and those which are too far away that no energy transfer can occur within the natural lifetime.

Future work on this polymer could include an examination in different solvent mixtures to see how this would affect its optical properties. Initial studies of the polymer in acetone:water

mixtures were also presented in Chapter 6, although, studies in this solvent system were and are expected to be limited by aggregation. In addition to considering FRET future work may also consider other energy transfer mechanisms such as Dexter transfer.

7.5 Final Remarks

There is an enormous and ever expanding literature detailing the luminescent properties of both inorganic and organic systems. The might be due to the vast range of technological applications that require luminescent materials. In order to determine how appropriate a material is for a particular application an in-depth photochemical examination is required in order to understand all processes which might be occurring in a system. In addition to a wide range of direct experimental methods, quantum mechanical computation and kinetic modelling techniques can be invaluable in obtaining further understanding of the photophysical and photochemical process consequent upon photon absorption. Whenever possible the full range of these methods, both experimental and theoretical should be utilised in evaluating a luminescent material for a specific application.